UNIVERSITY OF OKLAHOMA

GRADUATE COLLEGE

ORGANIC GEOCHEMICAL CHARACTERIZATION OF SOURCE ROCKS (SIRT SHALE) AND CRUDE OILS FROM CENTRAL SIRT BASIN, LIBYA

A DISSERTATION

SUBMITTED TO THE GRADUATE FACULTY

in partial fulfillment of the requirements for the

Degree of

DOCTOR OF PHILOSOPHY

By

ALSHAREF A. ALBAGHDADY
Norman, Oklahoma
2013

Downloaded from SHAREOK. Persistent Handle URL: https://hdl.handle.net/11244/319089

ORGANIC GEOCHEMICAL CHARACTERIZATION OF SOURCE ROCKS (SIRT SHALE) AND CRUDE OILS FROM CENTRAL SIRT BASIN, LIBYA

A DISSERTATION APPROVED FOR THE
CONOCOPHILLIPS SCHOOL OF GEOLOGY AND GEOPHYSICS

BY

_____
Dr. Paul Philp, Chair

_____
Dr. Roger Slatt

_____
Dr. Anna Cruse

_____
Dr. Michael Engel

_____
Dr. Ramadan Ahmed

© Copyright by ALSHAREF A. ALBAGHDADY 2013
All Rights Reserved.

Dedicated to my father and in memory of my mother

Acknowledgements

I would like to express my appreciation and extend my sincere gratitude to Dr. Paul Philp, my major advisor. I would probably never be able to complete this work without his guidance, encouragement and support throughout my research project. I favorably acknowledge the ministry of education of Libya for the economic support provided during the length of my degree and the School of Geology and Geophysics for being one of its students. I would also like to thank the members of my committee, Dr. Anna M. Cruse, Roger M. Slatt, Ramadan M. Ahmed, and Michael Engel for the time they invested for manuscript review, as well as, their valuable and encouraging suggestions.

This project would have also not been possible without the valuable contribution of Sirt Oil Company (SOC) and Arabian Gulf Oil Company (AGOCO) in Libya who provided the samples that were analyzed in this study. My most sincere thanks to Mr. Jon Allen, the lead lab specialist at the organic geochemistry laboratory of the School of Geology and Geophysics, for his valuable help with laboratory analyses needed for this research project. I would also like to express my gratitude to the laboratory specialist Rick Maynard, who analyzed the oil samples for carbon and hydrogen stable isotopes. My gratitude is also extended to all professors and staff of the School of Geology and Geophysics at the University of Oklahoma for their help, support and guidance during these years. I offer my appreciation to Mr. Brian Cardott from the Oklahoma Geological Survey for his help with vitrinite reflectance analysis. I am thankful to Dr. Wan Hasiah Abdullah, for introducing me to organic geochemistry and for her invaluable academic expertise, support and her encouragement during these

years. A special thanks to all of my friends in the Organic Geochemistry Group at University of Oklahoma and students who I have studied with them at the School of Geology and Geophysics at the University of Oklahoma.

Special admiration goes to all my friends Kendell George, Brandi VanAlphen and Carrie Mikker-DeBoer who have spent their time reading this manuscript and provide valuable suggestions. I want to thank my father, my sisters and my brothers for their constant encouragement. I know you faced some very hard times during the big political changes in our country while I was studying.

There are no words to express my gratitude to my brother Dr. Salah who always believes in me and continued to support me achieving my goals. I would like to offer my immense gratitude and infinite appreciation to Aisha, my wife; you are the best and I consider myself lucky to find you beside me whenever I need you. Finally, I would like to thank my children- Fatma, Arwa, Mohammed, and Abdassalam; all of are the best of my life, and the motivation that keeps me going.

Table of Contents

Acknowledgements iv
Table of Tables xi
Table of Figures xii
Abstract xvii
CHAPTER I 1
1. Introduction 1
1.1 Regional Setting 1
1.1.1 Structure 2
1.1.1.1 Hun Graben 2
1.1.1.2 Waddan Uplift 6
1.1.1.3 Zallah Trough 6
1.1.1.4 Az Zahrah-Al Hufrah Platform 7
1.1.1.5 Al Bayda Platform 7
1.1.1.6 Maradah Trough 7
1.1.1.7 Zaltan and Al Jahamah Platforms 8
1.1.1.8 Ajdabiya Trough 8
1.1.1.9 Hameimat Trough 9
1.1.2 Stratigraphy 9
1.1.2.1 Pre-Upper Cretaceous 10
1.1.2.2 Upper Cretaceous 10
1.1.2.3 Paleocene 14
1.1.2.4 Early Eocene 15
1.1.2.5 Middle Eocene 16
1.1.2.6 Miocene 16
1.1.3 Petroleum System 17
1.1.3.1 Source Rocks 18
1.1.3.2 Reservoirs 21
1.1.3.3 Seal Rock 24
1.1.3.4 Overburden Rock 25

1.1.3.5 Style of Traps 25
1.1.3.6 Sirt Shale Characterization 25
1.2 Location of Study Areas 33
1.3 Scope and Objective of Research 33
CHAPTER II 38
2. Organic Geochemistry 38
2.1 Biomarkers 38
2.2 Alkanes 39
2.3 Terpanes 39
2.4 Steranes 41
2.5 Biomarker Parameters 43
2.5.1 Pristane/Phytane Ratio 43
2.5.2 CPI Value 46
2.5.3 C_{27}/C_{17} Ratio 46
2.5.4 Isoprenoid/n-Alkane Ratios 47
2.5.5 Terpane Parameters 47
2.5.5.1 Homohopanes 47
2.5.5.2 Moretane/Hopane Ratios 48
2.5.5.3 Ts/Ts+Tm 48
2.5.5.4 C_{29}/C_{30} Hopane 49
2.5.5.5 Isomerization at C-22: 22S/(22S+22R) 49
2.5.5.6 Gammacerane 50
2.5.6 Steranes Parameters 51
2.5.6.1 C_{29} ααα 20R Sterane/C_{27} ααα 20R Sterane 51
2.5.6.2 C_{28}/C_{29} Sterane Ratios 51
2.5.6.3 (ββ/(ββ +αα) Ratio 52
2.5.6.4 20S/(20S+20R) C_{29} Sterane 52
2.5.6.5 Diasterane/ Sterane Ratio 53
2.6 Aromatic Hydrocarbons 53
2.6.1 Aromatic Steroids 53
2.6.1.1 MA(I)/MA(I+II) Ratio 55

2.6.1.2 TA(I)/TA(I+II) Ratio 55
2.6.2 Polycyclic Aromatic Hydrocarbons 56
2.6.2.1 Methylphenanthrene Indices 57
2.7 Biodegradation of Crude Oils 59
CHAPTER III 62
3. Experimental Investigation 62
3.1 Rock-Eval Analysis 62
3.2 Vitrinite Reflectance Measurements 63
3.3 Geochemical Techniques 68
3.3.1 Sample Preparation 68
3.3.2 Extraction of Soluble Organic Matter from Source Rocks 68
3.3.3 Isolation of Asphaltenes 68
3.3.4 Fractionation of Maltenes 69
3.3.5 Isolation of Branched and Cyclic Saturate Hydrocarbons 71
3.4 Analytical Methods and Instrumentation 71
3.4.1 Gas Chromatography 71
3.4.2 Gas Chromatography-Mass Spectrometry 71
3.4.3 Stable Carbon and Hydrogen Isotope 72
3.5 Compound Identifications 73
3.5.1 Identification of n-Alkane and Acyclic Isoprenoids 73
3.5.2 Identification of Terpanes 76
3.5.3 Hopanes and Moretanes 78
3.5.4 Homohopanes 78
3.5.4.1 Tricyclic and Tetracyclic Terpanes 80
3.5.4.2 Steranes and Diasteranes 82
3.5.5 Aromatic Hydrocarbons 86
3.5.5.1 Aromatic Steroids 86
3.5.5.2 Polycyclic Aromatic Hydrocarbons 90
3.6 Biomarker Quantitation 92
CHAPTER IV 97

4. Source Rock Analysis 97
4.1 TOC and Rock Eval Source rock Analysis 97
4.1.1 Organic richness 97
4.1.2 Hydrocarbon Generation Potential 100
4.1.3 Thermal Maturity 105
4.1.4 Organic Sequence Stratigraphy of Sirt Shale 109
4.1.4.1 Relative Hydrocarbon Potential (RHP) 110
4.2 Source rock Geochemistry 116
4.2.1 Environmental Conditions 116
4.2.2 Thermal Maturity 123
CHAPTER V 125
5. Oil Geochemistry 125
5.1 Crude oil classification 125
5.2 Source Input and Depositional Condition 127
5.2.1 n-Alkane and Isoprenoid 127
5.2.2 Terpane Parameters 131
5.2.3 Sterane Parameters 136
5.3 Thermal Maturity 139
5.3.1 Terpane Biomarker Parameters 139
5.3.2 Sterane Biomarker Parameters 140
5.3.3 Aromatic Hydrocarbons 142
5.4 Stable Isotopes 151
5.5 Principle Component Analysis 155
5.6 Extent of Biodegradation 158
CHAPTER VI 164
6. Oil-Source Rock Correlation 164
CHAPTER VII 173
7. Conclusions 173
References 176
Appendices 197

Appendix I. Sedimentary Organic Matter 197
Definition 197
Organic Matter in the Ocean 197
Settling of Organic Matter 200
Breakdown of Organic Matter 200
Preservation of Organic Matter 203
Types of Organic Matter 207
Kerogen 207
Kerogen Type 211
Organic Matter Content within Sequence Stratigraphy 214
Lowstand Systems Tracts 215
Transgressive Systems Tracts 215
Highstand Systems Tracts 215
Condensed Section 216
Geochemical Sequence Stratigraphy Parameters 216
Organic Matter Content and Type 216
Relative Hydrocarbon Potential 217
Appendix II. Total Organic Carbon and Rock Eval Pyrolysis Results for Source Rock Samples. 219
Appendix III Source Rock Geochemical Data 224
Appendix IV Crude Oil Geochemical Data 227
Appendix V. Absolute Concentration Of Source Rock Samples Normalized to Saturate Fraction (µg/g) 232
Appendix VI. Absolute Concentration of Crude Oil Samples Normalized to Saturate Fraction (µg/g) 234
Appendix VII Principal Component Analysis (PCA) 237

Table of Tables

Table 1-1. Classification of reserves by reservoirs in the Sirt Basin (Baird et al., 1996; Hallett, 2002)..... 20
Table 3-1. Description of oil samples in in this study. 65
Table 3-2. Identifications of tricyclic, tetracyclic and pentacyclic triterpanes from Figure 3-7. 77
Table 3.3. Identifications of steranes and diasteranes from Figure 3-13. 85
Table 3-4. List of monoaromatic steroid hydrocarbons at m/z 253 and their structure (El-Gayar, 2005). 87
Table 3-5. List of trioaromatic steroid hydrocarbons at m/z 231 and their structures (Younes and Philp, 2005)..... 89

Table of Figures

Figure 1-1. The location and the basin boundary of the Sirt Basin (modified after Bu-Argoub, 1996). 3
Figure 1-2. Map shows the structural elements of the Sirt Basin (modified after Abadi et al., 2008)..... 4
Figure 1-3. East–west structural cross section showing the major horsts and grabens across the Sirt Basin leveled to present-day sea level (After Abadi et al., 2008). 5
Figure 1-4. Stratigraphic section of the central Sirt Basin (modified after Ahlbrandt, 2001). 11
Figure 1-5. The total petroleum system of the Sirt Basin (modified after Ahlbrandt, 2001). 19
Figure 1-6. The Maradah Trough Petroleum System (after Hallett, 2002)..... 22
Figure 1-7. The Western Ajdabiya Trough petroleum systems (after Hallett, 2002). . 23
Figure 1-8. Map shows effective thickness of Sirt Shale source rock in the Sirt Basin (>1% TOC; Hallett, 2002). 29
Figure 1-9. Map shows Campanian source rock, kerogen facies, Sirt Basin (Hallett, 2002). 30
Figure 1-10. Map shows Campanian Sirt Shale, maturity and source kitchens. Four main source kitchens have been identified for the Campanian source rock in the Sirt Basin: the Zallah Trough, the A1 Kotlah Graben, the Maradah Trough, the Ajdabiya and the Hameimat Troughs (Hallett, 2002). 31
Figure 1-11. Burial history/TTI plot for Well 5P1-59 (Roohi, 1996a). 32
Figure 1-12. Map show the location the study area in Concession 6..... 34
Figure 1-13. Map shows the distribution of the wells included in this study in Concession 6. The black texts refer to the source rock wells and the green texts refer to the oil wells. 35
Figure 1-14. Map show the location the study area in Concession 47..... 36
Figure 1-15. Map shows the distribution of the wells included in this study in Concession 47. The black texts refer to the source rock wells and the green texts refer to the oil wells. 37

Figure 2-1. Diagenetic origin of pristane and phytane from chlorophyll (Peters and Moldowan, 1993). 45
Figure 2-2. A alignment diagram of the biodegradation scales of Peters and Moldowan (1993) and Wegner et al. (2001). The diagram illustrates the generalized sequence of the removal of selected molecular groups at increasing levels of biodegradation (Head et al., 2003). 61
Figure 3-1. Scheme for the analytical flow chart in this study. 66
Figure 3-2. Schematic pyrogram showing the evolution of organic compounds from a rock sample during pyrolysis (Peters et al., 2005). 67
Figure 3-3. Diagram illustrates the different fractions of the total organic matter analysis, the corresponding parameters and their recordings during Rock Eval (Lafargue et al., 1998). 67
Figure 3-4. Soxhlet continuous extractor for the extraction of the rock samples. 70
Figure 3-5. Structure of n-alkane and isoprenoids. 74
Figure 3-6. Gas chromatogram of saturated hydrocarbon fraction of sample C35-47 shows distributions of n-alkanes (nC_{10} to nC_{34}) and isoprenoids in the sample. 75
Figure 3-7. Mass chromatogram shows the distribution of terpane biomarkers (m/z 191) in Sirt Basin sample. See table 3-2 for peak identification. 76
Figure 3-8. Structures of a) Hopanes and b) C_{30} moretane. 79
Figure 3-9. Structures of a) Tricyclic terpanes and b) Tetracyclic terpanes. 81
Figure 3-10. Structures of a) 17α(H)-22,29,30-trisnorhopane (Tm), and b) 18α(H)-22,29,30-trisnorneohopane (Ts). 81
Figure 3-11. Structures of Steranes. 83
Figure 3-12. Structures of Diasteranes. 83
Figure 3-13. Mass chromatogram (m/z 217) of Sirt Basin sample shows the distribution of steranes and diasteranes. See Table 3-3 for peak identifications. 84
Figure 3-14. GC-MS chromatogram shows distribution of the monoaromatic steroid hydrocarbons in Sirt Samples. See Table 3.4 for peak identifications 86
Figure 3-15. GC-MS chromatogram shows distribution of the triaromatic steroid hydrocarbons in Sirt Samples. See Table 3.5 for peak identifications 88

Figure 3-16. Combination of mass chromatograms shows Phenanthrene (P), methylphenanthrene (MP) in m/z: 178+192; respectively. 90
Figure 3-17. Combination of mass chromatograms shows dibenzothiophene (DBT) and methyldibenzothiophenes (MDBTs) in m/z: 184+198; respectively. 91
Figure 3-18. Combination of mass chromatograms of m/z 66 with m/z 191and m/z 217 of crude oil shows the location of internal standard with terpanes (top), and steranes and diasteranes (bottom). 95
Figure 3-19. Combination mass chromatograms of 66 m/z with m/z: 191 and m/z 217 showing location of internal standard with terpanes (top), and steranes and diasteranes (bottom) in source rocks..... 96
Figure 4-1. Plot of S1 versus TOC, from which non-indigenous hydrocarbons can be distinguished from indigenous hydrocarbons (Hunt, 1996)..... 99
Figure 4-2. TOC versus total hydrocarbon generating potential of rock showing the generating potential of the studied source rocks. 102
Figure 4-3. Plot of hydrogen index versus oxygen index showing that the organic matter of Sirt Shale lies within the kerogen type II and III. 103
Figure 4-4. Plot of HI vs. TOC showing the type of organic matter..... 104
Figure 4-5. Plots of Production Index (PI) vs. T_{max} showing the level of thermal maturity of the samples of this study. 108
Figure 4-6. Gamma ray profile of Sirt Shale in the well BBB1-6, showing sea level changes within sequence stratigraphy. In this figure solid arrows refer to falling and rising of sea level at the larger scale and the dashed arrows refer to falling and rising of sea level at the smaller scale. 112
Figure 4-7. Rock Eval data, RHP, and GR log vs. depths. 113
Figure 4-8. GC trace for extracts of source rocks and show n-alkane distribution in the samples. The two samples at the top show a unimodal of n-alkanes the sample at the bottom shows biomodal distribution of n-alkanes. 117
Figure 4-9. Plot of pristane/nC_{17} versus phytane/nC_{18} showing source and depositional environments (Shanmugan, 1985). 118
Figure 4-10. GC-MS chromatograms are showing the distribution of terpanes (m/z 191) of the Sirt Shale..... 120

Figure 4-11. GC-MS chromatograms are show distribution of steranes (m/z 217) of the Sirt Shale. 121
Figure 4-12. Ternary diagram is showing the relative abundance of C_{27}, C_{28}, and C_{29} regular steranes in saturate hydrocarbon fraction of source rock extracts. 122
Figure 5-1. The carbon number profile of normalized C_{10} to C_{33} n-alkanes from oil samples of Sirt Basin. 129
Figure 5-2. Cross plot of Pr/Ph versus DBT/P indicates the shale lithology and the marine depositional environment of the Sirt Shale. 130
Figure 5-3. Plot of Pr/nC_{17} vs. Ph/nC_{18} of crude oils used in this study. The squares are oils from Concession 6 and triangles are oils from Concession 47. 132
Figure 5-4. Terpane (m/z 191) distribution of group A and B of Sirt Basin Oils. 134
Figure 5-5. Terpane distribution of group C and D of Sirt Basin Oils. 135
Figure 5-6. Sterane distribution (m/z 217) of group A and B of Sirt Basin Oils. Group A shows high C_{27} regular steranes (peak 41) compared to diasterane (peak 33). 137
Figure 5-7. Sterane distribution (m/z 217) of group C and D of Sirt Basin Oils. 138
Figure 5-8. C_{29} 20S/(20S + 20R) versus C_{29} $\beta\beta/(\beta\beta + \alpha\alpha)$ steranes ratios for oils from the Sirt Basin. 141
Figure 5-9. Mass chromatograms of m/z 253 showing the distribution of the monoaromatic steroid hydrocarbons in crude oil of Sirt Basin. 143
Figure 5-10. Mass chromatograms of m/z 231 showing the distribution of the triaromatic steroid hydrocarbons in crude oil of Sirt Basin. 145
Figure 5-11. Plot of monoaromatic versus triaromatic steroid hydrocarbon of crude oils. 148
Figure 5-12. Plot of Methylphenanthrene Index I versus Methylphenanthrene Index II of crude oils. 150
Figure 5-13. Cross-plot of $\delta^{13}C$ values of aromatic versus saturated hydrocarbons from crude oil samples from Sirt Basin with the boundary line separates marine and non-marine oils (Sofer, 1984). (Group A is not presented in the plot). 153
Figure 5-14. The plots $\delta^{13}C$ vs. δD for whole oil to delineate groupings of oils in the Sirt Basin. 154
Figure 5-15. Score (top) and loading (bottom) plots of PCA for oil samples 157

Figure 5-16. Gas chromatogram of the two samples from the Galio Formation showing removal of n-alkane while pristane and phytane are still present. 160
Figure 5-17. Mass chromatograms of m/z 191 and m/z 177 of the two samples from Galio Formation showing that the biodegradation does not affect the hopane which is supported by the absence of the25-norhopane biomarker..... 161
Figure 5-18. Mass chromatograms of m/z 217 of the two samples from the Galio Formation show absence of sterane degradation. 163
Figure 6-1. Plot of Pr/nC_{17} versus Ph/nC_{18} as an indicator of positive correlation between oils and source rocks in this study. The squares are oils and the triangles are source rocks..... 166
Figure 6-2. Ternary plot of regular steranes for oils (circles) and source rocks (squares) from Sirt Basin. 169
Figure 6-3. Sterane m/z 218 profiles showing the C_{27} isomers are greater than C_{28} and C_{28} are greater than C_{29} indicating marine organic matter for source rocks and oil of samples. 170
Figure 6-4. Distribution of absolute concentrations of source rocks and oils..... 172
Figure 1. Formation of source rocks. Only a small fraction of the organic matter is preserved. The formation organic-rich source rocks require restricted water circulation and oxygen supply (Bjørlykke, 2010). 202
Figure 2. Distribution of two organic carbons with similar texture deposited in different conditions (Pederson and Calvert, 1990). 205
Figure 3. Oxic (left) and anoxic (right) depositional environments generally result in poor and good preservation of deposited organic matter, respectively (modified by Peters et al., 2005 after Demaison and Moore, 1980). 206
Figure 4. Proposed mechanism for kerogen formation describing the interrelationships between extant biomass, kerogen and fossil fuels. LMW denotes low-molecular-weight (Tegelaar et al., 1989; Philp, 2007). 209
Figure 5. A geochemical fractionation of organic matter (Hantschel and Kauerauf, 2009). 210
Figure 6. Classification of kerogen to four types based on chemical analysis (Hunt, 1996). 213

Abstract

The Sirt Basin is located in the north of Libya, bordered on the north by the Gulf of Sirt in the Mediterranean Sea. Sirt Shale is dark-brown to black laminated organic-rich shale containing abundant foraminifera, deposited during Maastrichtian to lowermost Campanian. The samples analyzed in this study were collected from Sirt Basin, concession 6 and 47.

This organic geochemical study was performed on eighty-six samples taken from the Sirt Shale. The total organic carbon content is a poor to excellent source rock for oil generation and the kerogen types are type II and II/III. The samples from greater depths (more than 12000 ft) have kerogen type III with low HI and relatively high OI. T_{max} from Rock-Eval pyrolysis was found to be unreliable at the higher depths, and was in the mature range in Well BBB1-6 between depths of 10460 to 11425 ft.

Excellent source rock quality was observed in the well BBB1-6. In this well the samples have the highest TOC value, some greater even than 5%. This interval (10460-11425 ft) of well BBB1-6 is divided into two parts based on the Gamma Ray profile and Rock Eval data parameters. The lower strata were deposited during sea level rise within transgressive systems tracts and the upper strata were deposited within highstand systems tracts. The total organic carbon content increases with depth and supports sea level changes.

Organic geochemical analysis shows a relatively high abundance of low molecular weight n-alkanes compared to high molecular weight n-alkanes suggesting an absence, or low contribution of terrigenous organic matter. Pristane/phytane and isoprenoid/n-

alkane ratios, the presence of gammacerane, regular sterane distributions and the occurrence of C_{30} steranes suggest marine organic matter deposited under oxic to suboxic saline conditions. These rocks are mature and the main phase of oil generation has been reached.

Organic geochemical analysis of the eighteen crude oil samples shows pristane/phytane ratios between 1 and 3, which may suggest a marine depositional environment for the organic matter. The crude oils also show a high abundance of low molecular weight n-alkanes which suggests a high contribution of marine organic matter. A ternary diagram of regular steranes and the occurrence of C_{30} steranes also strongly suggest marine organic matter contributions. Geochemical parameters suggest that the lithology of the source rocks of these oils are shale deposited under oxic to suboxic marine conditions. According to the age parameters, the source rock of these crude oils is most likely Upper Cretaceous in age. The oils were divided into four groups (A, B, D and C) according to thermal maturity parameters and carbon stable isotope and hydrogen stable isotope analysis. Two of the shallowest samples from the Gialo reservoir show very slight biodegradation. These two samples show depletion of normal alkane while the isoprenoids, hopane, and steranes were unaffected which has been observed to be associated with light biodegradation.

The group A and B oils have a positive correlation with the source rock in well BBB1-6 according to the biomarker parameters. The absolute concentrations of biomarkers support this correlation where both oils (group A and B) and source rock extracts have relatively close biomarker concentrations; therefore, the crude oils in these groups could be sourced from similar source rocks.

CHAPTER I

1. Introduction

The Sirt Bain contains most of Libya's producing oilfields. It is located in northern Libya and stretches southward from the Gulf of Sirt. It contains marine clastic and carbonate sediments, formed during transgressions and regressions during the Upper Cretaceous period. The Sirt Basin is the sixth largest hydrocarbon producing province in the world, with oil and gas reserves estimated at 33 to 45 billion barrels of oil equivalent (BBOE; Macgregor and Moody, 1998). It contains most of the hydrocarbon reserves in Libya, and approximately 29% of Africa's total reserves (Chatelier and Slevein, 1988). In the Sirt Basin, oil is more abundant than gas. The oils have approximately 32 to 44 API gravity and sulfur content of 0.15 to 0.66% (Parsons et al., 1980). These oils are found in sandstone and limestone reservoirs ranging in age from Cambrian to Tertiary.

1.1 Regional Setting

The Sirt Basin covers an approximate area of 600000 km^2 (231660 mi^2) across central Libya and contains a succession of sedimentary deposits reaching a maximum thickness of approximately of 7500 m (24600 ft; Abadi, 2008; Figure 1-1). It is a continental rift area and part of the Tethyan rift system (Futyan and Jawzi, 1996; Guiraud and Bosworth, 1997). During much of the Paleozoic and Mesozoic, the Sirt Basin was an extensive uplift arch with NW-SE orientation (Selley, 1997). The uplift arch was rifted to form the Sirt Basin that began in the Late Cretaceous (Selley, 1997). Sedimentation started with Nubian sediment in the Early Cretaceous Period as non-

marine sediment began to accumulate in grabens (Selley, 1997; Hallett, 2002). Due to a full-scale rifting and block faulting in the Late Cretaceous Period, marine transgressions and associated facies changes across contemporaneous faults occurred in the basin (Bu-Argoub, 1996). In the Late Tertiary, all the platforms were covered by sediments. By the Mid-Paleocene Period, the region had developed into a distinct basin. During the Oligocene Period and the early Miocene Period, intense tectonic activity resumed. Finally, at the end of the mid-Miocene Period the present onshore part of the Sirt Basin had emerged (Bu-Argoub, 1996).

1.1.1 Structure

The Sirt Basin consists mainly of northwest-southeast, east-west and northeast-southwest arms with extended faults. These faults make the present basin and divide it into a large numbers of platforms and troughs (Hallett and El-Ghoul, 1996; Anketell, 1996; Figure 1-2 and 1-3). The sea covered both types of structures; the shale, mainly deposited in troughs and carbonate, formed on platforms. This resulted in complex stratigraphy and different names of the formations in the Sirt Basin due to different oil companies.

1.1.1.1 Hun Graben

The Hun Graben is one of the youngest tectonic elements of the Sirt Basin. This graben is located on the western side of the Sirt Basin (Tawadros, 2001). The Hun Graben is a NW-SE extended structure which appears as a huge depression (Cepek, 1979). The graben extends for 300 km (115 mi^2) from Wadi Zamam to Suknah with an average width of 40 km (15 mi^2; Hallett, 2002).

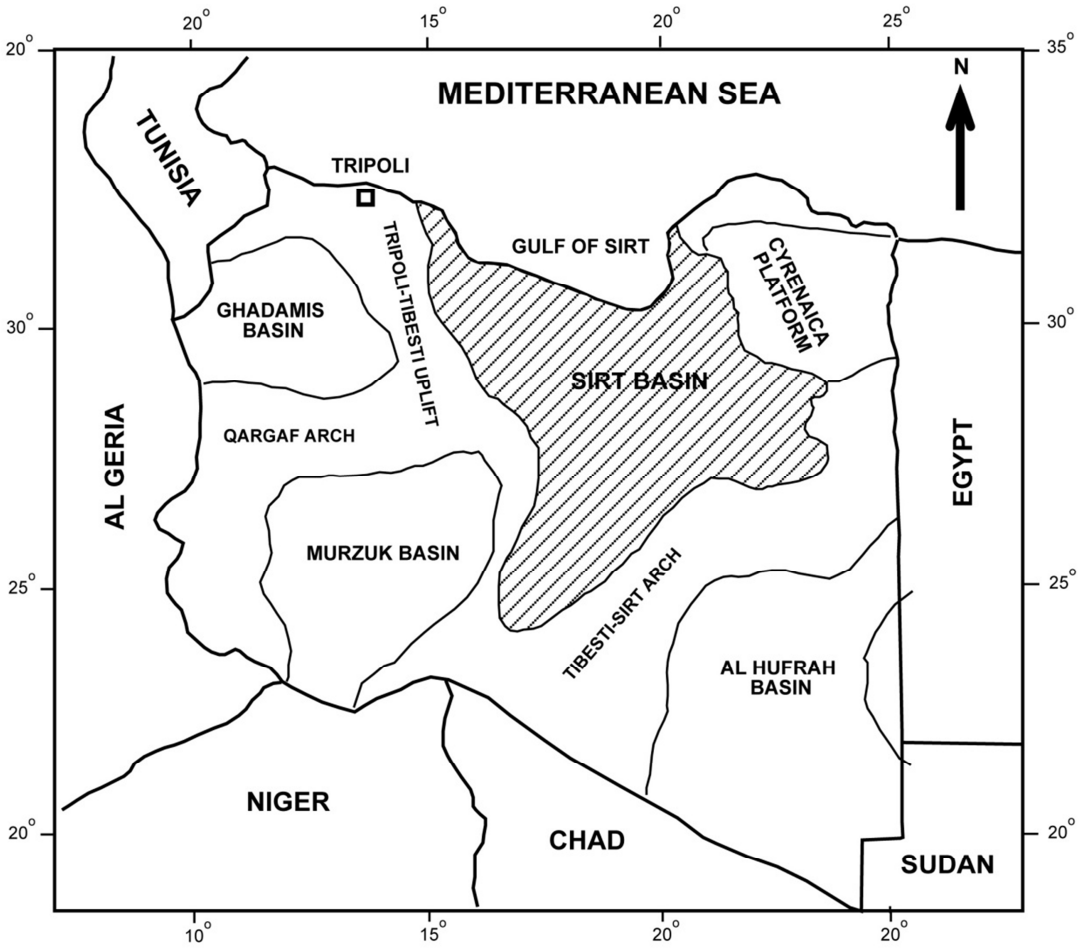


Figure 1-1. The location and the basin boundary of the Sirt Basin (modified after Bu-Argoub, 1996).

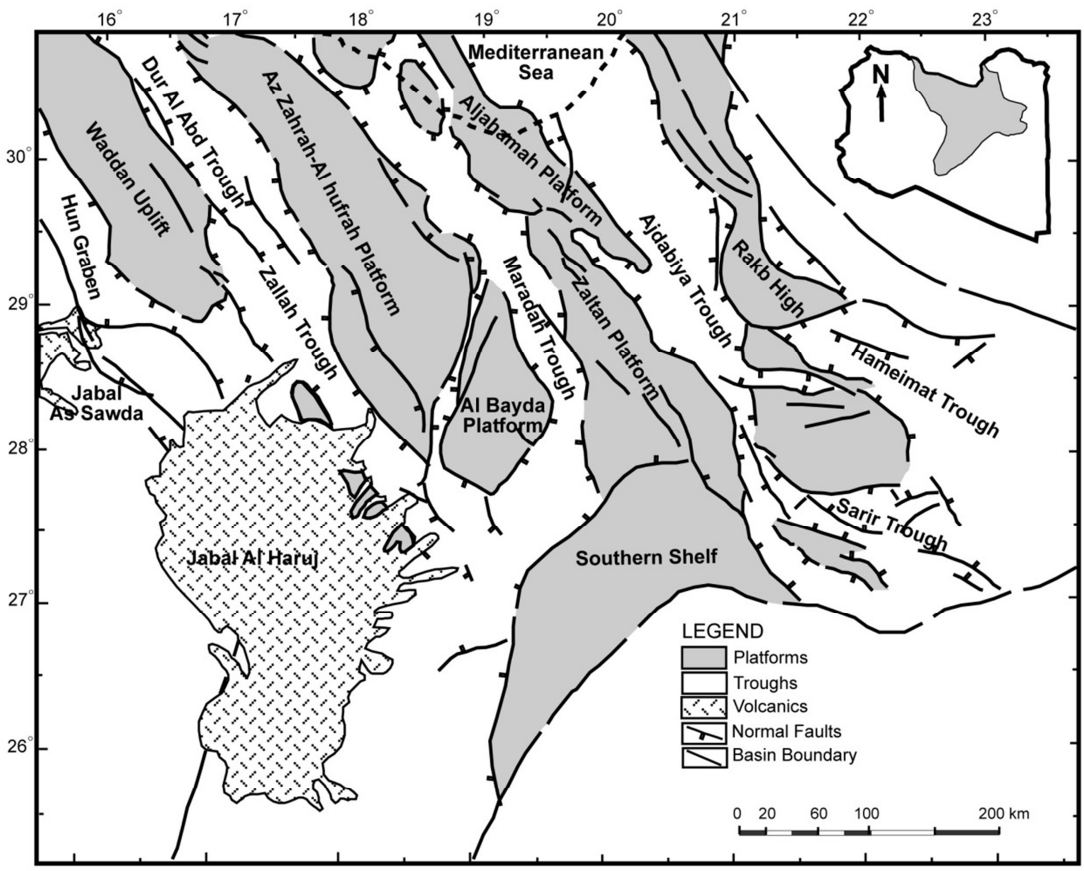


Figure 1-2. Map shows the structural elements of the Sirt Basin (modified after Abadi et al., 2008).

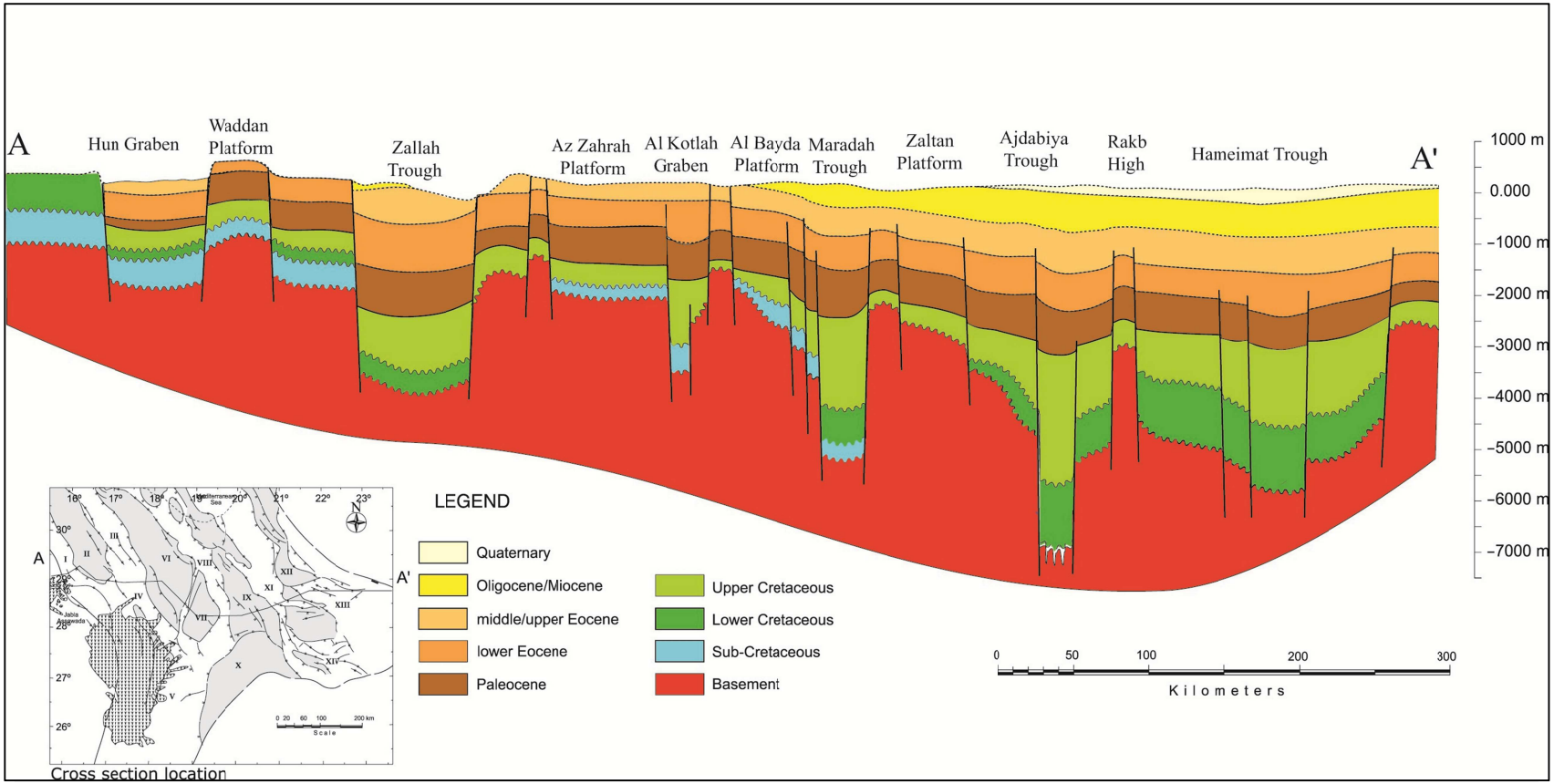


Figure 1-3. East–west structural cross section showing the major horsts and grabens across the Sirt Basin leveled to present-day sea level (After Abadi et al., 2008).

The Hun graben fill includes rocks of basement schist with a depth varying from 2300 m (7546 ft) to 3000 m (9843 ft; Hallett, 2002) with approximately 1500 m of sediments ranging in age from Triassic to Oligocene (Anketell, 1996; Hallett and El-Ghoul, 1996). The Hun Graben is the only outcropping graben in the Sirt Basin.

1.1.1.2 Waddan Uplift

The Waddan Uplift is located between the Hun Graben and the Zallah Trough as shown in Figure 1-2. It is a major platform area tilted towards the northeast, covering about 16,000 km^2 (6177 mi^2). The basement rocks are at a depth of only 1500 m (4921 ft) west of the Zallah Trough, and the depth to the basement in the Dur al Abd Trough is about 3000 m (9843 ft). The dominant trend of the fault direction is NNW-SSE with a set of ENE-WSW faults on the northern margin of the platform (Hallett, 2002).

1.1.1.3 Zallah Trough

The Zallah Trough is located between the Waddan Uplift in the west and the Az Zahrah-Al Hufrah platform on the east (Figure 1-2 and 1-3). The Zallah Trough narrows northwards and becomes shallower to form the Dur al Abd Trough. These toughs separate the Az Zahrah-Al Hufrah Platform from the Waddan Uplift in the area of the Mabrouk Field. The Zallah Trough also extends southwards to connect with the Abu Tumayam Trough and narrows to the east to connect with the Al Kotlah Graben in the region of the Dur Mansour and Al Kuf oil fields (Hallett, 2002). The Zallah Trough is divided into several sub-basins, including the Facha Graben, the Ar Ramlah Syncline, the Ayn An Naqah Subbasin and the Maamir Graben (Johnson and Nicaud, 1996; Schröter, 1996; Tawadros, 2001). The Zallah Trough does not appear to have developed before 60 million years. It appears to have had its maximum development

50 million years ago (Gumati and Nairn, 1991). The Zallah generally contains over 3600 m (11811 ft) of sediments (Hallett and El-Ghoul, 1996).

1.1.1.4 Az Zahrah-Al Hufrah Platform

The Az Zahrah-Al Hufrah Platform is bordered on the west by the Dur al Abd Trough and to the east by the Maradah Trough. It covers an area of 40000 km^2 (15444 mi^2). The Al Kotlah Graben forms the southern boundary of the Az Zahrah-Al Hufrah Platform. It trends NNE- SSW and separates it from the Al Bayda Platform. The depth to the top of the Cretaceous ranges from 900 m (2953 ft) on the western boundary near the Az Zahrah field and 1600 m (5249 ft) to the north (Hallett, 2002). The thickness of the Upper Cretaceous is about 300 m (Hallett, 2002).

1.1.1.5 Al Bayda Platform

The Al Bayda Platform trends from NNE to SSW. The Al Kotlah Graben separates the Al Bayda Platform from the Az Zahrah-Al Hufrah Platform to the north. The Al Bayda Platform is the western boundary of the Abu Tumayam Trough. The thickness of the Upper Cretaceous is 300 m (984 ft) and the depth to the top Cretaceous sediment ranges from 1300 m (4265 ft) to 1800 m (5906 ft; Hallett, 2002).

1.1.1.6 Maradah Trough

The Maradah Trough, also known as the Hagfah Trough, is bordered on the west by the Az Zahrah-Al Hufrah Platform to the north and Al Bayda Platform to the south and on the east by the Al Jahamah Platform to the north and the Zaltan Platform to the south. The shallowest parts of the trough are at the northern and southern margins while the deepest part is adjacent to the Al Jahamah Platform (Hallett, 2002). The

Maradah Trough did not exist before 60 million years. It became active about 40 million years (Gumati and Nairn, 1991). The Uppermost Cretaceous is found at a depth between 3000 m (9843 ft) in the basin's center and 2000 m (6562 ft) in the southern and northern parts (Hallett, 2002). The Upper Cretaceous sediments are very thick in the center of the basin, reaching up to 1800 m (Hallett, 2002).

1.1.1.7 Zaltan and Al Jahamah Platforms

The Zaltan and Jahamah Platforms extend from the Dayfah Field into the offshore north of An Nuwfaliyah. To the west these elements are bordered by the Maradah Trough and to the east by the Ajdabiya Trough. Southward the Zaltan Platform merges with the Southern Shelf. The depth to the top of the Cretaceous ranges from 1650 m (5413ft) to 2650 m (8694 ft) at the Dayfah Field and Hutaybah. The thickness of the Upper Cretaceous ranges from less than 200 m (656 ft) on the western margin thickening to 600 m (1967 ft) on the eastern margin (Hallett, 2002).

1.1.1.8 Ajdabiya Trough

The Ajdabiya Trough is also known as the Maragh Trough. It covers an area of 22500 km^2 (8687 mi^2). It is the largest and deepest trough of the Sirt Basin, containing about 8000 m (26247 ft) of sediment. The highest rate of sedimentation in the trough occurred during the Oligocene and Miocene Periods (Hallett, 2002). Oligocene sedimentations are about 1500 m (4921 ft) and reach about 2100 m (6890 ft) during the Miocene. Upper Cretaceous sediments reach 2400 m (7874 ft) in thickness in the southern part of the trough (Hallett, 2002). The trough was inactive during the Paleocene time and became active again during the Eocene epoch (Hallett and El Ghoul, 1996) and continues to be active (Hallett, 2002).

1.1.1.9 Hameimat Trough

The Hameimat Trough is located in the eastern part of the Sirt Basin. It is bordered by the Amal and Messlah Highs. Toward the east it connects with the Al Gaghbub-Siwa Trough through the Abu Attifel sub-basin (El-Arnauti and Shelmani, 1985) and westward into the Ajdabiya trough (Tawadros, 2001).

1.1.2 Stratigraphy

Sediment thicknesses in the Sirt basin are highly variable from the troughs and platforms, ranging from 1500 to 7000 m (Goudarzi, 1980) and represent deposits from the Cambrian to Tertiary (Tawadros, 2001). The basement rocks are represented by weathered and fractured granitic basement and metamorphic rocks from the Late Pre-Cambrian to Early Cambrian age (Koscec and Gherryo, 1996). The Paleozoic sequence is represented only by Cambro-Ordovician sediment with a wide distribution in the basin, except over some platforms. The Triassic and Jurassic sediments are characterized by a thin succession of sediments existing in the northeastern part of the Basin. The Lower Cretaceous is thicker and located more in the southeastern part of the basin. The thickness of the Upper Cretaceous marine sequence is the largest sequence in the basin, ranging in age from Cenomanian to Maastrichtian. These thicknesses are largely dependent on their positions in the basin with the thickest sediments found in the troughs (Hallett, 2002). The dominant stratigraphic section, which is present overlaying the basement in the subsurface of the Sirt Basin, is summarized in the Figure (1-4).

1.1.2.1 Pre-Upper Cretaceous

Nubian Formation: Nubian rocks are also known as the Sarir Sandstone (Ceriani et al., 2002), mainly non-marine sandstones, siltstone, shale and conglomerates (Barr and Weegar, 1972). In the northwest-southeast–trending troughs, it is rich in coccoliths (Bonnefous, 1972). In some place, the depositional environment of this formation is interpreted as tidal sand bodies in a marine setting with fluvial sedimentation that has formed under regressive conditions (El-Hawat et al., 1996).

1.1.2.2 Upper Cretaceous

Bahi Formation: The type section of the Bahi formation was first named in well A3-32 in the Bahi field (Barr and Weegar, 1972). It is poorly-sorted interbedded sandstones, siltstones, conglomerates, and shale, with glauconite occurring in the upper part of the formation (Barr and Weegar, 1972). It is a significant reservoir in the Sirt Basin. The environment of this formation is considered to be fluvial in the lower part of the formation (Barr and Weegar, 1972). The top part contains glauconite, deposited in a very shallow-marine environment (Hallett, 2002). The Bahi Formation is overlain by the Lidam Formation, but in some localities by younger Cretaceous units (Hallett, 2002).

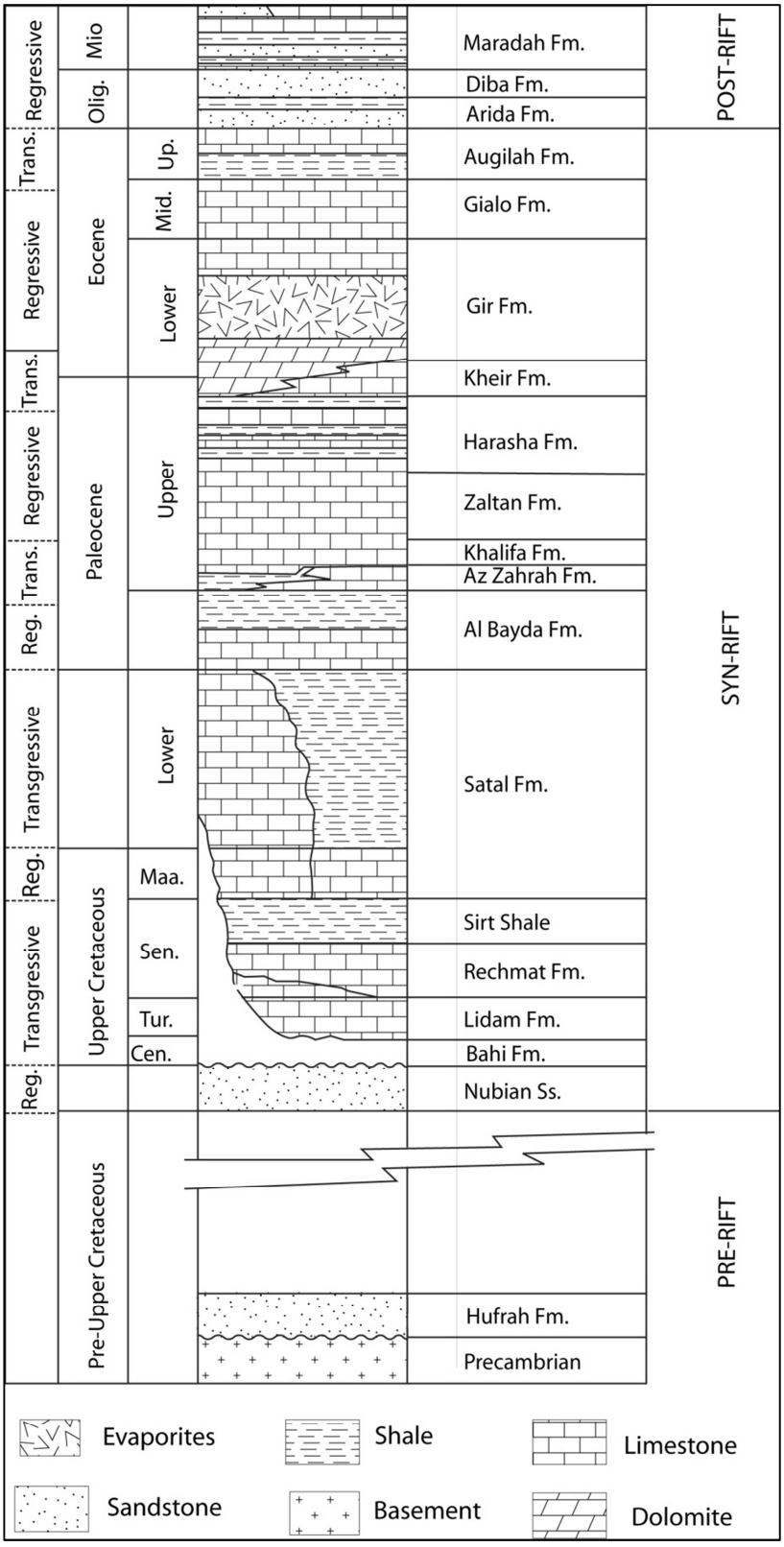


Figure 1-4. Stratigraphic section of the central Sirt Basin (modified after Ahlbrandt, 2001).

Maragh Formation: The Maragh Foundation is clastic sediment located in the north of the basin (Barr Weegar, 1972; Sghair and El Alami, 1996). The rocks are poorly sorted sandstones, conglomerates with quartz and volcanic pebbles. Glauconite and hematite are common in the Maragh Formation (Barr Weegar, 1972). The age of the Maragh Formation is Cenomanian to early Turonian and was deposited in a marginal marine environment (Thusu, 1996). It is an important reservoir in the eastern Sirt Basin (Hallett, 2002). Barr and Weegar (1972) named a type section in well N1-12 l of the Amal field.

Lidam Formation: The Lidam Formation was also named by Barr and Weegar (1972) and its type section was chosen in the G1-57 well in the southern Zallah Trough. The formation is dolomite and sandy dolomite in the lower part which indicates a local mixing with the underlying sands (Barr and Weegar, 1972). The abundance of quartz decreases upward in the formation and glauconite and oolites are sometimes present (Barr and Weegar, 1972). The depositional environment of the Lidam Formation is interpreted as shallow marine but in some locations lagoonal, and intertidal deposits may be present (Hallett, 2002). The Lidam Formation's age is considered to be Cenomanian (Barr and Weegar, 1972). The Lidam Formation is a significant hydrocarbon reservoir (Hallett, 2002) .

Argub Formation: The Argub Formation's name was given by Barr and Weegar (1972) in the D1-32 well, north of the Bahi field. The Argub Formation contains thin-bedded carbonates, shale, anhydrite, siltstone, and sandstone (Barr and Weegar, 1972). The facies vary from evaporites that characterize the basin's center to carbonates dominating the north of the Sirt Basin. The typical succession of the trough

depocenters includes interbedded black shale and anhydrite, covered by carbonate (El-Alami et al., 1989). Due to the absence of diagnostic fossils, the age was determined by its stratigraphic position and it is believed to be Turonian (Hallett, 2002).

Etel Formation: The Etel Formation is thin-bedded carbonates, shale, anhydrite, siltstone, and sandstone (Barr and Weegar, 1972). The type section was chosen in the well O2-59 by Barr and Weegar (1972), on the southeast margin of the Al Bayda Platform. The Etel Formation has a sharp contact with the underlying Lidam Formation. However, in other areas it occurs unconformably on the Bahi Formation or on pre-Cretaceous rocks. The contact with the overlying Rachmat Formation is gradational (Hallett, 2002). Based on its stratigraphic position, the age of the Etel Formation is considered Turonian (Barr and Weegar, 1972).

Rachmat Formation: The Rachmat Formation is fissile shale, with minor limestone, sandstone, and dolomite interbeds in some parts. The limestone interbeds are more common in the lower part (Barr and Weegar, 1972). The Rachmat Formation was established by Barr and Weegar (1972) in the O2-59 well on the Al Bayda Platform. The type section of the Rachmat Formation overlies the Etel Formation. Biostratigraphy indicates Coniacian-Santonian age (Barr and Weegar, 1972).

Tagrift Formation: The Tagrift Formation is a distinctive limestone horizon between the Rachmat Formation and the Sirt Shale. The name of the Tagrift Limestone was given by Barr and Weegar (1972) who defined a type section in the N1-59 well in the Awjilah Field. Its depositional environment is interpreted as very shallow water as indicated by the occurrence of rudistides, *Inoceramus,* and other pelecypods, gastropods, bryozoa, algae, ostracods and foraminifera (Barr and Weegar, 1972). The

formation is considered to be late Santonian to Early Campanian age (Hallett, 2002). The Tagrift Limestone is limited to an area along the southeastern margin of the basin, including the Rakb high area, and has been mapped between the Awjilah area and the Harash Field (Hallett, 2002).

Sirt Shale: The Sirt Shale is a shale succession with minor limestone interbeds. To the east, the Sirt Shale becomes calcareous in the lower part, and the shales grade laterally into and rest on the Maragh Sandstone (Barr and Weegar, 1972). The Sirt Shale unconformably overlies the Rachmat Formation and contact between the Sirt Shale and the Kalash Limestone is gradual (Barr and Weegar, 1972).

Kalash Formation: The Kalash Formation is mainly limestone, predominantly argillaceous calcilutite, with dark gray calcareous shale beds. Barr and Weegar (1972) selected the E1-57 well as type section in the southern Zallah Trough near the Al Kotlah Graben. Barr and Weegar (1972) interpreted that the depositional environment of this formation is an open marine environment. The abundance of planktonic foraminifera indicates a Maastrichtian age of the formation (Barr and Weegar, 1972).

1.1.2.3 Paleocene

Hagfah Formation: The Hagfah Formation includes the Upper Satal, Defa, and Lower Sabil members. It consists of shales and thin limestone interbeds in some parts (Barr and Weegar, 1972). Shales laterally grade into platform carbonates along the shelf (Upper Satal, Defa, and Lower Sabil).

Al Bayda Formation: The type section of the Al Bayda Formation is located in the Oasis BBB1-59 well (Barr and Weegar, 1972). It is mainly various interbedded limestones. In terms of environments, these rocks represent carbonate shelf deposits,

with dolomite and calcareous shales, deposited in a variety of shallow-marine environments (Barr and Weegar, 1972).

Khalifa Formation: The Khalifa Formation is defined by Barr and Weegar (1972) in the Oasis AA1-59 well. It consists of lower shale and upper argillaceous limestone. The environment of the upper limestone unit is interpreted as a marginal marine environment whereas the shale is interpreted as an open marine environment (Hallett, 2002). The Khalifa Formation conformably overlies the Dahra, Al Bayda and Hagfah Formations (Barr and Weegar, 1972).

1.1.2.4 Early Eocene

Jabal Zaltan Group: The Jabal Zaltan Group is comprised of two formations: the Lower is the Zaltan Limestone and the Upper is the Harash Formation (Barr and Weegar, 1972). The Zaltan Limestone Formation is widespread across the central and western Sirt Basin and consists of shale, chalky fossiliferous calcilutite and calcarenite, and dolomite (Abadi, 2008). The Harash Formation is predominantly chalky, argillaceous, and muddy calcarenite, with thin interbeds of fissile shale that are dominant in the lower part of the formation (Abadi, 2008).

Kheir Formation: The Kheir Formation is extremely variable in lithology. It is mainly shale, though marl and limestone are present. The formation is conformably overlain by the Lower Eocene Gir Formation (Barr and Weegar, 1972).

Gir Formation: The Gir Formation is typically a sequence of interbedded dolomites and anhydrites with varying amount of limestone and shale. Its environments and facies vary from shallow marine carbonates and evaporites to deeper marine facies in the northern Ajdabiya Trough. In some areas, the Gir Formation is subdivided into the

Facha Dolomite Member that contains dolomite with minor amount of anhydrite, the Hun Evaporite Member which is interbedded anhydrites and dolomites with minor shale, and the Mesdar Limestone Member (Barr and Weegar, 1972).

Gialo Formation: The Gialo Limestone is a thick succession of gray to brown, shallow marine mudstones that contain nummulite (Barr and Weegar, 1972). This formation is highly fossiliferous. In the eastern Sirt Basin, it includes limestone, dolomite, and minor anhydrite (Belazi, 1989), and in the Sarir Trough, nummulitic limestone, marl, and beds of calcareous sandstone (Sandford, 1970). The interpreted depositional environment of the Gialo Formation is shallow marine environments (Barr and Weegar, 1972).

1.1.2.5 Middle Eocene

Augila Formation: The Augila Formation consists of shales, limestones and sandstones (Weegar, 1972). The formation is subdivided into three units or members. The lower unit is light gray to green shale with thin argillaceous limestone or interbedded dolomite. The middle unit contains soft, friable, porous, glauconitic, quartz sandstone. The upper unit is light to dark gray, hard, sandy, slightly glauconitic limestone that is very argillaceous in some places. In the eastern margin the lower part of the Augila Formation is mainly limestone facies, known as the Rashda Member (Barr and Weegar, 1972). The Augila Formation was deposited in shallow-water open-marine envirnments (Hallett, 2002).

1.1.2.6 Miocene

Najah Group: The Najah Group is subdivided into the Arida and Diba Formations (Barr and Weegar, 1972). The Arida Formation mainly consists of sandstones and

shale. The Arida Formation varies dramatically in both lithology and environment of deposition, ranging from continental in the southeast to marine in the in the north of the basin (Bezan, 1996). The Diba Formation includes sandstones and thin shales with sandy limestone at the top. The interpreted depositional environment of the shale is open marine and continental for the sandstones (Bezan, 1996).

Maradah Formation: The Maradah Formation is a clastic unit containing interbedded shales, sandstone, sandy limestone, calcarenite, and gypsum beds (Selley, 1966, 1971; Barr and Weegar, 1972; Benfield and Wright, 1980; Gammudi et al., 1996). The interpreted depositional environment varies from continental to shallow marine environments (Barr and Weegar, 1972).

1.1.3 Petroleum System

The term *petroleum system* refers to all controlling factors which determine the presence of oil and gas in reservoirs and traps, including the identification of source rocks, the condition of hydrocarbon generation from the source rocks, the timing of hydrocarbon migration, and other events that may affect accumulation (Magoon and Dow, 1994). These factors can be summarized as charge, migration and entrapment (Demaison and Huizinga, 1991). These include the occurrence of source, reservoir, seal rock and overburden as well as hydrocarbon generation-migration-accumulation along with trap formation. The important components of a petroleum system include the following: source rock, reservoir rock, seal rock, and overburden rock. Petroleum systems generally have two processes, trap formation and generation–migration–accumulation of hydrocarbons (Magoon and Beaumont, 1999).

The petroleum system of the Sirt Basin is distinctive among other petroleum systems in Libya due to three reasons: 1) the Mesozoic-Cenozoic age of the basin, 2) the presence of a rich and productive source rock in the Upper Cretaceous, mainly the Sirt Shale, and 3) the late age of oil generation and migration in the Cenozoic period (Hallett, 2002). Figure 1-5 shows a chart summarizing the petroleum system of the Sirt Basin (Ahlbrandt, 2001). According to Parsons et al. (1980) the most prolific reservoirs are Nubian sandstones followed by Paleocene carbonates and Upper Cretaceous clastics. More than 50% of fields occur from 2400 (7874 ft) to 3200 m (10499 ft) depth with temperatures ranging from 66°C (150.8 °F) to 93°C (199.4 °F). Most of the oils are found in structural traps (more than 80%). Recently, the known reserves were categorized by reservoir and were consistent with earlier classifications as seen in Table 1.1 (Baird et al., 1996; Hallett, 2002).

1.1.3.1 Source Rocks

The Al Kotlah Graben contains rich Sirt Shale and therefore, is considered to be the source kitchen. The Sirt Shale has reached peak maturity in the south west of the graben and may have charged some fields like Al Kotlah in the Al Kotlah Graben, and Haram on the south of the Az Zahrah-Al Hufrah Platform. However, this kitchen may have different kerogen types as reflected by different chemical compositions and carbon isotope values in the oils of the Abu Alwan Field (Hallett, 2002).

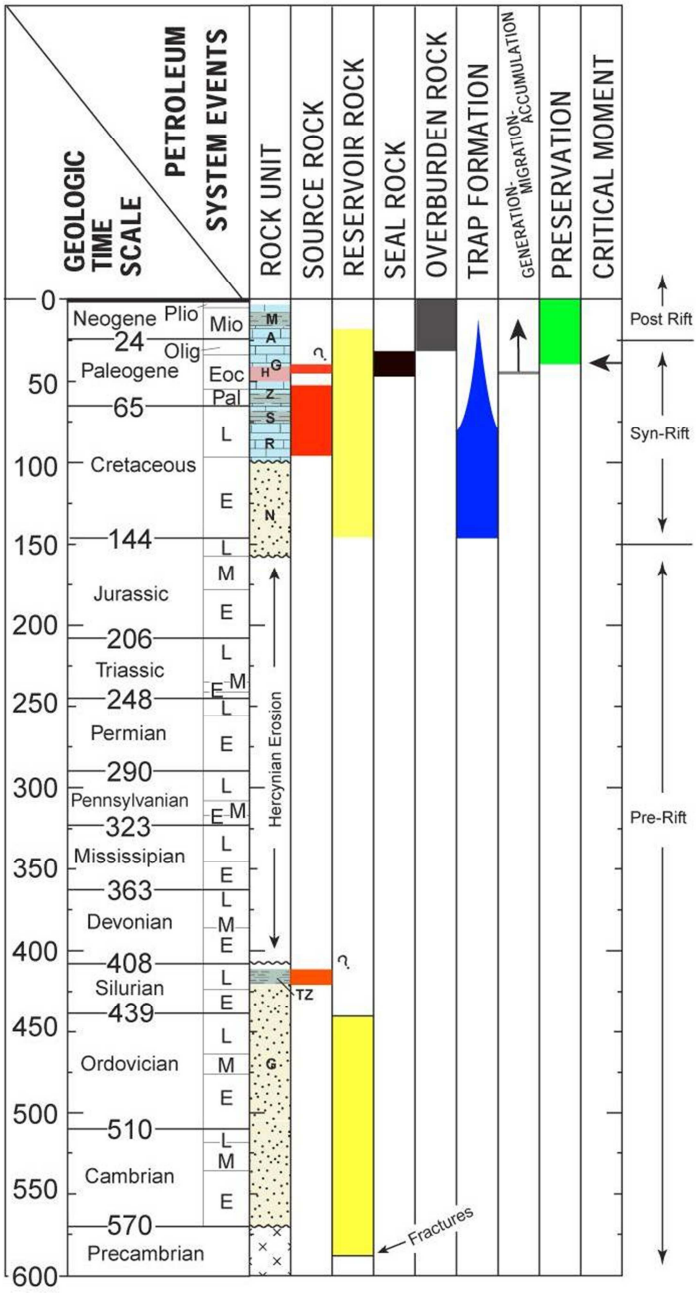


Figure 1-5. The total petroleum system of the Sirt Basin (modified after Ahlbrandt, 2001).

Table 1-1. Classification of reserves by reservoirs in the Sirt Basin (Baird et al., 1996; Hallett, 2002).

Age	Reservoirs	Reserves MMB	%
Oligocene, Rupelian	Arida	1,468	4
Eocene, Lutetian	Jalu	1,834	5
Eocene, Ypresian	Al Jir, Facha	734	2
Palaeocene, Thanetian	Zaltan, U. Sabil, Harash	6,239	17
Palaeocene, L. Thanetian	Az Zahrah	1,101	3
Palaeocene, Montian	Al Bayda	734	2
Palaeocene, Danian	Dayfah, U. Satal	5,140	14
U. Cret., Maastrichtian	Wahah, Kalash	4,038	11
U. Cret., Camp.-Con. + Precambrian	Taqrifat + Basement	2,203	6
U. Cret. Cenomanian	Bahi, Maragh	1,834	5
Lower Cretaceous	Upper Nubian	2,203	6
Lower Cretaceous	Lower and Middle Nubian	6,973	19
Mesozoic/Palaeozoic	Quartzites	1,834	5
	Minor reservoirs	365	1
Total		36,700	100

The main source rock in the Maradah Trough is Sirt Shale (Figure 1-6). It has total organic carbon value greater than 1% with an effective thickness of about 330 m and has reached peak maturity in most of the trough. Type II kerogen is present in the southern part of the trough while the northern part is dominated by Type III kerogen where there is gas generation. The Sirt Shale in the Maradah Trough is thought to be the main source for the oil found in the Az Zahrah-Al Hufrah and Al Bayda Platforms (Roohi, 1996 a and b; Hallett, 2002). The Sirt Shale kitchen in the Ajdabiya Trough may be responsible for 60% of all oil found in the Sirt Basin. Further, it is also assumed that the oil found on the Zaltan Platform (Figure 1-7) was sourced from this trough. Total organic carbon is more than 1% and reaches up to 760 m (2493 ft) in the Intisar area. The oil generation peak is at about 3800 m and the top of gas window is at 4200 m (13780 ft; Hallett, 2002).

1.1.3.2 Reservoirs

The distribution and quality of reservoirs in the Sirt Basin are generally connected to tectonic events in the region, related to pre-rift, syn-rift, and post-rift sequences (Ahlbrandt, 2001). The reservoirs are characterized by formations from Precambrian to Oligocene age (Gumati et al., 1996). The Sirt Basin deeps from west to east and also from south to the north which is influenced the reservoir formation. The basin is produced from the fractured basement of Precambrian, Cambrian-Ordovician Sandstones, Triassic rocks through Lower Cretaceous, Paleocene, and Eocene rocks.

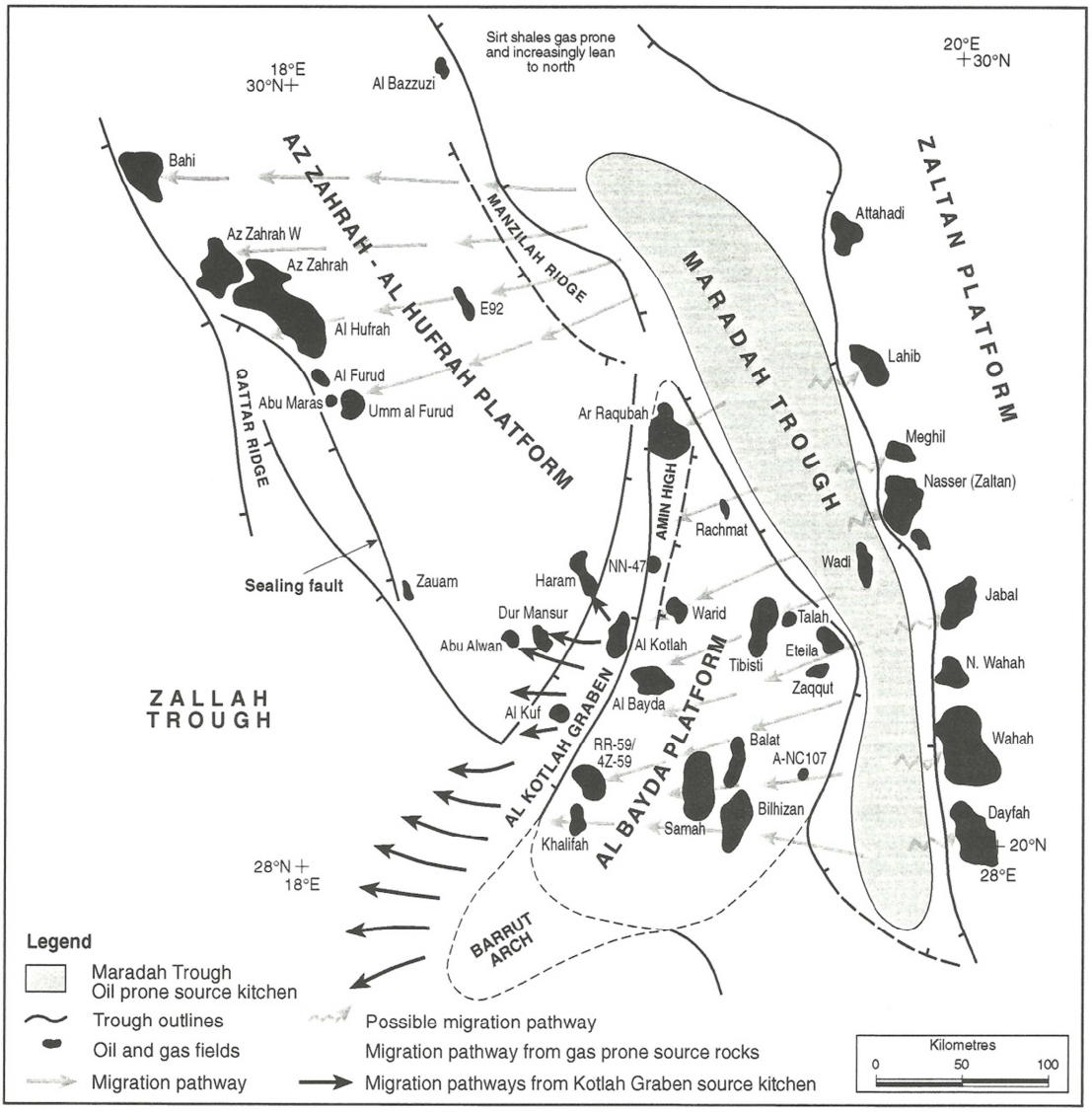


Figure 1-6. The Maradah Trough Petroleum System (after Hallett, 2002).

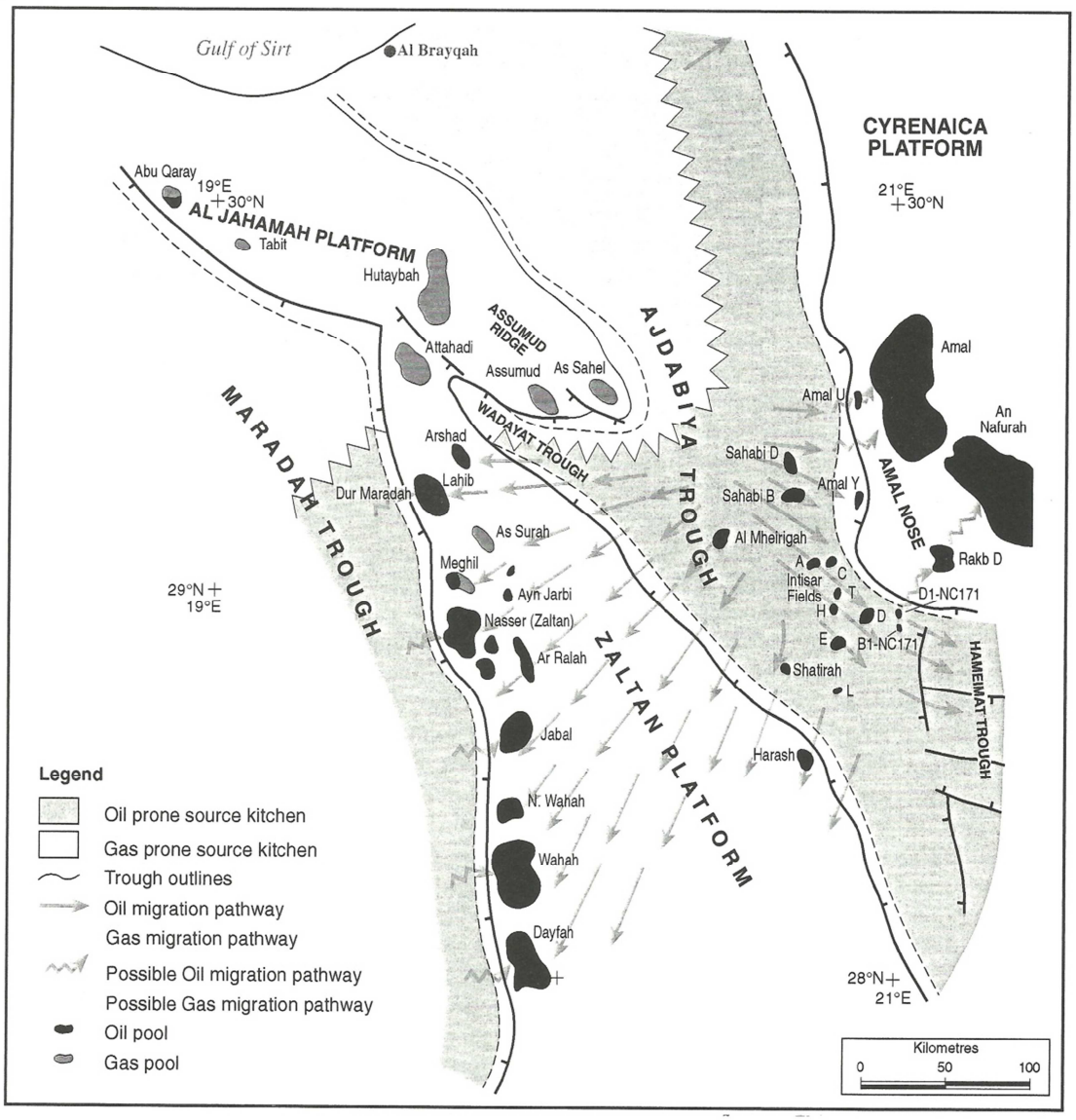


Figure 1-7. The Western Ajdabiya Trough petroleum systems (after Hallett, 2002).

The main reservoirs are carbonate rocks of Tertiary age, which contain 42% of the oil and clastics, mostly of pre-Tertiary age that contain 58% of the oil (Harding, 1984; Ahlbrandt, 2001). Carbonates of the Paleocene Zaltan Group have 33% of the discovered oil making this is the single largest reservoir interval. However, the clastics of Early Cretaceous age (Nubian or Sarir Sandstone) contain 28%, and clastics of Cambrian-Ordovician age (Gargaf, Hufrah or Amal Group) have 29% of known petroleum volume (Ahlbrandt, 2001). In the study areas the main reservoirs are sandstones of the Gargaf Formation from the Cambro-Ordovician, and carbonate rocks from Upper Cretaceous to Oligocene as in the Zaltan and Al Bayda formations (Philip, 1992). The Wahah Carbonate of the Upper Cretaceous is productive on the Wahah, Jabal, SE Nasser, Lahib, and Hutaybah fields.

1.1.3.3 Seal Rock

The Upper Cretaceous Etel Shale and evaporite deposits at the Sirt unconformity provide the main seal rock for pre-rifting formations. In some places these rocks may show a lack of an effective seal because the Bahi sandstone or Lidam dolomite directly overlies it (Rusk, 2001). The Etel Shale and evaporites act as seal rock for the Bahi and Lidam Formation in some areas. The Paleocene is the seal rock in the platforms. The Khalifa Shale is the most important seal rock since it is present over the entire area (Hallett, 2002). The Wahah Formation is covered by tight micritic limestone of the Kalash Formation and the Al Hagfah Formation.

1.1.3.4 Overburden Rock

The overburden is rock from post-rift sedimentation that deposited during the Oligocene and younger. These deposits are mostly shales and carbonates with greater thickness in the deepest troughs (Ahlbrandt, 2001).

1.1.3.5 Style of Traps

Since the basin resulted from a rifting system, the dominant traps are structural traps. Stratigraphic traps are widely found as well as combinations between stratigraphic and structural traps (Clifford et al., 1980). Bioherm traps were found in the basin particularly in the Zaltan Formation on the Zaltan Platform (Bebout and Poindexter, 1975).

1.1.3.6 Sirt Shale Characterization

The Sirt Shale, which contains minor amounts of carbonates (Tagrift Limestone) of Upper Cretaceous, Campanian/Turonian is the main source rock (Parsons et al., 1980; Gumati and Schamel, 1988; Montgomery, 1994; El-Alami, 1996; Ghori and Mohammed, 1996; Mansour and Magairhy, 1996; Macgregor and Moody, 1998; Ambrose, 2000). Several other potential source rocks of ages other than Late Cretaceous have been observed; Burwood (1997), for example, recognized source potential in four mudstones within deeper parts of the Sirt Basin including the Sirt Trough. These potential source rocks occur in the Sirt Shale (Upper Cretaceous), a lower part of the Nubian Formation (Triassic–Lower Cretaceous), the Harash Formation (Paleocene), and the Antelat Formation (Eocene, Gir Formation equivalent; Ahlbrandt, 2001). The Cenomanian-Turonian Etel Formation contains evaporites, shale, and minor carbonates deposited in shallow lagoonal to supratidal zone

environments and show good source-rock features (Figure 1-8), with TOC values ranging from 0.6% to 6.5% in the Hameimat Trough (El-Alami, 1996).

The Sirt Shale is a dark-brown to black laminated organic shale, rich in foraminifera. This suggests that the upper water layers were not anoxic, but the subsiding troughs in which the shales deposited may have been isolated from the open sea by sills which led to water stratification and anoxic conditions on the floor of the troughs. The lack of bioturbation in the Sirt Shale supports the hypothesis that the Campanian sea floor was an improper environment for burrowing organisms. In the eastern Sirt Basin, the lower part of the Sirt Shale passes into a Tagrift Limestone, which also provides evidence of a lack of oxygen and low-energy conditions, but with limited areal extent (Hallett, 2002).

The thickness of the Sirt Shale ranges from about 300 m to as much as 900 m in the troughs. These rocks are within the oil-generating window between depths of 2700 m and 3400 m in the central and eastern Sirt Basin (Futyan and Jawzi, 1996).

In the Sirt Shale the distribution of kerogen facies is closely related to the Campanian paleogeography. Type IV kerogen is found on the platforms, mostly on the Az Zahrah-A1 Hufrah, A1 Jahamah, Zaltan and Waddan Platforms. Kerogen type grades from type III around the trough margins, to type II in the center of the troughs (Figure 1-9). Type I kerogen has not been found in the Sirt Shale (Hallett, 2002).

The active thermally mature Upper Cretaceous source rock is at depths of at least 2865 m (9380 ft; Goudarzi, 1980; Gumati and Kanes, 1985; Ibrahim, 1996), where conditions are considered favorable for oil generation (time temperature index (TTI) = 15, vitrinite reflectance (Ro) = 0.7; Gumati and Schamel, 1988; Montgomery, 1994).

The Ajdabiya and Maradah Troughs were the principal places of major hydrocarbon generation for the accumulations discovered in the western Sirt Basin (Roohi, 1996a and b). The source rock of the Sirt Shale in the Maradah Trough is very similar to the Sirt Shale in the Ajdabiya Trough. It has not been possible to chemically distinguish the oils generated from the two kitchens (Hallett, 2002). Only minor generation occurred in the Zallah Trough. Low generation in the Zallah Trough is due either to the shallow burial depths of the rich source rocks, or to the poor development of the source rocks or both. However, the source rocks in the Hun Graben are also unable to generate hydrocarbons (Hallett, 2002). The source rock deep in the Ajdabiya Trough could be the major source of the hydrocarbons found in the Zaltan Platform, and the source rock in the Maradah Trough is believed to be the main area for hydrocarbon generation of the Al Bayda and Az Zahrah-Al Hufrah platforms. A lack of hydrocarbon accumulation in the Waddan Uplift is due to an absence of hydrocarbon generation from the rocks in the Zallah Trough (Roohi, 1996a and b).

The levels of thermal maturity of Sirt Shale show variation from troughs to platforms (Figure 1-10). The highest levels of thermal maturity were found in the troughs. Since the Sirt Shale has the highest TOC values in the troughs where it is deeply buried, Lopatin's method can be used to estimate its maturity and the timing of oil generation of these rocks. The application of Lopatin's method on the deepest well drilled (Well 5P1-59) with 5855 m (19210 ft) in the southern part of the Ajdabiya Trough (Figure 1-11), show that hydrocarbon generation at the base of the Upper Cretaceous shale started (TTI = 15) about 48 million years ago (Middle Eocene) and passed the oil generation window (TTI = 160) about 26 million years ago (Late

Oligocene). The top part of the unit entered the oil generation stage 28 million years ago and is presently at the peak oil generation window (TTI = 75). Therefore, the major oil generation was mainly during the Oligocene-Miocene time when the burial depth of the potential source rock was between about 3000 m and 4260 m (Roohi, 1996a).

Modeling of geothermal gradients in the Sirt Basin (Gumati and Schamel, 1988) has shown that a geothermal gradient between 25 and 33°C/km existed in the Late Cretaceous and that a lower geothermal gradient of 22°C/km existed from the beginning of the Tertiary onwards. The modeling indicates that the basin had probably reached its present thermal gradient by the Early Tertiary. This study also indicated that Lower Paleocene shales are at an early mature stage with Ro values of 0.67-0.71% in the deepest part of the Ajdabiya Trough, but are submature with Ro values of 0.5% in the Tagrift Trough. Generally, the Tertiary rocks are immature. The differences in geothermal gradients in the basin are related to thermal conductivity (a function of porosity and lithology) more than to the depth of burial (Gumati and Schamel, 1988). Recently, geothermal gradients of the eastern part of the Sirt Basin have been calculated, ranging from less than 24°C/km to over 30°C/km, averaging 27°C/km (Ghori and Mohammed, 1996).

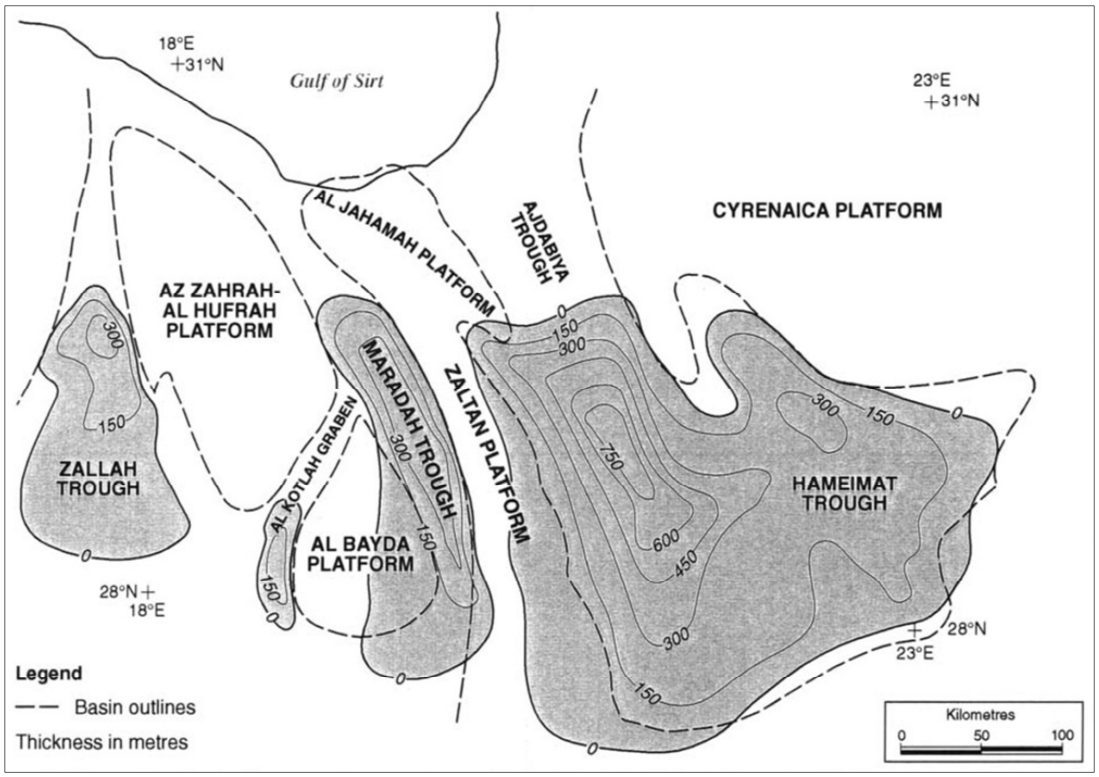


Figure 1-8. Map shows effective thickness of Sirt Shale source rock in the Sirt Basin (>1% TOC; Hallett, 2002).

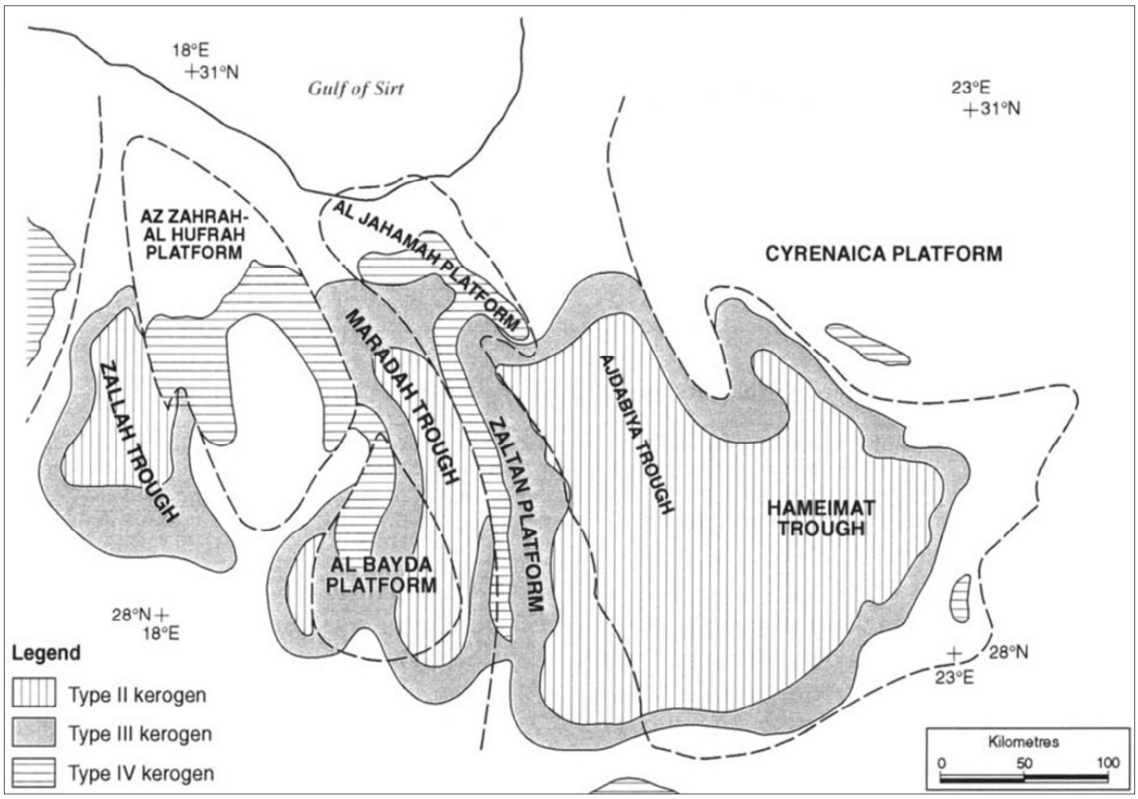


Figure 1-9. Map shows Campanian source rock, kerogen facies, Sirt Basin (Hallett, 2002).

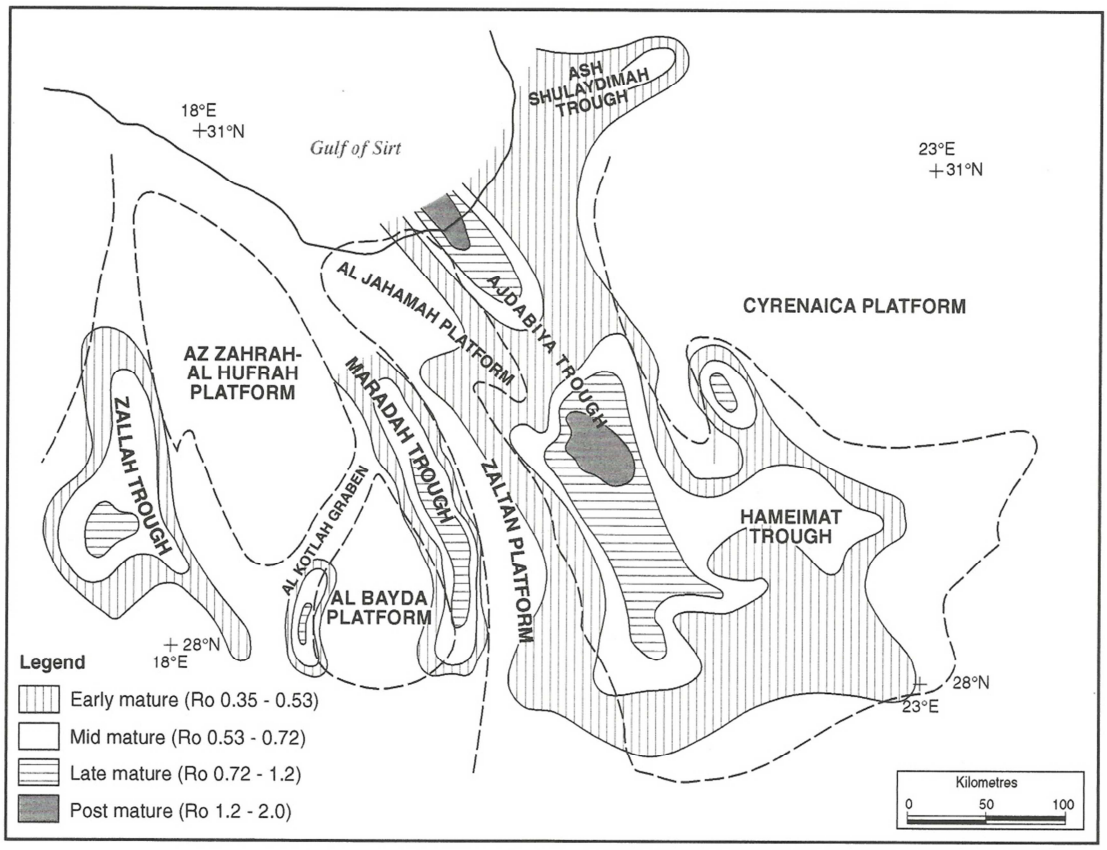


Figure 1-10. Map shows Campanian Sirt Shale, maturity and source kitchens. Four main source kitchens have been identified for the Campanian source rock in the Sirt Basin: the Zallah Trough, the A1 Kotlah Graben, the Maradah Trough, the Ajdabiya and the Hameimat Troughs (Hallett, 2002).

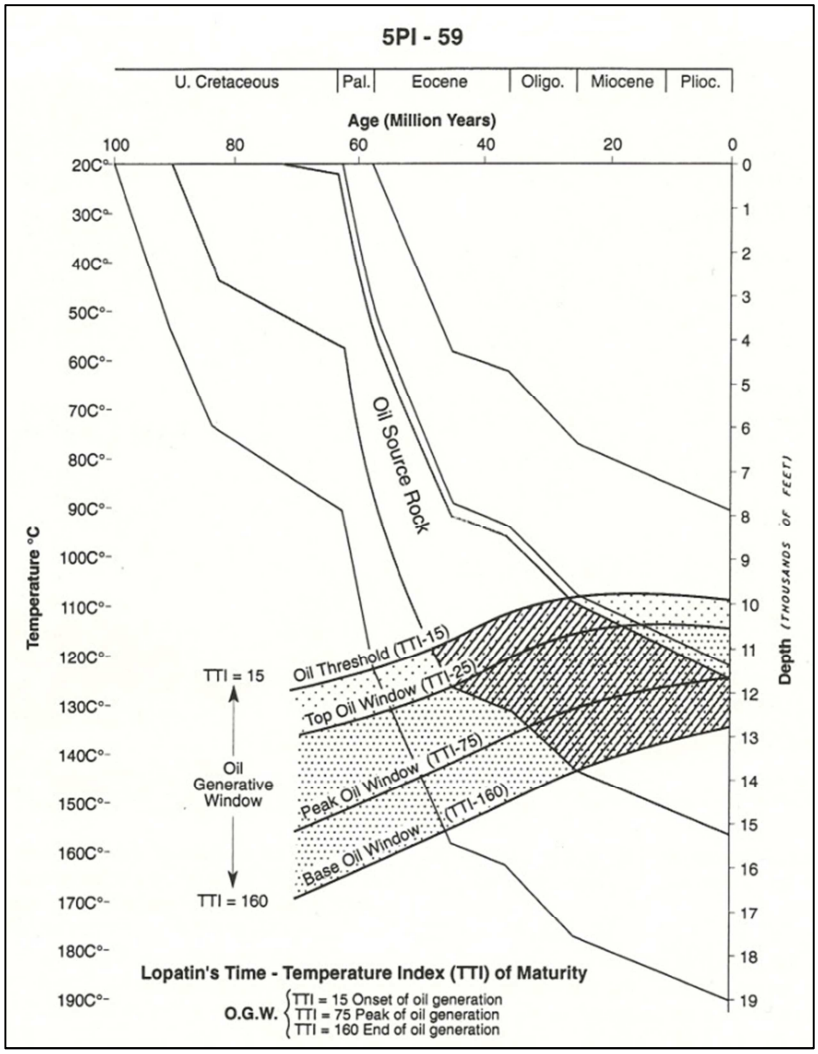


Figure 1-11. Burial history/TTI plot for Well 5P1-59 (Roohi, 1996a).

1.2 Location of Study Areas

The samples were collected from two concessions. Concession 6 is located 50 km in south of Marsa Al Brayqah. The first commercial well in Sirt Basin is in this concession, the Zaltan No. 1 Well. It is located on the Zaltan Platform and Maradah Trough (Figure 1-12 and 1-13; the Zaltan Platform is bounded by the Maradah and Ajdabiya Troughs. Concession 47 is on the Az Zahrah-Al Hufrah Platform and the Al Bayda Platform, including the Al Kotlah Graben (Figure 1-14 and 1-15).

1.3 Scope and Objective of Research

This research project is based on field trip data and laboratory analysis of samples collected during the trip. As the geology of the Sirt Basin has been thoroughly investigated by previous researchers, this study will mainly concentrate on the characterization of crude oils within the study areas and organic facies of Sirt Shale, based on organic geochemical parameters. The main objectives of the study are to:

1- Investigate the quality of organic matter within Sirt Shale in different wells (e.g. Rock-Eval pyrolysis analysis, GC, GC-MS)
2- Interpret the depositional environments based on geochemical data
3- Evaluate the petroleum generating potential of the Sirt Shale within the area
4- Determine the thermal maturity of the organic constituents
5- Undertake oil/oil and oil/source rock correlations

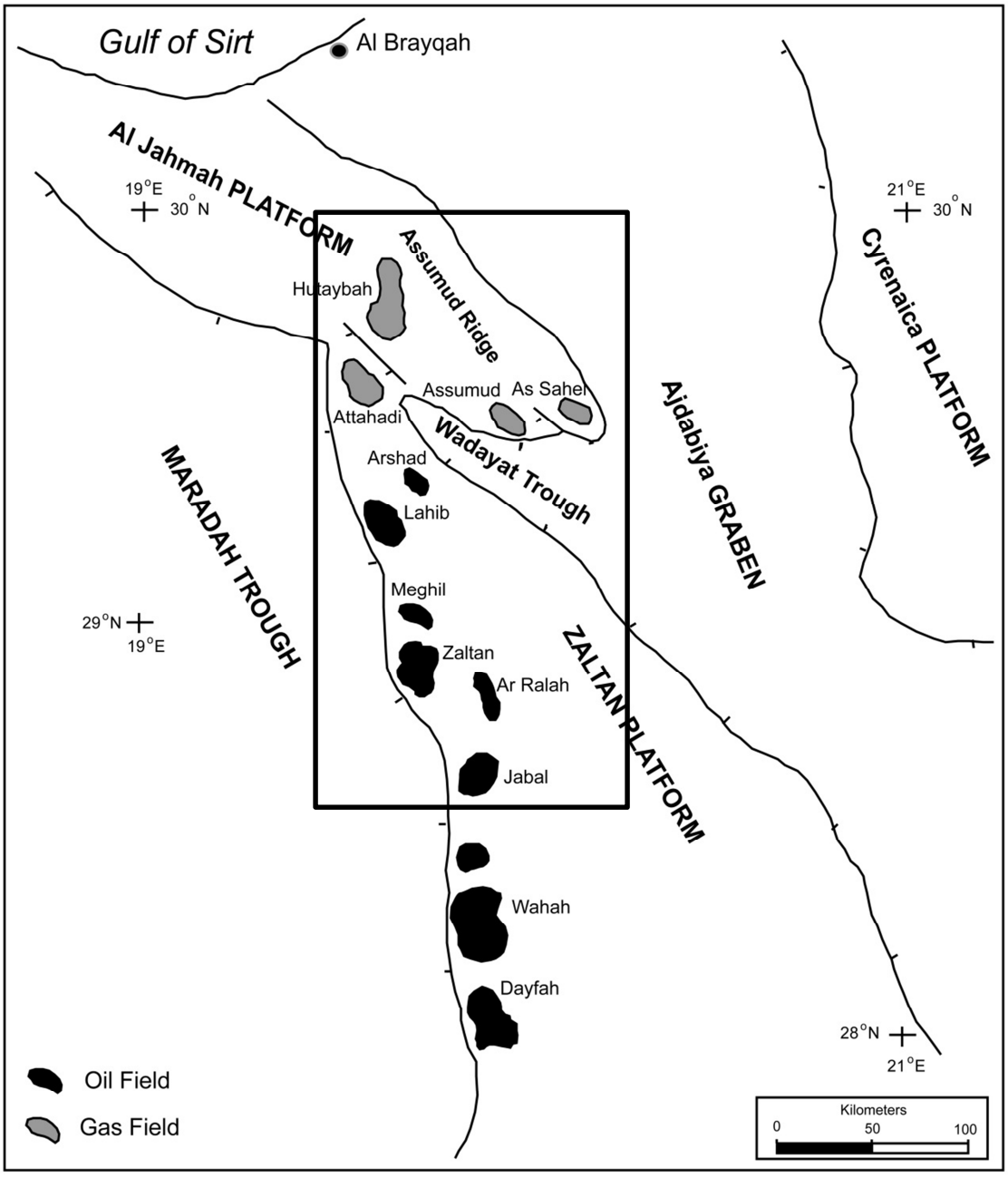


Figure 1-12. Map show the location the study area in Concession 6.

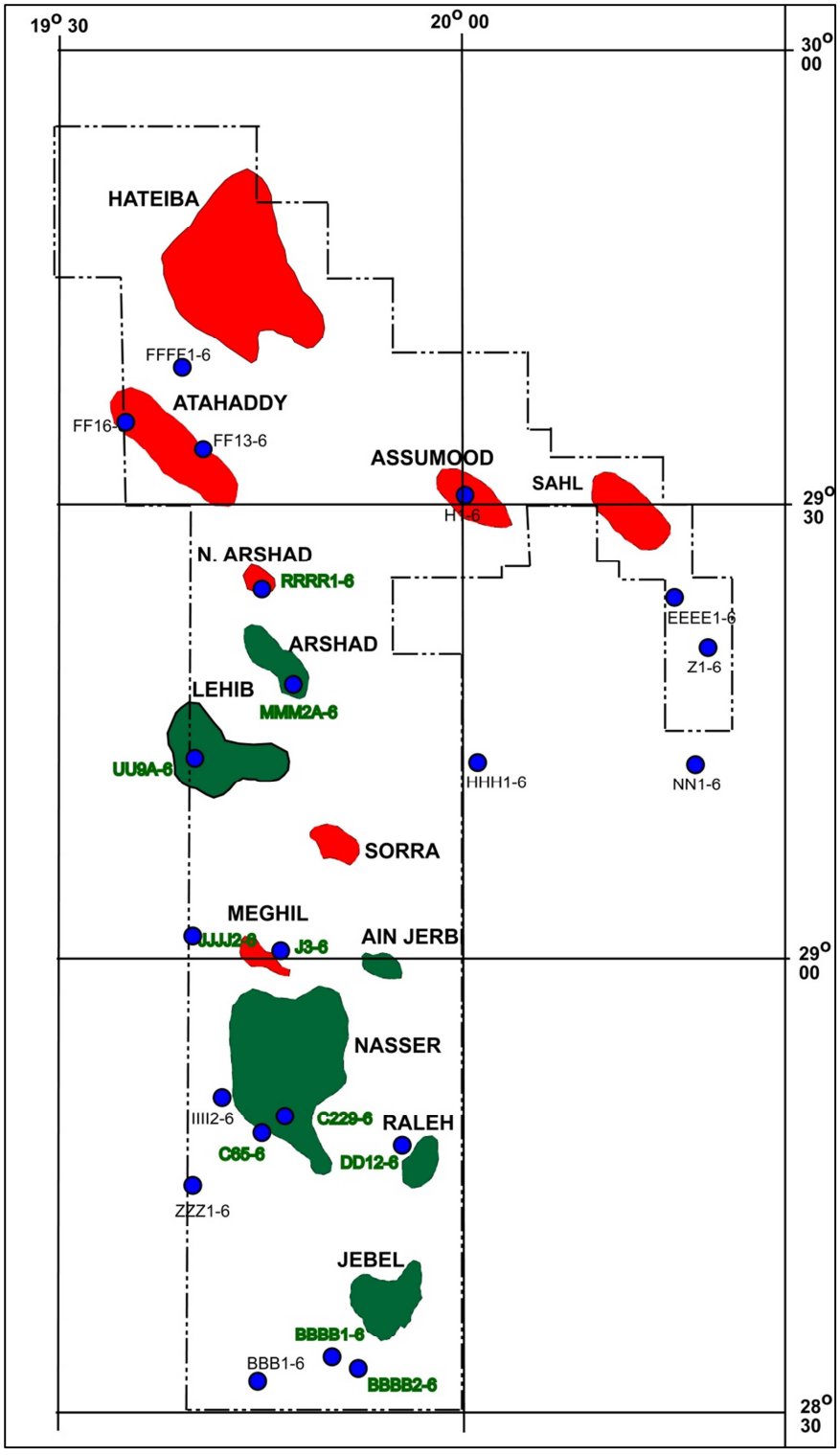


Figure 1-13. Map shows the distribution of the wells included in this study in Concession 6. The black texts refer to the source rock wells and the green texts refer to the oil wells.

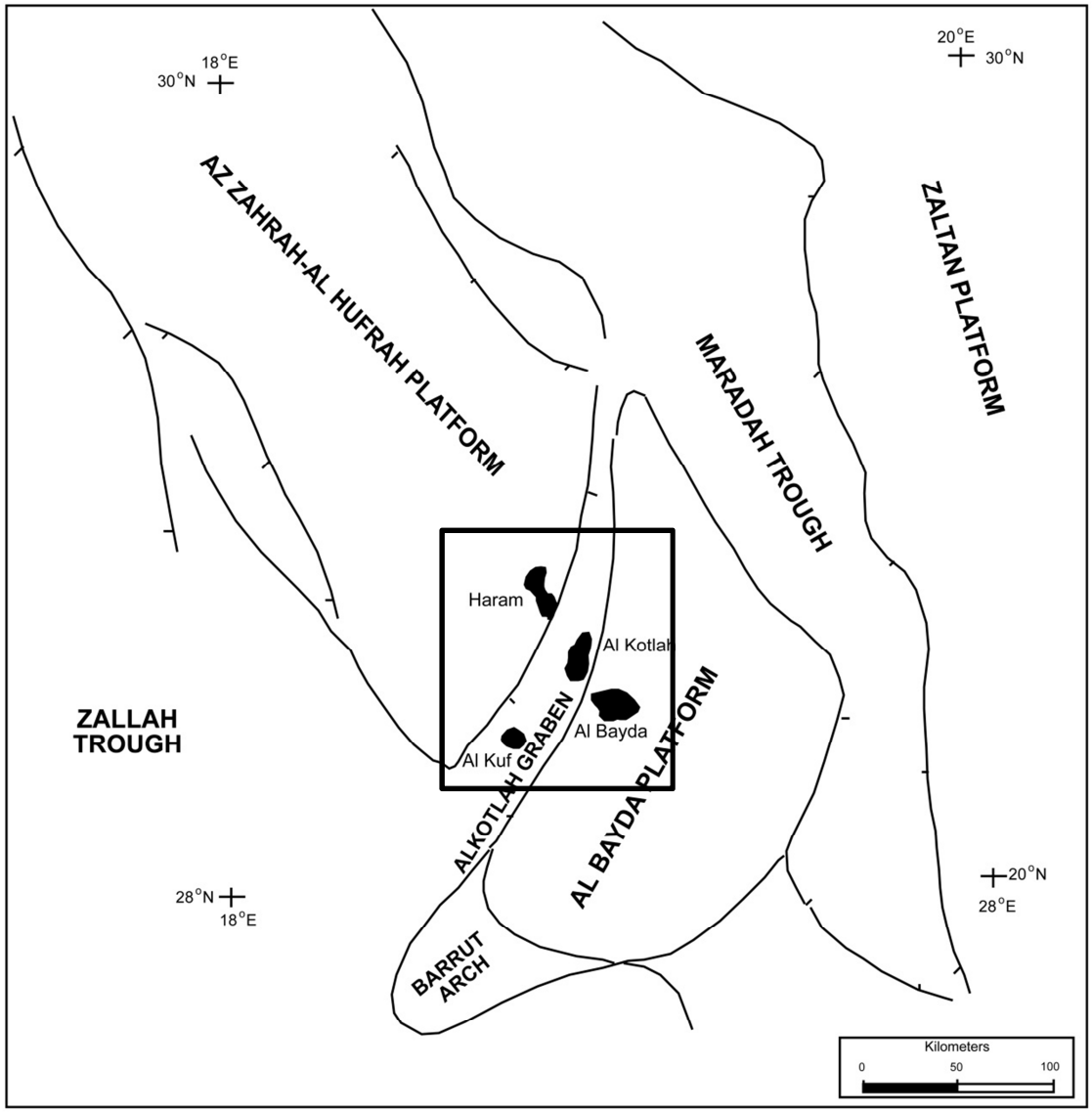


Figure 1-14. Map show the location the study area in Concession 47.

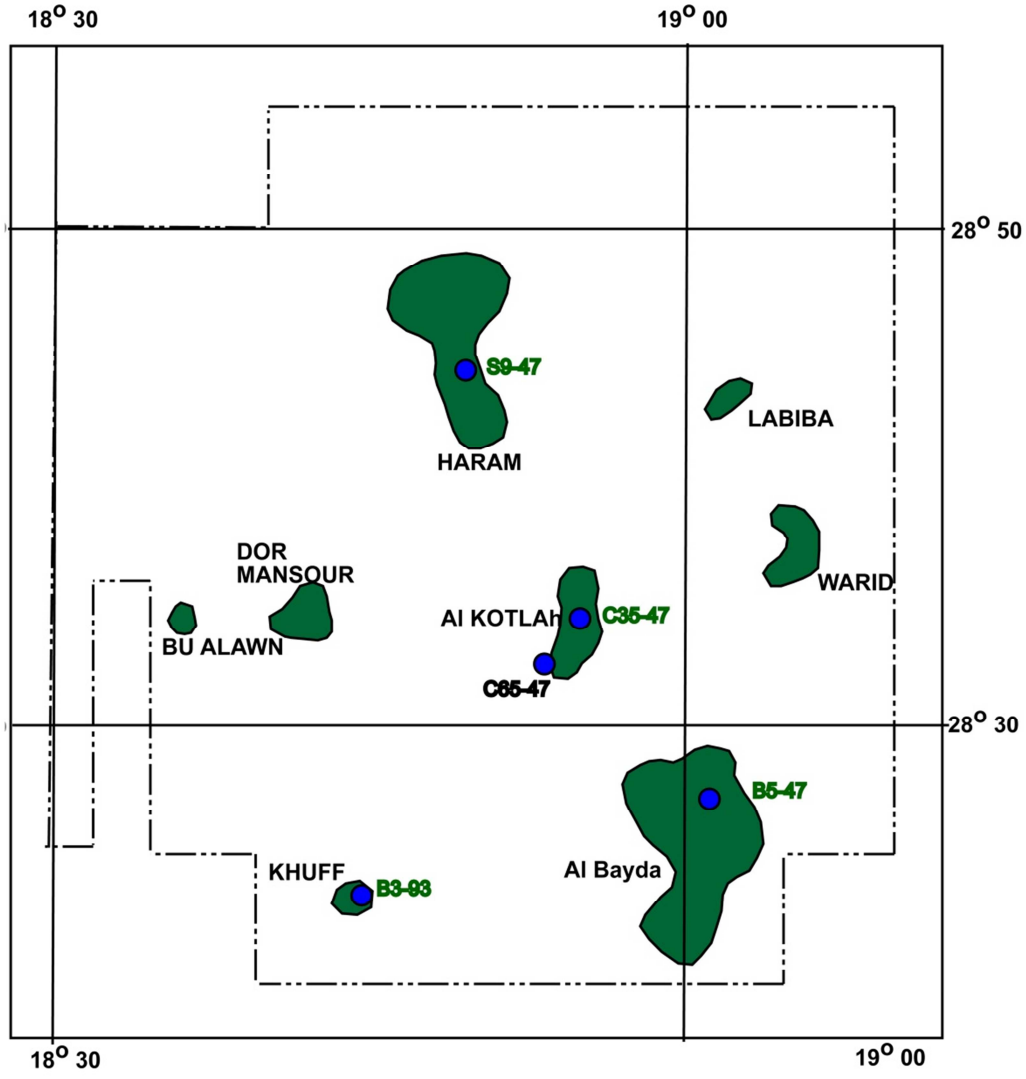


Figure 1-15. Map shows the distribution of the wells included in this study in Concession 47. The black texts refer to the source rock wells and the green texts refer to the oil wells.

CHAPTER II

2. Organic Geochemistry

2.1 Biomarkers

Biomarkers are compounds found in oils and source rocks. Their biological molecular precursors can usually be identified. The common precursors for biomarkers are chlorophyll, sterols, and hopanoids (Peters and Moldowan, 1993). Even though biomarkers are present in very low concentrations in oil and source rock extracts, their parameters are good tools for understanding the transformation processes of organic matter after deposition (Philp, 1985).

The biomarker compounds of oils and rock extracts are used to explore the original type of organic matter, the depositional environment, and the level of thermal maturity. Biomarkers can also be used to identify biodegradation and other alteration processes in oils and source rocks, and for oil-to-oil or oil-to-source rock correlations (Mackenzie, 1984; Philp, 1985; Peters and Moldowan, 1993). Biomarkers are useful tools in oil exploration of because their structures are stable enough to survive during the maturation processes in oil formation. Biomarkers provide more detailed information than the use of only screening (Rock Eval analysis) and microscopic analysis. However, biomarkers and Rock Eval data are powerful tools if used together study the depositional environment of crude oil and source rocks. Generally, biomarkers are used in petroleum geochemistry to: (1) indicate the depositional environment of source rocks (Didyk et al., 1978; Brassell and Eglinton, 1986; Jiamo, et al., 1990; Peters et al., 2005), (2) to identify the type of organic matter from which

oil is derived (Tissot and Welte, 1984), and (3) to estimate the maturity of source rocks and crude oils (Seifert and Moldowan, 1979; Mackenzie, 1984).

2.2 Alkanes

n-Alkanes are the most abundant hydrocarbons in organisms and organic matter. They have been found in bacteria, marine and terrestrial organisms. The major alkanes identified from organisms, source rocks extracts and crude oils are n-alkanes and isoprenoids. The alkanes show relatively higher concentrations in source rocks and crude oils, as compared to those found in living organisms. This difference in concentration is due to their low chemical and catabolic activity which results in a preferential preservation and therefore relative high abundance of n-alkane in the organic matter of sediments (Tissot and Welte, 1984).

2.3 Terpanes

A wide group of hydrocarbons is commonly detected using m/z 191 mass chromatograms (Peters et al., 2005). Terpanes have been observed to have originated from bacterial membrane lipids (Ourisson et al., 1982). The bacterial terpanes include homologous groups such as tricyclic, and tetracyclic and pentacyclic terpanes. These compounds are used to characterize depositional environments, source of organic matter and thermal maturity of oils and source rocks. Terpanes are usually divided into hopanoids and non-hopanoids. Hopanoids include the 17α(H), 21β(H) hopane and 17β(H), 21α(H)hopane (moretanes). Two important C_{27} hopane compounds, 17α(H)-22,29,30-trisnorhopane (Tm) and 18α(H),21β(H)-22,29,30-trisnorhopane (Ts), are widely used for investigating source rock and crude oils. Tm is believed to represent as the biologically produced structure while Ts is converted form during thermal

maturity processes (Peters and Moldowan, 1993). The common non-hopanoids terpane is oleanane which occurs in Cretaceous or younger rock and oils. The precursor of oleanane is thought to be terrigenous angiosperms (Ekweozor and Udo, 1987).

Tricyclic terpanes are identified in most oils and source rock extracts (Aquino Neto et al., 1983). These compounds could originate from precursor organisms such as prokaryotes (Ourisson et al., 1982), algae (Volkman et al., 1989; Simoneit et al., 1993). Generally, tricyclic terpanes may be generated from the same bacteria that produced the pentacyclic terpanes, or by other microorganisms that generate only tricyclic terpanes (Waples and Mashihara, 1990). The carbon number distributions of tricyclic terpanes commonly range from C_{19} to C_{29} but compounds up to C_{54} have been identified (De Grande et al., 1993). The tricyclic compounds with high carbon number (more than C_{29}) usually co-elute with hopanes which make their identification by GC-MS sometimes difficult (Farrimond et al., 1999). The most abundant tricyclic terpane compound is the C_{23} 13β(H),14α (H) (Farrimond et al., 1999).

The ratio of tricyclic terpanes/17α(H)-hopanes is dependent mainly on source of organic matter or depositional environment, but the ratio generally increases with maturity due to their higher thermal stability compared to the hopanes. Tricyclic terpanes are generated from kerogen at higher quantities compared to 17α(H)-hopanes at high thermal maturity (Peters et al., 1990). It have been also reported that the increasing maturity decreases the abundance of the C_{23} relative to the C_{21} and C_{24} tricyclics (Ekweozor and Strausz, 1983; Cassani et al., 1988; Shi et al., 1988). However, Farrimond et al., (1999) observed increases in C_{23}/C_{24} and C_{26}/C_{23} tricyclic terpane ratios through the oil window. This increase is opposite to the trends of source

rocks that observed by Cassani et al. (1988). The difference between the carbon number distributions of tricyclic terpanes may be attributed to the faster heating of the organic matter (Farrimond et al., 1999).

Tetracyclic terpanes are another class, containing carbon numbers from C_{24} to C_{27}, and could have up to C_{35} compounds (Aquino Neto et al., 1983), and can be monitored on the m/z 191 chromatograms. The C_{24} is the common compound among tetracyclic terpanes (Peters and Moldowan, 1993). The high abundance of C_{24} tetracyclic terpanes has been reported in evaporitic and carbonate environments (Connan et al., 1986, Clark and Philp, 1989; Jones and Philp, 1990). However, Philp and Gilbert, (1986) have found high concentrations of C_{24} tetracyclic to be related to a high input of organic matter of terrestrial origin.

2.4 Steranes

Steranes represent one of the main eukaryotes products (McCaffrey et al., 1994; Othman, 2003), and are believed to be derived from the sterols that are commonly found in higher plants and algae and with low concentrations or absent in prokaryotes (Volkman, 1986). Four main sterol precursors containing 27, 28, 29, and 30 carbon atoms have been identified in many organisms and plants. These sterols make four different regular steranes during diagenesis (Waples and Machihara, 1990). The C_{27}-C_{30} steranes are named as cholestane, 24-methylcholestane, 24-ethylcholestane, and 24-n-propylcholestane, respectively. The relative abundance of C_{27}, C_{28} and C_{29} steranes has been used to indicate the type of organic matter (Samuel et al., 2009). Therefore, these compounds are useful parameters for identifying organic matter type and correlating the oil with oil and oil with source rocks (Seifert and Moldowan, 1978;

Peters et al., 1989). C_{27} steranes are believed to be derived from marine organic matter, while abundant C_{29} steranes indicate a contribution from higher plant organic matter and an abundance of C_{28} compounds may indicate the influence of lacustrine algae (Waples and Machihara, 1990; Peters and Moldowan, 1993; Peters, 2005; Othman, 2003; Duan, 2012).

However, the abundance of C_{29} steranes are also identified in many algal sources not related to an influence of terrestrial organic matter (Grantham, 1986; Rullkötter et al. 1986). In addition, Volkman (1986, 1988) found that some rocks in deep marine environments and less terrigenous influence, showed a high concentration of C_{29} steranes. Ternary diagram of C_{27}–C_{29} sterol concentration are used to characterize the distributions of these compounds to differentiate between marine, lacustrine and land plant sources (Huang and Meinschein, 1979). Marine organic matter is strongly indicated by the presence of C_{30} steranes in crude oils and source rocks (Moldowan *et al.*, 1985).

Diasteranes are rearranged steranes (Murray and Boreham, 1992) where the rearrangement involves the migration of methyl groups from ring positions C-10 and C-13 (in regular sterane) to C-5 and C-14, forming diasteranes (Waples and Machihara, 1990; Peters and Moldowan, 1993).

The smaller carbon number compounds, C_{21} (pregnane), C_{22} (homopregnane) respectively can also be important in oil and rock samples from certain environments (Peakman et al., 1989). Pregnanes are believed to be to be derived from the hormones pregnanol and pregnanone and also result from side-chain cleavage of regular steranes

during thermal processes (Huang, 1984; Huang et al., 1994). However, the precursors of pregnane and homopregnane are related to hyper saline environments (ten Haven et al., 1985; Mueller et al., 1995) and therefore can be used as indicators of these environments.

2.5 Biomarker Parameters

Biomarker indicators differ from the other organic parameters because they represent single molecules found in organic matter of crude oils and source rocks. Their structure provides valuable information about their origin, depositional environment, and thermal maturity and geological age of the source rocks. Biomarkers can also be used to determine relative contributions of marine, lacustrine, and terrestrial organic matter and estimate redox conditions of deposition. Biomarkers and other maturation parameters such as vitrinite reflectance can be used to adjust models of generation of oil and gas versus the time of fault and trap formation. These kinds of models are useful to predict the volume of crude oil available for migration to a reservoir (Waples, 1994).

2.5.1 Pristane/Phytane Ratio

Pristane (Pr) and phytane (Ph) are regular isoprenoids that are present in relatively high concentrations in oils and organic matter. They are easily detected by using only GC (Philp, 1985). The pristane/phytane ratio is one of the most widely used geochemical parameters and has been commonly found a good indicator to estimate depositional environments of organic matter (Powell and McKirdy, 1973; Didyk et al., 1978). Under oxic conditions the phytol side-chain of chlorophyll is believed to form pristane, while under anoxic conditions, phytane is produced from diagenesis of phytol

(Figure 2-1). The high Pr/Ph ratios generally indicate that the organic matter has undergone some degree of oxidation. Therefore, oils originating generally from organic matter environment in anoxic conditions would have low Pr/Ph ratios because of low or absence of oxygen, while oils originating from organic matter in oxic conditions would have high Pr/Ph ratio (Brooks et al., 1969; and Powell and McKirdy, 1973). Generally, Pr/Ph ratios greater than 3.0 have been documented to be related to terrestrial organic matter deposited under oxic and suboxic conditions. Low Pr/Ph ratios (less than 1) indicate anoxic conditions while Pr/Ph ratios between 1 and 3 have been found in marine oxic and suboxic conditions (Hunt, 1996; Peters et al 2005). However, it should be noted that different origins of these isoprenoids has been recognized. Risatti et al., (1984) suggested archaebacteria could also be another source of phytane while tocopherols could be a source for pristane (ten Haven et al., 1987).

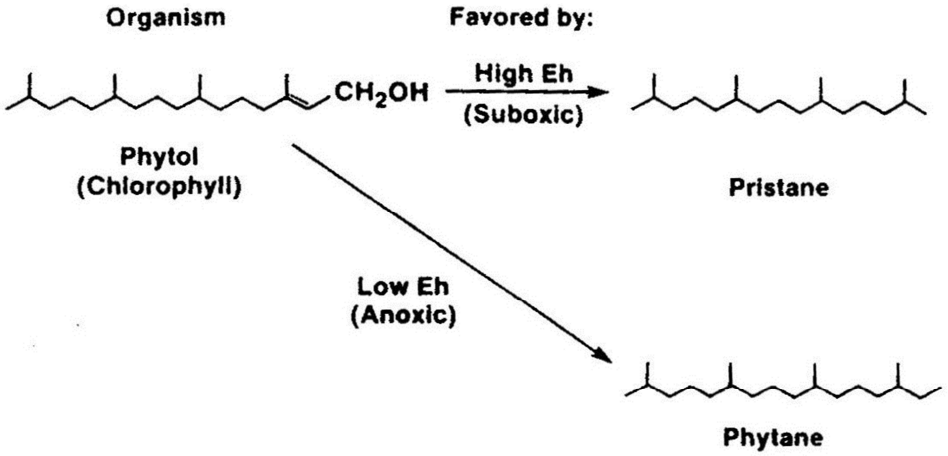


Figure 2-1. Diagenetic origin of pristane and phytane from chlorophyll (Peters and Moldowan, 1993).

2.5.2 CPI Value

The relative abundance of odd versus even carbon-numbered n-alkanes is called the carbon preference index (CPI; Bray and Evans, 1961). It can be used to estimate the thermal maturity of rocks and crude oils. It is calculated as:

$$CPI= \{[(C_{25}+C_{27}+C_{29}+C_{31}+C_{33})/(C_{24}+C_{26}+C_{28}+C_{30}+C_{32})]+[(C_{25}+C_{27}+C_{29}+C_{31}+C_{33})/(C_{26}+C_{28}+C_{30}+C_{32}+C_{34})]\}/2$$

Even though CPI values are useful as indicators of maturity, it should be used in association with other independent indices. High CPI values (greater than 1.5) generally indicate relatively immature samples while CPI values close to 1 indicate high maturity (Simoneit, 1978). However, Low CPI values do not always indicate higher maturity; they can also indicate a lack of higher n-alkanes from terrestrial organic matter. CPI values of 0.8 or less which may be found in carbonate-evaporate sediments could indicate immature organic matter (Tissot and Welte, 1984).

2.5.3 C_{27}/C_{17} Ratio

The dominant n-alkanes in marine organic matter are C_{15} to C_{19} while terrestrial organic matter shows high abundance of n-alkanes C_{27} to C_{31}. This difference between land plants and marine organic matter is used to characterize the type and origin of organic matter. Oils generated from waxes derived from land organic matter will contain an abundance of high molecular weight n-alkanes (C_{27} through C_{31}). It should be noted that lacustrine organic matter and lacustrine oils can be very waxy. These waxes come from freshwater algae. The low molecular weight n-alkanes (C_{15} through-

C_{19}) are found in crude oils that generated from source from marine organisms (Hunt, 1996). Therefore, C_{27}/C_{17} ratio can be used to show the type of organic matter input.

2.5.4 Isoprenoid/n-Alkane Ratios

Pristane/n-C_{17} and phytane/n-C_{18} are sometimes used in oil-oil and oil-source correlations studies. Didyk et al. (1978) suggested that high Pr/nC_{17} ratios (less than 1) for crude oils indicate that non-marine plants have a contribution in the origin of the crude oil and organic matter. The high ratios of Ph/nC_{18} are used as indicator to oxic conditions. Lijmbach (1975) indicated that oils originating from organic matter deposited in marine conditions are characterized by Pr/nC_{17} ratios lower than 0.5, while oils from continental environments have ratios higher than 1. Ratios between 0.5 and 1.0 indicate transitional depositional environments. Thermal maturity affects this ratio by decreasing the relative values of Pr/nC_{17}. These ratios are also affected by biodegradation in which the n-alkanes are generally attacked by aerobic bacteria before the isoprenoids (Peters and Moldowan, 1993).

2.5.5 Terpane Parameters

2.5.5.1 Homohopanes

The homohopanes (C_{31} to C_{35}) are extended hopanes, derived from bacteriopolyhopanol present in prokaryotic cells. An abundance of C_{35} homohopane may be associated with the bacteria activity in the depositional environment (Ourisson et al., 1979, 1984). Low C_{35} presence of homohopanes is generally associated with oxic condition during deposition. High C_{35} homohopane indicates anoxic marine conditions during deposition (Peters and Moldowan, 1991; Ahmed et al., 2012).

Therefore, the distribution of homohopanes 22R+22S $C_{35}/(C_{31}-C_{35})$ ratio, known as homohopanes index in crude oils and source rocks, is used to determine the redox conditions of deposition environments (Peters and Moldowan, 1991).

2.5.5.2 Moretane/Hopane Ratios

Moretane is absent in living organisms but forms from hopanes at higher levels of maturity (Hunt, 1996). The biological 17β(H),21β(H)-hopane in organisms is thermally unstable and converted 17β(H),21α(H)-hopane (moretane) and 17α(H),21β(H)-hopane during diagenesis. Therefore, 17β(H),21β(H)-hopane is not found in crude oils. The occurrence of biological 17β(H),21β(H)-hopane in the crude oils indicates contamination by immature organic matter. During catagenesis, both moretane and hopane decrease in concentration but moretane concentration decreases more rapidly than hopane (Peters and Moldowan, 1993). Therefore, the moretanes/hopane ratio is used as a maturity parameter (Grantham, 1986). A ratio of 0.8 indicates immature organic matter while values of less than 0.15 to minimum of 0.05 suggest mature organic matter (Mackenzie et al., 1980; Seirfert and Moldowan, 1980).

2.5.5.3 Ts/Ts+Tm

With increasing maturity, 17α(H),21β(H)-22,29,30-trisnorhopane(Tm) shows a lower relative stability to thermal processes than 18(H),21β(H)-22,29,30 trisnorneohopane (Ts) and Ts/Tm ratio increases due to the relatively greater destruction of Tm (Farrimond et al. 1996). Therefore, the Ts/Tm ratio is usually used to determine the level of thermal maturity. This ratio is affected by organic matter type and clay minerals of the source rock in the depositional environments (Seifert and

Moldowan, 1978; McKirdy et al., 1983; Rullkötter and Marzi, 1988). Therefore, the Ts/Tm or Ts/(Ts+Tm) ratio would be more reliable if used with other maturity parameters. Farrimond et al. (1996) considered the increase in Ts/Tm ratio is attributed to the relatively greater destruction of Tm.

2.5.5.4 C_{29}/C_{30} Hopane

Hopanes are pentacyclic terpanes that are derived from bacteria (Ourisson et al., 1984; Prince, 1987). The C_{29} and C_{30} 17α(H),21β(H)-hopanes are the most common terpanes in most crude oil and source rock (Waples and Machihara, 1990) and used as environmental indicators. High concentrations of C_{29} 17α(H),21β(H)-hopane in oils indicates they are originated from organic-rich carbonates (Zumberge,1984; Connan et al., 1986) and evaporates (Connan et. al., 1986). High concentrations of C_{30} hopane over 30-norhopane (C_{29}/C_{30} hopane <1) indicate that the organic matter oils are derived from clay-rich, shale source rocks (Gürgey, 1999; Othman, 2003). The high concentrations of C_{29} 17α(H),21β(H)-hopane are used as indicators in oils and organic matter originated from organic-rich carbonate and evaporite source rocks (Clark and Philp, 1989).

2.5.5.5 Isomerization at C-22: 22S/(22S+22R)

22S/(22S+22R) parameter is the most widely used of the hopane maturity parameters. It is a calculation the concentration of the more thermally stable 22S isomer relative to the 22R isomer (biological form; Kolaczkowska et al., 1990). The 22S/(22S+22R) ratio for homohopanes is a good maturity parameter for oils in the early oil window. During maturation, the ratio 22S/(22S+22R) increases from 0 to 0.60. Samples having ratios in the range 0.50 to 0.54 have entered the oil the early

stage of generation window (Peters et al., 2005). The equilibrium value of this ratio occurs between 0.57 and 0.62 (Seifert and Moldowan, 1986; Peters and Moldowan, 1993). However, this ratio is affected by lithology. It has been found that immature organic matter from carbonate rocks (Moldowan et al., 1992) and from evaporitic rocks (ten Haven et al., 1986) show values of this ratio consistent with a higher level of maturity.

A decrease in the 22S/(22S+22R) homohopane ratio was observed with increasing depth in pyrolysis experiments (Lewan et al., 1986; Lu et al., 1989; Abbott et al., 1990; Peters et al., 1990) and sediments rapidly heated by igneous intrusions (Raymond and Murchison, 1992; Bishop and Abbott, 1993; Farrimond et al., 1996). This is the opposite of what is normally expected. However, this reversal of isomerization ratios of 22S/(22S+22R) was also reported in source rock with increasing depth by Curiale and Odermatt (1989) in the Monterey Formation, Santa Maria Basin, USA. Farrimond et al. (1996) observed that within the oil window, the increase in the 22S/(22S+22R) ratio is due to fast destruction of 22R isomer compared to 22S. At the later stages of the oil window or close to an igneous intrusion, the concentration of both S and R isomers are reduced but with faster destruction of the S isomer which causes the decrease of the ratio.

2.5.5.6 Gammacerane

Gammacerane is also a pentacyclic triterpane, used to investigate the salinity of a depositional environment. High concentrations of gammacerane are usually related to highly reducing hypersaline conditions during the deposition of organic matter (Peters and Moldowan, 1993). Gammacerane can also be used as an indicator of a stratified

water column in marine and non-marine depositional environments of source rock which resulted from hypersalinity (Sinninghe Damsté et al. 1995).

2.5.6 Steranes Parameters

2.5.6.1 C_{29} ααα 20R Sterane/C_{27} ααα 20R Sterane

Steranes are mainly derived from eukaryotic organisms (Ourisson et al., 1979). Generally, sterane distributions reflect the variations in algal input to source rocks and can be used to differentiate crude oils based on genetic relationships. Oils generated from kerogen containing organic matter derived from a marine source usually show low ratios of C_{29} relative to C_{27} steranes (Mackenzie et al., 1982; and Czochanska et al., 1988). C_{29} steranes are often used as indicators of land-plant-derived organic matter in source rocks and oils.

2.5.6.2 C_{28}/C_{29} Sterane Ratios

This ratio of C_{28}/ C_{29} steranes is good parameter to estimate the age of organic matter and oil from marine source rock that has minimum or absence of higher plant organic matter. The ratio generally increases from the Paleozoic to the Present time due to an increase in phytoplankton diversity. It has been observed that the C_{28} steranes increase while C_{29} steranes decrease through geologic time (Grantham and Wakefield, 1988, Peters et al., 2007). Therefore, this ratio is used to differentiate between Paleozoic oils from Upper Cretaceous and Tertiary oils (Grantham and Wakefield, 1988). A ratio of less than 0.5 suggests oils from Lower Paleozoic age and older while ratios between 0.4 and 0.7 for oils of Upper Paleozoic to Lower Jurassic age, and oils with a ratio greater than 0.7 indicate Upper Jurassic to Tertiary oils.

Schwark and Empt, (2006) used these ratios to age Late Devonian extinction events (a major extinction events in the history of the Earth's biota). They found a sharp increase in the C_{28}/C_{29}-sterane ratio from <0.55 to >0.70 at the Devonian/Carboniferous boundary. This increase is consistent with the change in the green algae from more primitive algae that produces C_{29} steranes to modern algae which yields C_{28} sterane (Schwark and Empt, 2006).

2.5.6.3 (ββ/(ββ +αα) Ratio

C_{29}ββ/αα parameter is widely used to determine the thermal maturity level. The αββ sterane isomers show greater thermal stability relative to the biologically-derived form of ααα. The αα isomer gradually converts to a mixture of both αα and ββ. The ratio (ββ/(ββ+αα) increases from 0 to a value of about 0.7 and reaches equilibrium values between 0.67 and 0.71 (Seifert and Moldowan, 1986). Heating rate, clay minerals and depositional environment influence this ratio; therefore, it should be used with caution (Philp, 2007). The reaction of steroids with clay minerals during diagenesis may also influence the of (ββ/(ββ+αα) ratio, causing high concentrations of the ββ compounds (ten Haven et al., 1986; and Rullkötter and Marzi, 1988),

2.5.6.4 20S/(20S+20R) C_{29} Sterane

The 20S/(20S+20R) parameter that is usually calculated using the C_{29} ααα steranes is also one of the most widely used maturity parameters for oil and source rock. This ratio is based on the relative concentration of the more stable 20S isomer compared with the biologically 20R isomer (Peters and Moldowan, 1993). With increasing maturity, the biologically produced form 20R converts to 20S and the ratio changes from 0 to about 0.5. This ratio reaches its equilibrium values between 0.52 and 0.55.

When equilibrium is reached, no changes in the level of maturity can be observed using this ratio (Seifert and Moldowan, 1986; Waples and Machihara, 1990).

2.5.6.5 Diasterane/ Sterane Ratio

This ratio is used to differentiate the level of thermal maturity and depositional conditions of the source rock and crude oils (Peters et al. 2005) and also to differentiate crude oils derived from carbonate versus clastic source rocks (Mello et al., 1988). Diasteranes are more stable than regular steranes; therefore the ratio of diasterane/ sterane increases after the peak oil generation window (Peters et al. 1990). Generally, high ratios may indicate that the crude oils are generated from organic matter containing an abundance of clays, whereas low ratios may indicate source rock deposited in an oxic and clay poor carbonate (Peters and Moldowan, 1993). However, diasterane/sterane ratios are useful for oils of similar maturity since the diasteranes increase with increasing maturity (Moldowan et al., 1986).

2.6 Aromatic Hydrocarbons

2.6.1 Aromatic Steroids

Aromatic steroid molecules are an organic compounds formed by diagenesis and maturation of sterols (Hussler et al., 1981; Mackenzie et al., 1982; El-Gayar, 2005). Monoaromatic and triaromatic steroids are two groups of aromatic hydrocarbons that have been identified from the aromatic fraction of crude oils and source rocks. The monoaromatic steroid hydrocarbons are present in immature organic matter while triaromatic steroids may form in organic matter at a later stage of diagenesis.

Triaromatic steroids have not so far been found in significant amounts in recent organic matter (Hussler et al., 1981, El-Gayar, 2005).

Aromatic steroids have been widely used in petroleum geochemistry to estimate thermal maturity the level and oil-oil and oil-source rock correlations (Peters and Moldowan, 1993; Jiang et al., 2001; El-Gayar, 2005). Aromatic steroid hydrocarbons remain unaffected in the severely biodegraded oils which makes them a good correlation tools for biodegraded oils (Peters et al., 2005). Moldowan et al., (1985) used the ternary diagram of monoaromatic C_{27}, C_{28}, and C_{29} steroid hydrocarbons to differentiate between the types of source organic matter. Oils derived from marine organic matter have less C_{29} monoaromatic steroids than oils generated from terrigenous organic matter; terrigenous organic matter generally has a low concentration of C_{27} and C_{28} monoaromatic steroid hydrocarbons (Peters et al., 2005). Moldowan et al., (1985) used the ternary diagram of C-ring monoaromatic C_{27}, C_{28}, and C_{29} steroid hydrocarbons to differentiate between types of source organic matter. The monoaromatic steroid is a powerful tool for correlation throughout the oil generation window (Peters et al., 1989; El-Gayar, 2005) especially when used with ternary diagrams of steranes since both of them have different origins (Peters et al., 2005). Monoaromatic steroid hydrocarbons are believed to be converted to triaromatic steroid hydrocarbons during maturation and the ratio between them therefore increases from 0 to 100% during thermal maturity (Peters et al., 2005). The ratios of short- to long-side chain monoaromatic and triaromatic steroids and triaromatic to monoaromatic steroids are both increase with maturation; therefore, these ratios have

been used as parameters to determine level of the thermal maturity for crude oils and source rocks (Mackenzie et al., 1981).

2.6.1.1 MA(I)/MA(I+II) Ratio

The ratio of MA(I)/MA(I+II) increases from 0 to 100% during maturation. Therefore it has been used to estimate the level of thermal maturity of oil and source rocks particularly when other biomarker parameters are not useful as maturity indicators in the late oil window (Pesters et al., 2005). The oxidation and reduction during diagenesis in source rocks influenced this ratio (Moldowan et al., 1986). Many possibilities were suggested as the causes of an increase in this ratio with maturity. The increase is due to: 1) conversion of long chain to short chain monoaromatic steroids by cracking, 2) preferential thermal degradation of long chain versus short chain, or 3) both conversion and thermal degradation of long chain to or versus short chain (Peters et al., 2005).

2.6.1.2 TA(I)/TA(I+II) Ratio

Triaromatic steroid hydrocarbons are thought to be formed by the conversion of monoaromatic steroids at higher maturity level which makes the ratios of short to long chain triaromatic steroids more useful than monoaromatic steroids. Beach et al., (1989) suggested that the increases in this ratio are due to preferential cracking of long chain triaromatic steroids rather than due to conversion of long to short chain triaromatic steroid hydrocarbons.

2.6.2 Polycyclic Aromatic Hydrocarbons

Aromatic hydrocarbons are common organic compounds which have been found in crude oils and source rock extracts throughout geological time (Radke et al., 1982a and b; Radke et al. 2001; Asif, 2010). Polycyclic aromatic hydrocarbons are absence in the living organisms (Hase and Hites, 1976). Most aromatic hydrocarbons in crude oils and organic matter in source rock are formed by complex chemical reactions between biological compounds during thermal maturation (Albrecht et al., 1971; Radke, 1987). Due to their high resistance to thermal alteration, aromatic hydrocarbons are widely used as parameter to estimate maturation particularly in higher maturity levels crude oils and source rocks (Peters et al., 2005).

Maturity determination of crude oil and source rock based on biomarker parameters is not reliable in high maturity (Stojanović et al., 2007) which makes the aromatic hydrocarbon parameters valuable tool in these levels. The maturity parameters of saturated compounds are limited at higher maturity levels due to alteration. The distribution and abundance of n-alkanes are influenced by organic matter type, the environment of deposition, biodegradation and maturity as well. Terpanes and steranes are also limited in the higher level of maturity due to reaching equilibrium values before the last stage of oil generation window (Pesters and Moldowan, 1993). Ts/(Ts+Tm), sterane maturity parameters and diasterane/regular steranes are also affected by clay minerals (Peters and Moldowan, 1993; Seifert and Moldowan, 1978).

Aromatic maturity parameters are proposed based on aromatization reactions (Norgate et al., 1999). Generally, the α-configuration compounds are less stable than

related isomers with β- configurations. Therefore, during maturation, the β/α ratio for particular groups of compounds usually shows a regular increase due to the α-position being transferred to thermally more stable forms in the β-position (Radke et al., 1982a; Alexander et al., 1985 and 1994; van Aarssen et al., 1999; Stojanović et al., 2007). The thermal maturity parameters of aromatic hydrocarbons were established based on the relative abundances of isomers with increasing in thermal maturity. Therefore, many ratios and parameters such as the methylphenanthrene index have been proposed.

2.6.2.1 Methylphenanthrene Indices

The methylphenanthrene Index (MPI) was proposed by Radke et al., (1982a), is probably one of the most widely used aromatic maturity parameters to estimate the level of thermal maturity of oils (Asif, 2010). The parameters have been generated from the distribution of phenanthrene and four or three methylphenanthrene isomers (1-, 2-, 3-, and 9-MP). Three indices were suggested:

MPI 1 = 1.5 (2-MP + 3-MP)/(P + 1-MP + 9-MP) which was suggested by Radke et al. (1982a)

MPI 2 = 3 (2-MP)/(P + 1-MP + 9-MP) which was suggested by Radke et al. (1982b)

MPI 2 is thought to provide a more reliable value than MPI 1 and it has been proposed to replace the MPI 1 (Radke, 1987; Othman, 2003, Asif, M., 2010). The difference between them reflects a minor dominance of 2- over 3-MP, which is usually observed in the methylphenanthrene distribution (Radke et al., 1982b). MPI1was calibrated with vitrinite reflectance values particularly within the oil generation

window, used to calculate vitrinite reflectance for crude oils (Radke et al., 1982a, 1982b; Radke and Welte, 1983) as follows:

$R_{C(rw)}$ = 0.6 MPI 1 + 0.4 for the R_m<1.35%

$R_{C(rw)}$ = - 0.6 MPI 1 + 2.3 for the R_m>1.35%

Therefore, the MPI is used as a proxy for the vitrinite reflectance of oils and to correlate them to the corresponding organic matter in the source rocks (Othman, 2003). This parameter is useful to estimate the level of maturity of crude oils and organic matter that has low or absent vitrinite macerals (Tissot and Welte, 1984). MPI1 can be influenced by the type of organic matter present(Radke et al., 1986; Budzinski et al., 1995); therefore, calibrations of MPI1 with the vitrinite reflectance values of oils or source rocks which derived from different organic matter types are not always reliable (Radke, 1987). Boreham et al. (1988) suggested an alternative calibration of MPI1 to vitrinite reflectance MPI 1 as follows:

$R_{c(b)}$ = 0.7 MPI 1 + 0.22 for R_m < 1.7%

$R_{c(b)}$= - 0.55 MPI 1 + 3.0 (for R_m > 1.7%

Based on the ratio of (2-MP)/(I-MP), MPR was also suggested by Radke et al. (1982b). MPR increases with increasing the level of thermal maturity. (Budzinski et al. (1995) proposed MPI3. The MPI3 is based on the distribution of methylphenanthrene isomers (1-, 2-, 3- and 9-MP). It increases with increasing level of thermal maturity and is calculated as follows:

MPI 3 = (%3-MP + %2-MP)/(%9-MP + %1-MP).

2.7 Biodegradation of Crude Oils

Crude oil biodegradations are alteration processes by aerobic or anaerobic activity of living organisms in oil reservoirs (Connan, 1984) with a low temperatures below 80°C (Wenger et al., 2001). These organisms use hydrocarbon compounds for their metabolic processes. It has long been observed that only oxic conditions in water reservoirs can cause aerobic biodegradation of crude oils (Peters et al., 2005). Recently, it has been found that anaerobic sulfate reducing and fermenting bacteria can also degrade oils in deep reservoirs (Peters et al., 2005). Highly saline waters in reservoirs may reduce the biodegradation. The alteration of crude oil compositions by biodegradation within reservoir decreases the volume of crude oil, its quality, and its API gravity; biodegradation also increases oil's the viscosity, and its sulfur, asphaltene and metals content (Wenger et al., 2001).

Organic geochemistry has provided reliable parameters to understand the mechanisms of biodegradation and whether a sample represents non-degraded oil, a degraded or a mixture of both degraded and non-degraded crude oils. A determination of the presence of degraded and non-degraded oils in a reservoir can provide good information on whether a reservoir represents a single filling period or a filling period followed by degradation and an influx of fresh oil (Philp, 2007).

Alexander (1983) proposed the concept of scaling biodegradation by observing the sequence by which organic compounds degrade within an oil sample since the organic compounds have different levels of resistance to biodegradation (Peters et al., 2005). Various biodegradation scales have been developed following this same method (See Figure 2-2; Peters and Moldowan, 1993; Wenger et al., 2001; Head et al., 2003). The

n-alkanes degrade first because the other compounds have greater structural complexity (Philp, 2007). Isoprenoids such as pristane and phytane are degraded later because they are more resistant to biodegradation than the n-alkanes. Biodegradation of steranes usually occurs after the complete removal of isoprenoids. Steranes degrade before or after hopanes. Diasteranes are more resistant to biodegradation than steranes (Peters and Moldowan, 1993). Within each class of biomarker compound, the biological configurations are more affected by biodegradation than thermally stable isomers. For example, steranes 20R and hopanes 22R isomers are degraded before the S isomers (Peters and Moldowan, 1993; Philp, 2007).

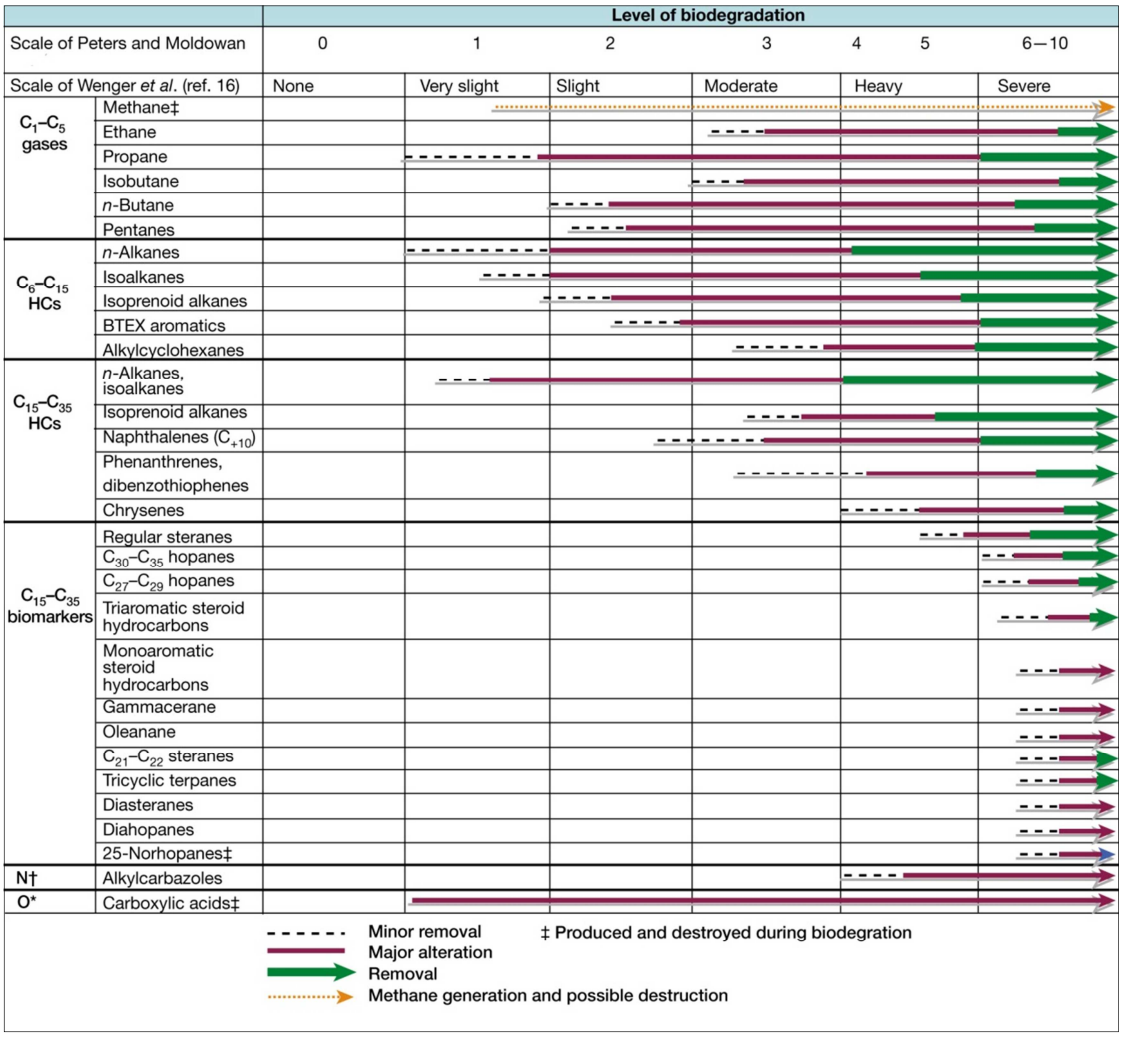


Figure 2-2. A alignment diagram of the biodegradation scales of Peters and Moldowan (1993) and Wegner et al. (2001). The diagram illustrates the generalized sequence of the removal of selected molecular groups at increasing levels of biodegradation (Head et al., 2003).

CHAPTER III

3. Experimental Investigation

The collected cutting shale samples from wells were subjected to Rock-Eval and geochemical analysis using gas chromatography (GC) and gas chromatography–mass spectrometry (GC- MS). The rock samples were taken from the platforms and troughs. The oil samples are from the Zaltan Platform, the Az Zahrah-Al Hufrah Platform, the Al Bayda Platform and Al Kotlah Graben of the Sirt Basin (Table 3.1). Figure 3-1 shows the analytical flow chart of the analysis in this study.

3.1 Rock-Eval Analysis

Eighty six samples were analyzed by Rock-Eval pyrolysis (Espitalie et al., 1977) to determine the hydrocarbon generating potential of the organic matter. The experimental procedure followed for Rock-Eval pyrolysis was that described by Peters (1986) and Peters and Cassa (1994). GeoMark, LTD at Humble, Texas, used a Rock-Eval II apparatus to analyze crushed samples of 100 mg by heating them in a helium atmosphere at 300°C for 4 min. This was followed by programmed pyrolysis at 25°C/min from 300 to 550°C. A flame ionization detector (FID) measured the hydrocarbons generated from these rocks. A thermal conductivity detector (TCD) measured the CO_2 generated from the rocks. Figure 3-2 is representative of the peaks and parameters obtained from typical Rock-Eval pyrolysis. The first peak (S1 mg HC/g) represents the free hydrocarbons already present in the rocks and can be obtained at 300°C. The second peak (S2 mg HC/g) represents the hydrocarbons that attach to the kerogen generated by cracking the kerogen by increasing the temperature

from 300 to 550°C at 25°C/min. The third peak (S3 mg CO_2/g) represents the amount of CO_2 that is detected at 390°C per one gram of rock during the pyrolysis. T_{max} represents the temperature at which the maximum amount of hydrocarbon is generated from the sample. Figure 3-3 summarizes the different fractions of the total organic matter of rocks analyzed by Rock Eval.

The pyrolysis values collected on the computer can be used to generate some parameters to determine the quality of organic matter; these measurements include values such as PI, S2/S3, HI, OI and RHP (Appendix I). The S2/S3 ratio represents a measure of the amount of hydrocarbons which can be generated from a rock relative to the amount of organic CO_2 released during temperature programming up to 390º C. The hydrogen index (HI) corresponds to the quantity of cracking organic compounds from S2 relative to the TOC in the sample (mg HC/g TOC). The oxygen index (OI) corresponds to the quantity of carbon dioxide from S3 relative to the TOC (mg CO_2/g TOC). Production index (PI) is defined as the ratio S1/(S1 +S2). PI is an indication of the amount of hydrocarbon which has been produced geologically relative to the total amount of hydrocarbon which the sample can produce. RHP (relative hydrocarbon potential) represents the free hydrocarbons and the hydrocarbons formed by thermal cracking of kerogen relative to total organic carbon (S1+S2)/TOC (Fang et al., 1993). The quantity of organic matter or total organic carbon (TOC) was determined using a LECO carbon analyzer for each sample.

3.2 Vitrinite Reflectance Measurements

Vitrinite reflectance is a comparative measure of light intensity reflected from a standard of known reflectance, such as sapphire to that of the sample. In this study,

vitrinite reflectance measurements of source rocks were obtained using the Oklahoma Geological Survey petrographic laboratory. Vitrinite Reflectance (VR) is the most commonly used organic maturation indicator used in petroleum exploration. This is because it is reasonably accurate, quick, non-destructive and inexpensive, it extends over a longer maturity range than other indicators, and is not affected significantly by pressure, only by temperature (Hunt, 1996). Samples with vitrinite reflectance values from 0.5% to 1.3% are considered mature and within the oil generation window. Samples with vitrinite reflectance values less than 0.5% are thermally immature. Samples with vitrinite reflectance greater than 1.3% are post-mature and at the gas generation window (Tissot & Welte, 1984).

Table 3-1. Description of oil samples in in this study.

Sample	Formation	Age	Field	No. of Sample
C65	Gialo	Mid. Eocene	S E Nasser	2
BBBB2-6			S. Jebel	
C98-6	Zaltan	Uper. Paleocene	N E Nasser	6
IIII2-6			S Nasser	
C229-6			S E Nasser	
J3-6 II			E. Meghil	
GGGG1-6			N Nasser	
JJJJ2-6			W Meghil	
B5-47	Al Byada	Paleocene	Al Byada	1
C35-47	Kalash	Upper Cretaceous	Al Kotlah	2
B3-93			Khuf	
BBBB1-6	Wahah		S. Jebel	1
DD12-6			Ralah	2
S9-47	Tagrife		Haram	
RRRR1-6	Gargaf	Cambrian–Ordovician	E Arashad	4
MMM2A-6			Arashad	
FF16-6			Attahaddy	
UU9A-6			Lehib	

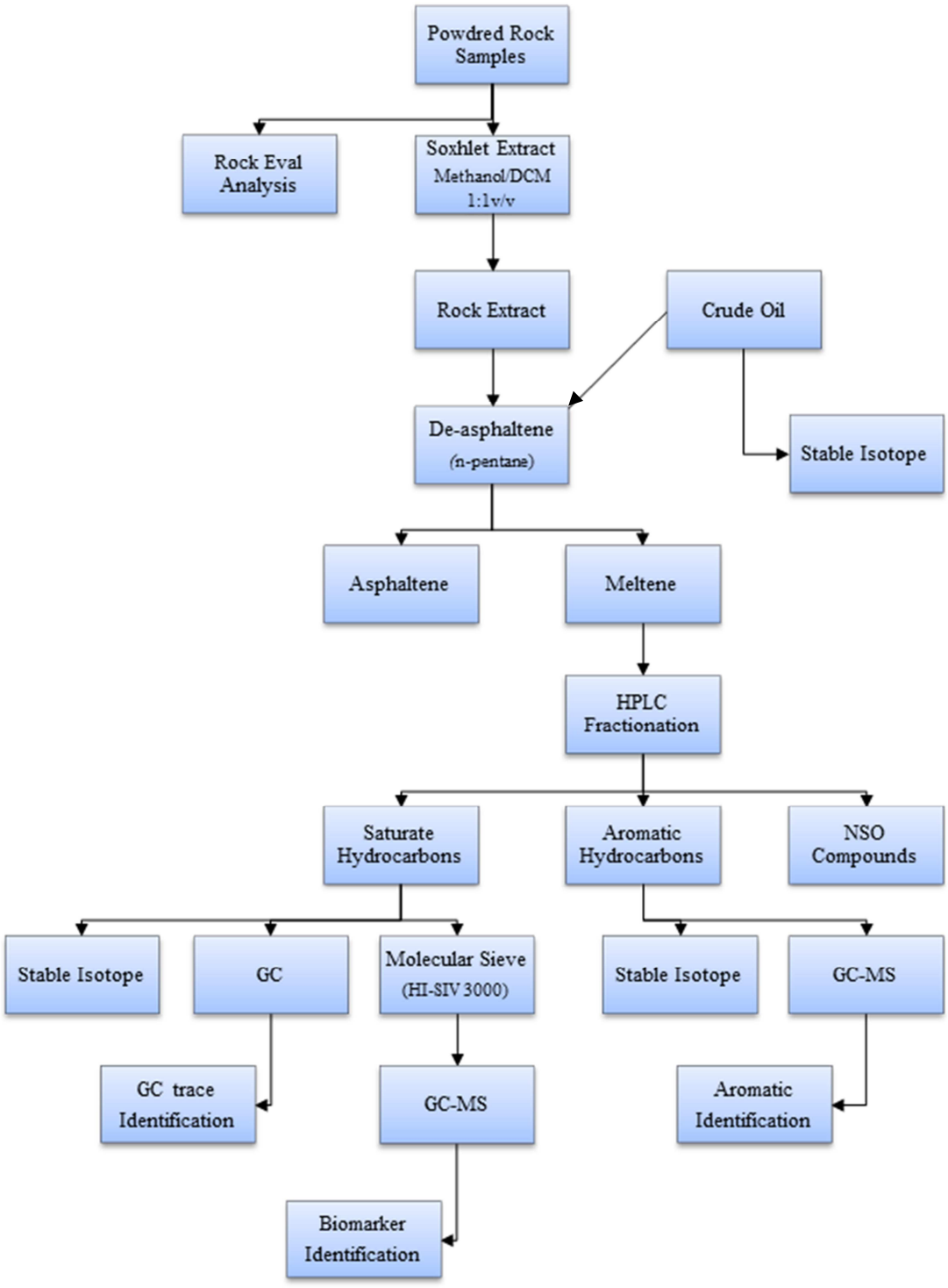


Figure 3-1. Scheme for the analytical flow chart in this study.

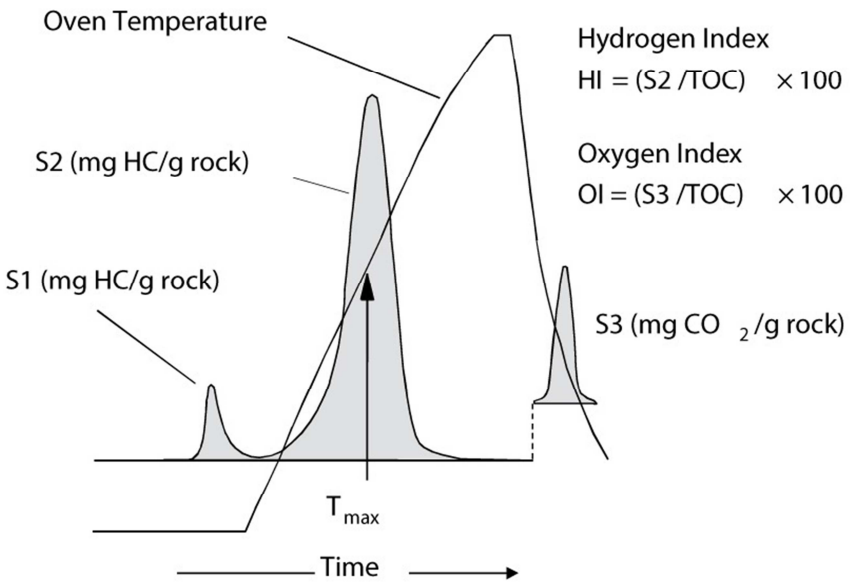


Figure 3-2. Schematic pyrogram showing the evolution of organic compounds from a rock sample during pyrolysis (Peters et al., 2005).

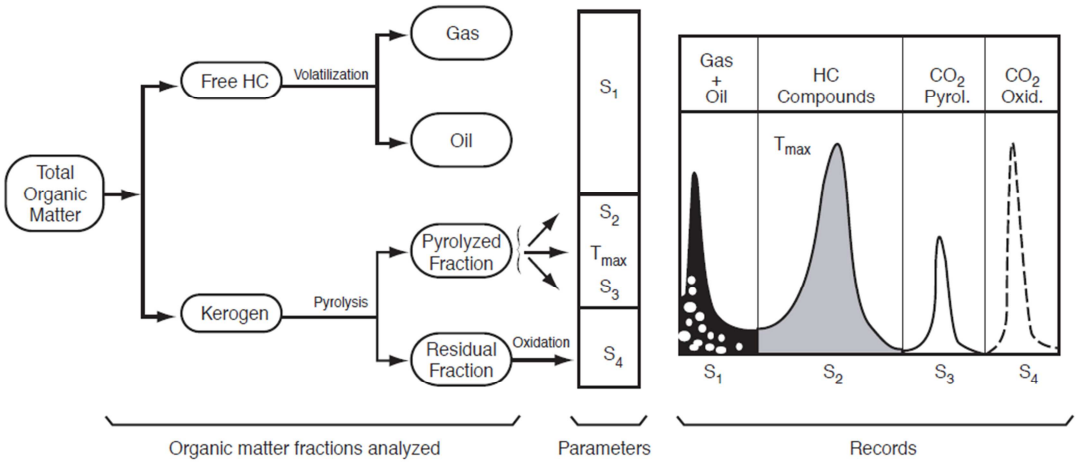


Figure 3-3. Diagram illustrates the different fractions of the total organic matter analysis, the corresponding parameters and their recordings during Rock Eval (Lafargue et al., 1998).

3.3 Geochemical Techniques

3.3.1 Sample Preparation

The rock samples (well cuttings) were washed with distilled water and air dried prior to grinding. The samples were ground to particle size of about 425μm or less. The crude oil samples were shaken carefully to make the oils homogeneous.

3.3.2 Extraction of Soluble Organic Matter from Source Rocks

Based on Rock Eval parameters, twelve samples were selected for organic geochemical analysis. For extraction of the source rocks, a known amount of crushed sample (about 40g) is placed in a pre-weighed, pre-extracted thimble, capped with pre-extracted glass wool and extracted in a Soxhlet apparatus (Figure 3-4) with 250 ml of dichloromethane and methanol (1:1 v/v). After 24 hours, when the solvent surrounding the thimble became clear, the extraction was stopped and the solvent in the reservoir flask was reduced using a Buchi rotary evaporator.

3.3.3 Isolation of Asphaltenes

Asphaltenes were removed from the extracts and crude oils by precipitation with *n*-pentane. The extracts were dissolved by adding 1 ml of dichloromethane and transferred into a small glass vial. The volume of the extracts was increased by adding 40 ml of *n*-pentane and transferred into a 50 ml centrifuge tube which was stored in a refrigerator for 12 hours in order to precipitate the asphaltenes. The suspended asphaltenes were separated by centrifuging for 20 minutes at 1000 RPM. The maltenes were concentrated and separated from asphaltenes by filtration and evaporating the n-pentane solution and transferring it in a pre-weighed glass vial. The residual

precipitate was dissolved in dichloromethane, transferred to a vial and dried under a stream of nitrogen to yield the asphaltenes.

3.3.4 Fractionation of Maltenes

High-Performance Liquid Chromatography (HPLC) in a Hewlett Packard 1050 series HPLC was used to separate the maltene fraction into three fractions (saturate hydrocarbons, aromatic hydrocarbons and NSO compounds). The maltene fraction was dissolved in hexane using a ratio of 20:50 (mg/µl) and 50 µl of this solution was injected into the HPLC.

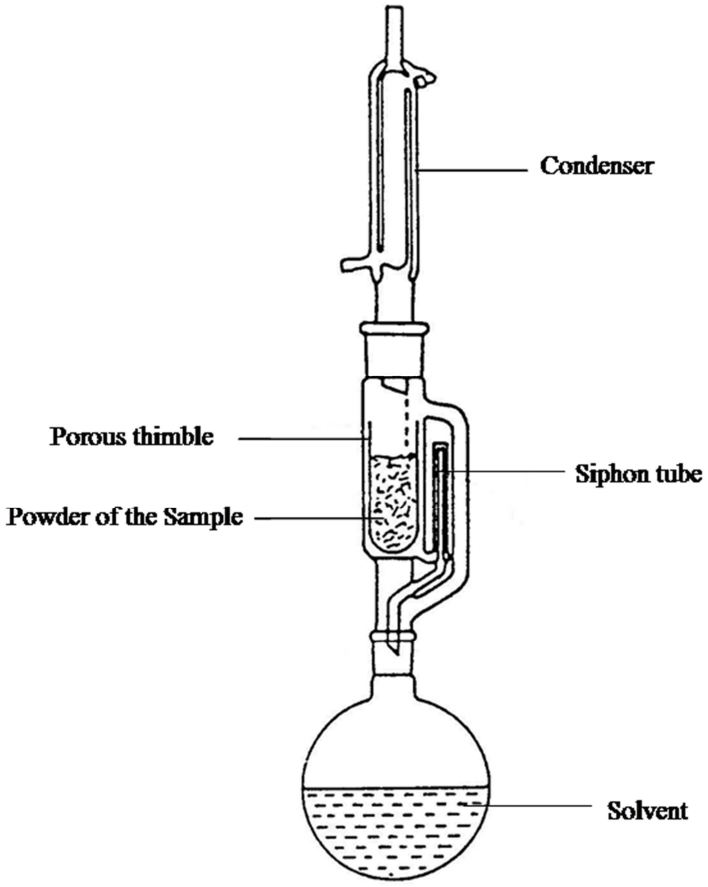


Figure 3-4. Soxhlet continuous extractor for the extraction of the rock samples.

3.3.5 Isolation of Branched and Cyclic Saturate Hydrocarbons

Separation of branched and cyclic compounds from n-alkanes was achieved using HI-SIV 3000 molecular sieve. The activated sieve was packed into a clean (rinsed with methanol, dichloromethane and n-hexane) and dry Pasteur pipette, plugged with non-absorbent cotton wool using light air pressure. The saturate fraction was dissolved in a small volume of n-hexane and loaded onto the column. The saturate hydrocarbon vial was then rinsed with n-hexane and also transferred to the top of the column. Three bed volumes of hexane were added to insure complete separation of the branched and cyclic compounds from the n-alkanes.

3.4 Analytical Methods and Instrumentation

3.4.1 Gas Chromatography

The gas chromatography (GC) used for analyzing the saturate fractions was a Hewlett Packard 6890 coupled with flame ionization detector (GC/FID) equipped with an Agilent J&W DB-Petro column (100m x 0.25mm 0.5µm film thickness). The samples were injected using a splitless injector and helium used as the carrier gas. The oven was initially maintained at 40°C for 1.5 min, subsequently temperatures were programmed from 40 to 300° at 4°C/min and held isothermal for 14 min. The injector and detector temperature were kept at 300 °C.

3.4.2 Gas Chromatography-Mass Spectrometry

An Agilent 7890A gas chromatography interfaced with a 5975C mass selective detector (MSD) and equipped with an Agilent J&W 60m x 0.25µm DB-5MS fused silica capillary column was used. 1µl of fraction solution in dichloromethane was

injected onto the column. The samples were injected using a splitless injector and helium used as the carrier gas. The oven was initially maintained at 40°C for 1.5 min, subsequent temperatures were programmed from 40 to 300°C at 4°C/min and held isothermal for 14 min. The injector and detector temperatures were kept at 300°C. The column was linked directly to the ion source through a transfer line operated at 300°C; the electronic impact ion source was operated at 70 eV. Data were acquired in a selected ion monitoring (SIM) mode and processed with the Hewlett Packard Chemstation software.

3.4.3 Stable Carbon and Hydrogen Isotope

For 18 whole oil samples, the stable carbon and hydrogen isotope ratios were measured by the isotope laboratory at the University of Oklahoma. The stable carbon isotope ratio was also measured for saturate and aromatic fractions of seven of these samples.

For the measurements of the stable carbon isotope ratios, the 200-300 μg organic samples were weighed on micro-balance and wrapped in tin capsules (Costech 041074) and then placed in sequence in a Costech zero blank autosampler which was mounted on the Costech 4010 elemental analyzer (EA). The EA was equipped with a furnace reactor column packed with the reagents chromium oxide (Costech 011001) and silvered cobalt oxide (Costech 011007). The samples were purged with high purity helium (99.9999%) to remove air and then analyzed by flash combustion. In the flash combustion process, the autosampler dropped the samples one at a time onto the top of a furnace reactor column. The reactor column was held at 1000°C to provide a pulse of high purity O_2 for the complete sample combustion. Carbon gases were

completely converted to CO_2 with the presence of chromium oxide. Nitrogen gases were then converted to N_2 in the reduction column packed with copper reduced wire (Costech 011013) at a temperature of 650°C. Finally, CO_2 was separated from N_2 by a short GC column held at 55°C and carried by a helium stream at a flow rate of 100ml/min to a Thermo Conflo III interface with dilution which is connected to the source of a Thermo Delta V plus isotope ratio mass spectrometer. δC was reported relative to the Vienna Pee Dee Belemnite (VPDB) scale.

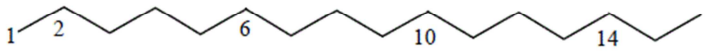
For the stable hydrogen isotope analysis, the approximately 300 μg samples were wrapped in silver capsules (Costech 041066) and then placed in sequence in a Costech zero blank autosampler equipped with an isolation valve mounted on a Thermo TCEA (Temperature Conversion Elementary Analyzer). In the TCEA, The reactor furnace was held at 1400°C to decompose the sample into CO and H_2. Subsequently, H_2 was separated from CO by the GC column at 100°C and carried by a helium stream at a flow rate of 100 ml/min to the Conflo III interface with dilution which is connected to the source of a Thermo Delta V plus isotope ratio mass spectrometer. After H3+ corrections, δD was reported relative to the Vienna Standard Mean Ocean Water (VSMOW) scale.

3.5 Compound Identifications

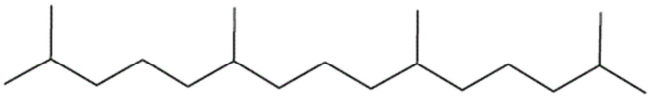
3.5.1 Identification of n-Alkane and Acyclic Isoprenoids

n-Alkanes are abundant compounds in the oils and source rocks and can be identified by gas chromatography alone (Philp, 1985) or by gas chromatography mass spectrometry. The n-alkane and isoprenoids (pristane and phytane) are saturated

hydrocarbons and have a simple straight chain (Figure 3-5). In this study these compounds were identified using GC chromatogram by comparing the compound's positions with publication data (Figure 3-6).

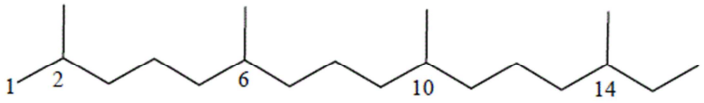


n-alkane (n-C_{16})

Pristane 

pristane (C_{19})

2, 6, 10, 14-tetramethylpentadecane

Phytane 

phytane (C_{20})

2, 6, 10, 14-tetramethylhexadecane

Figure 3-5. Structure of n-alkane and isoprenoids.

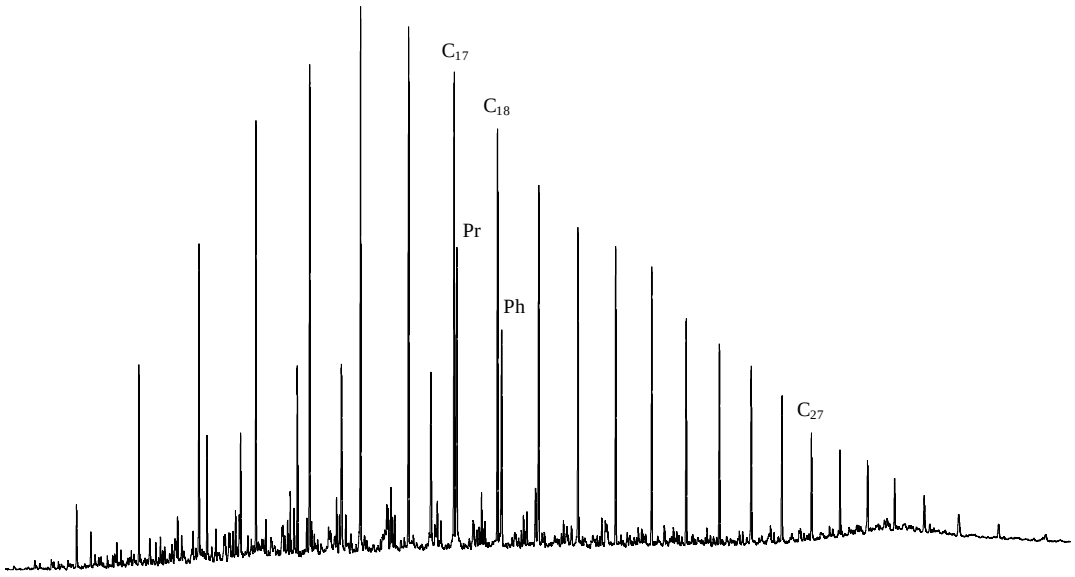


Figure 3-6. Gas chromatogram of saturated hydrocarbon fraction of sample C35-47 shows distributions of n-alkanes (nC_{10} to nC_{34}) and isoprenoids in the sample.

3.5.2 Identification of Terpanes

The terpane biomarkers in this study were identified on the m/z 191 chromatograms of GC-MS (Figure 3-7)

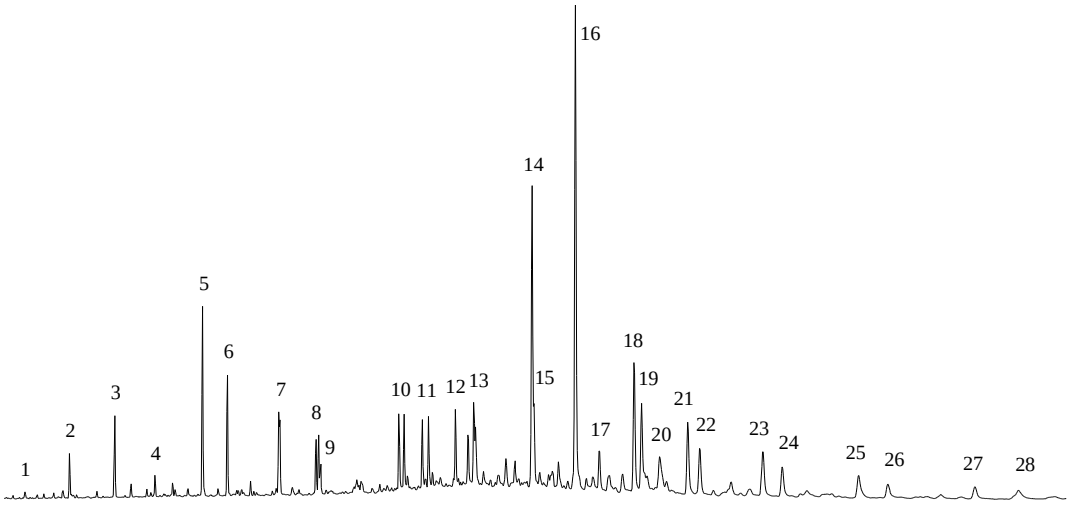


Figure 3-7. Mass chromatogram shows the distribution of terpane biomarkers (m/z 191) in Sirt Basin sample. See table 3-2 for peak identification.

Table 3-2. Identifications of tricyclic, tetracyclic and pentacyclic triterpanes from Figure 3-7.

Peak No.	Compounds
1	C_{19} Tricyclic terpane
2	C_{20} Tricyclic terpane
3	C_{21} Tricyclic terpane
4	C_{22} Tricyclic terpane
5	C_{23} Tricyclic terpane
6	C_{24} Tricyclic terpane
7	C_{25} Tricyclic terpane
8	C_{26} [22S] Tricyclic terpane + C_{26} [22R] Tricyclic terpane
9	C_{24} Tetracyclic terpane
10	C_{28} [22S] Tricyclic terpane + C_{28} [22R] Tricyclic terpane
11	C_{29} [22S] Tricyclic terpane + C_{29} [22R] Tricyclic terpane
12	18α Trisnorneohopane [C_{27} Ts]
13	17α Trisnorneohopane [C_{27} Tm]
14	Norhopane [C_{29}]
15	18α Neonorhopane [C_{29}Ts]
16	Hopane [C_{30}]
17	17β21α Moretane [C_{30}]
18	22S Homohopane [C_{31}]
19	22R Homohopane [C_{31}]
20	Gammacerane [C_{30}]
21	22S Bishomohopane [C_{32}]
22	22R Bishomohopane [C_{32}]
23	22S Trishomohopane [C_{33}]
24	22R Trishomohopane [C_{33}]
25	22S Tetrakishomohopane [C_{34}]
26	22R Tetrakishomohopane [C_{34}]
27	22S Pentakishomohopane [C_{35}]
28	22R Pentakishomohopane [C_{35}]

3.5.3 Hopanes and Moretanes

Hopanes are a group of the triterpane compounds. They are cyclic compounds containing five rings. Four rings are having six carbon atoms and one ring is having five carbon atoms. The side chain of hopanes contains up to 8 carbon atoms. The common compound is 17α(H),21β(H) hopane and has 30 carbon atoms, three of them are in the side chain (Figure 3-8a). The hopanes are composed of three groups of compounds, 17α(H),21β(H) hopanes (Figure 3-8b), 17β(H),21β(H)hopanes, and 17β(H),21α(H) hopanes (moretanes; Peters and Moldowan, 1993).

3.5.4 Homohopanes

These compounds are extended hopane compounds containing more than 30 carbon atoms. Homohopanes show an extended side chain with an additional asymmetric center at C-22, resulting in two compounds (22S and 22R) and are identified as two peaks in the GC-MS (Peters and Moldowan, 1993).

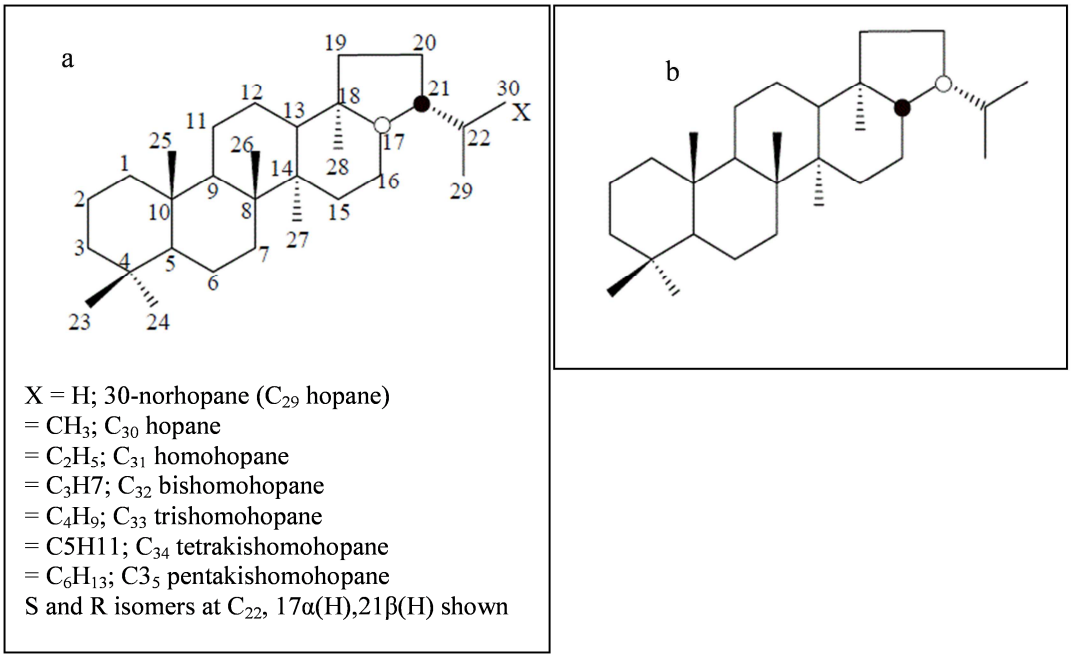


Figure 3-8. Structures of a) Hopanes and b) C_{30} moretane.

3.5.4.1 Tricyclic and Tetracyclic Terpanes

Tricyclic terpanes range from C_{19} to $C_{29.}$ The C_{23} compound is usually the abundant one (Figure 3-9a). Compounds with up to C_{54} carbon atoms have also been identified in oils and source rocks (De Grande et al., 1993). Tricyclic terpanes having more than 25 carbon atoms are identified in GC-MS as S and R epimers (Kruge et al., 1990a, 1990b). Tricyclic terpanes with more than C_{29} carbon atoms may co-elute with hopanes in GC-MS which make their identification difficult (Farrimond et al., 1999). Tetracyclic terpanes are another class which can also be identified in m/z 191 of GC-MS. They range from C_{24} to C_{27} compounds (Figure 3-9b) and possibly up to C_{35} (Aquino Neto et al., 1983). The C_{24} tetracyclic terpane is the most important compound among them and is used to investigate conditions of depositional environments (Peters and Moldowan, 1993).

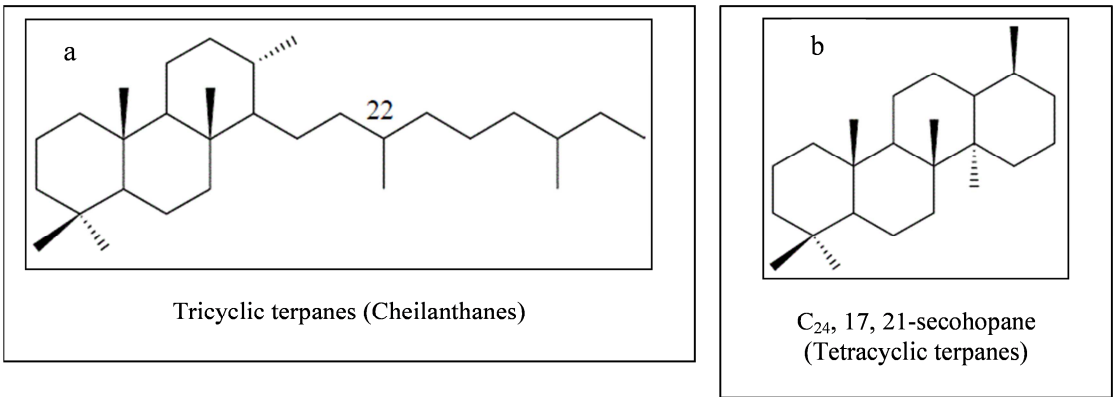


Figure 3-9. Structures of a) Tricyclic terpanes and b) Tetracyclic terpanes.

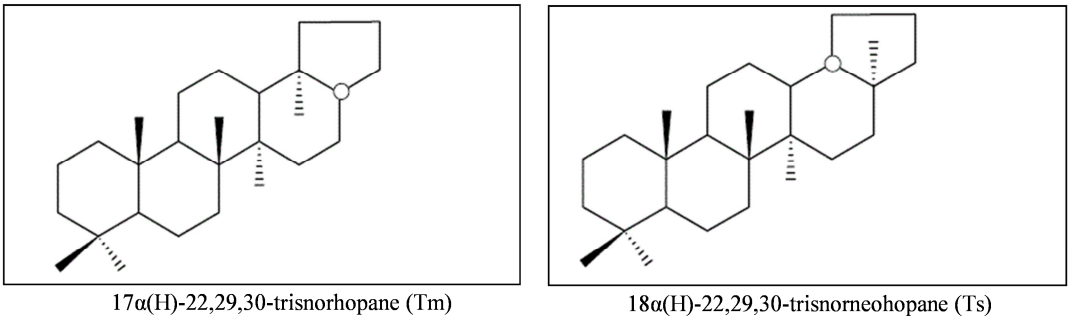
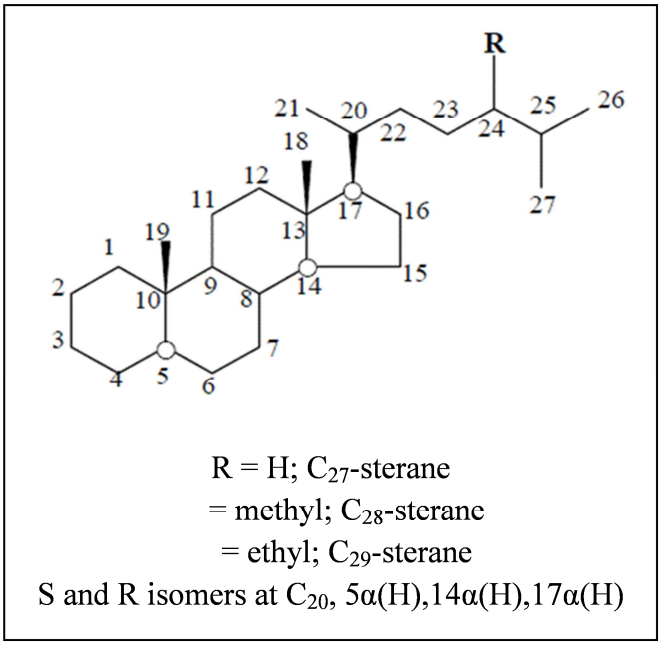


Figure 3-10. Structures of a) 17α(H)-22,29,30-trisnorhopane (Tm), and b) 18α(H)-22,29,30-trisnorneohopane (Ts).

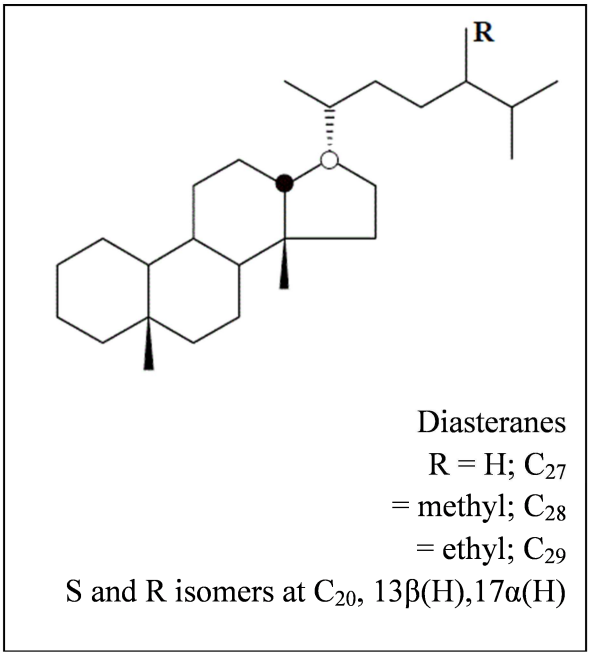
3.5.4.2 Steranes and Diasteranes

Steranes are an important class of biomarkers identifying using m/z 217 in GC-MS (Peters and Moldowan, 1993). Steranes usually consist of four rings, three of them having six sides (Figure 3-11), and one containing five carbon atoms (Waples and Machihara, 1990). Diasteranes (Figure 3-12) are rearranged steranes (Murray and Boreham, 1992) where the rearrangement includes a change of methyl groups from ring positions C-10 and C-13 (in sterane) to C-5 and C-14 (Waples and Machihara, 1990; Peters and Moldowan, 1993). Figure 3-13 show a typical distribution of sterane and diasterane biomarkers which are detected by GC-MS in the oil sample from the Sirt Basin.



R = H; C_{27}-sterane
= methyl; C_{28}-sterane
= ethyl; C_{29}-sterane
S and R isomers at C_{20}, 5α(H),14α(H),17α(H)

Figure 3-11. Structures of Steranes.



Diasteranes
R = H; C_{27}
= methyl; C_{28}
= ethyl; C_{29}
S and R isomers at C_{20}, 13β(H),17α(H)

Figure 3-12. Structures of Diasteranes.

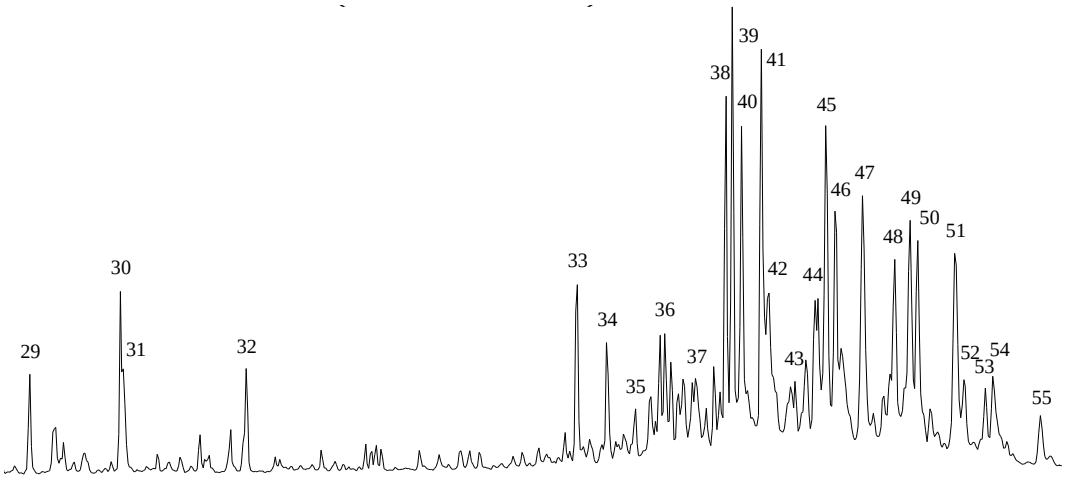


Figure 3-13. Mass chromatogram (m/z 217) of Sirt Basin sample shows the distribution of steranes and diasteranes. See Table 3-3 for peak identifications.

Table 3.3. Identifications of steranes and diasteranes from Figure 3-13.

Peak No.	Compounds
29	Diapregnane
30	5α(H), 14β(H), 17β(H) Pregnane
31	Diahomopregnane
32	5α(H), 14β(H), 17β(H) Homopregnane
33	13β (H), 17α(H), 20(S)- diacholestane
34	13β(H), 17α(H), 20(R)- diacholestane
35	13α(H), 17β(H), 20(R)- diacholestane
36	24-methyl-13β(H), 17α(H), 20(S)- diacholestane
37	24-methyl-13β(H), 17α(H), 20(R)- diacholestane
38	24-methyl-13α(H), 17β(H), 20(R)- diacholestane + 5α(H), 14α(H), 17α(H), 20(S)-cholestane
39	24-ethyl-13β(H), 17α(H), 20(S)- diacholestane + 5α(H), 14β(H), 17β(H), 20(R)-cholestane
40	24-methyl-13α(H), 17β(H), 20(S)- diacholestane +5α(H), 14β(H), 17β(H), 20(S)-cholestane
41	5α(H), 14α(H), 17α(H), 20(R)-cholestane
42	24-ethyl-13β(H), 17α(H), 20(R)- diacholestane
43	24-ethyl-13α(H), 17β(H), 20(R)- diacholestane
44	24-methyl-5α(H), 14α(H), 17α(H), 20(S)-cholestane
45	24-ethyl-13α(H), 17β(H), 20(S)- diacholestane + 24-methyl-5α(H), 14β(H), 17β(H), 20(R)-cholestane
45	24-methyl-5α(H), 14β(H), 17β(H), 20(S)-cholestane
47	24-methyl-5α(H), 14α(H), 17α(H), 20(R)-cholestane
48	24-ethyl-5α(H), 14α(H), 17α(H), 20(S)-cholestane
49	24-ethyl-5α(H), 14β(H), 17β(H), 20(R)-cholestane
50	24-ethyl-5α(H), 14β(H), 17β(H), 20(S)-cholestane
51	24-ethyl-5α(H), 14α(H), 17α(H), 20(R)-cholestane
52	24-propyl-5α(H), 14α(H), 17α(H), 20(S)-cholestane
53	24-propyl-5α(H), 14β(H), 17β(H), 20(R)-cholestane
54	24-propyl-5α(H), 14β(H), 17β(H), 20(S)-cholestane
55	24-propyl-5α(H), 14α(H), 17α(H), 20(R)-cholestane

3.5.5 Aromatic Hydrocarbons

3.5.5.1 Aromatic Steroids

The aromatic steroids were identified using the GC-MS chromatograms at m/z 253 (Figure 3-14) for monoaromatics and m/z 231 for triaromatics (Figure 3-15).

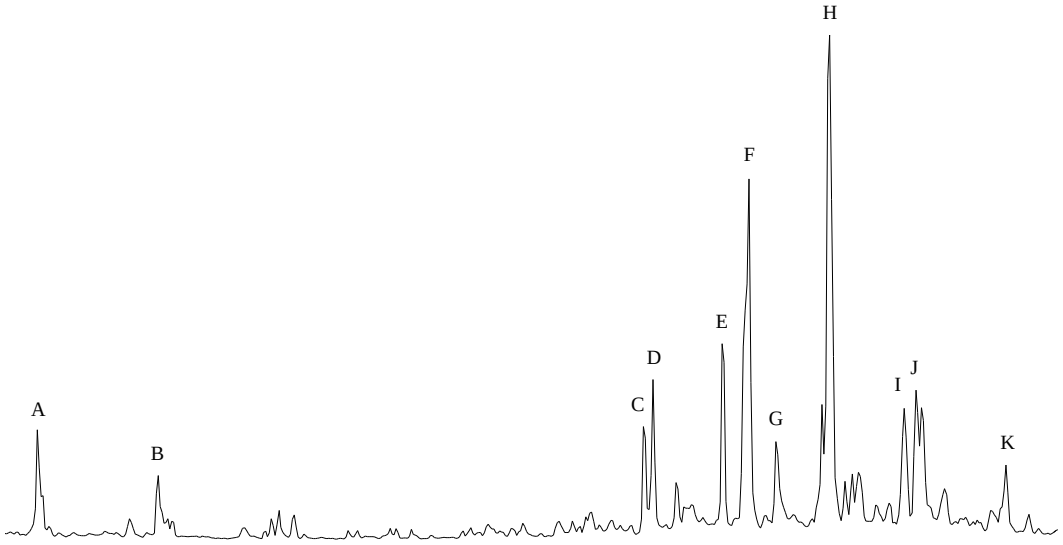
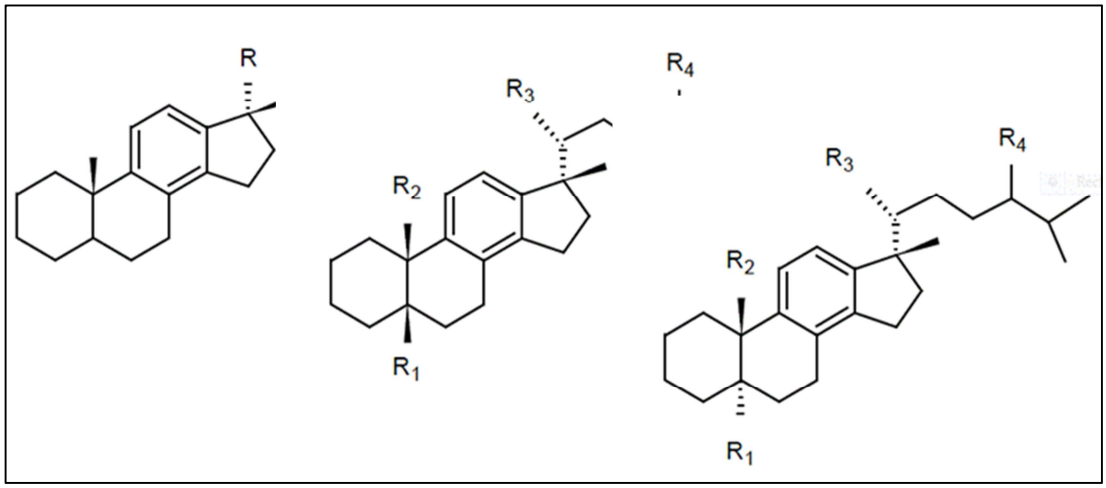


Figure 3-14. GC-MS chromatogram shows distribution of the monoaromatic steroid hydrocarbons in Sirt Samples. See Table 3.4 for peak identifications.

Table 3-4. List of monoaromatic steroid hydrocarbons at m/z 253 and their structure (El-Gayar, 2005).

Beak	compound	Structure
A	17-methyl-18-norpregna-8,11,13 trienes	I, R = C_2H_5
B	17,20-dimethyl-18-norpregna-8,11,13 trienes	I, R = CH $(CH_3)_2$
C	5*β*(H), 10*β*(CH3)-cholest-8,11,13 trienes (20S)	II, R1 & R4 = H, R2 & R3 = CH_3
D	5*β*(CH3), 10*β*(H)-diacholest-8,11,13 trienes (20S)	II, R1 & R3 = CH3, R2 & R4 = H
E	5*β*(CH3), 10*β*(H)-diacholest-8,11,13 trienes (20R) +	II, R1 & R3 = CH3, R2 & R4 = H
	5*β*(H), 10*β*(CH3)-cholest-8,11,13 trienes (20R) +	II, R1 & R4 = H, R2 & R3 = CH_3
	5*α*(H), 10*β*(CH3)-cholest-8,11,13 trienes (20S)	III, R1 & R4 = H, R2 & = CH_3
F	24-methyl-5*β*(H), 10*β*(CH3)-cholest-8,11,13 trienes (20S) +	II, R1 = H, R2, R3 & R4 = CH_3
	5*β*(CH3), 10*β*(H)-diacholest-8,11,13 trienes (20R) +	III, R1 & R3 = CH_3, R2 & R4 = H
	24-methyl-5*β*(CH3), 10*β*(H)-diacholest-8,11,13 trienes	II, R1, R3 & R4 = CH_3, R2 = H
G	5*α*(CH3), 10*β*(H)-diacholest-8,11,13 trienes (20S)	III, R1 & = CH3, R2 & R4 = H
H	5*α*(H), 10*β*(CH3)-cholest-8,11,13 trienes (20R) +	III, R1 & R4 = H, R2 & R3 = CH_3
	24-methyl-5*α*(H), 10*β*(CH3)-cholest-8,11,13 trienes (20S) +	III, R1 = H, R2, R3 & R4 = CH_3
	24-methyl-5*β*(H), 10*β*(CH3)-cholest-8,11,13 trienes (20R) +	II, R1 = H, R2, R3 & R4 = CH_3
	24-methyl-5*β*(CH3), 10*β*(H)-diacholest-8,11,13 trienes (20R) +	II, R3 & R4 = CH_3, R2 = H
	24-ethyl-5*β*(H), 10*β*(CH3)-cholest-8,11,13 trienes (20S) +	II, R1 = H, R2 & R3 = CH_3, R4= C_2H_5
	24-ethyl-5*β*(CH3), 10*β*(H)-diacholest-8,11,13 trienes (20S)	II, R1 & R3 = CH3, R2 = H, R4 = C2H_5
I	24-ethyl-5*α*(H), 10*β*(CH3)-cholest-8,11,13 trienes (20S)	III, R1 = H, R2 & R3 = CH_3, R4 = C2H_5
J	24-methyl-5*α*(H), 10*β*(CH3)-cholest-8,11,13 trienes	III, R1 = H, R2, R3 & R4 = CH3
	24-ethyl-5*β*(H), 10*β*(CH3)-cholest-8,11,13 trienes	II, R1 = H, R2 & R3 = CH_3, R4 = C_2H_5
	24-ethyl-5*β*(CH3), 10*β*(H)-diacholest-8,11,13 trienes (20R)	II, R1 & R3 = CH3, R2 = H, R4 = C_2H_5
K	24-ethyl-5*α*(H), 10*β*(CH3)-cholest-8,11,13 trienes (20R)	III, R1 = H, R2 & R3 = CH_3, R4 = C_2H_5



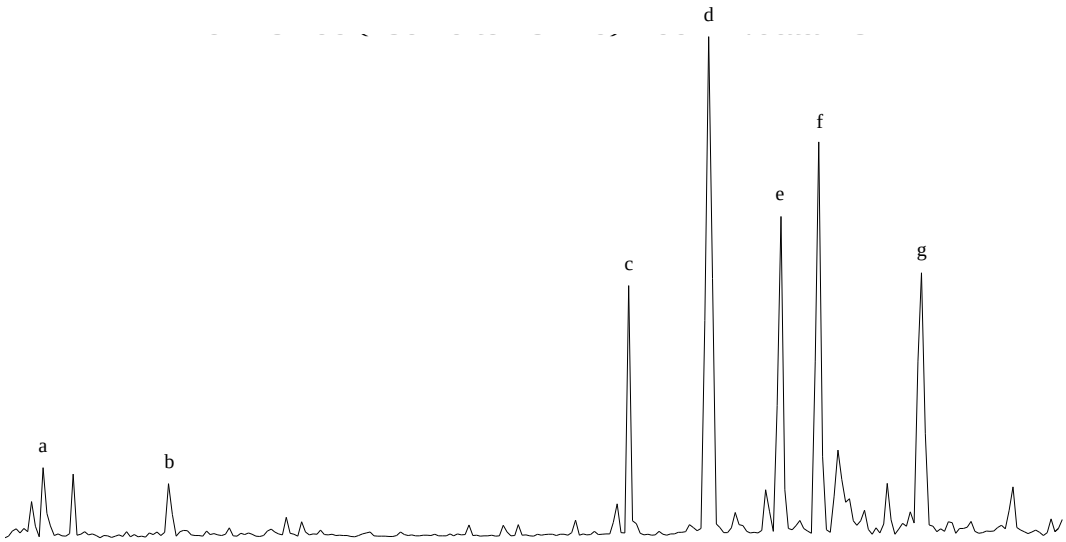
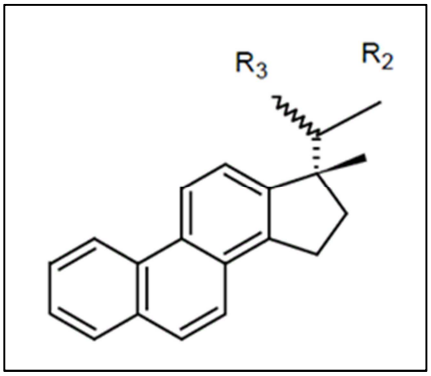


Figure 3-15. GC-MS chromatogram shows distribution of the triaromatic steroid hydrocarbons in Sirt Samples. See Table 3.5 for peak identifications.

Table 3-5. List of trioaromatic steroid hydrocarbons at m/z 231 and their structures (Younes and Philp, 2005).

Beak	**Compound**	**Structure**
a	C_{20} Triaromatic Sterane	R1 = CH_3, R2 = H
b	C_{21} Triaromatic Sterane	R1 = CH_3, R2 = CH_3
c	C_{26} Triaromatic Sterane (20S)	R1 = S(CH_3), R2 = C_6H_{13}
d	C_{26} Triaromatic Sterane (20R)+	R1 = R(CH_3), R2 = C_6H_{13}
	C_{27} Triaromatic Sterane (20S)	R1 = S(CH_3), R2 = C_7H_{15}
e	C_{28} Triaromatic Sterane (20S)	R1 = S(CH_3), R2 = C_8H_{17}
f	C_{27} Triaromatic Sterane (20R)	R1 = R(CH_3), R2 = C_7H_{15}
g	C_{28} Triaromatic Sterane (20R)	R1 = R(CH_3), R2 = C8H_{17}



3.5.5.2 Polycyclic Aromatic Hydrocarbons

Aromatic hydrocarbon compounds identified for this study were identified using GC-MS of the aromatic fraction. Several compounds of various molecular ion groups were used in this study. Methylphenanthrene (MP) were identified using m/z 192 mass chromatogram, whereas Phenanthrene (P), DBT Dibenzothiophene (DBT) and methyl Dibenzothiophenes (MDBT) were detected respectively using m/z 178, m/z 184 and m/z 198 mass chromatograms (Figure 3-16 and 3-17).

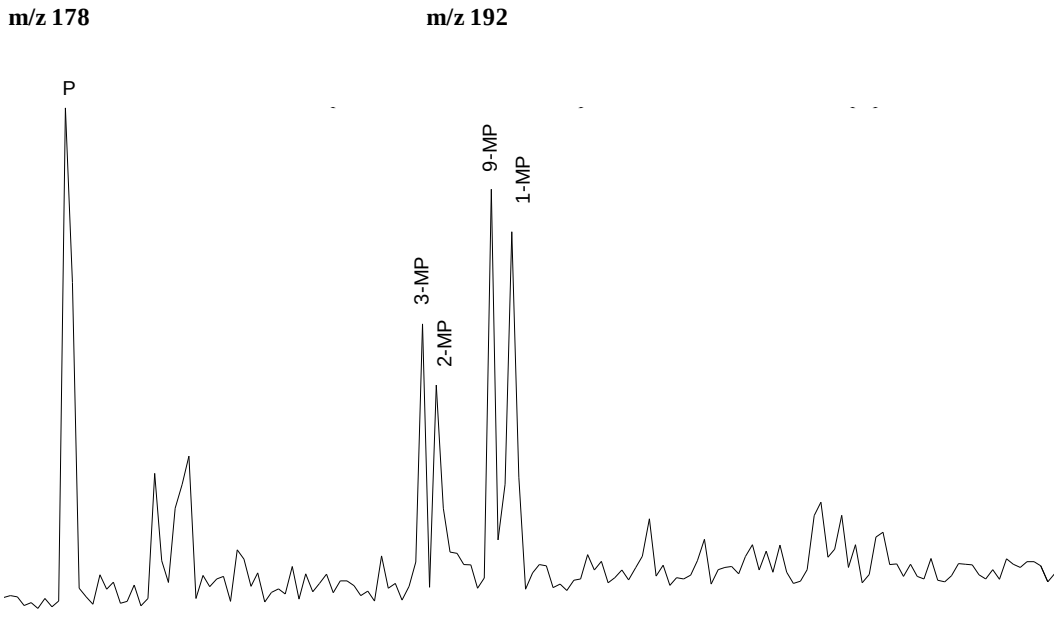


Figure 3-16. Combination of mass chromatograms shows Phenanthrene (P), methylphenanthrene (MP) in m/z: 178+192; respectively.

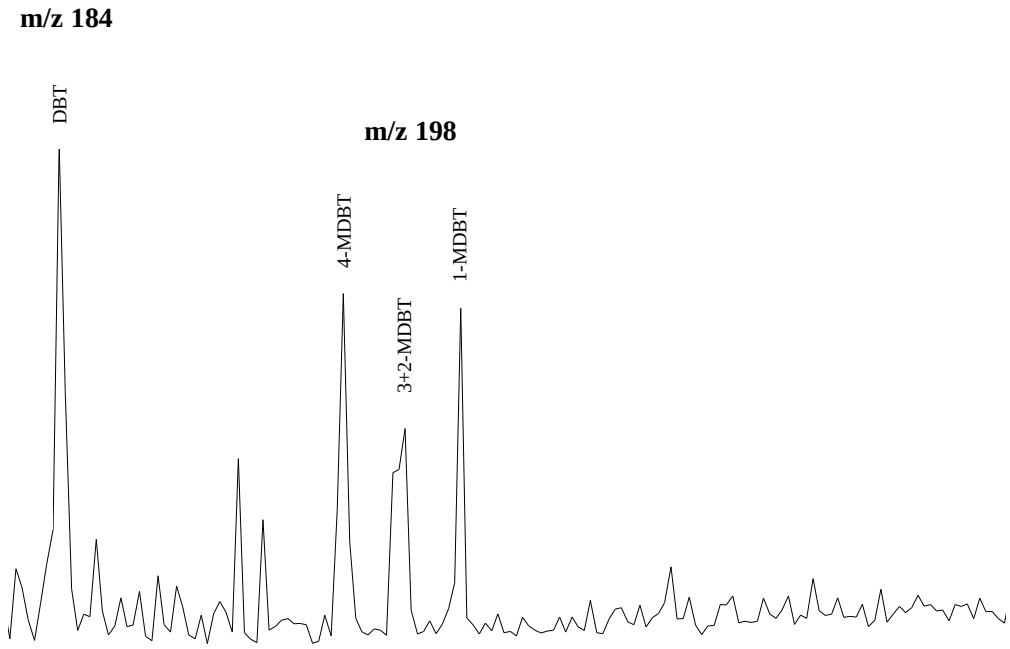


Figure 3-17. Combination of mass chromatograms shows dibenzothiophene (DBT) and methyldibenzothiophenes (MDBTs) in m/z: 184+198; respectively.

3.6 Biomarker Quantitation

The absolute concentration of biomarkers in crude oils and source rocks are dependent on depositional environment, maturation and alteration of the source rocks and oils in the reservoirs (Hunt 1996). Mixing of crude oils in the reservoir from different sources also affects the biomarker concentration (Rullkötter et al., 1984). Biomarkers are present in very low concentrations compared to the main groups of compounds in the crude oils such as n- alkanes. The availability of non-co-eluting internal standards, when used in GC-MS analysis, has allowed the petroleum geochemist to accomplish accurate quantitative analysis and therefore provides a good tool of studying the biomarkers by quantitative analysis (Elington and Douglas, 1988).

Calculation of the absolute Biomarker concentration:

The n-tetracosane-d50 is used as an internal standard. It is added to the saturate fraction for quantification of the individual molecular compounds. Quantitation of biomarkers was accomplished by using combined mass chromatograms containing one fragment from the standard and one fragment from the compound of interest to quantify. In this study, the quantitation was applied on peak areas of hopane and sterane (m/z 191 and m/z 217; respectively) and the peak areas of the internal standard were calculated in m/z 66 (Figure 3-18 and 3-19).

The absolute concentrations of crude oils were normalized to the saturate fraction since it is impossible to be normalized to TOC values. The absolute biomarker concentrations of source rocks were also normalized to the saturate fraction to obtain a better correlation between crude oils and source rock. It should be noted that the

organic matter extracts and its saturate fraction in source rock can be affected by migration, contamination or thermal maturity; therefore, these alteration processes should be considered in correlation with source rock extracts and crude oils (Wang, 1993). The modified equation from Wang (1993) was used to calculate the absolute concentration of the biomarkers. The following is the modified equation for calculating absolute biomarkers of the source rock normalized to Saturates:

$$C_{ABS} = (C_{bio} \times V_{b/c} \times 1{,}000{,}000)/SAT \times W_{sample} \times \% H_{sie} \times \% HLPC) \ (\mu g/g \ TOC)$$

- C_{ABS} is the absolute concentration of a biomarker group normalized to the SAT values expressed in a unit of micrograms of biomarker per gram TOC (µg/g SAT).
- C_{bio} is the relative concentration of biomarker expressed in a unit of µg biomarker per ml solvent and was calculated by: $C_{bio}=(A_{bio} \times C_{STD})/ A_{STD}$, where C_{bio} is the integrated peak area of the biomarker; C_{STD} is the known concentration of the internal standard; and A_{STD} is the integrated peak area of the internal standard.
- $V_{b/c}$ is the volume of the branched and cyclic fraction expressed in a unit of ml and calculated by: $V_{b/c} = W_{b/c}/9$ (mg/ml, where W_b/c is the branched and cyclic fraction and 9 (mg/ml) is the concentration utilized in the analysis of biomarkers.
- 1,000,000 is the number used to cancel the three percentages in the denominator of the equation.

- SAT is the total saturate fraction of the source rock or oil expressed in a unit of percent.
- W_{sample} is the weight of the bitumen used in extraction expressed in grams.
- H_{sie} is the percentage of saturate fraction used for preparing branched and cyclic saturate fraction HI-SIV 3000 molecular sieve.
- % HLPC is the percentage of extract used for fractionation analysis by High-Performance Liquid Chromatography.

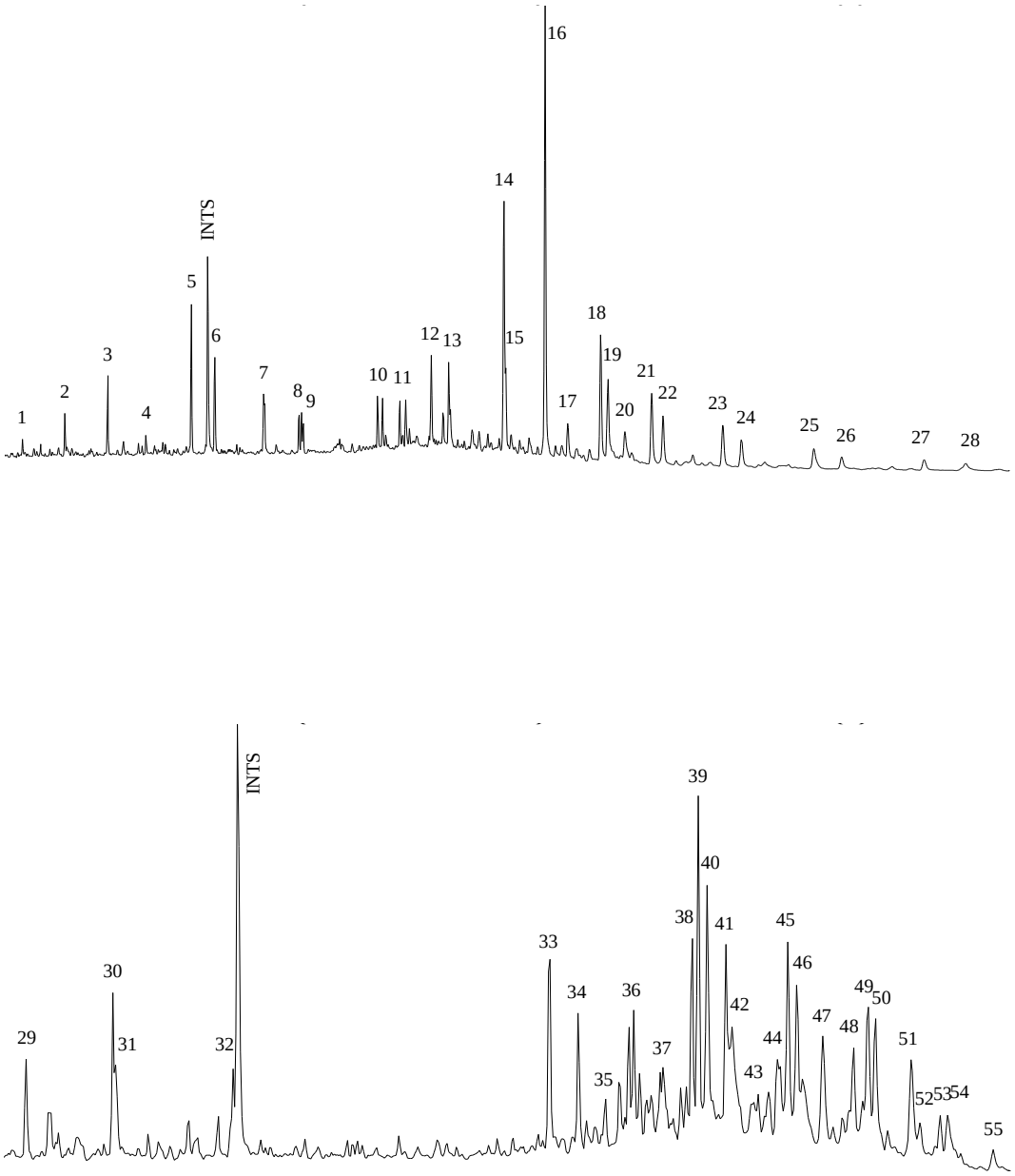


Figure 3-18. Combination of mass chromatograms of m/z 66 with m/z 191and m/z 217 of crude oil shows the location of internal standard with terpanes (top), and steranes and diasteranes (bottom).

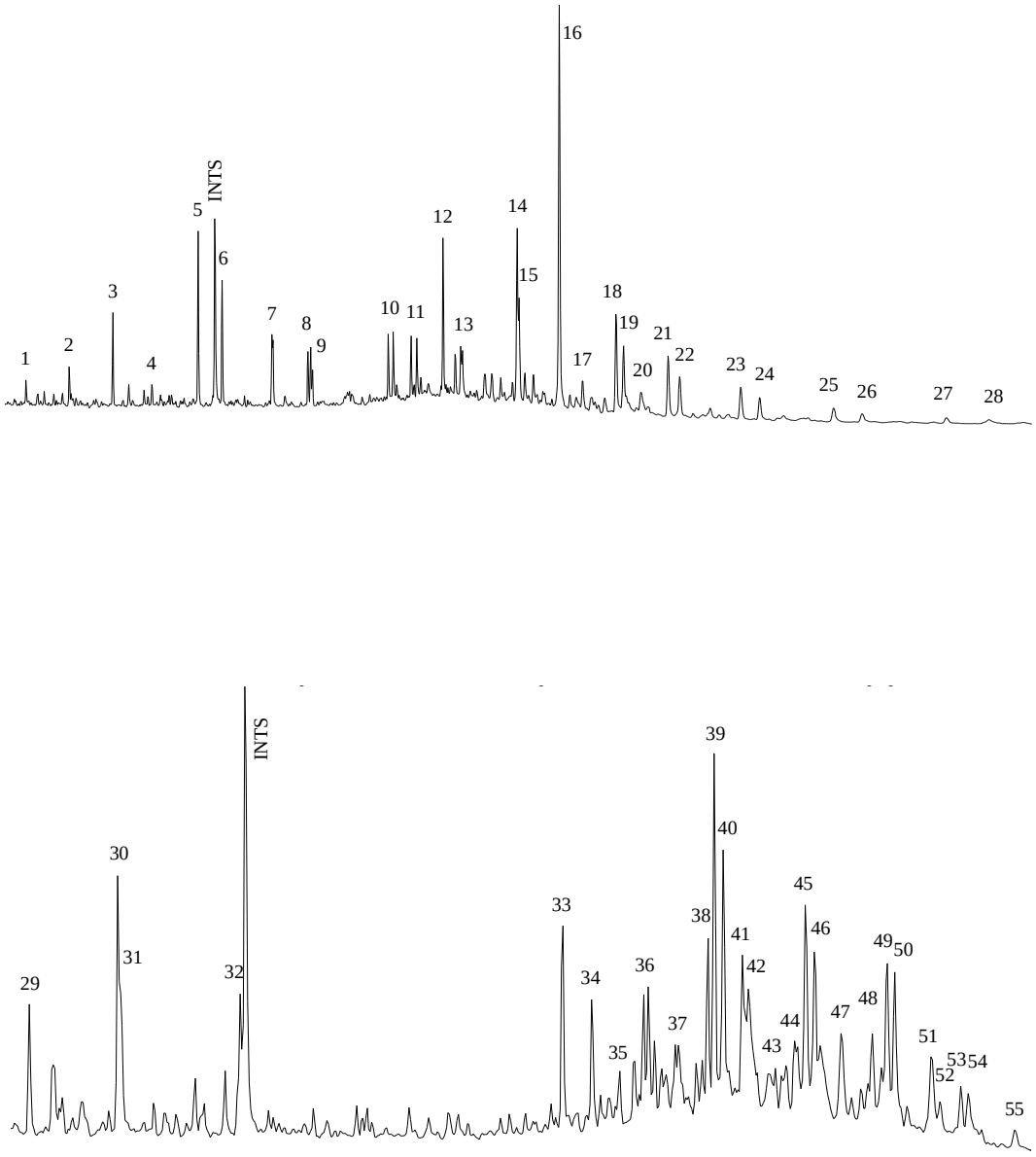


Figure 3-19. Combination mass chromatograms of 66 m/z with m/z: 191 and m/z 217 showing location of internal standard with terpanes (top), and steranes and diasteranes (bottom) in source rocks.

CHAPTER IV

4. Source Rock Analysis

4.1 TOC and Rock Eval Source rock Analysis

The total organic carbon content of the source rock varies from poor to excellent with respect to oil generation and the kerogen types are type II and II/III. The samples at greater depths (more than 12000 ft) show kerogen type III with low HI and relatively high OI. T_{max} from Rock Eval pyrolysis is not reliable in most samples and shows generally low values in higher depths. However, in the in Well BBB1-6 (10460 to 11425 ft.), T_{max} values are within the early generation window. Excellent source rock quality was observed in well BBB1-6 where the TOC values were the highest among all the studied wells. The Rock Eval analysis of samples from well 3B1-6 shows pattern consistent with the Gamma Ray profile. Therefore, the well is divided into two parts. The lower strata were deposited during a sea level rise within transgressive systems tracts and the upper strata were deposited within highstand systems tracts. The total organic carbon content increases with depth and supports sea level changes.

4.1.1 Organic richness

TOC values of the samples in the study vary with depth and location. Generally, TOC values are low in the plat forms and deepest samples in the troughs. TOC values for samples collected from wells FFFF1-6 and FFF13-6 located on the north part of Concession 6 are all low, ranging between 0.24 to 0.89%. According to El- Alami et al. (1989) the entire northern part of the basin has low TOC content due partly, to

unsuitable kerogen facies and the high level of maturity. In the southern part of Concession 6, the TOC values vary among the two studied wells. The samples from well ZZZ1-6 (12135 to 13715 ft) show fair TOC values ranging from 0.64 to 2.00 while well BBB1-6 (10465 to 11425 ft) have much higher values ranging, from about 0.69 to 5.35% showing that these samples exhibit fair to excellent TOC for oil generation (Appendix I). The samples from H1-6 and 3H1-6 wells located on the Zaltan Platform in the East of the Concession at depth from 9990 to 10475 ft have low TOC values ranging from 0.11 to 0.56% while well Z1-6 (13225 to 14515 ft) located in Ajdabiya Trough have values from 0.75 to 1.27%. This is inconsistent with Baric et al. (1996) conclusion about the lower part of Sirt Shale. Baric et al. (1996) reported that these rocks at depths of more than 11010 ft show a decrease in organic matter with an average of 0.56%. The well Z1-6 samples have a depth exceeding 13000 ft and a TOC of up to 2.0%. The TOC of samples from well EEEE-6 (13275 - 14045 ft) and well NN1-6 (12885 to 13245 ft) that located also in Ajdabiya through between have values from 1.8 to 2.9% and 0.64 to 2.00%, respectively. The high TOC in these wells are inconsistent with the depth as in Z1-6 since they are close to each other. The high TOC in well EEEE-6 is probably due contamination as observed from high S1 peak (Figure 4-1). The samples from Al Kotlah Graben from Well C65-47 have low TOC with values of 0.42 to 0.86% at depth between 6715 and 7505 ft. However, TOC analyses alone give limited information about petroleum potential. It is well known that samples containing low TOC value can be related to poor preservation in depositional environments or to the oil generation from these rocks (see Appendix I).

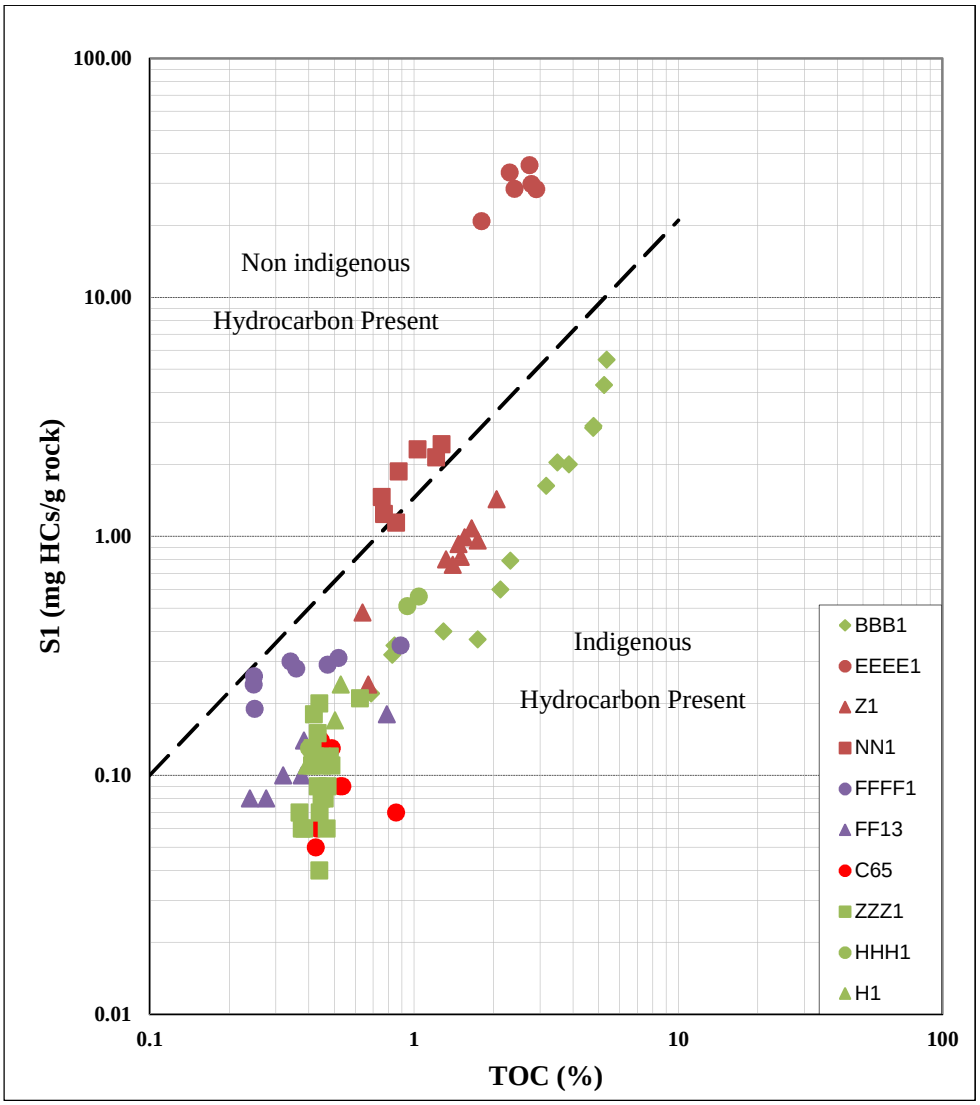


Figure 4-1. Plot of S1 versus TOC, from which non-indigenous hydrocarbons can be distinguished from indigenous hydrocarbons (Hunt, 1996).

4.1.2 Hydrocarbon Generation Potential

The type of kerogen in a potential source rock determines the nature and amount of hydrocarbons produced by Sirt Shale. Hydrogen Index (HI) and Oxygen Index (OI) are parameters used to characterize the origin of organic matter type (Appendix I; Tissot and Welte, 1984; Cornford et al., 1998). The HI corresponds to the quantity of cracking organic compounds from kerogen, or hydrocarbons from S2, relative to the TOC in the sample, measured in mg hydrocarbon/g TOC (mg HC/g TOC). The OI corresponds to the quantity of carbon dioxide from S3 relative to the TOC (mg CO2/g TOC; Peters, 1986). Hydrocarbon source rock evaluation parameters for Rock-Eval pyrolysis data are shown in Appendix II. Sirt Shale in well BBB1- contains (TOC) in the fair to excellent range and S1 and S2 show very good potential in terms of generated hydrocarbons. The S2/S3 of well BBB1-6 shales is greater than 5.0, indicating oil-prone source rocks. A plot of S1 plus S2 versus TOC values (Figure 4-2) indicates the oil shales to be excellent source rocks. Tmax, 439-443 °C indicates that shale is at the early stage of hydrocarbon generation. The hydrogen index (HI) is in the range of 206 to 518 mg/g TOC, suggesting both type II and type II/III kerogen are the main components of OM. In the well C65-47 (6415-7505 ft), the shale contains poor to low amount of TOC. The generation potential of the shale in this well is poor where S1 shows poor genetic potential (0.09 to 0.14). HI range from 38 to 208 mg/g TOC indicating both oil and gas prone OM (Type-III and II/III kerogen). A plot of HI versus OI shows that most of the samples plot in the field of Type III kerogen but the samples from well BBB1-6 fall into Type II and Type II/III kerogen fields. Generally, the samples of this study vary from kerogen type II, II/III and type III (Figure 4-3).

However, this plot may be affected by kerogen mixtures, thermal maturity during pyrolysis (Cornford et al., 1998). This variation indicates that Sirt Shale does not usually have type II kerogen even at the greatest depths. Samples with depths greater than 12000 ft. could be affected by thermal maturity. Samples with shallower depths indicate their origin kerogen type III since the major oil generation of Sirt Shale is between 10000 and 14000 ft. (Roohi, 1996) as indicated by Lopatin's time-temperature index of maturity (TTI). It should be noted that a late mature stage of gas/condensate generation has been reached in the Ajdabiya source rocks (Hallett, 2002) which supported vitrinite reflectance of sample from Z1-6 that has value of 2.1 at depth 13745 ft. The variation in kerogen types is also supported in Figure 4-4 which is an alternative method for assessing kerogen type by plotting S2 values against TOC (Cornford et al., 1998).

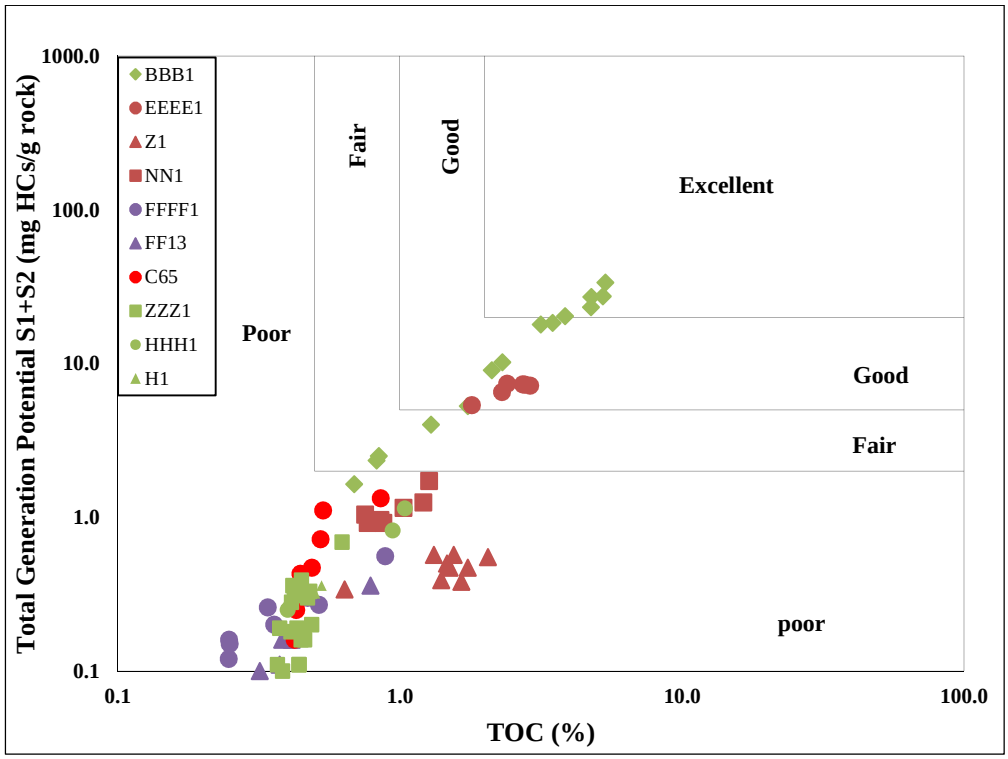


Figure 4-2. TOC versus total hydrocarbon generating potential of rock showing the generating potential of the studied source rocks.

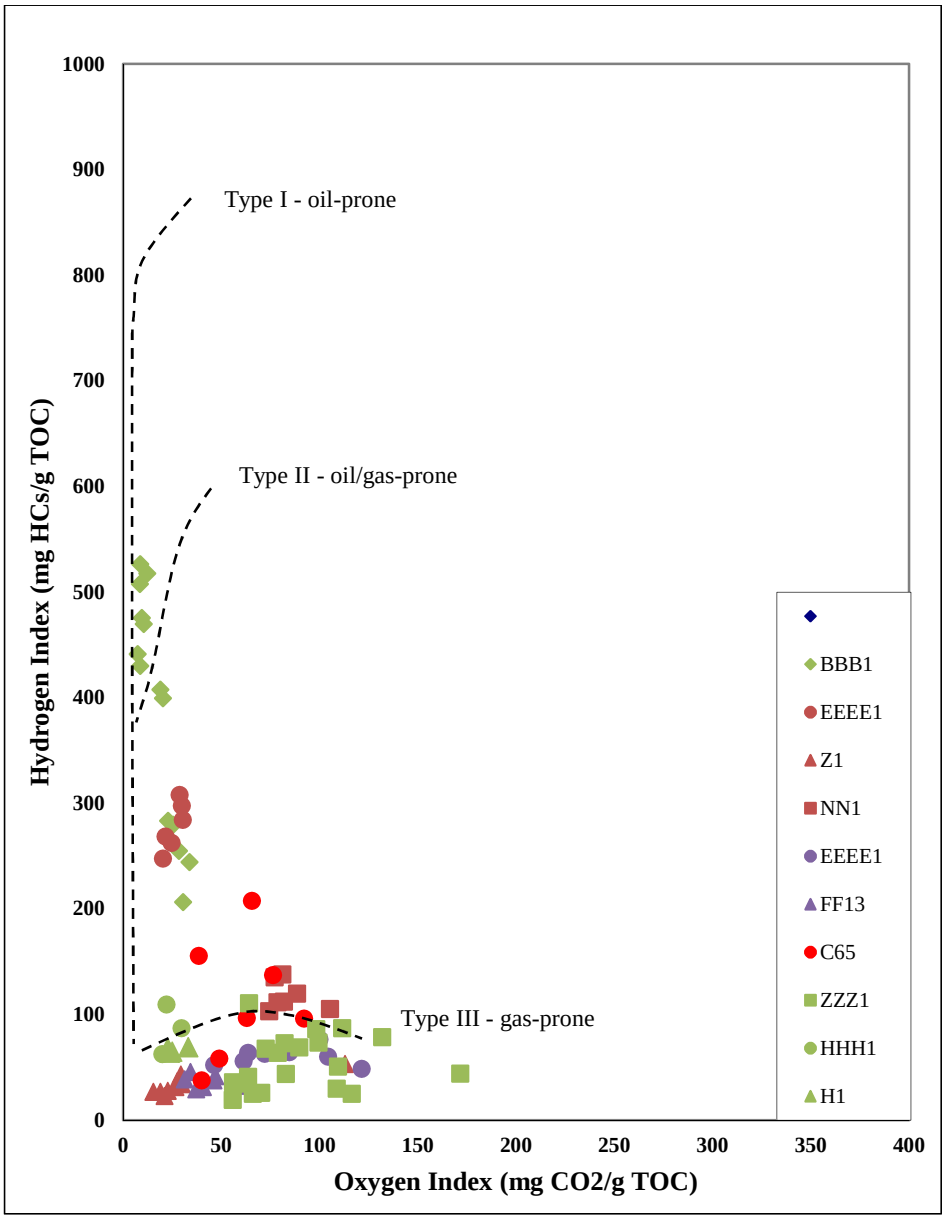


Figure 4-3. Plot of hydrogen index versus oxygen index showing that the organic matter of Sirt Shale lies within the kerogen type II and III.

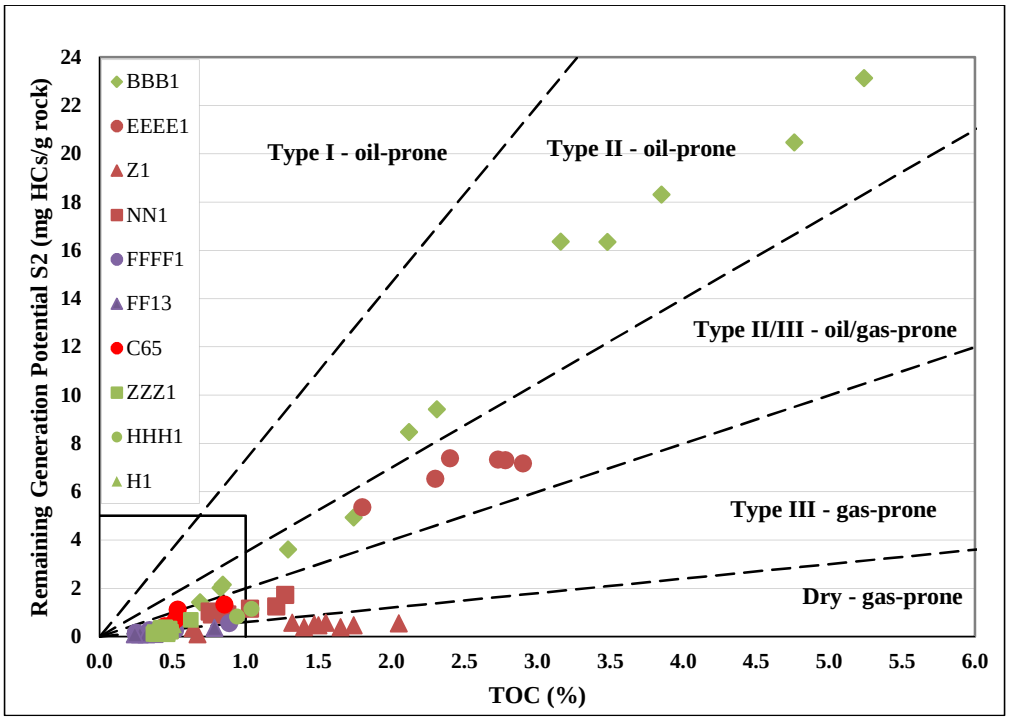


Figure 4-4. Plot of HI vs. TOC showing the type of organic matter.

4.1.3 Thermal Maturity

The T_{max} values represent the temperature at which the largest amount of hydrocarbons is generated from the kerogen of the OM in source rock where the S2 peak reaches its maximum during Rock-Eval pyrolysis (Peters, 1986; Tissot et al., 1987). Rock-Eval T_{max} values can be used to estimate the level of thermal maturity for OM within the sediments, their values increase progressively along with the level of thermal maturity (Tissot and Welte, 1984; Waples, 1985; Peters, 1986; Tissot et al., 1987. Peters (1986) suggests that T_{max} of samples with S2 peak values less 0.2 mg HC/g rock values are unreliable due to the broad nature of the S2 peak and should be rejected. Empirical evidence suggests that samples with T_{max} and S2 values less than 0.5 mg HC/g rock and TOC values less than 0.5% should be considered unreliable when estimating thermal maturity (Riediger, 1997).

There are some problems associated with T_{max}. Even though its value may increase regularly with depth, variations can result due to contaminants, such as drilling-mud additives and natural bitumen (Hunt, 1996; Peters, 1986). In addition to, solid bitumen can increase S2 peaks (Hunt, 1996).

The Production Index (PI) also used in estimating the maturity of OM. In absence of migration, the S1/(S1+S2) ratio is an evaluation of the transformation ratio. The continuous increases of this ratio along with increasing depths make it a valuable maturation parameter (Tissot and Welte, 1984). The ratio gradually increases with depth and the components in the kerogen (S2) are converted to free hydrocarbons (S1) thermally (Peters and Cassa, 1994). PI values less than 0.1 indicate immature OM while a ratio of 0.4 indicate that the late of the oil window has been reached. The ratio

increases to reach 1 when the hydrocarbon generative potential capacity of kerogen has been exhausted (Peters, 1986). PI and T_{max} data for most of the Sirt Shale in this study vary from well to well according to well location and well depth (Figure 4-5). Most of the studied samples are located in the zone of hydrocarbon staining or contamination. In the Figure 4-5, the BBB1-6 samples are located in the mature zone as well as C65-47 and HHH1-6. The samples of well NNN-6 show mature T_{max} (434-437) and high PI values (0.54-0.67) which placed them in the contamination zone. Peters and Cassa (1994) reported that T_{max} values between 390 °C to 435 °C, and 436 °C to 445°, the PI values should be equal to or less than 0.1 and 0.3, respectively. Samples differing from these conditions are considered to be contaminated by drilling additives or migrated oil. The remaining wells show decreasing T_{max} values with depth and are as low as 363 in some wells. The decreasing T_{max} values with depth can be attributed to a low S2 (HC/g rock) peak (Bordenave et al., 1993). The solid bitumen and the heavy oil may produce a low T_{max} such as 350 (Clementz, 1979). S2 peak in a bitumen-rich source rock may not be totally attributable to the kerogen. The solid bitumen in this study was observed in a selected sample for study under microscope during the measurement of vitrinite reflectance. Vitrinite reflectance indicated that OM of upper Cretaceous at a depth of 10000 to 12000 feet has values of 0.65 to 1.21% R_o. Generally the levels of maturity of OM within the Sirt basin are variable and immature in a range of 0.35 to 1.62 R_o (Gumati and Schamel, 1988).

Futyan and Jawzi, (1996) demonstrate that these rocks are within the oil window between depth of 8860 ft and 11160 ft in the central and eastern Sirt Basin. The application of Lopatin's method of maturity also indicates that the major oil generation

of the source rocks in Maradah Trough was at a depth between about 9840 ft and 13120 ft (Brennan, 1992). This window includes the entire section of this study (10460 ft to 11425 ft). Hydrocarbon generation at the base of the Upper Cretaceous Sirt Shale entered the oil window during the mid-Eocene and reached peak generation at the beginning of the Oligocene (Brennan, 1992; Hallett, 2002). In this study the values of 0.8 to 1.0 vitrinite reflectance and T_{max} values of the well BBB1-6 also support that these rocks are within the oil window.

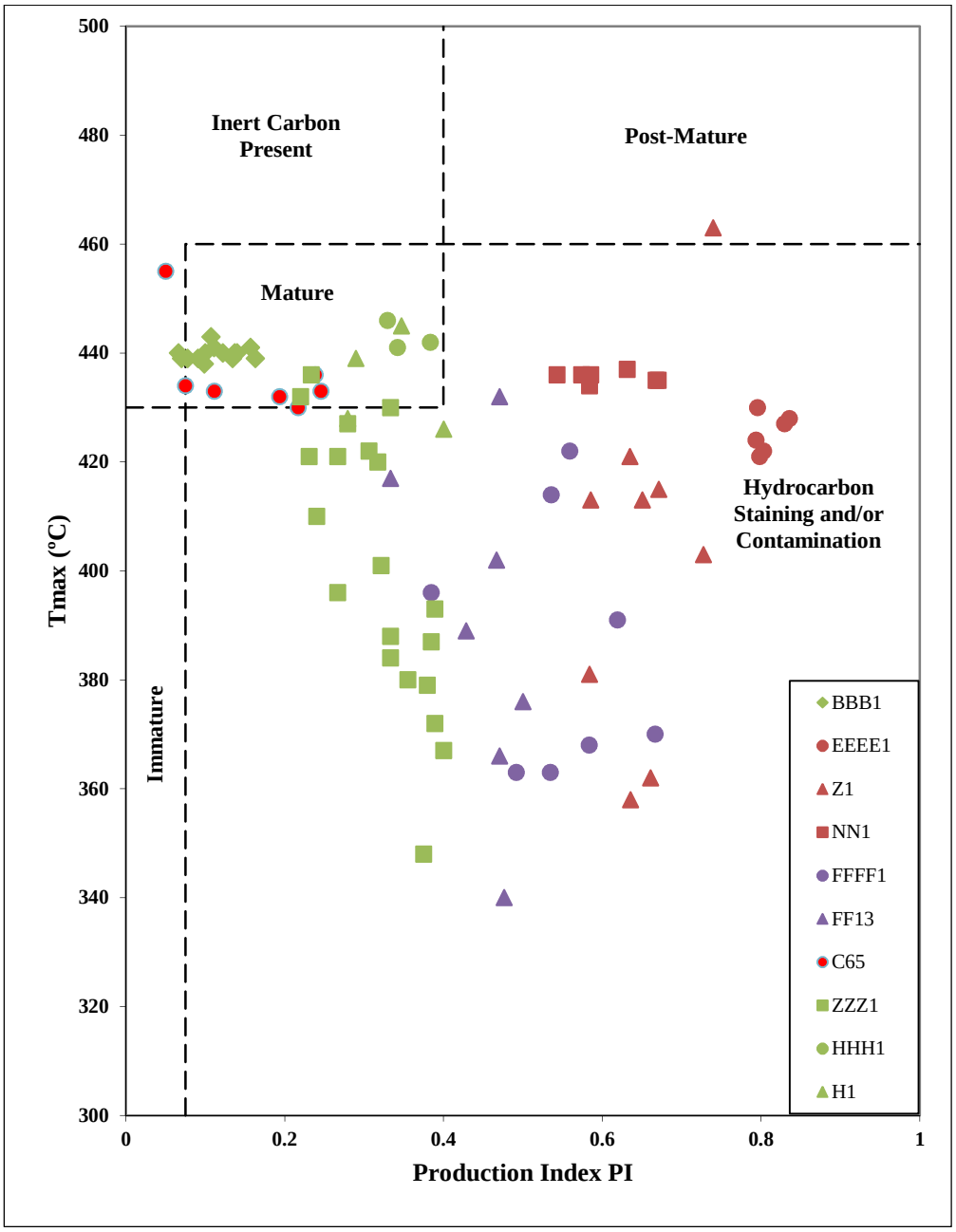


Figure 4-5. Plots of Production Index (PI) vs. T_{max} showing the level of thermal maturity of the samples of this study.

4.1.4 Organic Sequence Stratigraphy of Sirt Shale

The BBB1-6 well in this study can be used to determine the relation between organic matter and sequence stratigraphy. The well was divided to Highstand and Regressive Systems Tract (HST) and Transgressive Systems Tract (TST) of sequence stratigraphy using the gamma ray curve (Figure 4.6). the Transgressive Systems Tract strata was deposited during a rapid rate of rise in relative sea level with the maximum flooding surface at the top while the HST was deposited during a slower rate of rise (Appendix I). Recently, understanding the sequence stratigraphy of shale provides a powerful tool for high-grading stratigraphic intervals most favourable for preservation of organic matter (Slatt and Rodriguez, 2012). The OM which is usually determined by the TOC will reflect changes of sea level within sequence stratigraphy. Potential source rocks can be found in lowstand systems tracts (LST), transgressive systems tracts (TST), and highstand systems tracts (HST). The richest source rocks are found in the condensed section of the transgressive systems tracts (Bohacs, 1991and Isaksen; Creaney and Passey, 1993; Philp, 2007), and also in HST but directly above the maximum flooding surface (MFS; Slatt and Rodriguez, 2012). However, the reducing in OM within HST is due to higher sedimentation rate during these systems tracts (Meijun, et al., 2003).

In this study, Rock-Eval pyrolysis indicate good to excellent source rock and correlate with sea level changes as in the Figure 4-7. HST samples show relatively low TOC ranging from 0.69 to 3.85. In Figure 4-7, the local drop in the HST strata is reflected also in organic matter content where the shallowest strata shows the lowest TOC values (greater than 1) in the study interval (Appendix II). Deeper sediments

which represent TST were comparatively organic-rich suggested by TOC (greater 3%) and S1 and S2 of <2-4 and 16-28 mg HC/g rock, respectively. The samples of the condensed section show the highest TOC which reached up to 5.35.

4.1.4.1 Relative Hydrocarbon Potential (RHP)

Relative hydrocarbon potential (RHP) proposed by Fang et al. (1993) is used to investigate the depositional conditions of organic matter (Appendix I).

RHP reflects oxygenation conditions in the depositional environment. It can be related to sea level fluctuations within a sequence stratigraphic framework. Therefore, the sequence stratigraphy of shale is a powerful tool not only for regional-to-local stratigraphic correlations but also for high-grading stratigraphic intervals most favorable for preservation of OM (ductile), gas storage, and hydraulic fracturing (organic-poor, relatively brittle; Slatt and Rodriguez, 2011).

The deeper samples of the well 3B6 contain high quantities of OM, which may indicate deposition during rising sea level which agrees with the gamma ray profile. Changes in the abundance of OM from the bottom to top of the studied section can be due to sea level changes. The HST strata show higher RHP than TST and CS, which indicate that the HST was deposited in more oxic environment compared to the TST and CS. The changes in the organic matter content and RHP can be reflected in the plot of HI, OI, PI, S1/TOC, S1+S2, RHP and gamma ray profile against depth (Figure 4-7).

The gamma ray log represents the response of uranium which is usually associated with organic matter. Therefore, it serves as an indirect tool for assessing good preservation of organic matter. The Sirt Shale in this study shows increasing gamma

radiation with increasing TOC values for these rocks. This observation can be explained by sea level changes within sequence stratigraphy (Slatt and Rodriguez, 2012). During rising sea level in the TST, the organic matter has excellent conditions for accumulation and preservation as shown in the lower part of the studied section. The upper part represents the HST, reflecting more oxic conditions and therefore less organic matter content. The RHP parameter in this study reflects the fluctuations in oxygenation conditions; showing a positive correlation with fluctuations in relative sea level. This further observation in Sirt Shale is supported by increasing OI and decreasing HI along with increasing gamma response, and therefore rising sea level. The high content of HI and low OI in this Sirt Shale are associated with TST where the gamma ray profile has higher readings

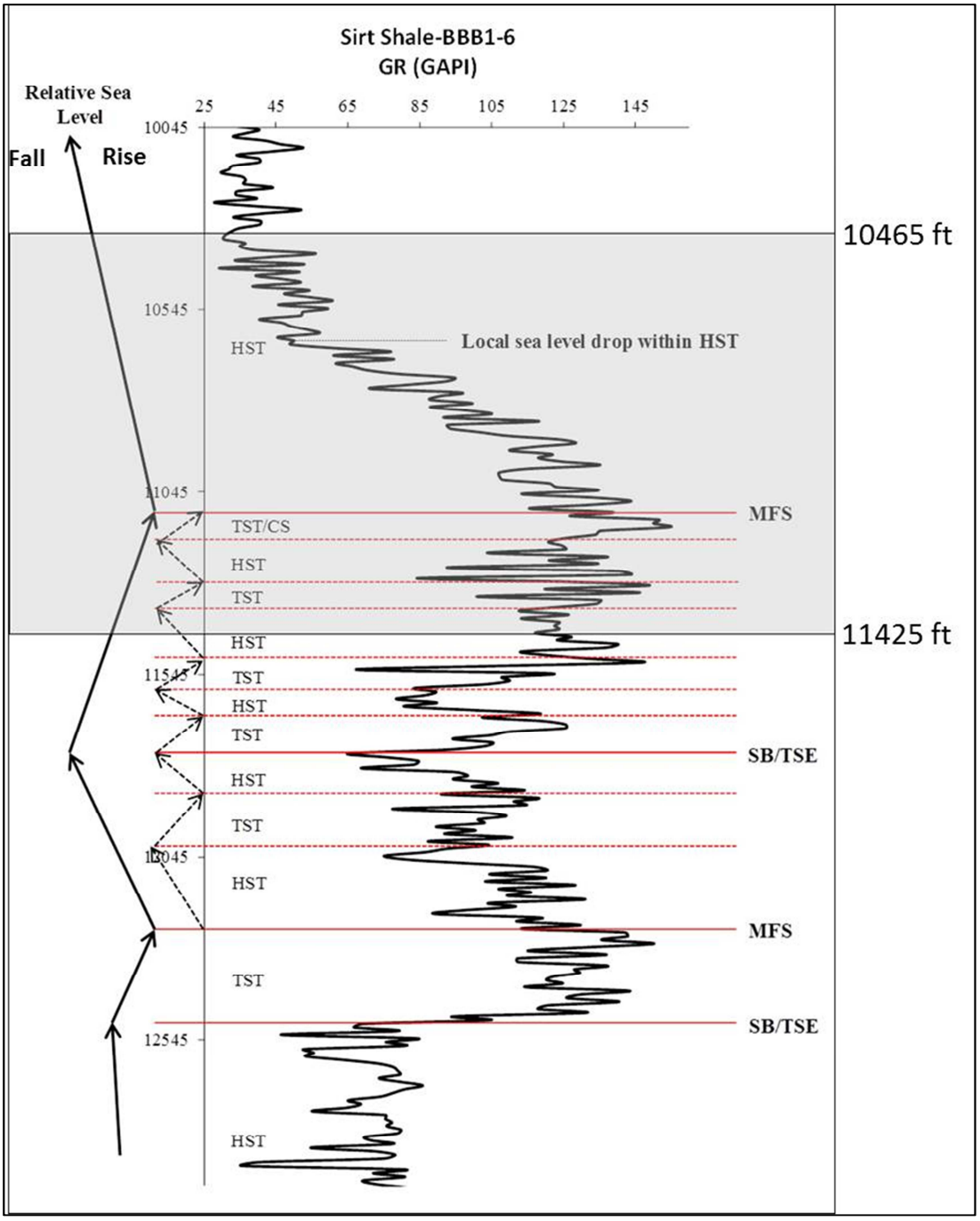


Figure 4-6. Gamma ray profile of Sirt Shale in the well BBB1-6, showing sea level changes within sequence stratigraphy. In this figure solid arrows refer to falling and rising of sea level at the larger scale and the dashed arrows refer to falling and rising of sea level at the smaller scale.

Shaded area= Interval which included in this study; SB= Sequence Boundary; TSE Transgressive Surface of Erosion; TST=Transgressive Systems Tract; CS= Condensed Section; MSF= Maximum Flooding Surface; HST=Highstand Systems Tract.

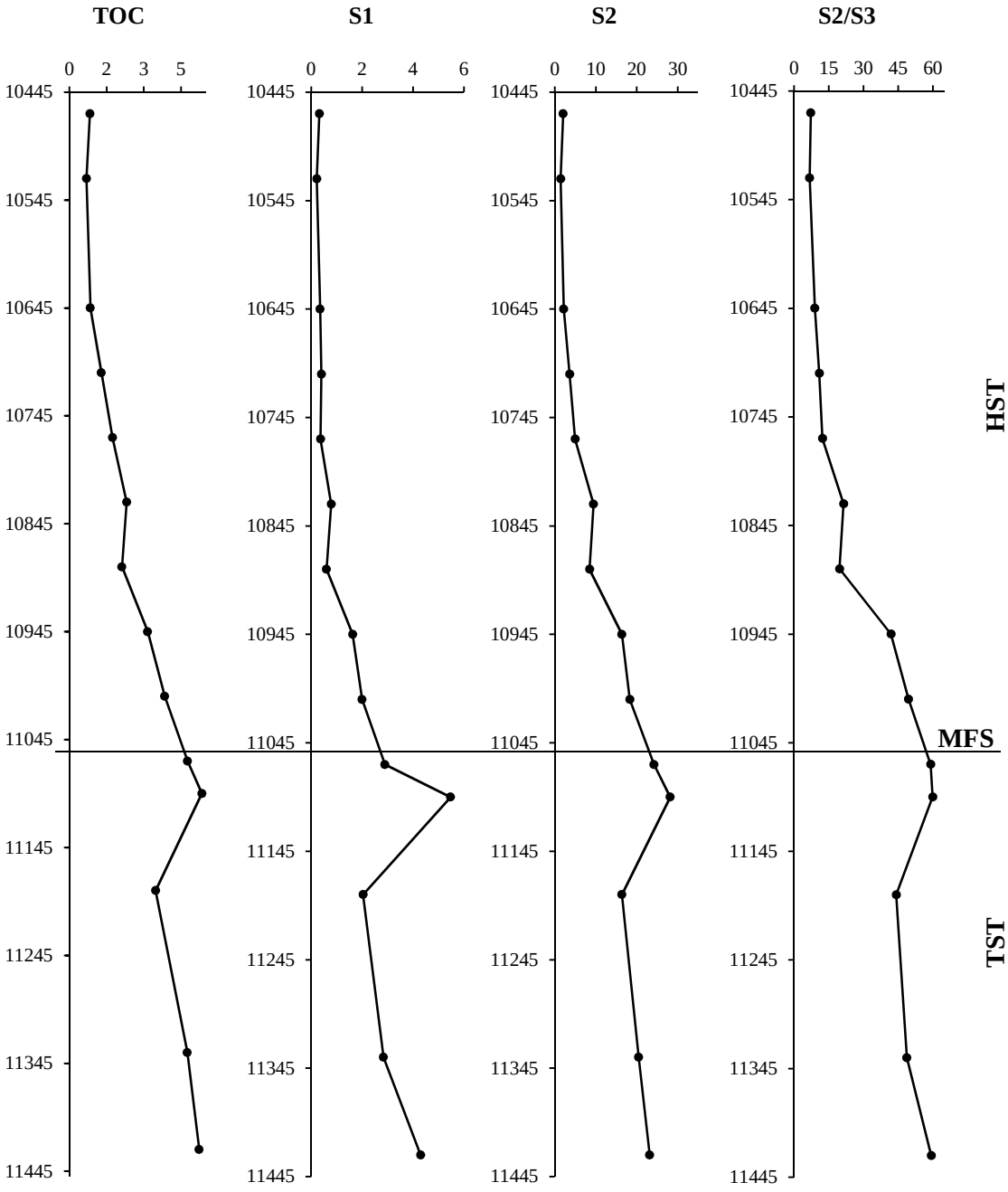


Figure 4-7. Rock Eval data, RHP, and GR log vs. depths.

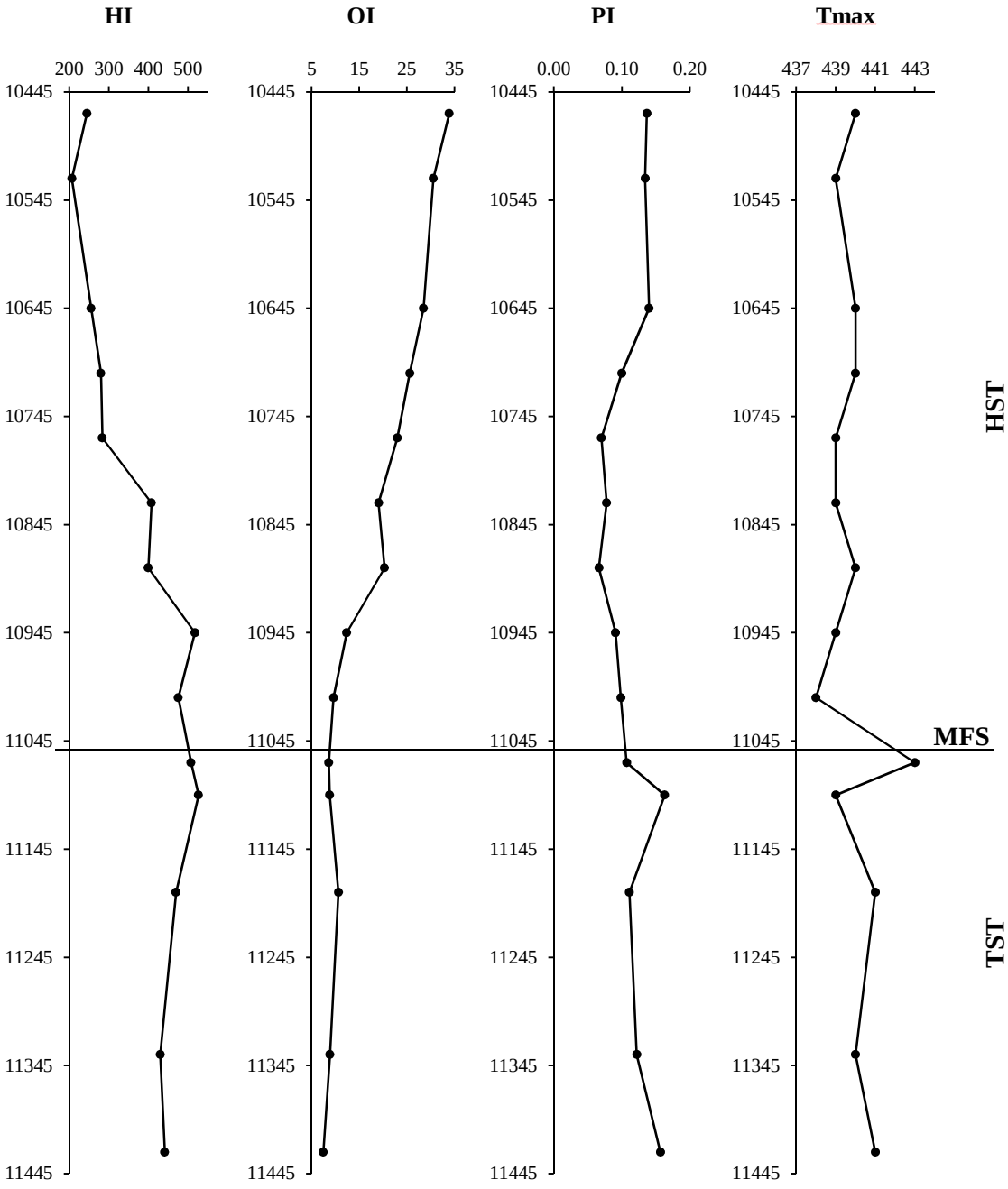


Figure 4-7..... Continued...

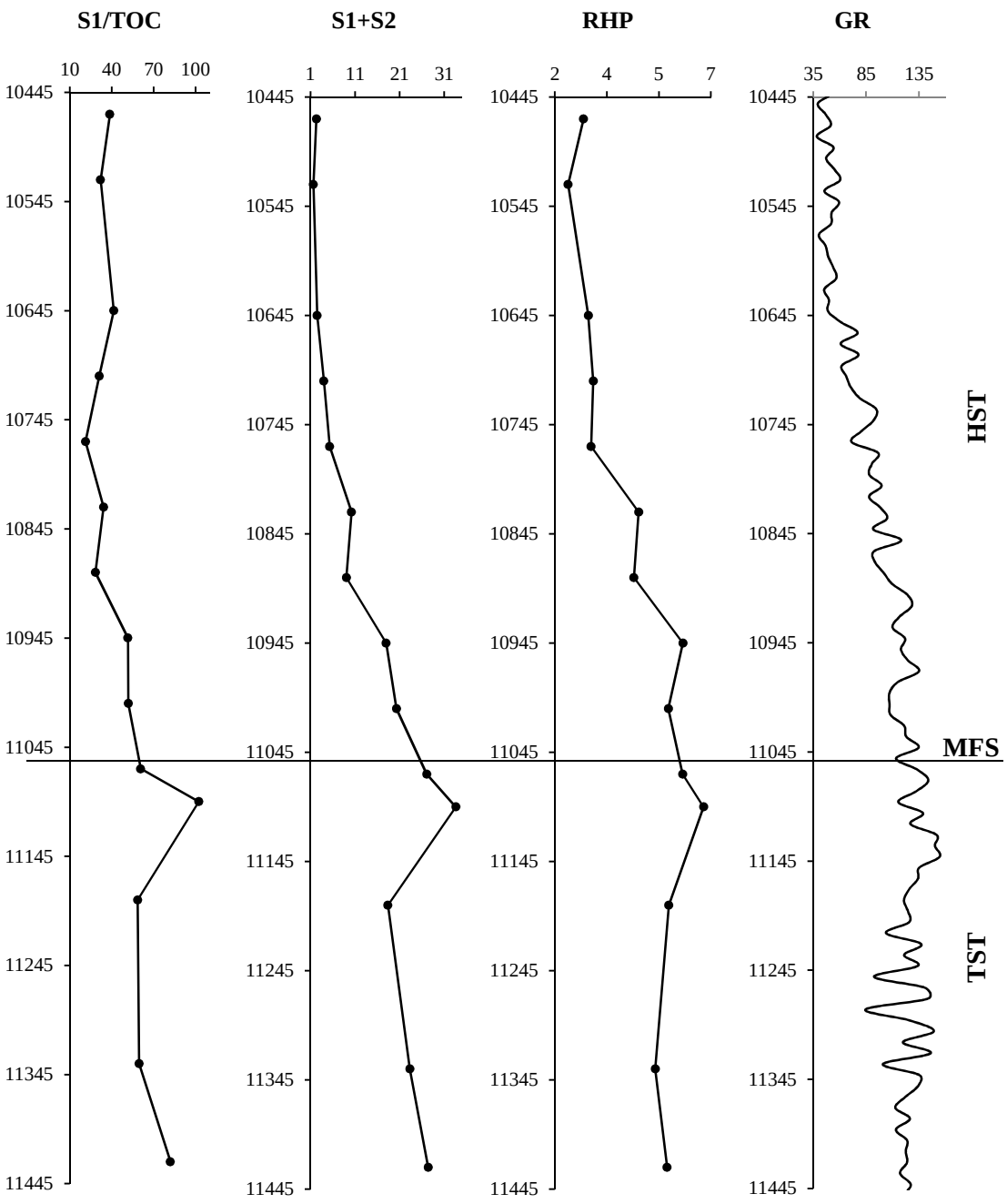


Figure 4-7..... Continued...

4.2 Source rock Geochemistry

4.2.1 Environmental Conditions

The distribution of n-alkanes in Sirt shale source rocks may reflect the organic matter source. The n-alkanes of samples from this study range from C_{14}–C_{35} with maxima between nC_{16}–nC_{18} (Figure 4-8). The samples in the upper part of the well 3B-6 display unimodal distributions, while the lower part shows biomodal distribution of n-alkanes (Figure 4-8). The high abundance of low molecular weight n-alkanes relative to the higher molecular weight n-alkanes (nC_{27}/nC_{17} ratios), suggests an absence, or low contribution, of terrigenous organic matter. The nC_{27} indicates higher plant input and the nC_{17} shows a contribution from algae (Hunt, 1996; Tissot and Welte, 1984). The pristane/phytane ratios in all samples range from 0.89-1.68 and may suggest organic matter deposited in a marine environment Sirt Shale.

The low Pr/nC_{17} and Ph/nC_{18} ratios (0.47 to 0.55 and 0.47 to 0.56, respectively) support a marine of environment (Lijmbach, 1975). A plot of Pr/nC_{17} versus Ph/nC_{18} can be used to indicate types of organic matter (Figure 4-9) and the distribution of the samples on this plot support the marine depositional environment for the OM within these Sirt Shale source rocks (Shanmugam, 1985).

The samples generally have similar biomarker distributions in the m/z 191 and 217 ion mass chromatograms shown in Figures 4-10 and 5.11. For peak identifications of biomarkers see Table 4.2 and 4.3. The C_{29} and C_{30} 17α(H)-hopanes are the two dominant triterpanes in the samples (Figure 4-10), and ratios of C_{29}/C_{30} hopanes are between 0.33 and 0.48 in the Sirt Shale, which are consistent with the clay-bearing character samples in the study.

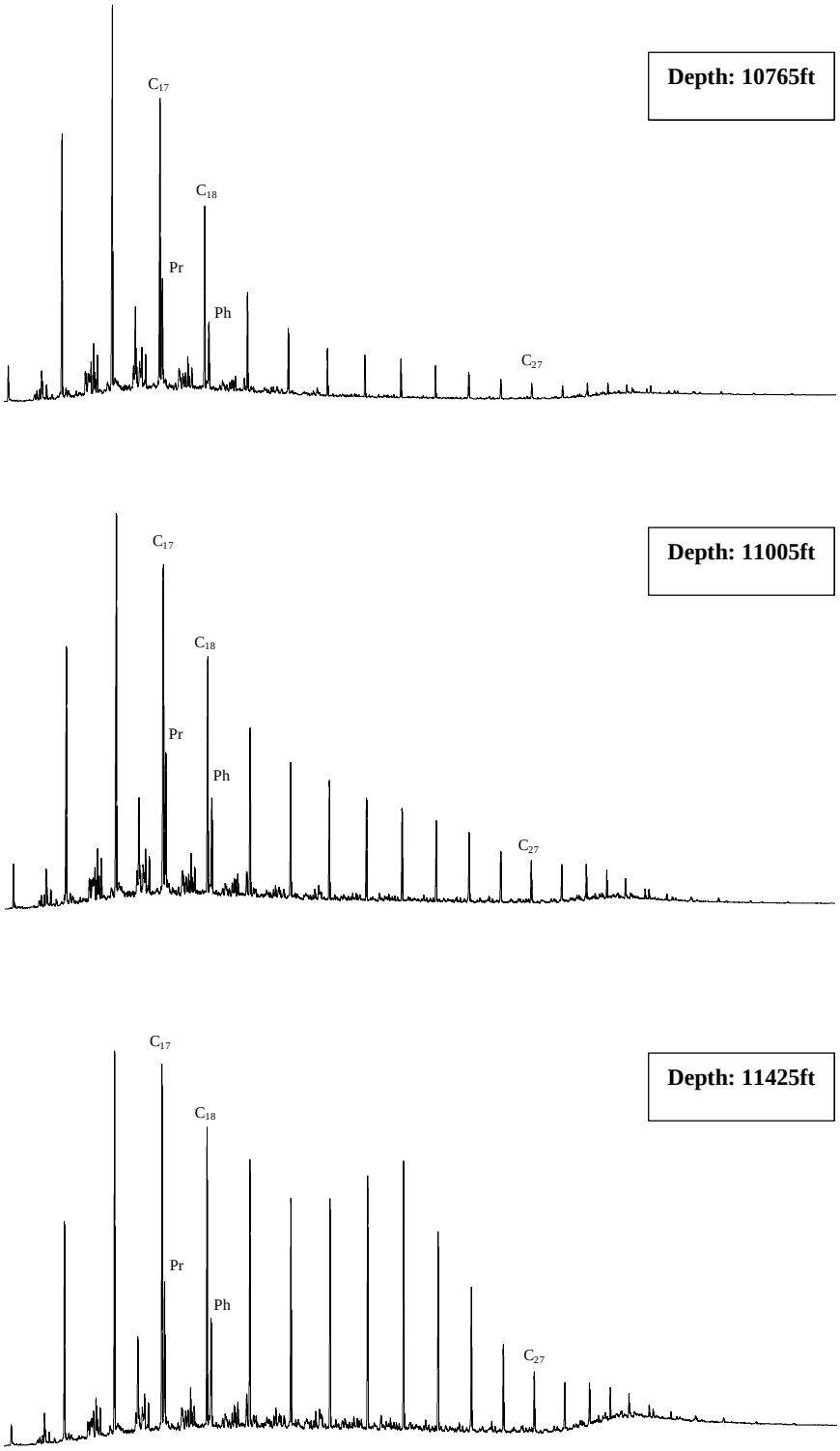


Figure 4-8. GC trace for extracts of source rocks and show n-alkane distribution in the samples. The two samples at the top show a unimodal of n-alkanes the sample at the bottom shows biomodal distribution of n-alkanes.

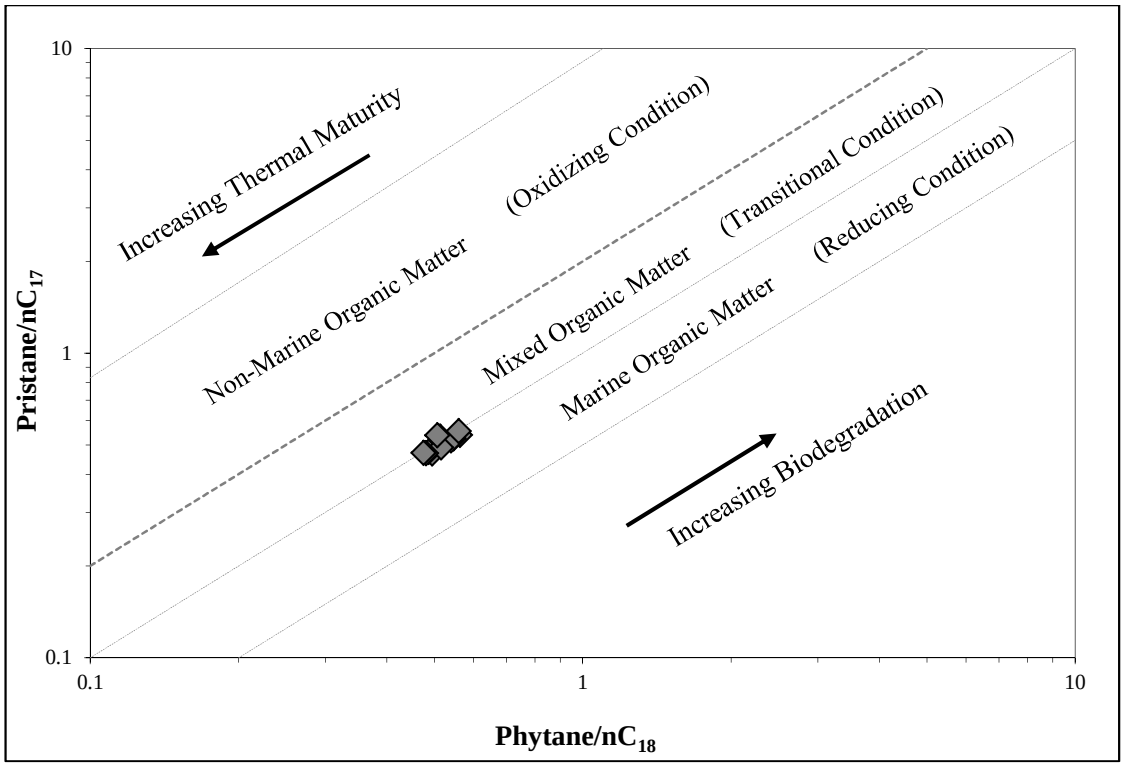


Figure 4-9. Plot of pristane/nC_{17} versus phytane/nC_{18} showing source and depositional environments (Shanmugan, 1985).

Gammacerane/C_{31}R hopane ratios range from 0.24 to 0.33 in the Sirt Shale samples. The considerable amount of gammacerane present may indicate salinity in the source rock depositional environment. The low abundance of C_{24} tetracyclic terpanes in the Sirt Shale samples may result from the impact of marine OM. The low abundance of C_{24} tetracyclic terpanes in this study could be used as a characteristic for clastic marine depositional environments. Carbonate and evaporite depositional environments have high C_{24} tetracyclic terpanes (Clark and Philp, 1989).

The distribution of regular steranes of these rocks reflects marine organic matter type. Organic matter is derived from marine phytoplankton which has high abundance of C_{27} steranes. This is supported by the high C_{27}/C_{29} sterane ratios which range from 1.45 to 1.89. In this study, the relative abundance of C_{27}, C_{28} and C_{29} steranes, $C_{27} > C_{28} > C_{29}$ (Figure 4-11), reflects a dominant contribution from marine source organic matter. A ternary plot of C_{27}, C_{28}, and C_{29} steranes has been widely used to characterise organic facies based on the relative abundance of these steranes and is also consistent with marine type organic matter (Figure 4-12). The presence of C_{30} steranes in all of the samples strongly suggests accumulation from marine organic matter in these rocks (Moldowan et al., 1985). The diasteranes in the Sirt Shale are present in relatively high concentrations as reflected in the ratio of C_{27} diasterane/C_{27}R sterane (0.82 to 1.31). High ratios of diasterane/C_{27}R sterane indicate that the hydrocarbons are generated from source rocks containing an abundance of clays minerals. Pregnane/sterane ratios in these samples range from 0.96 to 2.04; a relatively high abundance of pregnane in the Sirt Shale may indicate hypersaline conditions (ten Haven et al., 1985; Huang et al., 1994; Mueller et al, 1995).

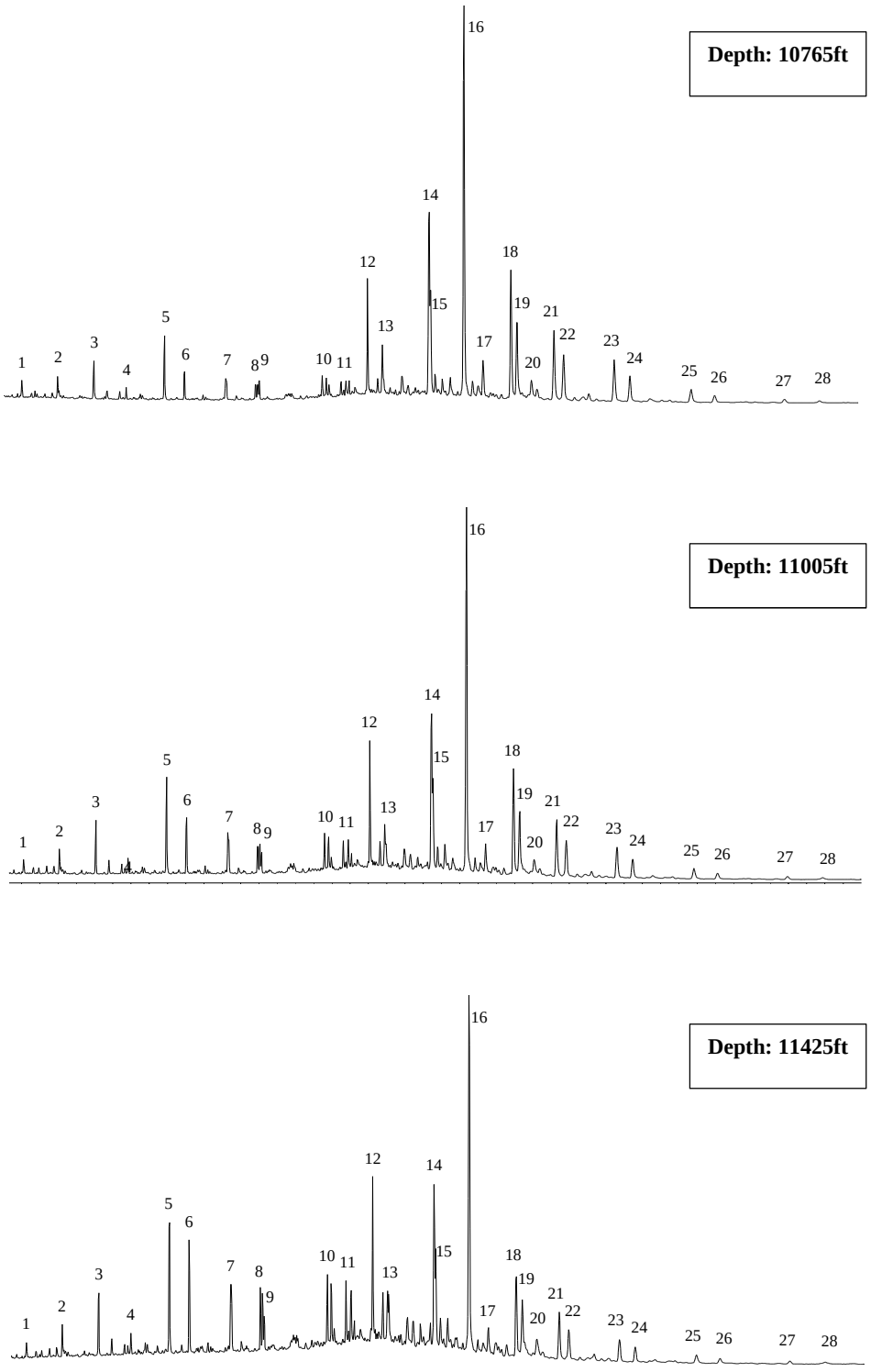


Figure 4-10. GC-MS chromatograms are showing the distribution of terpanes (m/z 191) of the Sirt Shale.

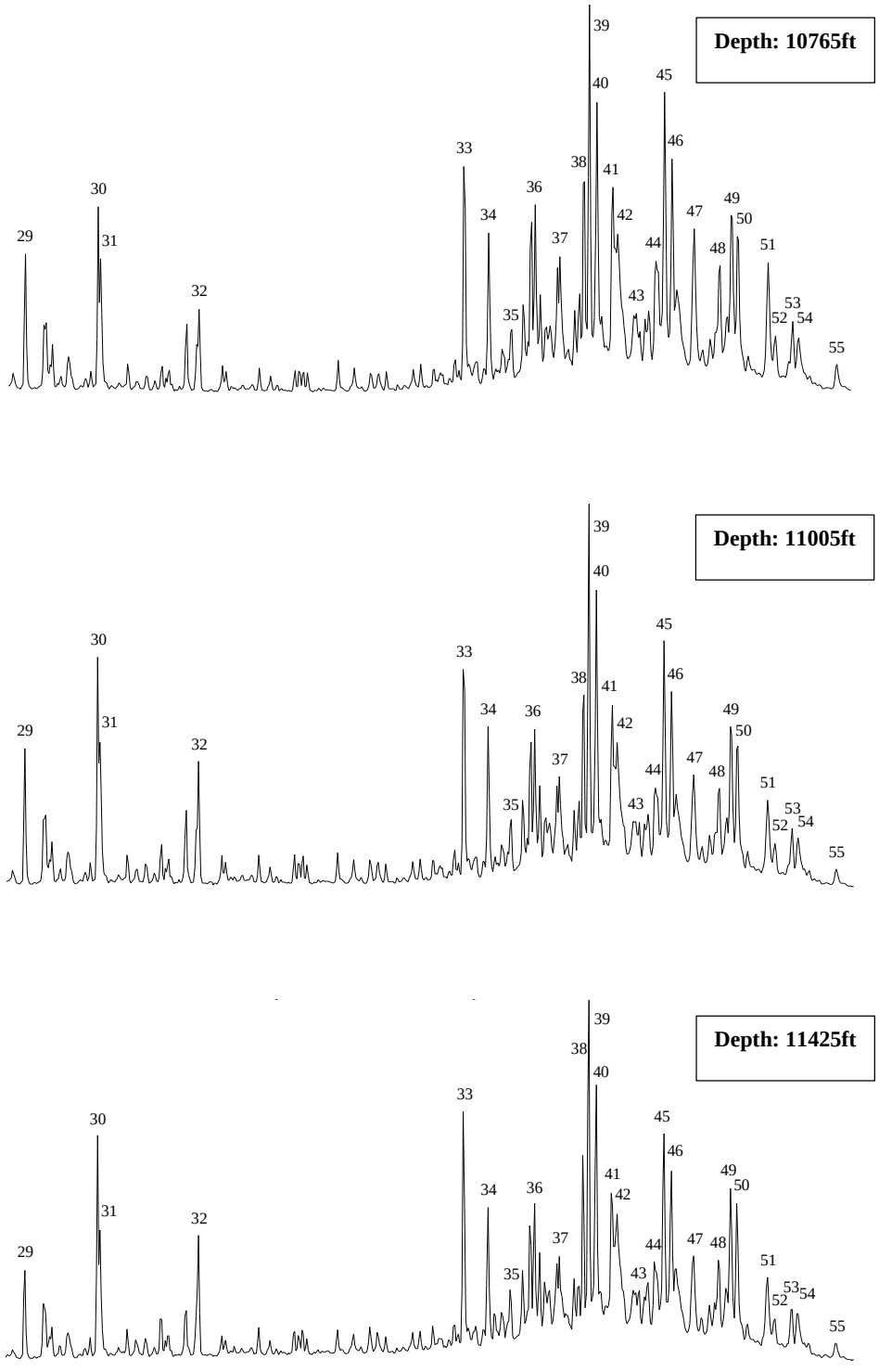


Figure 4-11. GC-MS chromatograms are show distribution of steranes (m/z 217) of the Sirt Shale.

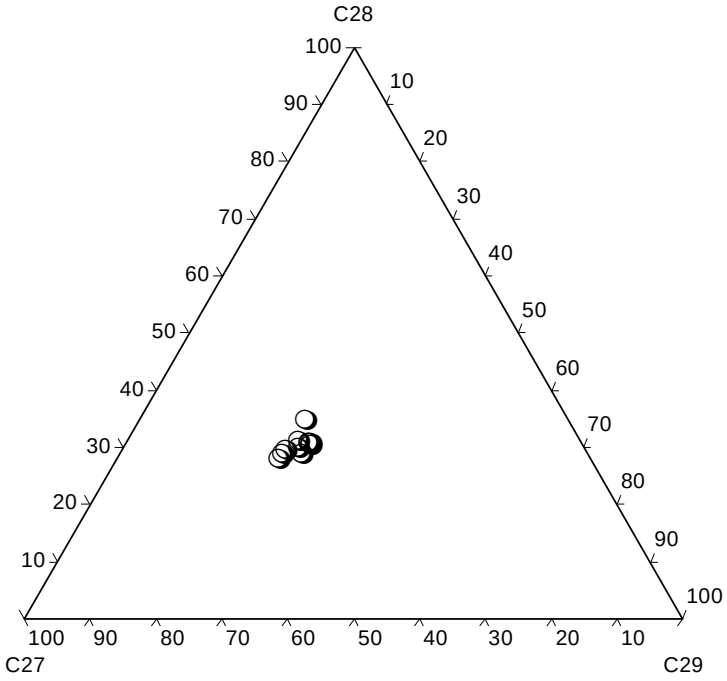


Figure 4-12. Ternary diagram is showing the relative abundance of C_{27}, C_{28}, and C_{29} regular steranes in saturate hydrocarbon fraction of source rock extracts.

4.2.2 Thermal Maturity

The samples exhibit CPI (carbon preference index) values of about 1.02 to 1.26 and CPI values close to 1.0 indicating high maturity (Simoneit, 1978). The hopane ratio of 22S/(22S+22R) is a widely used as biomarker maturity parameter in the early oil generation window (Kolaczkowska et al., 1990; Peters and Moldowan, 1993; Peters et al., 2005). The ratios of the samples in this study range from 0.54 to 0.59, indicating that the main phase of generation has been reached or surpassed (Peters and Moldowan, 1993). The samples at the top of the section reached equilibrium values, while the samples at the bottom show decreasing values with increasing depth which is inconsistent with the reflected normal maturity trend. The decreasing trend could be due to differential increases in the rate of producing 22R isomer versus the 22S isomer, due to the effect of thermal maturity or due to rapid destruction of the S isomer comparing to the R isomer.

Values for the Ts/(Ts+Tm) ratio range from 0.66 to 0.74 for Sirt Shale samples and support the idea that these rocks are thermally mature. This parameter is commonly used for maturity assessment, although it varies with the source of organic matter (Seifert and Moldowan, 1978). The moretane/C_{30} hopane ratios are low in all samples and range from 0.08 to 0.11. Anything less than 0.15 indicates that the rocks are mature (Peters and Moldowan, 1993). Moretanes are less stable than hopanes, and decrease in concentration more rapidly than regular hopanes with increasing maturity and all or most, of the moretane loss occurs at very low values of maturity.

The ratios of tricyclics to hopanes have been found to be a good parameter for investigating the thermal maturity of oils and source rocks. Generally, in this study

the carbon number distributions of tricyclic terpanes are dominated by the C_{23} tricyclic terpane as found in most geological samples (Farrimond et al., 1999). The ratios of the C_{23} tricyclic to C_{30} hopane range from 0.12 to 0.28 and generally these ratios are consistent with increasing depth and maturity. At high levels of maturity tricyclics are released from kerogen at higher rates than 17α(H)-hopanes due to their stability at the higher level of thermal maturity (Peters et al., 1990). The ratios of C_{24}/C_{23} tricyclics range from 0.40 to 0.73 and increase with depth. Cassani et al. (1988) have observed that with increasing maturity there was a decrease in the abundance of the C_{23} tricyclic compounds relative to the C_{21} and C_{24} tricyclics in the La Luna Formation, Maracaibo Basin, Venezuela which is also Upper Cretaceous in age. However, Farrimond et al. (1999) observed a decrease in the C_{24}/C_{23} and C_{26}/C_{23} tricyclic terpane ratios through the oil window. This trend is dissimilar to the trends observed for source rocks in this study and trends of Cassani et al. (1988) because of rapid igneous intrusive heating which is not present in the samples from Sirt Shale where the heating occurred as a result of burial and increasing maturity.

The 20S/(20S+20R) ratios in this study range from 0.44 to 0.53, and ββ/(ββ+αα) ratio range from 0.51 to 0.63. The sterane ratios for all samples indicate that the equilibrium values have not been reached with the exception of one sample which has an 20S/(20S+20R) ratio of 0.53. These values for the sterane ratios suggest that these samples are mature according to Huang et al. (1991). Huang et al. (1991) suggested that a value of 0.25 for the C_{29} sterane 20S/(20S+20R) ratio and ββ/(ββ+αα) as a margin between immature and low thermal maturity while a value of 0.42 was considered as boundary between low maturity and maturity.

CHAPTER V

5. Oil Geochemistry

Eighteen crude oil samples were collected from the Zaltan Platform, Az Zahrah-Al Hufrah platform, Al Bayda platform and Al Kotlah Graben of the central Sirt Basin. The organic geochemical parameters indicate that these oils were sourced form marine organic matter deposited under oxic to suboxic conditions. The oils were divided into four groups according to the stable carbon and hydrogen isotope analysis of the whole oils and thermal maturity of the oils based on saturate and aromatic parameters. The highest maturity crude oils were observed in the deepest reservoir. Oils at shallower depths were less mature. Two samples from the shallowest reservoir in the area show slight biodegradation. These two samples show depletion of n-alkanes and an increase in the isoprenoid/n-alkane ratios. The isoprenoids, hopanes, and steranes were unaffected which has been observed to be associated with minor biodegradation. This evidence suggests that there were at least two different sources for the crude oil in this area.

5.1 Crude oil classification

Gas chromatography (GC) was performed on saturate fractions to identify the n-alkane/isoprenoid (pristane and phytane) distribution. GC-MS analysis was performed using the branched and cyclic portion of the saturate fractions to identify the biomarkers and aromatic fraction for use in this study. Data analysis of each saturate fraction obtained triterpanes (m/z 191, steranes (m/z 217) and monoaromatic steroids (m/z 253) while data containing the aromatic fraction consisted of triaromatic steroids

(m/z 231), phenanthrene (m/z 178), methylphenanthrene (192) and dibenzothiophene (m/z 184). The samples in this study are divided into four groups (A, B, C and D) with one (B) containing two subgroups (B1 and B2).

Group A: oils were collected from the Upper Cretaceous Kalash Formation of the Al Kotlah and Khuf oilfields at Al Kotlah Graben in between the Az Zahrah-Alhufrah and Al Bayda platforms. The oils can be characterized by relatively low diasterane/C_{27} R regular sterane, pregnane/ C_{27} R regular sterane, C_{29} ββ/(ββ+αα) and C_{23} tricyclic/ C_{30} hopane ratios. The ratio of short to long chain monoaromatics and triaromatics contain relatively low values. They have high Pr/C_{17} and Ph/C_{18} ratios if the biodegraded samples are excluded.

Group B: oils were divided into two subgroups (B1 and B2) according to the age of the formations and their n-alkane distributions. Subgroup B1 consists of two crude oils from the Middle Eocene Gialo formation. One is from South East Zaltan and the other is from South Jebel fields, located in the Zaltan Platform. Both show slight biodegradation where some n-alkanes were removed. Subgroup B2 came from the Upper Cretaceous Tagrift Formation and Paleocene Al Bayda and Zaltan formations. One sample is from the Al Bayda formation in the Al Bayda oilfield on the Al Bayda Platform and other is from the Tagrift Formation in the Haram oilfield in the Az Zahrah-AL Hufrah Platform. This subgroup consists of also five samples from the Zaltan and one sample from the West Meghil oilfields from the Zaltan formation. Group B oils show relatively moderate diasterane/C_{27} R regular sterane, pregnane/C_{27} R regular sterane, C_{29} ββ/(ββ+δδ) Pr/C_{17} and Ph/C_{18} ratios. They also have low C_{23} tricyclic/ C_{30} hopane ratios.

Group C: these oils came from fields located on the North Zaltan Platform. Reservoirs were from the Gargaf Formation and of Cambrian-Ordovician age from the East Arashad, and Lahib oilfields. These oil samples are characterized by a relatively high abundance of tricyclic compounds compared to hopanes. This group of oils had the highest diasterane/C_{27} R regular sterane, pregnane/C_{27} R regular sterane, C_{29} ββ/(ββ+αα) and C_{23} tricyclic/ C_{30} hopane ratios. However, Pr/C_{17} and Ph/C_{18} ratios are lower than that of Group B.

Group D: consists of only one sample collected from the Cambrian-Ordovician age in the Gargaf Formation on the North Zaltan Platform. This sample contains low C_{23} tricyclic/ C_{30} hopane, diasterane/C_{27} R regular sterane and pregnane/C_{27} R regular sterane ratios. It is characterized by relatively low Pr/C_{17} and Ph/C_{18} ratios, low abundance of steranes and hopanes, with little to no tricyclic terpanes compared to the hopanes. The C_{29} ββ/(ββ+αα) ratio is moderate like that of Group B.

5.2 Source Input and Depositional Condition

5.2.1 n-Alkane and Isoprenoid

The n-Alkane distributions in crude oils and source rocks may reflect the origin of the organic matter of the source (Volkmann et al., 1986). GC performed on saturate fraction of Sirt Basin oil shows a normal alkane distribution range from C_{12} to C_{35} maximizing at C_{16} and C_{17}, indicating the oil samples are of marine algal origin (Appendix III and Figure 5-1). The n-alkane distributions in representative oil samples from the studied fields of the Sirt Basin show generally similar carbon number distribution (Figure 5-1). The n-alkane distribution and carbon number distribution

curve of normalized C_{10} to C_{33} n-alkanes show that the oils are dominated by low molecular weight compounds and the high molecular weight n-alkanes are less abundant, which may suggest that these oils are derived from kerogen deposited in marine environments. However, two samples from the Gialo formation show slight biodegradation where some of n-alkanes have been removed, but were excluded.

The pristane/phytane ratio is commonly used as an indicator of redox conditions in the depositional environment of organic matter (Powell and McKirdy, 1973; and Didyk et al., 1978). During oxic condition, the phytol side-chain of chlorophyll is believed to form pristane, while under anoxic conditions, phytane is produced. All oil groups in this study show pristane/phytane ratios between 1.24 and 2.12 which may suggest oxic to suboxic condition for the depositional environment (Hunt, 1996; Peters et al., 2005). Hughes et al. (1995) suggested a cross plot of DBT/P vs. Pr/Ph to identify lithology and the depositional environment of the source rock that produced the oils. The crude oil samples of Sirt Basin show low DBT/P ratios. The plot of the studied oils indicates these crude oils were most likely generated from shale source rocks deposited in marine environment (Figure 5-2).

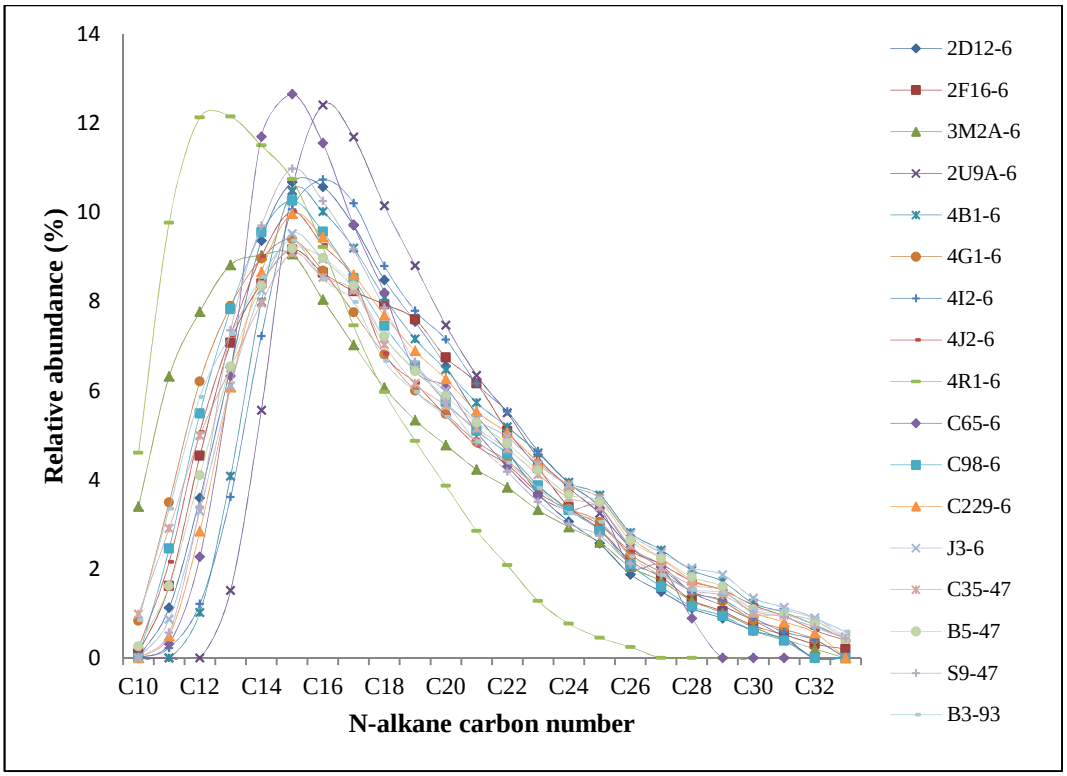


Figure 5-1. The carbon number profile of normalized C_{10} to C_{33} n-alkanes from oil samples of Sirt Basin.

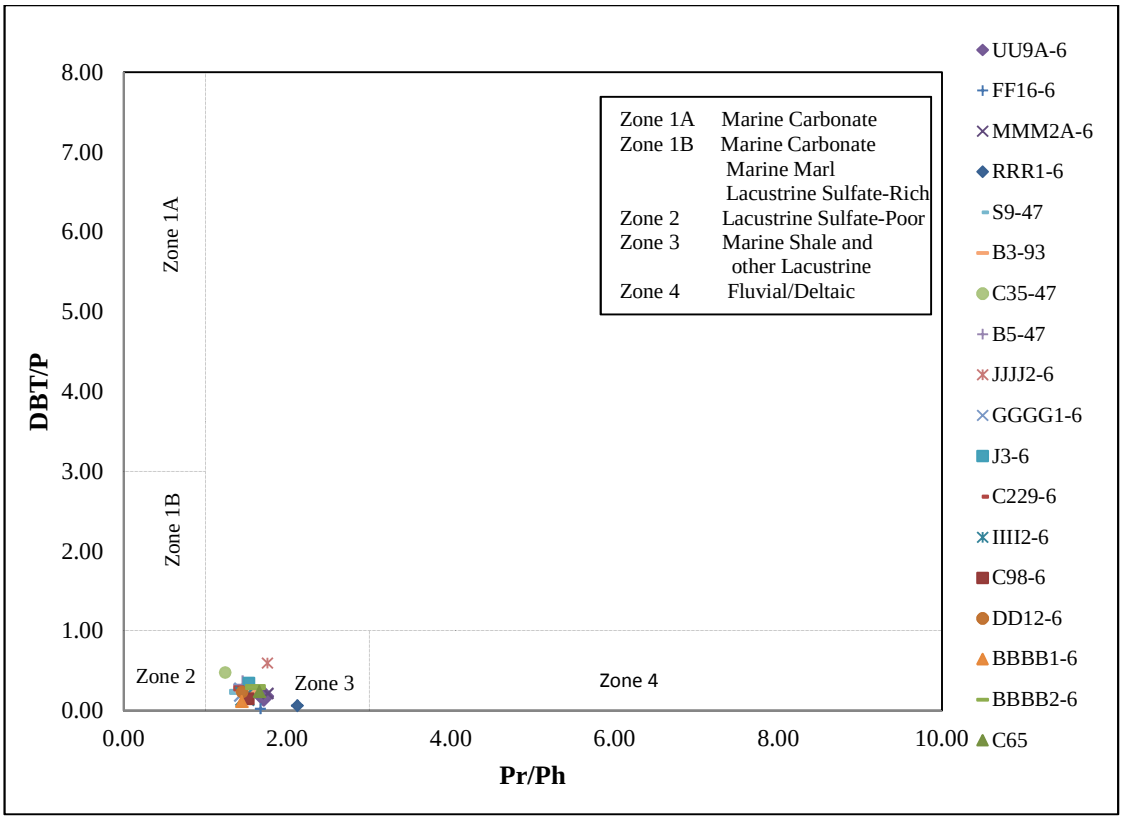


Figure 5-2. Cross plot of Pr/Ph versus DBT/P indicates the shale lithology and the marine depositional environment of the Sirt Shale.

The low Pr/nC_{17} and Ph/nC_{18} ratios range from 0.11 to 0.76 and 0.07 to 0.72, respectively in non-biodegraded samples. These values suggest deposition in an open marine environment (Lijmbach, 1975). A plot of Pr/nC_{17} versus Ph/C_{18} can be used to indicate the type of organic matter (Figure 6-3). The distribution of samples on this plot suggests a marine environment for organic matter within the rocks. This plot also shows the effect of thermal maturity and biodegradation on the oils. In the Figure 5-3 all samples are found in the marine organic matter type. Two of the analyzed oils are located in the upper right area of the diagram and have the highest values (one of them is out area plot) due to the effect of biodegradation. Three other oils can be easily recognized on the left hand side of the diagram as having the lowest values due to the high level of maturity. The sample in Group D does not fit plotted area and would be found outside the lower left corner of the diagram. It has the lowest n-alkane/isoprenoid ratio value among the studied oils.

5.2.2 Terpane Parameters

In this study, crude oil samples from Sirt Shale have different terpane distributions among the different oil groups. Group A and B have similar terpane distributions and show a high number of hopanes than tricyclic terpanes which may indicate that they have similar organic matter type (Figure 5-4). Group C oils have higher tricyclic terpanes than hopanes while group D lack tricyclic and tetracyclic terpanes but the hopanes are presented, which indicate that this group has different organic sources from the others (Fig 5-5).

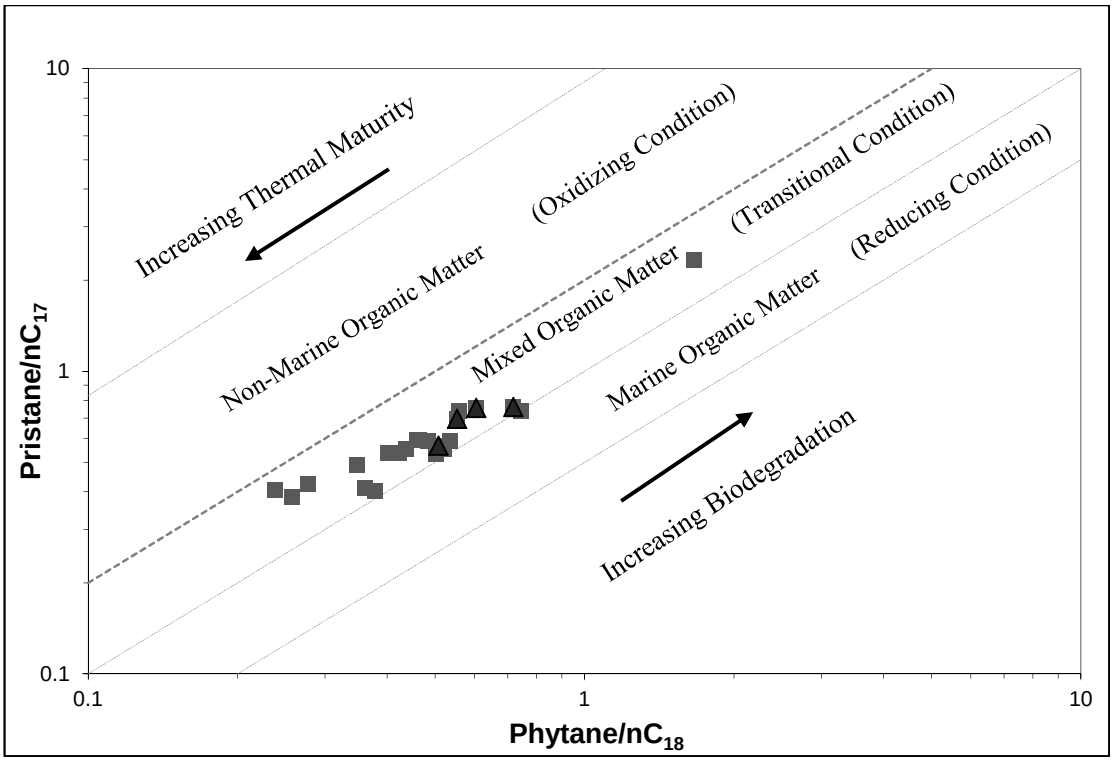


Figure 5-3. Plot of Pr/nC_{17} vs. Ph/nC_{18} of crude oils used in this study. The squares are oils from Concession 6 and triangles are oils from Concession 47.

High C_{35} homohopanes is an indicator of oxic marine conditions during deposition which is reflected in the 22R+22S $C_{35}/(C_{31}\text{-}C_{35})$ homohopane ratio. This ratio is used to estimate the redox conditions of the depositional environment of the source rocks. These ratios studied in all groups are very low, ranging from 0.03 to 0.11 which may indicate oxic conditions in the depositional environment. This is consistent with the conditions suggested by high pristane/phytane ratios. In the studied samples, C_{29} and C_{30} 17α (H)-hopanes, the two most abundance terpanes and the C_{29}/C_{30} hopane ratios between 0.37 and 0.91 may indicate the clay-bearing character of the source rocks

$G/C_{31}R$ homohopane ratio ranges from 0.27 to 0.62 which may indicate a saline environment. The oil groups show low abundance of C_{24} tetracyclic terpanes which could be used as a characteristic of clastic marine depositional environments since a high abundance of C_{24} tetracyclic has been reported to be associated with a high input of terrestrially derived organic matter (Philp and Gilbert, 1986) and carbonate (Zumberge, 1984; Connan et al., 1986; Prince et al., 1987; Clark and Philp 1989) and evaporate (Connan et al., 1986; Clark and Philp 1989) depositional environments. The ratios of C_{23} tricyclic to C_{30} hopane range from 0.22 to 8.75 and support the nature of the marine environment even though the sample shows a maturity effect for this ratio.

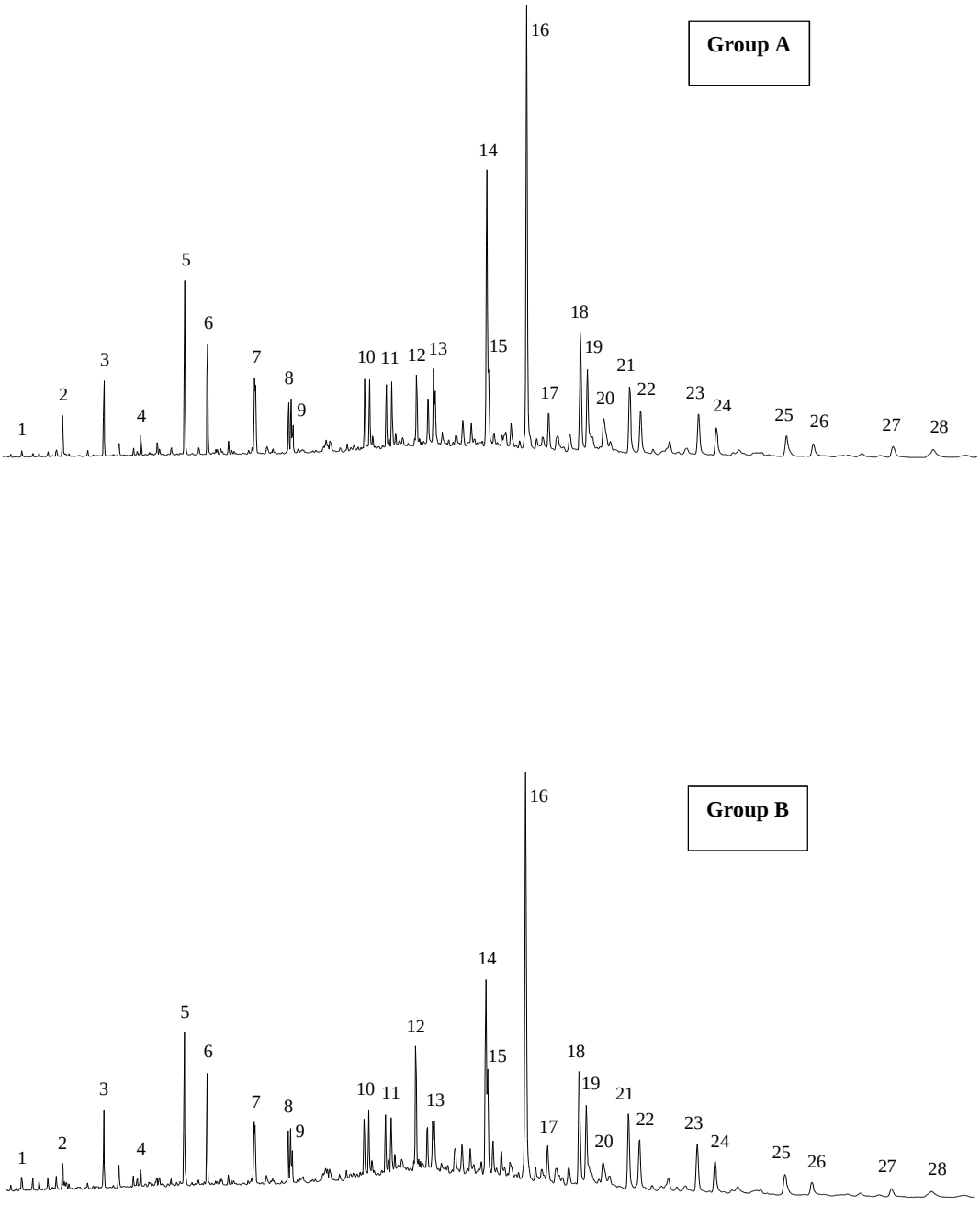


Figure 5-4. Terpane (m/z 191) distribution of group A and B of Sirt Basin Oils.

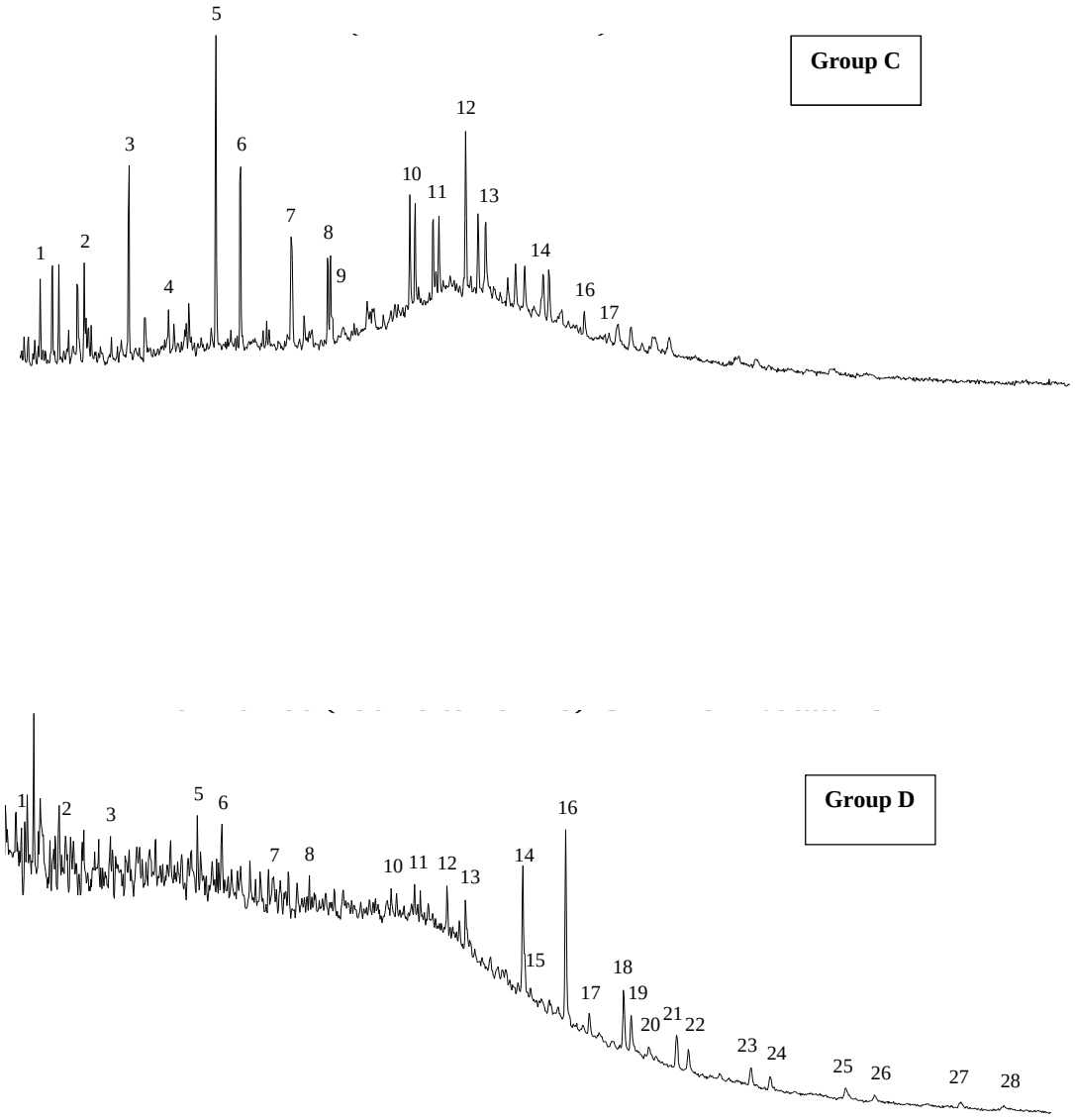


Figure 5-5. Terpane distribution of group C and D of Sirt Basin Oils.

5.2.3 Sterane Parameters

Figure (5-6 and 5-7) show the distribution of steranes for all groups (see Table 4.3 for peak identifications). The relative abundance of C_{27}, C_{28} and C_{29} steranes have been found to be a good indicator for organic matter type. All of the studied samples show a high abundance of C_{27} steranes that are believed to be derived from marine organic matter (phytoplankton) and a relatively low abundance of C_{29} steranes indicate a low contribution from higher plant organic matter evident in the high ratios of C_{27}/C_{29} steranes (Appendix III). The samples show moderate abundance of C_{28} compounds, which indicates a contribution by lacustrine algae. The diagram of Huang and Meinschein (1979) supports the marine source type of organic matter. The presence of C_{30} steranes (Figure 5-6 and 5-7) in the studied crude oil samples strongly indicates marine organic matter for these rocks. The ratio of C_{28}/ $C_{29}\alpha\alpha$ steranes is considered to be parameter to estimate the age of oils in marine settings as it increases from Precambrian to Tertiary due to the relative increase of C_{28} steranes and the decrease of C_{29} steranes through geological time. In the studies, this ratio ranges from 1.04 to 1.36 (Appendix III) which suggests they could be generated from Upper cretaceous source rocks.

C_{27} Diasteranes/ C_{27} R regular steranes ratios are generally high in Groups B, C and D but low in Group A which may reflect the effect of thermal maturity on these. In these samples these ratios can be an additional indicator of rich clay content in the source rocks.

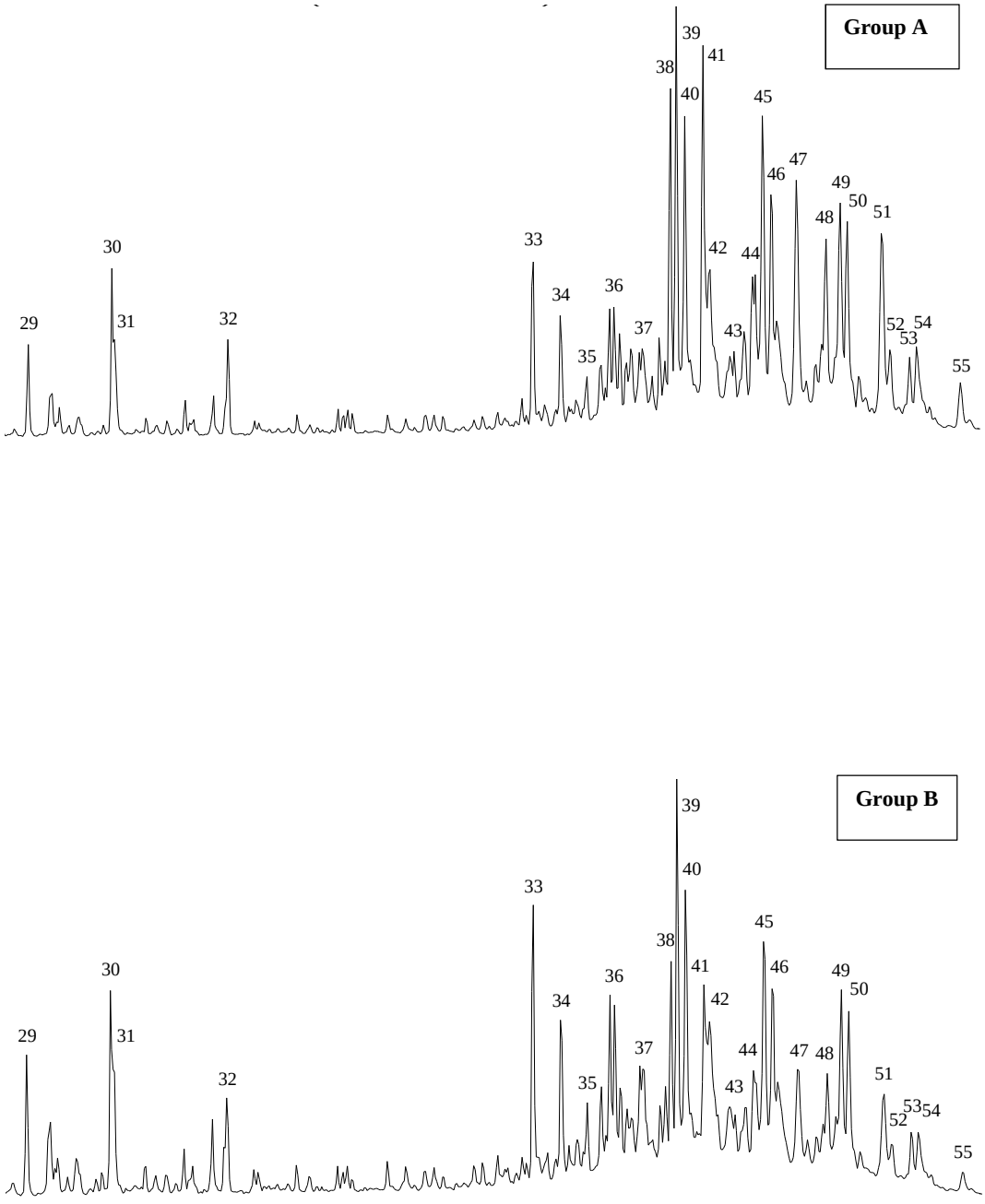


Figure 5-6. Sterane distribution (m/z 217) of group A and B of Sirt Basin Oils. Group A shows high C_{27} regular steranes (peak 41) compared to diasterane (peak 33).

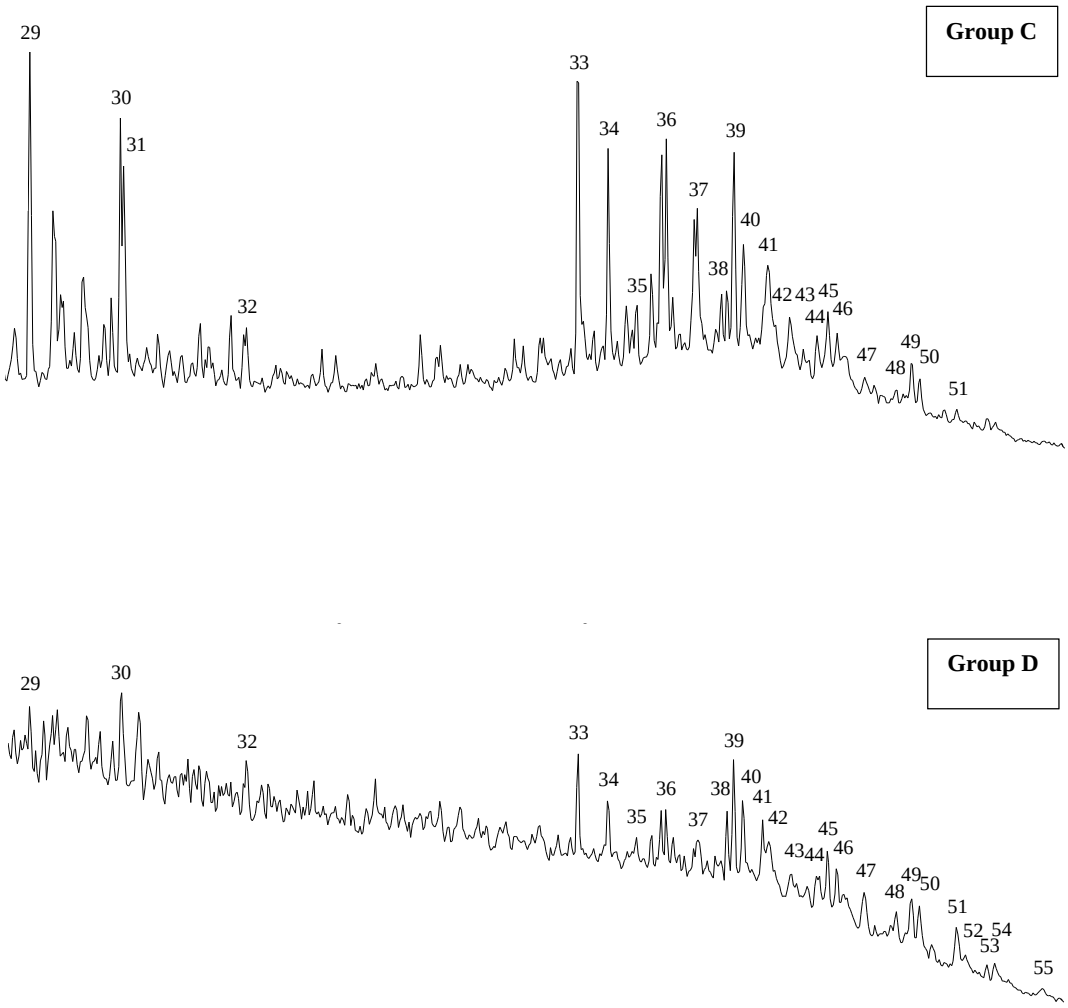


Figure 5-7. Sterane distribution (m/z 217) of group C and D of Sirt Basin Oils.

5.3 Thermal Maturity

5.3.1 Terpane Biomarker Parameters

Both moretanes and hopanes are used to estimate the level of thermal maturity of the oil and source rock (Peters and Moldowan, 1993). In this study the Moretane/ Hopane ratio is low, 0.09 and 0.14 for A and B groups while it is below the detection limit for group C and D. The ratio of the Ts/(Ts+Tm) ratio values range from 0.48 to 0.76 for all oil groups. This biomarker could be influenced by either maturity or source type.

The ratios 22S/(22S+22R) of hopane of Group A range from 0.52 to 0.54. Group B1 contain values ranging from 0.53 to 0.54 while Group B2 show values in between 0.52 and 0.59, indicating that these samples have not reached the oil generation window. Peters et al. (2005) proposed that samples containing ratios in the range of 0.50 to 0.54 have barely entered the oil generation window while ratios in the 0.57 to 0.62 oil range indicate the main phase of generation has been reached or surpassed (Peters and Moldowan, 1993). Group C oils show a ratio that has reached equilibrium values (0.59 to 0.68) with one exception for the sample with the low value of 0.53 which could be caused by faster destruction of the S isomer in higher stages of the oil window (Farrimond et al. 1996). The Group D sample reached the equilibrium value 0.62. However, this ratio indicates the source rocks of all oils have entered the oil generation window as seen in Groups A and B, or passed it as in C and D Groups.

5.3.2 Sterane Biomarker Parameters

The ratio of 20S/(20S+20R) is the most common used steranes to estimate the level of maturity for oil and source rock. The biologically produced form is 20R decrease with increasing maturity while 20S increases with increasing of the maturity. The equilibrium between the two forms is reached within the range of 0.52 and 0.55 where recordable changes in maturity can be observed (Seifert and Moldowan, 1986; Waples and Machihara, 1990, Peters and Moldowan, 1993). Group A samples have the same value for this ratio (0.49). Group B1 have high values (0.50 & 0.53) while Group B2 samples have values ranging from 0.44 to 0.53 showing equilibrium. Group C oils have the highest values ranging from 0.54 to 0.56 while the Group D sample has value of 0.52. Groups C and D are considered to have reached equilibrium values.

The relative abundance of $C_{29}\beta\beta$ to $C_{29}\alpha\alpha$ is another maturity parameter that operates beyond the start of the oil window; therefore, this ratio is more reliable when applying to higher levels of maturity than 22S/ (22S+2sR) homohopane ratios. Group A oils show relatively low values of ($\beta\beta/(\beta\beta+\alpha\alpha)$ ratios, that range from a 0.50 to a 0.52 while Groups B1 and B2 exhibit moderate values, ranging from 0.57 to 0.64 that do not reach equilibrium. Group C samples reach equilibrium between 0.67 and 0.71. The sample of Group D shows a moderate 0.64 value (Figure 5-8). This ratio can be influenced by several factors such as heating rate, presence of clay minerals, the nature of the source material and the depositional environment (Philp, 2007) or lithology (ten Haven et al., 1986; and Rullkötter and Marzi, 1988).

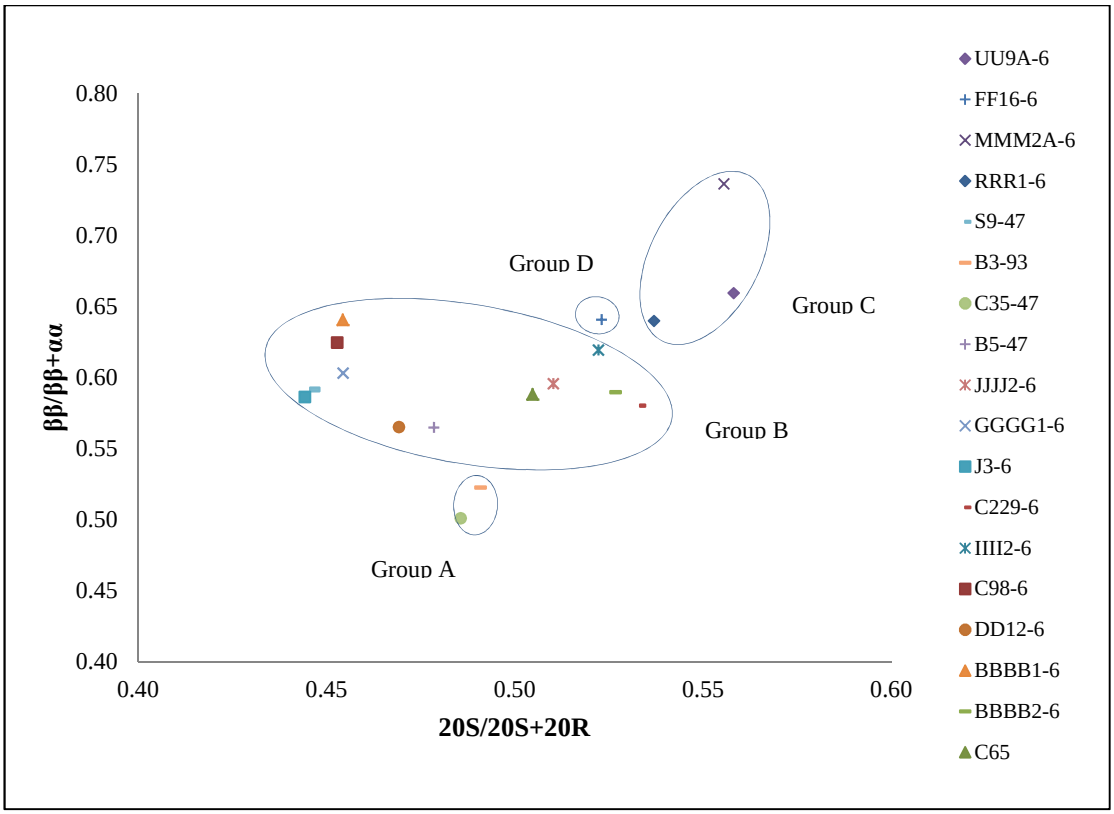


Figure 5-8. C_{29} 20S/(20S + 20R) versus C_{29} ββ/(ββ + αα) steranes ratios for oils from the Sirt Basin.

5.3.3 Aromatic Hydrocarbons

Aromatic hydrocarbons can be used to assess thermal maturity of crude oils. Two series of aromatic steroids were recognized using GC-MS analysis, the monoaromatic and triaromatic hydrocarbon steroids with mass chromatogram of m/z 253, m/z 231 respectively (Philp, 1985). The distribution of aromatic steroids has been commonly used as parameter for the study of crude oil thermal maturity as well as source rocks (Peters and Moldowan, 1993).

Mass chromatograms of the investigated oils clearly show a significant difference in the distribution pattern of monoaromatic and triaromatic steroids (Figure 5-9 and 5-10). Even though Groups A and B show all monoaromatic and triaromatic compounds in typical a distribution. Compared to Group A, Group B has a higher ratio of short chain to long chain compounds. These differences could be due to different maturation, where Group B shows a higher maturity level than Group A, as seen from biomarker analysis. Groups C and D are highly mature, which can be observed from the low concentration of biomarker compounds and the noise in the chromatograms (Aldahik, 2010). The difference between triaromatic hydrocarbon steroids in Group C and D can be related to the difference of organic matter type which is consistent with the biomarker distribution.

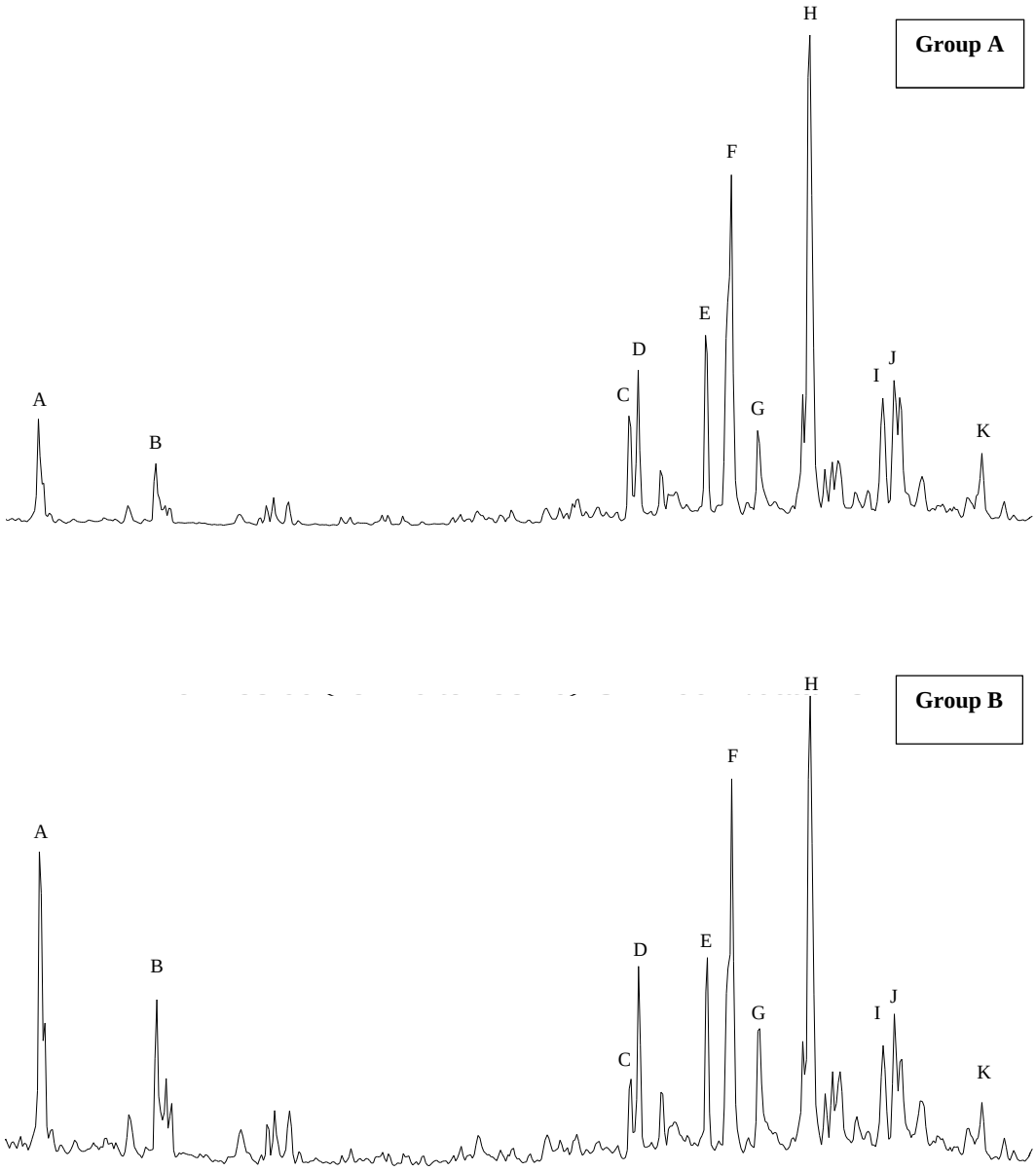


Figure 5-9. Mass chromatograms of m/z 253 showing the distribution of the monoaromatic steroid hydrocarbons in crude oil of Sirt Basin.

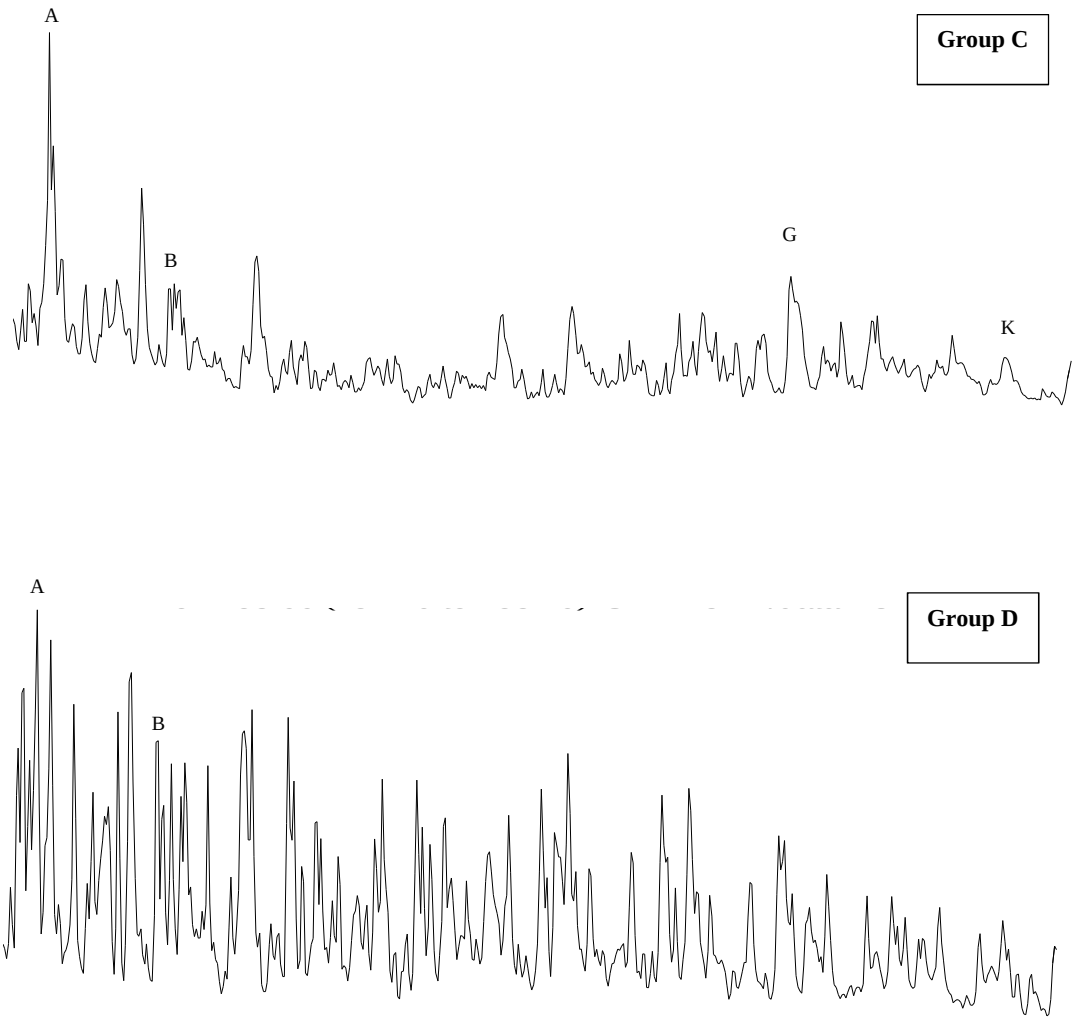


Figure 5-9.…….continued

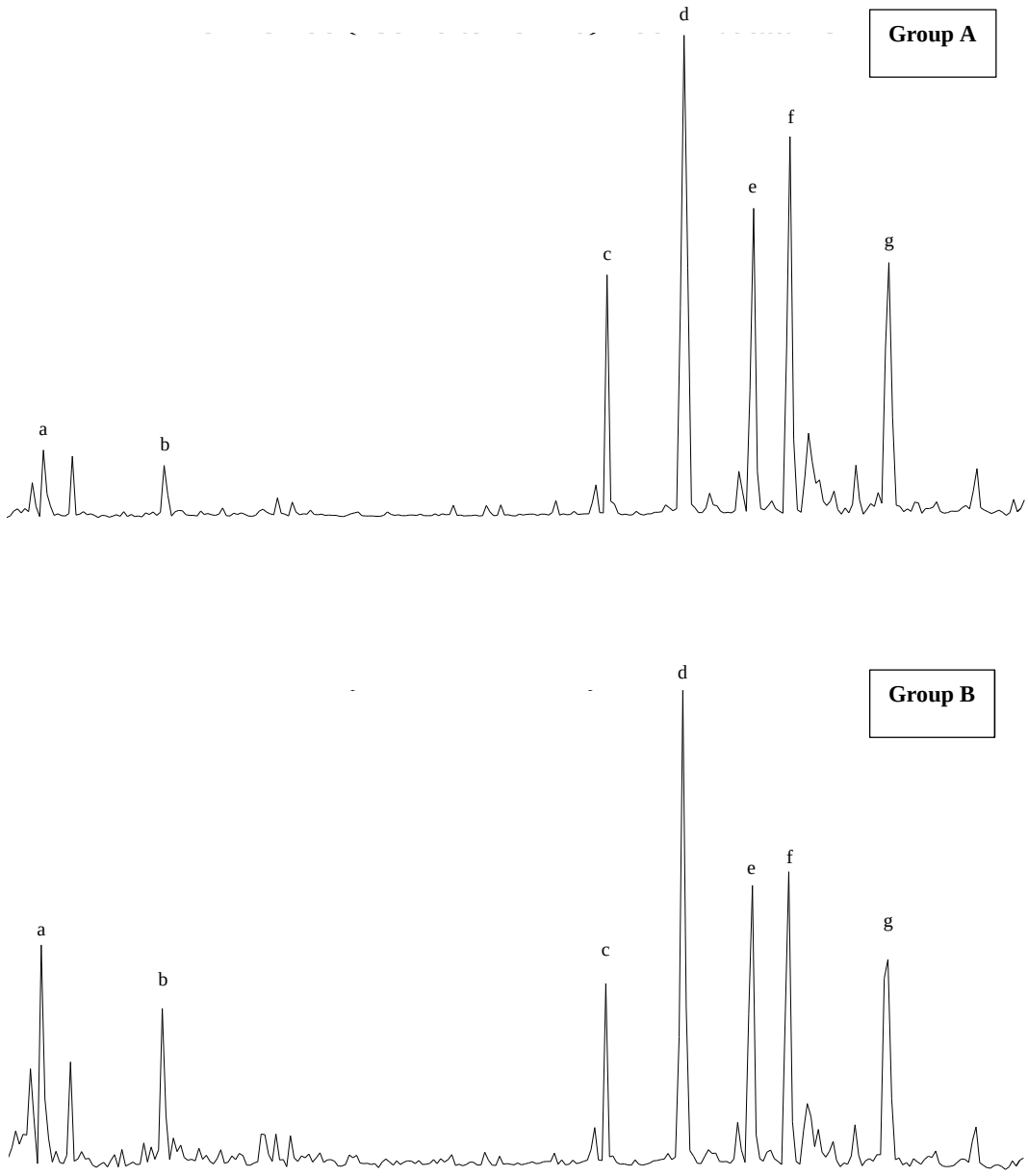
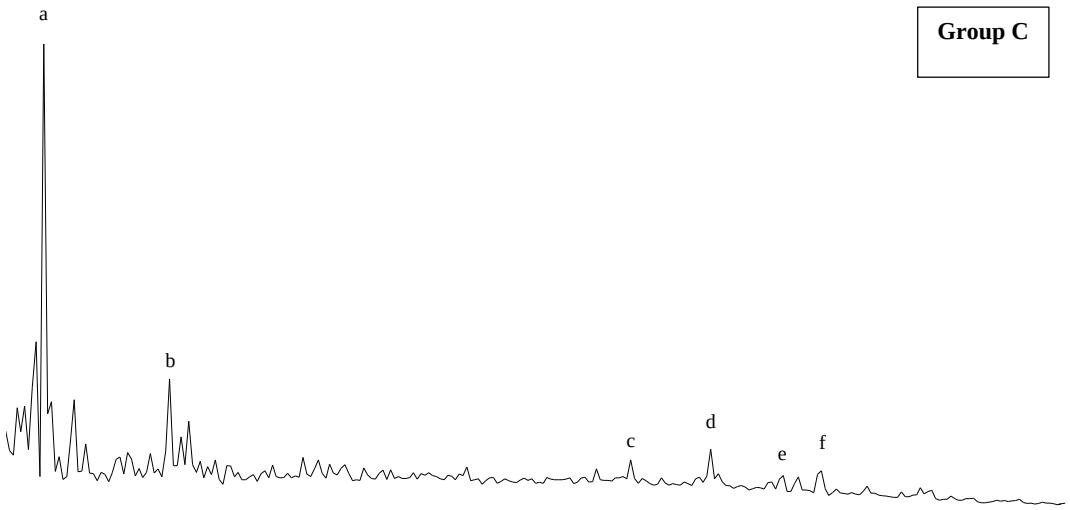


Figure 5-10. Mass chromatograms of m/z 231 showing the distribution of the triaromatic steroid hydrocarbons in crude oil of Sirt Basin.



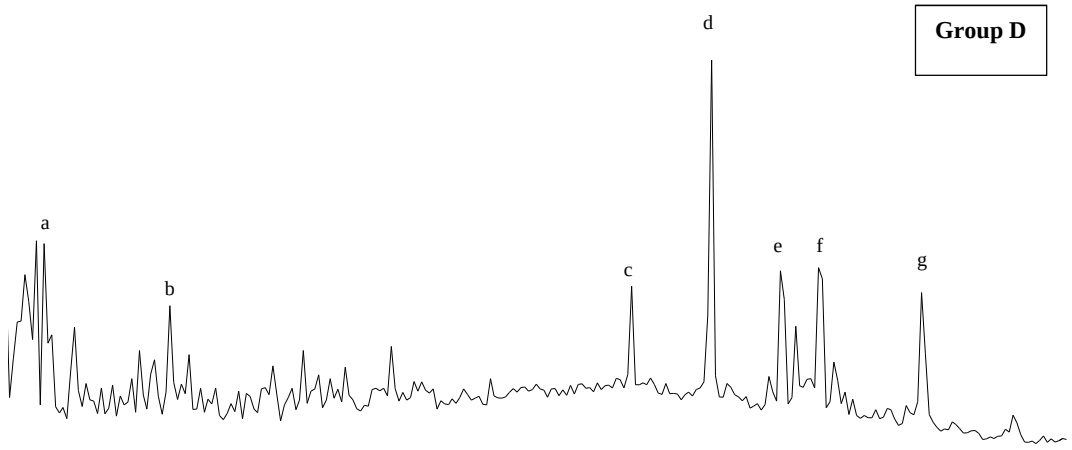


Figure 5-10.……continued

The relative abundance of short chain to compared long chain monoaromatic (MA(I)/MA(I+II) and triaromatic (TA /(TA+MA)) hydrocarbon steroids ratio increases during maturation and is applied to estimate thermal maturation of oil and source rocks particularly in the late oil window, when other maturity biomarkers cannot be used to estimate the level of thermal maturity. The calculated (MA(I)/MA(I+II)) and (TA / (TA+MA)) ratios for crude oils investigated in this study are shown in Appendix IV. A plot of (MA(I)/MA(I+II) versus TA / (TA+MA) show the sample groups from Sirt Basin are clearly distinguished (Figure 5-11). This plot indicates that Groups A and B (B1 and B2) show only slight differences in the distribution of aromatic steroids which could be explained by similar organic matter within different facies. The Group D sample is characterized by a different plot from group C that indicates it contains a different type of organic matter.

The Methylphenanthrene Index (MPI-1) has been derived from the distribution of phenanthrene and methylphenanthrene isomers. Even though, it is influenced by the lithology, source and the organic matter type (Cassani et al., 1988), MPI-1 is the most widely applied parameter for estimating the level of maturity (Radke & Welte, 1983). MPI-1 values within crude oils increase in accordance with maturity. In studied oils, the methylphenanthrene indices (MPI-1 and MPI-2) show evidence of the different thermal maturity of the three groups (Appendix IV and Figure 5-12).

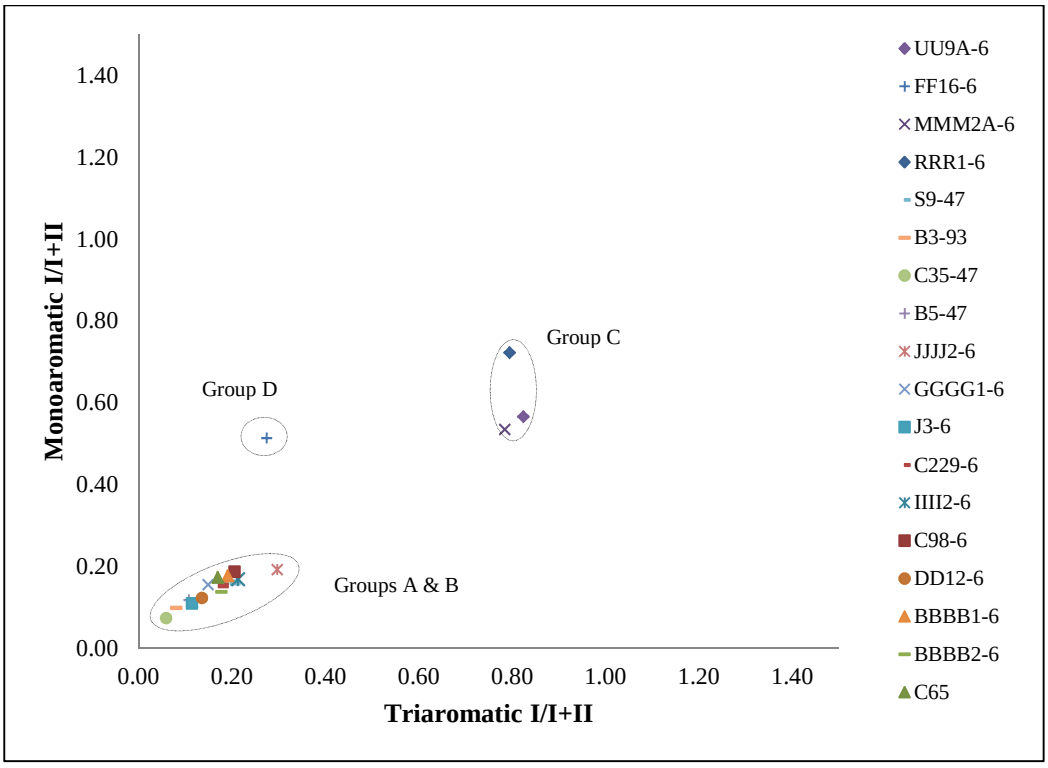


Figure 5-11. Plot of monoaromatic versus triaromatic steroid hydrocarbon of crude oils.

Using the MPI-1 parameter, the vitrinite reflectance (% Rc) can be calculated using two equations (Equation 6.1 and Equation 6.2) of Radke et al. 1987.

%Rc = 0.6*MPI-1 + 0.4 for the Rm<1.3 (Equation 5-1)

%Rc = 0.6*MPI-1 + 2.3 for the Rm. 1.3 (Equation 5-2)

Group A and B samples show typical distributions of hopanes and steranes, characterizing of low maturity. Therefore using equation 5-1 should be used to calculate vitrinite reflectance. However, the second equation5-2 was used to calculate the % Rc for Groups C and D, because the hopanes and steranes of these samples are low in concentration due to high level of maturity. The % Rc of Group A and B oils range from 0.75-0.82 and from 1.46 to 1.82 for Group C while the Group D oil has a value of 1.08.

The calculation of Rc can also be calculated using Boreham et al. (1988) equations.

%Rc = 0.7 MPI-1 + 0.22 for the Rm<1.7 (Equation 5-3).

%Rc = 0.55 MPI-1 + 0.3 for the Rm<1.7 (Equation 5-4).

The % Rc of oils in the range 0.62-0.71 for Group A and B, and C oils range from 2.23 to 2.56 while the % Rc of Group D oil is 1.88. The % Rc shows the rocks generated from Group A and B oils are mature within the oil generation window while the oils of Groups C and D show a post mature level. The difference between Groups C and D in % Rc calculations could be due to the source of the type of organic material.

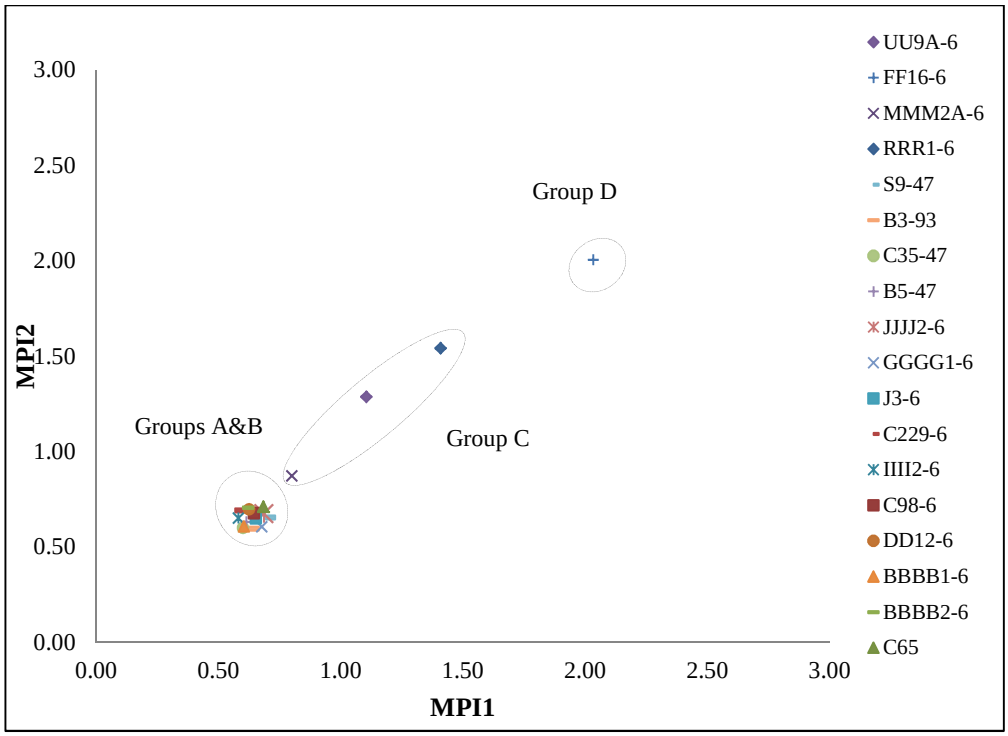


Figure 5-12. Plot of Methylphenanthrene Index I versus Methylphenanthrene Index II of crude oils.

5.4 Stable Isotopes

The stable isotopes of carbon and hydrogen analysis are excellent tools for correlating and analyzing crude oils and source rocks. The different physical and chemical processes cause variations in stable isotopic compositions. In this study the bulk isotope analysis for whole oil was used to measure stable isotopes of total carbon and hydrogen in the samples. Bulk analysis for saturated and aromatic fractions of crude oils was used for selected samples only. Bulk carbon stable isotope analysis of saturated and aromatic fractions in crude oils have been widely used to indicate the source of organic matter origin in crude oils; stable isotope compositions represent various types of organic matter (Sofer, 1984; Andrusevich et al., 1998). In addition to the origin-related differences of δD, hydrogen isotopic compositions are also affected by level of thermal maturity. It was thought that increasing of thermal maturity level can increase heavier hydrogen isotope in the organic matter within the source rock (Dawson et al. 2005, Radke et al., 2005). This is thought to caused by hydrogen exchange between the hydrocarbons in sediment during deposition and deuterium enriched formation waters (Schimmelmann et al., 1999). In addition to thermal maturity, biodegradation can change the stable isotope composition and have a minor effect on the whole oil (Sun et al. 2005).

Cross plots of $\delta^{13}C$ versus aromatic fractions in saturate fraction were used to separate oil groups of petroleum in the Sirt Basin (Figure 5-13.). The crude oils in Group C show higher values of $\delta^{13}C$ (isotopically the heaviest). More negative $\delta^{13}C$ values are observed in Group D while Group B plotted between Group C and D, indicating that they are isotopically lighter than Groups C and D. The difference in

isotopic composition of crude oils within Groups B and C are likely related to the different level of thermal maturity while the sample in Group D reflects a different organic meter source. Evidence of differences between groups are made clear and supported in plot δ13C versus δD for whole oil and the same results were accomplished (Figure 5-14). Crude oils were separated due to their similarity and therefore provided support for the existence of at least three oil groups in samples from the Sit Basin used in this study. The differences in stable carbon and hydrogen isotopic compositions of whole oil between oil groups are consistent with source and maturity variations observed by biomarkers.

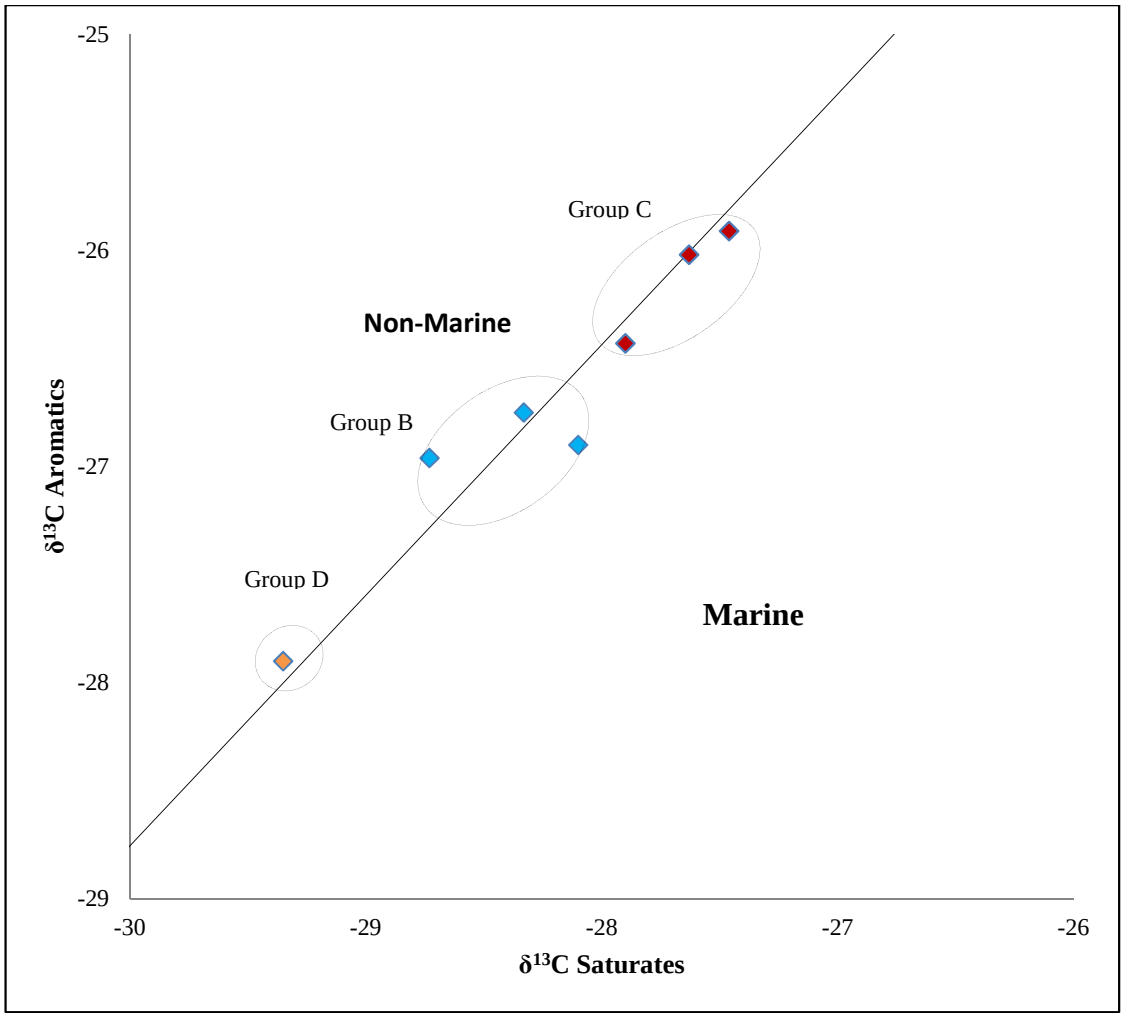


Figure 5-13. Cross-plot of $\delta^{13}C$ values of aromatic versus saturated hydrocarbons from crude oil samples from Sirt Basin with the boundary line separates marine and non-marine oils (Sofer, 1984). (Group A is not presented in the plot).

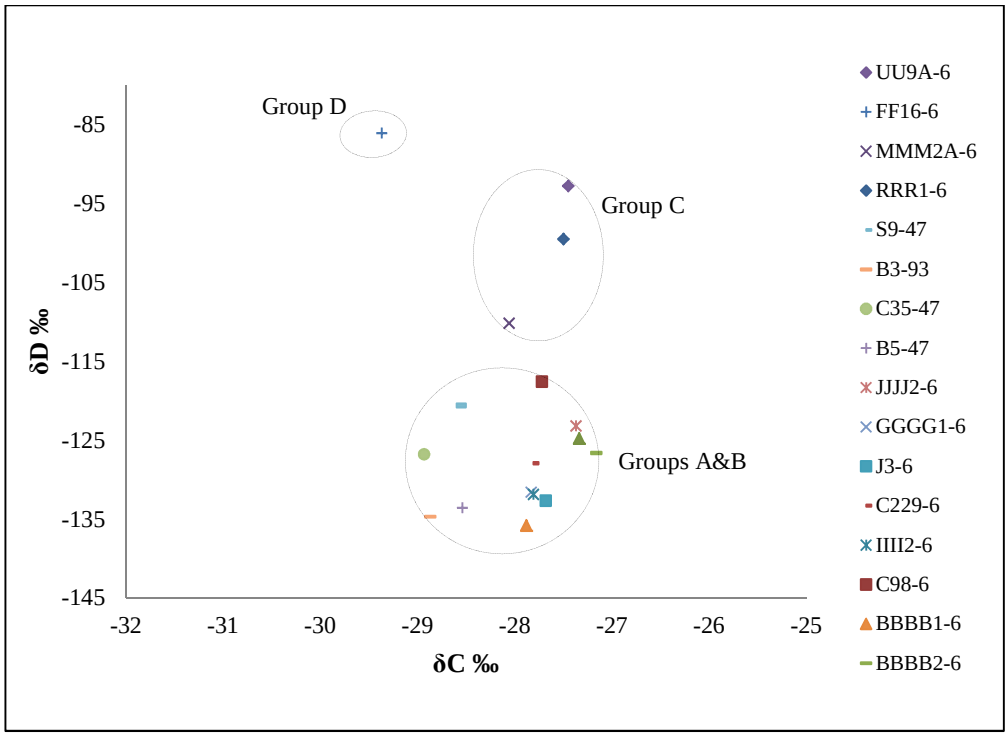


Figure 5-14. The plots $\delta^{13}C$ vs. δD for whole oil to delineate groupings of oils in the Sirt Basin.

5.5 Principle Component Analysis

The principle component analysis (PCA) is a powerful tool to classify and group oils using different geochemical parameters. In the PCA, the set of geochemical parameters are reduced to a few components that best explain variations in the data set. These geochemical parameters may have a difference in significance with regard to organic matter and oil. Therefore, some geochemical parameters may be controlled by thermal maturity, type of organic matter, lithology, or other processes.

New variables (principal components; also known as factors) will be generated from original geochemical parameters. The factors are organized according to their contribution to the geochemical parameters. In the PCA results are usually represented by score plots and loading plots. A score plot shows the distribution of the samples based on factors. A loading plot displays the distribution of geochemical parameters (Azevedo et al., 2008; Hur et al., 2009, Abdi and Williams, 2010).

Using Xlstat software, two factors were used to examine the distributions of geochemical parameters and to group the oil samples of Sirt Basin based on selected geochemical parameters. PCA data analyses of the crude oils are shown in the Appendix VII. The grouping of the samples was identified using the factors (factor 1 and 2) with the greatest contribution of geochemical parameters, 53.21% and 17.47% of explained variance. The score plot and loading plot (Figure 5-15) shows the sample distribution and the relations between them. Most of variation vectors representing the maturity parameters (the ratios of short chain to long chain of monoaromatic and triaromatic steroids, calculated vitrinite reflectance, pregnane/C_{27}R sterane ratio, C_{27}R Sterane/C_{29}R sterane ratio and C_{23}Tricyclic terpane /C_{30} hopane ratio) have

predominant factor 1(F2) over factor 2 (F2), as illustrated in the Figure (5-15). As a result, F1 axis represents the maturity. Whereas, the variation vectors representing Ts/(Ts+Tm) and $\delta^{13}C$, which can be influenced by both organic matter source and maturity. These vectors have predominant factor F2 over F1 (Figure 5-15; Appendix VII). Accordingly, F2 indicates the organic matter source (Pieri et al., 1996).

This analysis supports previous geochemical parameter result achieved by biomarker analysis. The bi-plot shows the distribution of the geochemical parameter and the relationships between them, as well as the contribution each geochemical parameter has on data variability. The PCA plot shows the oils can be grouped into three groups where Group A and B are related. Group C and D samples can be distinguished. The separation between Group A and B oils is not clear by PCA analysis. This may also support that Group A and Group B oils have originated from similar organic matter source rocks.

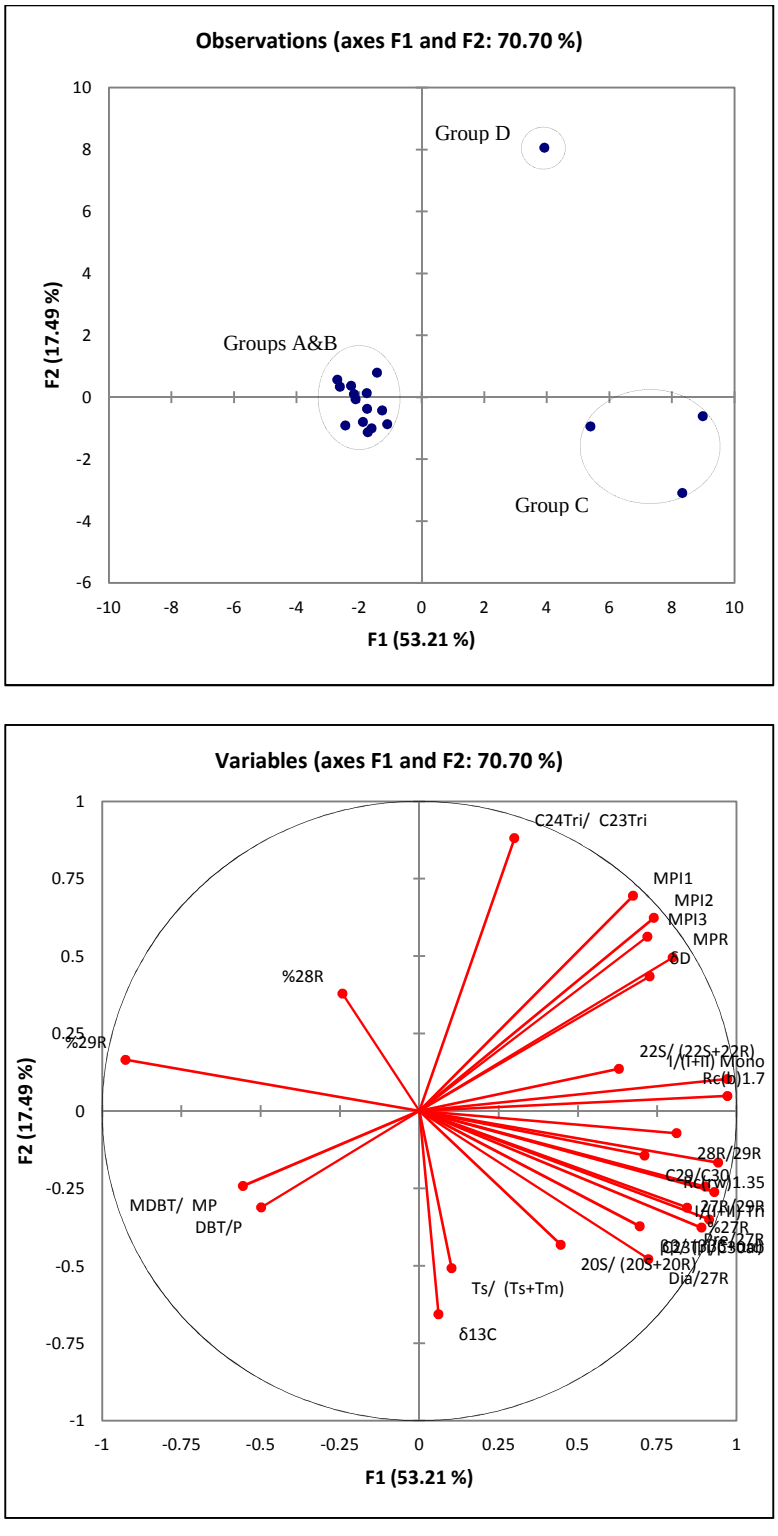


Figure 5-15. Score (top) and loading (bottom) plots of PCA for oil samples

5.6 Extent of Biodegradation

Biodegradation can change biomarker ratios if compounds in the oil were subjected to different degrees of bacterial attack. Biodegradation leads to a selective removal of certain compounds in crude oil (Peters and Moldowan, 1993; Wenger et al., 2001), starting with the saturated hydrocarbons first. Typically, the selective removal of n-alkanes indicates minor crude oil biodegradation. Normal alkanes degrade earlier than isoprenoids (Peters et al., 2005).

The two biodegraded oils in this study were found at shallower depths and are from the Mid Eocene Gialo formation. Both of them show a biodegradation rank in the range of 0 to 2 (Peters and Moldowan, 1993). At these biodegradation levels, isoprenoids, hopanes and steranes are not generally affected. Biomarker degradation typically occurs after isoprenoids are completely removed (rank 5). This is consistent with accepted requirements for aerobic bacterial degradation of crude oil, including abundance of oxygen and nutrients (e.g. nitrate), temperatures below about 80°C in circulating meteoric water, and low levels of hydrogen sulfide (Tissot and Welte, 1984; Hunt, 1996, and Peters et al., 1996). The ratios of Pr/nC_{17} and Ph/nC_{18} are widely accepted parameters used to determine the extent of oil biodegradation. In general, isoprenoids, such as pristane and phytane, are not removed during light to moderate biodegradation, while n-alkanes are obviously affected (Peters and Moldowan, 1993, Wenger et al., 2001). The two biodegraded samples in this study have higher Pr/nC_{17} and Ph/nC_{18} ratio (Figure 5-16), indicating the removal of n-alkanes by microbial activity. There was no biodegradation observed for hopanes and steranes Figure 5-17 and Figure 5-18).

However, on some occasions oils can contain n-alkanes and/or isoprenoids that show significant biomarker biodegradation. These cases are commonly due to mixing within a reservoir of multiple oil charges that have been degraded to different extents. However, in this study biodegraded oils were observed without evidence of mixing. Enrichment of 25-norhopanes is used to determine biodegradation in multiple charges of oil, where an abundance of 25-norhopanes is generally believed to be associated with severe biodegradation levels (Peters and Moldowan, 1993; Bennett et al., 2009). The absence of 25-norhopanes in these samples, indicate a lack of mixing of severely degraded and non-degraded oils (Figure 5-17). The study indicates that oils in Sirt Basin may have undergone biodegradation, inconsistent with previous studies conducted with Sirt Basin crude oils (e.g. Burwood et al., 2003; Aboglila et al., 2010). The rest of the oils analyzed in this study show no sign of biodegradation. Mixed-system hybrid oils have been observed in Sirt Basin without evidence of any biodegraded oil (Burwood et al., 2003).

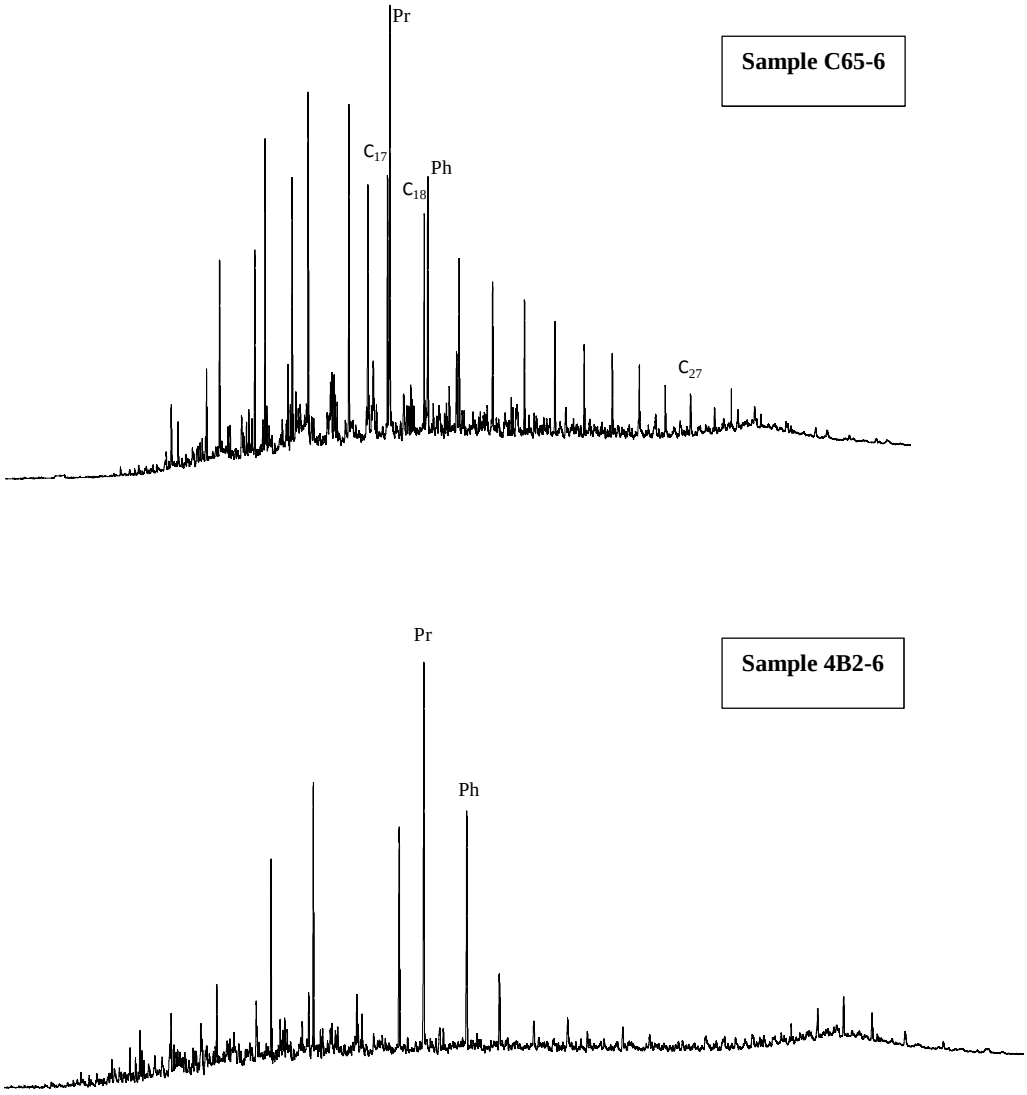


Figure 5-16. Gas chromatogram of the two samples from the Galio Formation showing removal of n-alkane while pristane and phytane are still present.

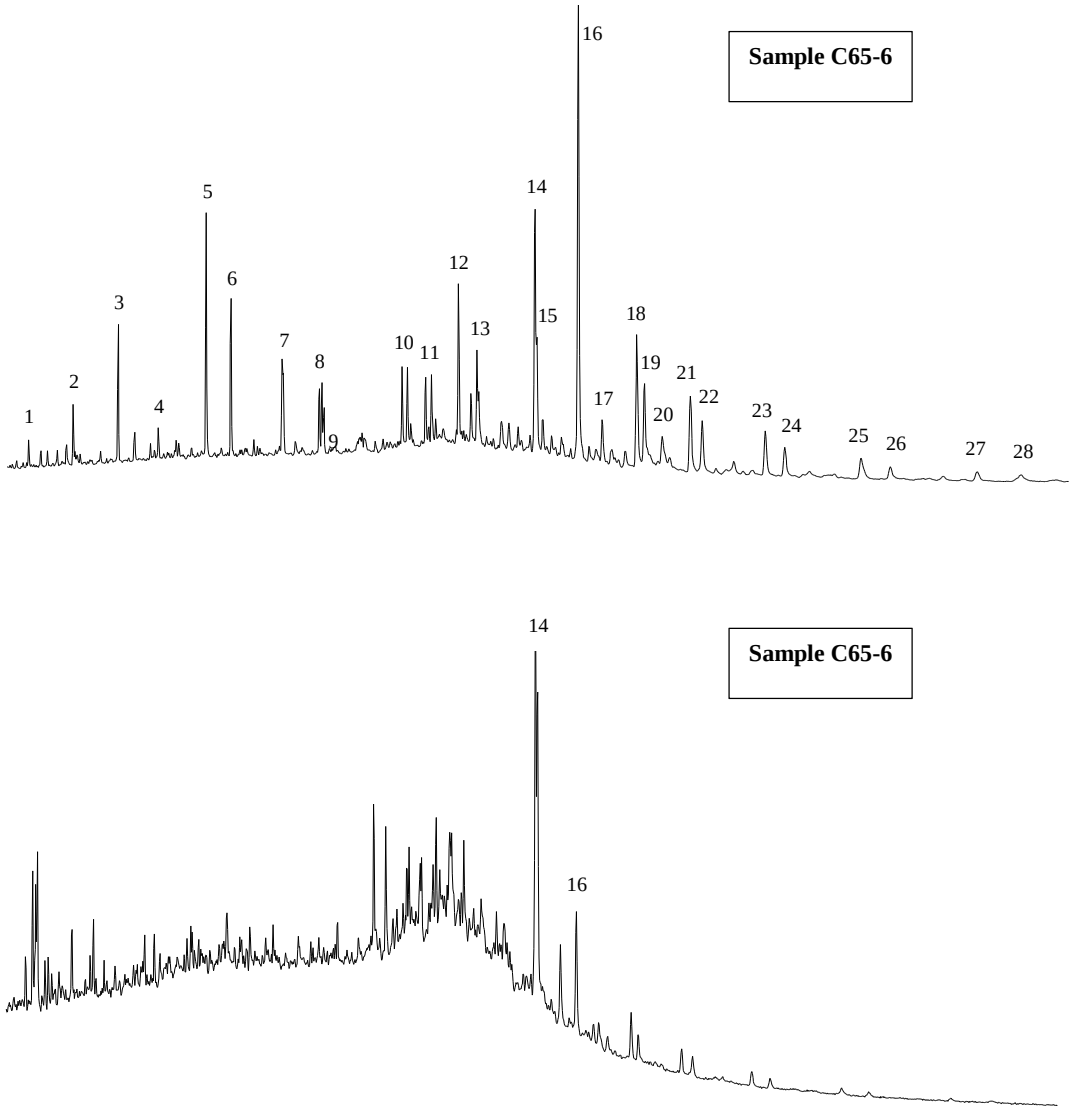


Figure 5-17. Mass chromatograms of m/z 191 and m/z 177 of the two samples from Galio Formation showing that the biodegradation does not affect the hopane which is supported by the absence of the25-norhopane biomarker.

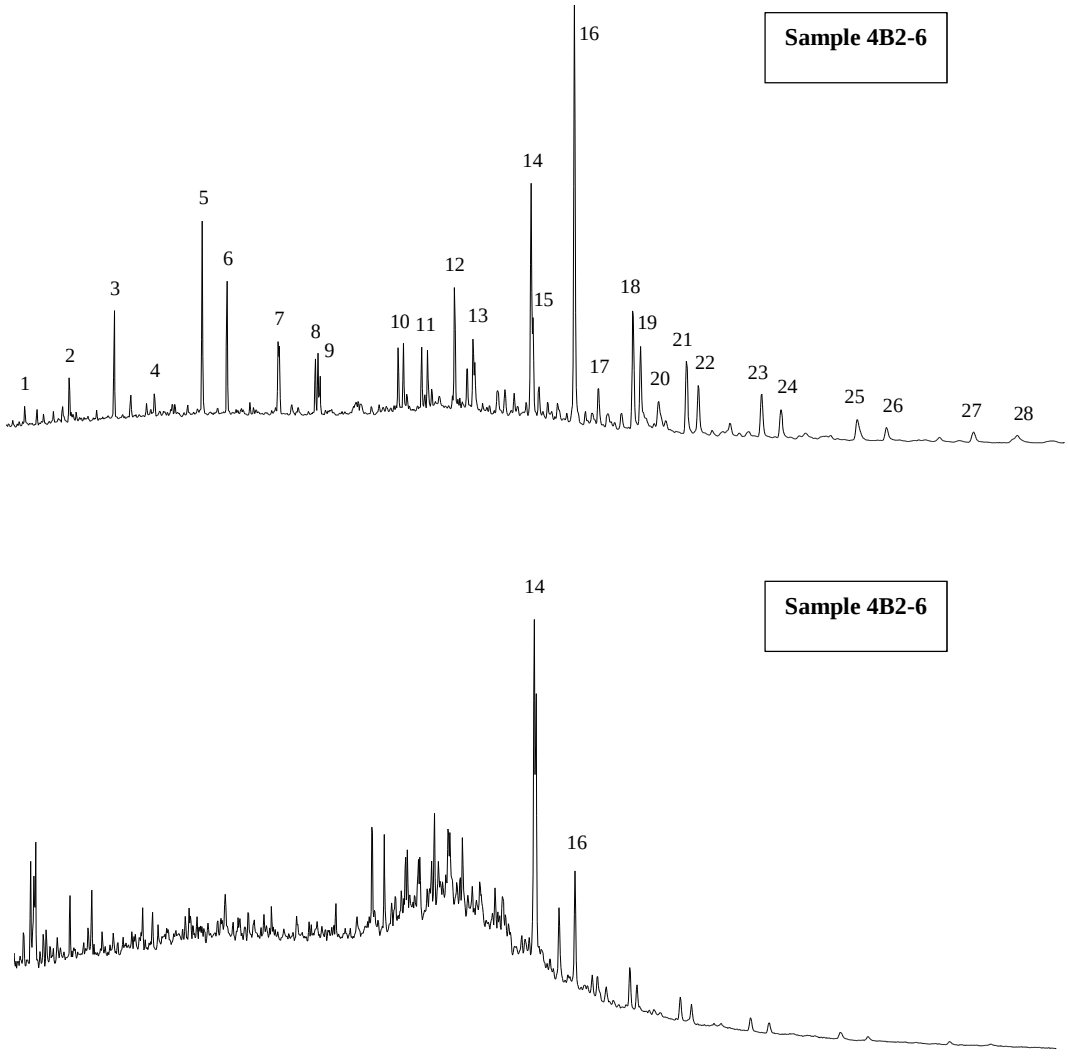


Figure 5-17……continued

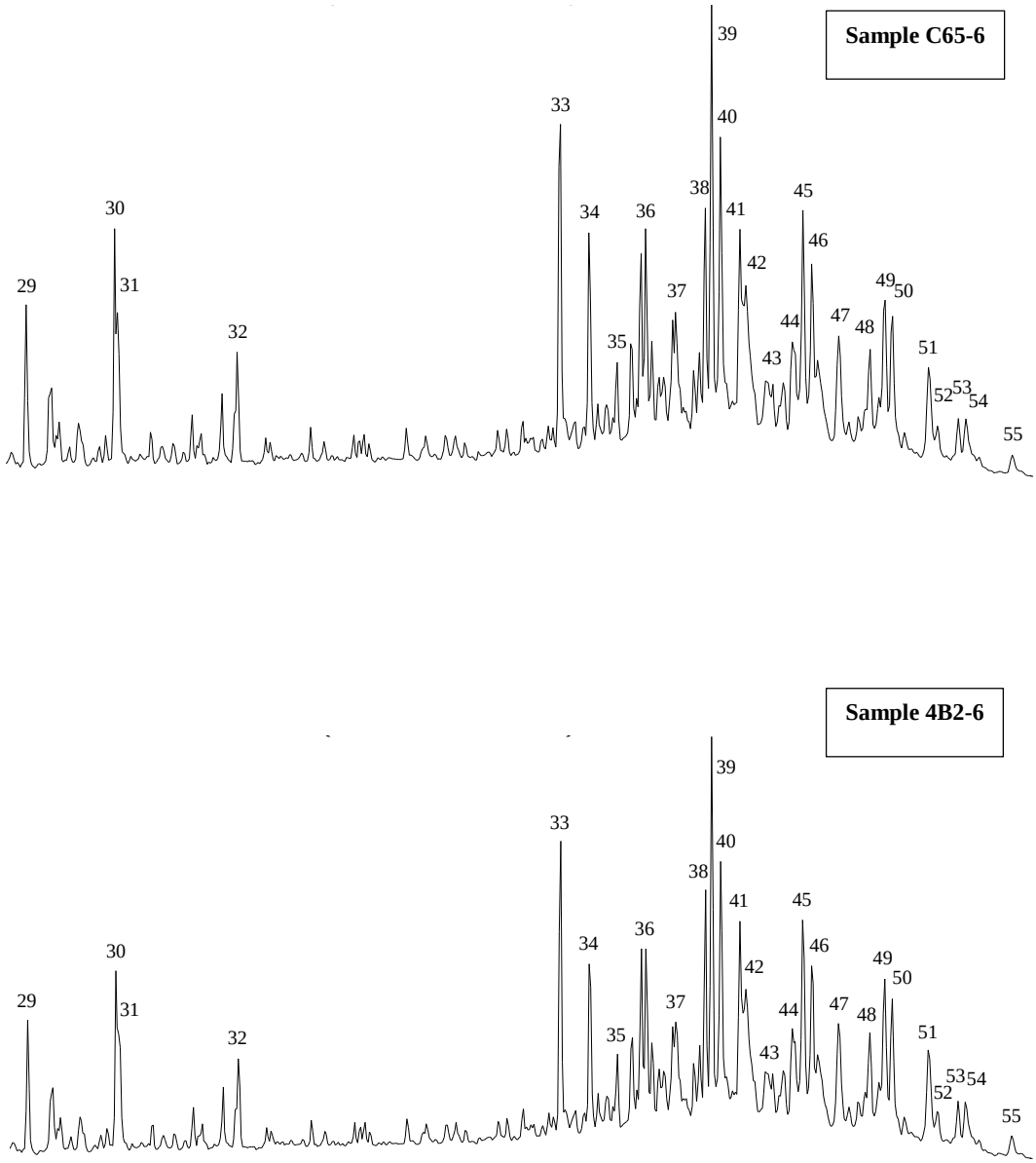


Figure 5-18. Mass chromatograms of m/z 217 of the two samples from the Galio Formation show absence of sterane degradation.

CHAPTER VI

6. Oil-Source Rock Correlation

The concept of oil-source rock correlation is based on the organic matter in both components containing similar chemical compounds that do not change significantly during migration. The correlation of oil and source rock relies on biomarker composition to find the genetic relationship between the two components. Similar biological sources will reflect strongly in similar biomarker distributions (Peters and Moldowan, 1993). However, there are other processes which can alter correlation parameters such as thermal maturity and biodegradation. These effects need to be considered when making oil-source rock correlations. Peters (2005) discussed the effects of oil-source correlation:

- Oil generated from several horizons of source rock and the analyzed source rock samples may not be representative of the whole source rock section.
- Migrated hydrocarbons or contamination of the source rock or oil may alter the extracted bitumen from the source rock or oil sample.
- Huge differences in maturity levels between oils and source rock samples make correlation difficult.
- Expulsion from the source rock and migration might alter the oil composition; for example, migrated oils are typically enriched with saturated and aromatic hydrocarbons but are typically low in NSO compounds.
- Mixed oils are sometimes derived from multiple source rocks and will affect interpretation.

A comparison of the geochemical signatures in the analyzed oils and organic extracts shows they generally exhibit similarities in n-alkane and biomarker fingerprints. The source rocks are comparable with broad n-alkane distributions for the majority of oils. The overall similarities are highlighted by close ratios of Pr/Ph which is present in both oil and source rock samples. They range between 2 and 3 which mean the organic matter was deposited in marine conditions. However, the ratios of isoprenoids relative to n-alkanes are variable even and less than one. Pr/nC_{17} and Ph/nC_{18} ratios are similar in both source oils of group A and B. These ratios are relatively very low in group C and D, with D being the smallest. Furthermore, on the cross-plot of these two parameters (Figure 6-1) group A and B oils appear to follow a similar path to that of the source extracts.

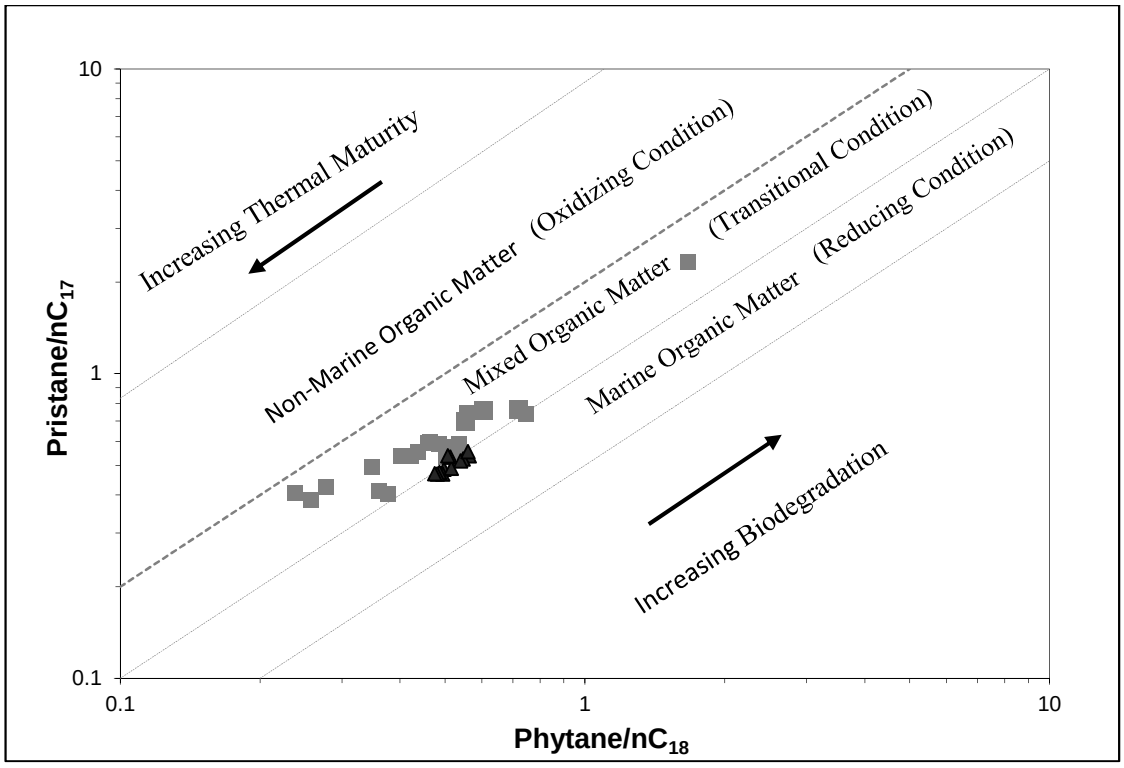


Figure 6-1. Plot of Pr/nC_{17} versus Ph/nC_{18} as an indicator of positive correlation between oils and source rocks in this study. The squares are oils and the triangles are source rocks.

All of the oils and source rock extracts show considerable amounts of gammacerane, a very specific biomarker for highly saline environments, indicating that the source rocks were deposited under saline conditions. Biomarker distribution and thermal maturity of crude oils and source rocks show at least two types of source rocks for these oils even though they all are of marine origin as indicated by the presence of C_{30} steranes (Moldowan, et al., 1985). A marine source rocks other than Sirt Shale are found in the Sirt Basin such as Rachmat and Tegrifet (Burwood et al., 2003). The data shows that the group A and B oils have the closest geochemical characteristics to the source rock extracts. Group C has a low concentration of terpanes and steranes due to its higher maturity compared to Group A and B as shown in the figures. In Group D, unlike most samples that exhibt low biomarker concentration due to high thermal maturity, the terpane and steranes contain a unique distribution. Both sets of biomarkers show an absence of low molecular weight isomers. The biomarkers, detected in the branched and cyclic fractions of Group A and B and source rock samples show similar distributions. A high abundance of hopanes in these oils and the extracts of source rocks support a large microbial contribution to the source organic matter. A low abundance of C_{24} tetracyclic terpane indicate that the oils were generated from clay rich source rocks which is supported by high ratio of diasterane/ regular steranes. The lithology of source rocks which generate these oils are having shale characteristic consistent, with shale lithology of the source rocks.

The oils studied display very similar sterane and diasterane distributions, indicating these oils were derived from similar source facies. Generally, steranes and diasterane distributions, which reflect variation in algal input to source rocks, are

effective parameters to differentiate source rock facies and are used widely to group oils according to their genetic relationships. Distributions of steranes C_{27}, C_{28}, C_{29}, are usually presented in ternary plots to show if the source facies are same among the studied oils. The ternary plot of sterane distributions of oils Figure 6-2 shows that most oils (Group A and B) are characterized by sterane distributions and that these oils were derived from similar marine source rock. A good agreement can be seen between source rocks and crude oils and the ββ steranes chromatograms (m/z 218) as shown in Figure 6-3.

Normalizing the absolute biomarker concentrations to saturate fraction of oil and source rock extracts allow quantitative study and correlation. Therefore the quantification of biomarkers is a useful tool to distinguish if the oils come from similar source rock. Oil-source rock correlations based on absolute concentration show similar results. The absolute concentrations of hopanes are higher than the steranes (Figure 6-4). A good correlation between source rocks and oils of group A and B were found using the absolute biomarker concentrations. The oils of groups C and D exhibit a low absolute concentration of biomarkers, which may indicate that they originate from different source rocks. In Figure 6-4, it is clear to observe the similarity between source rocks and oils of group A and B. Both of them have high concentrations of C_{30} hopanes compared to C_{29} hopane. The absolute concentrations of tetracyclic terpane are low in the source rock and oil of these groups.

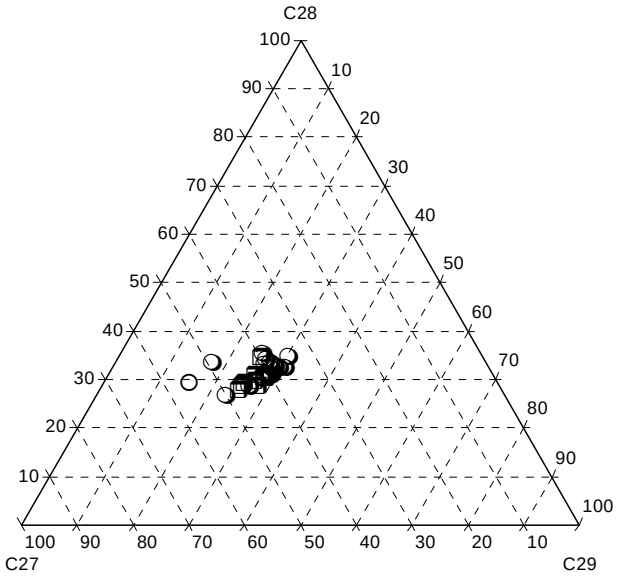


Figure 6-2. Ternary plot of regular steranes for oils (circles) and source rocks (squares) from Sirt Basin.

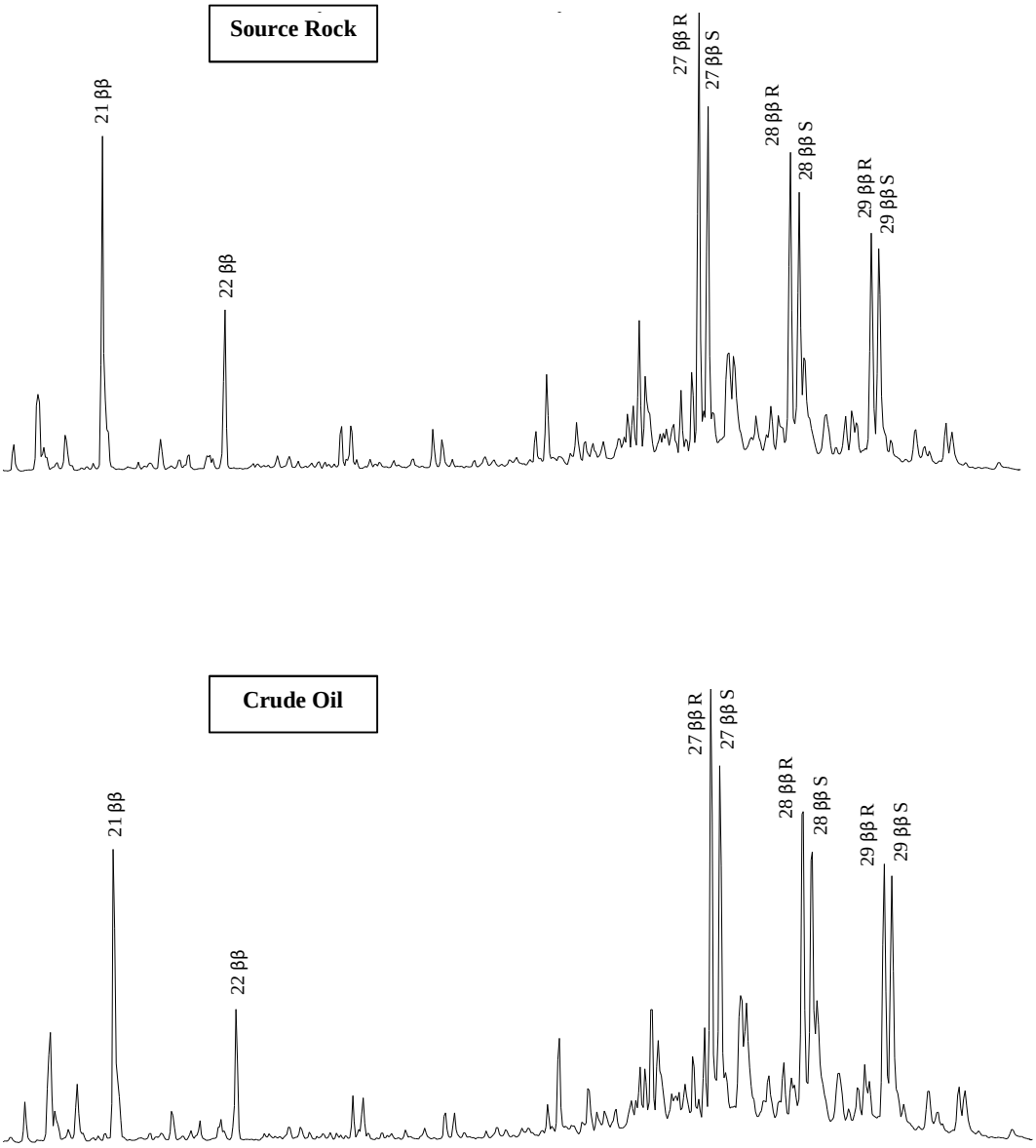


Figure 6-3. Sterane m/z 218 profiles showing the C_{27} isomers are greater than C_{28} and C_{28} are greater than C_{29} indicating marine organic matter for source rocks and oil of samples.

The absolute concentration of the selected biomarkers of oil and source can be matched in Figure 6.4. The high biomarker concentrations may indicate that the oil from these did not significantly migrate from the source rocks.

The above results indicate that the oils in A and B were sourced primarily from the Sirt Shale while group C oils show source from higher maturity source rock and Group D was sourced from different marine organic matter at high thermal maturity. Group C and D oils are most likely derived from the Ajdabiya Trough source rocks because it has the higher thermal maturity in the basin and is geographically closed. Group A could be sourced from the Al Kotlah Graben or possibly from the Maradah Trough. Group B can be generated from the Ajdabiya or Maradah Trough. Random sampling and near identical biomarkers of the oils from Sirt Shale makes identification of the source rocks incredibly difficult (Hallett, 2002).

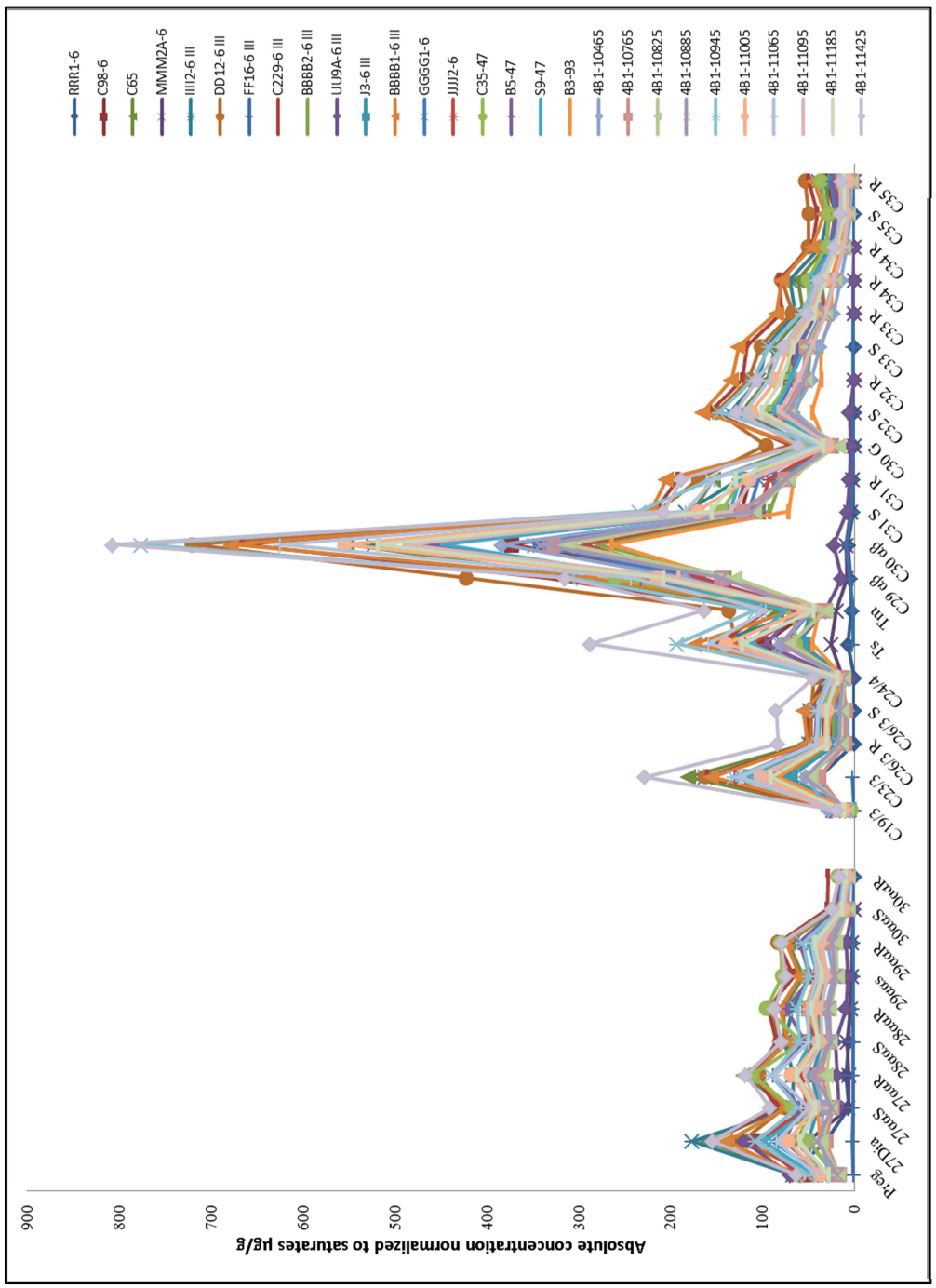


Figure 6-4. Distribution of absolute concentrations of source rocks and oils

CHAPTER VII

7. Conclusions

TOC values for source rock samples collected from the Zaltan Platform on the north part of Concession 6 are all low, ranging between 0.24% and 0.89%. In the southern part of Concession 6, the TOC values vary among the two studied wells. The samples from the Maradah through (12135 to 13715 ft) show fair TOC values ranging from 0.64 to 2.00 while well BBB1-6 (10465 to 11425 ft) have much higher ranges, from about 0.69 to 5.35 % showing that these samples have afair to excellent TOC for oil generation. The samples from the Zaltan Platform in the east of Concession 6 at depth from 9990 to 10475 ft have low TOC values ranging from 0.11 to 0.56 wt% while samples at depth exceeding 12885 ft located in the Ajdabiya Trough have values from 0.64 to 2.9 %. The samples from the Al Kotlah Graben have low TOC with values of 0.42 to 0.86% at depth between 6715 and 7505 ft. Most of the samples show kerogen type III except for those from Al Kotlah Graben and South of Maradah trough which have type II and type II/III kerogen. The variation in TOC in the wells can be explained by different types of organic matter in lower depths and the deepest wells by oil generation from these rocks.

However, the Sirt Shale samples from the south of the Maradah Trough having TOC values ranging from 0.69-5.36%, HI 206-527 mg HC/g TOC and OI value < 34 mg CO_2/g TOC, indicate that these rocks have good to excellent oil generation potential. Therefore, these rocks have been investigated using more geochemical parameters to assess the type of organic matter, depositional conditions, and thermal

maturity. The organic matter gets richer with increasing depth which indicates strata changes with increasing sea level. These strata were deposited during rising sea level within transgressive systems tracts for the lower part and highstand systems tracts for the upper part. Organic matter type is mainly kerogen type II although II/III OM is present.

The pristane/phytane ratios in all samples range from 0.89 to 1.62, which suggests a marine depositional environment for the organic matter. The high abundance of low molecular weight n-alkanes compared to high molecular weight alkanes, suggests a low contribution of terrigenous organic matter. C_{29}/C_{30} hopane ratios less than one are consistent with the clay-bearing character of the samples studied. The presence of a marine source signature can be seen from the high ratio of C_{27}/C_{29} steranes. A ternary diagram of regular steranes and the occurrence of C_{30} steranes strongly suggest a contribution from marine organic matter. High values for the pregnane/C_{27}R sterane ratio and the presence of gammacerane indicates a saline condition for the depositional environment.

These rocks are thermally mature; T_{max} values are between 438 and 443°C and the main phase of generation has been reached. The thermal maturity is also reflected in the low ratios of moretane/C_{30} hopane. The level of maturity for this unit also can be seen in the C_{29} sterane isomerization, Ts/(Ts+Tm), C_{23} tricyclic terpanes/C_{30} hopane, and C_{24} tricyclic terpanes/C_{23} tricyclic terpanes. These ratios show generally increasing maturity with depth.

The depositional environment and type of organic matter of crude oil samples show generally similar characteristic as the source rocks. Pristane/phytane ratios

suggest a marine depositional environment for the organic matter deposited under oxic to suboxic marine condition. The high abundance of low molecular weight n-alkanes of crude oils supports a high contribution of marine organic matter. A ternary diagram of regular steranes and occurrence of C_{30} steranes strongly suggest marine organic matter contributions. Geochemical parameters suggest that the lithology of the source rocks of these oils is shale and most likely Upper Cretaceous in age. These crude oils are generally thermally mature. The thermal maturity is reflected in the low ratios of moretane/C_{30} hopane. The high maturity for this unit also can be seen in the C_{29} sterane isomerization, Ts/(Ts +Tm), C_{23} tricyclic terpanes /C_{30} Hopane, C_{24} tetracyclic terpanes /C_{23} tricyclic terpanes, 22S/(22S+22R) ratios for C_{31} and C_{32} hopanes and aromatic hydrocarbons. The oils were divided into four groups according to thermal maturity.

The oils from group A and B have similar organic geochemical characteristics and are classified as from similar source rocks but different facies. Group C is characterized by relatively high maturity. Group D oils are unlike any of the other oil groups. No oil source-rock correlation could be determined for groups C and D due to lack of source rocks samples, but based on biomarker characteristics for these oils, the hydrocarbon source rock is likely thermally highly mature shale. The shallowest reservoir showed very slight biodegradation where the n-alkanes have been removed with no affect in the hopane and steranes. A positive correlation can be observed between source rock in the south part of Maradah trough with the oils of Group A and B. Source rock and the oils of these groups show similar a distribution of biomarkers and their absolute concentrations.

References

Abadi, A. M., van Wees, J. D., van Dijk, P. M., and Cloetingh, S. A. P. L. (2008). Tectonics and subsidence evolution of the Sirt Basin, Libya. *American Association of Petroleum Geologists Bulletin* **92**, 993-1027.

Abdi, H. and Williams, L.J., (2010). Principal component analysis. *Wiley Interdisciplinary Reviews: Computational Statistics*, **2,** 433-459.

Abbott, G. D., Wang, G. Y., Eglinton, T. I., Home, A. K., and Petch, G. S. (1990). The kinetics of sterane biological marker release and degradation processes during the hydrous pyrolysis of vitrinite kerogen. *Geochimica et Cosmochimica Acta* **54**, 2451-2461.

Aboglila, S., Grice, K., Trinajstic, K., Dawson, D., and Williford, K. H. (2010). Use of biomarker distributions and compound specific isotopes of carbon and hydrogen to delineate hydrocarbon characteristics in the East Sirte Basin (Libya). *Organic Geochemistry* **41**, 1249-1258.

Ahlbrandt, T. S. (2001). "The Sirte Basin Province of Libya: Sirte-Zelten Total Petroleum System," US Department of the Interior, US Geological Survey Bulletin **2202–F**.

Ahmed, M., Volk, H., Allan, T. and Holland, D., (2012). Origin of oils in the Eastern Papuan Basin, Papua New Guinea. *Organic Geochemistry*, **53** 137–152.

Albrecht, P., and Ourisson, G. (1971). Biogenic substances in sediments and fossils. *Angewandte Chemie International Edition in English* **10**, 209-225.

Aldahik, A., (2010). Crude Oil Families in the Euphrates Graben Petroleum System, Ph. D. Dissertation, Berlin Institute of Technology.

Alexander, R., Kagi, R., Rowland, S., Sheppard, P., and Chirila, T. (1985). The effects of thermal maturity on distributions of dimethylnaphthalenes and trimethylnaphthalenes in some ancient sediments and petroleums. *Geochimica et Cosmochimica Acta* **49**, 385-395.

Alexander, R., Kagi, R. I., Singh, R. K., and Sosrowidjojo, I. B. (1994). The effect of maturity on the relative abundances of cadalene and isocadalene in sediments from the Gippsland Basin, Australia. *Organic Geochemistry* **21**, 115-120.

Alexander, R., Kagi, R. I., Woodhouse, G. W., and Volkman, J. K. (1983). The geochemistry of some biodegraded Australian oils. *Australian Petroleum Exploration Association Journal* **23**, 53-63.

Ambrose, G. (2000). The geology and hydrocarbon habitat of the Sarir Sandstone, SE Sirt Basin, Libya. *Journal of Petroleum Geology* **23**, 165-191.

Andrusevich, V., Engel, M., Zumberge, J., and Brothers, L. (1998). Secular, episodic changes in stable carbon isotope composition of crude oils. *Chemical Geology* **152**, 59-72.

Anketell, J. M. (1996). Structural history of the Sirt Basin and its relationships to the Sabratah Basin and Cyrenaican platform, northern Libya. *In* "Geology of the Sirt Basin" (M. J. Salem, A. S. El-Hawat and A. M. Sbeta, eds.), Vol. 3, pp. 57-88. Elsevier, Amsterdam.

Aquino Neto, F. R., Trendel, J., Restle, A., Connan, J., and Albrecht, P. (1983). Occurrence and formation of tricyclic and tetracyclic terpanes in sediments and petroleum. *Advances in Organic Geochemistry 1981*, 659-667.

Asif, M., (2010). Geochemical Applications of Polycyclic Aromatic Hydrocarbons in Crude Oils and Sdiments from Pakistan, Ph. D. Dissertation, University of Engineering & Technology, Lahore.

Azevedo, D., Tamanqueira, J., Dias, J., Carmo, A., Landau, L., Gonçalves, F. (2008). Multivariate statistical analysis of diamondoid and biomarker data from Brazilian basin oil samples. *Fuel*, **87**, 2122-2130.

Baird, D. W., Aburawi, R. M., and Bailey, N. J. L. (1996). Geohistory and petroleum in the central Sirt Basin. *In* "Geology of the Sirt Basin " (M. T. B. M.J. Salem, A.A. Misallati and M.J. Sola, ed.), Vol. 3, pp. 3-56. Elsevier, Amsterdam.

Baric, G., Maricic, M., and Spanic, D. (1996). Geochemical Characterization of Source Rocks in NC-157 Block (Zaltan platform), Sirt basin. *In* "The Geology of Sirt Basin" (M. J. Salem, A. S. El-Hawat and A. M. Sbeta, eds.), Vol. 3, pp. 1086-1097. Elsevier, Amsterdam.

Barr, F. T., and Weegar, A. A. (1972). "Stratigraphic Nomenclature of the Sirte Basin, Libya," The Petroleum Exploration Society of Libia.

Beach, F., Peakman, T. M., Abbott, G. D., Sleeman, R., and Maxwell, J. R. (1989). Laboratory thermal alteration of triaromatic steroid hydrocarbons. *Organic Geochemistry* **14**, 109-111.

Bebout, D. G., and Pendexter, C. (1975). Secondary carbonate porosity as related to early Tertiary depositional facies, Zelten Field, Libya. *American Association of Petroleum Geologists Bulletin* **59**, 665-693.

Belazi, H. S. (1989). The geology of the Nafoora oilfields. *Journal of Petroleum Geology* **12**, 353-366.

Benfield, A. C., and Wright, E. P. (1980). Post-Eocene sedimentation in the eastern Sirt Basin, Libya. *In* "The geology of Libya" (M. J. Salem and M. T. Busrewil, eds.), Vol. 2, pp. 463-500. Academic Press, London.

Bennett, B., Jiang, C. and Larter, S.R., (2009). Identification and occurrence of 25-norbenzohopanes in biodegraded bitumen from Palaeozoic carbonates in northern Alberta. *Organic Geochemistry*, **40,** 667-670.

Bezan, M. A., and Emil, K. M. (1996). Oligocene sediments of Sirt Basin and their hydrocarbon potential. *In* "The geology of the Sirt Basin: Amsterdam, Elsevier" (M. J. Salem, M. T. Busrewil, A. A. Misallati and M. A. Sola, eds.), Vol. 1, pp. 119-127. Elsevier, Amsterdam.

Bishop, A. N., and Abbott, G. D. (1993). The interrelationship of biological marker maturity parameters and molecular yields during contact metamorphism. *Geochimica et Cosmochimica Acta* **57**, 3661-3668.

Bissada, K. K., Elrod, L. W., Robison, C. R., Darnell, L. M., Szymczyk, H. M., and Trostle, J. L. (1993). Geochemical inversion. A modern approach to inferring source-rock identity from characteristics of accumulated oil and gas. *Energy exploration & exploitation* **11**, 295-328.

Bjørlykke, K. (2010). "Petroleum geoscience: From sedimentary environments to rock physics," Springer Verlag.

Bohacs, K.M., Grabowski Jr, G.J., Carroll, A.R., Mankiewicz, P.J., Miskell-Gerhardt, K.J., Schwalbach, J.R., Wegner, M.B., Simo, J.A.T. (2005). Production, destruction, and dilution—the many paths to source-rock development. SEPM Special Publication No. 82, 61-101.

Bohacs, K. M., and Isaksen, G. H. (1991). Source quality variations tied to sequence development: Integration of physical and chemical aspects, Lower to Middle Triassic, western Barents Sea. *American Association of Petroleum Geologists Bulletin* **75**, 544.

Bonnefous, J., 1972. Geology of the quartzitic" Gargaf Formation" in the Sirt basin. Libya: Bulletin du Centre de Recherches de Pau, Societe Nationale des Petroles d'Aquitaine, **6**, 225-261.

Bordenave, M. L., Espitalie, J., Leplat, P., Oudin, J. L. and Vandenbroucke, M.,. (1993). Screening Techniques for Source Rock Evaluation. *In* "Applied Petroleum Geochemistry" (M. L. Bordenave, ed.), pp. 217-278. Editions Technip Paris.

Boreham, C., Crick, I., and Powell, T. (1988). Alternative calibration of the

methylphenanthrene index against vitrinite reflectance: application to maturity measurements on oils and sediments. *Organic Geochemistry* **12**, 289-294.

Brassell, S. C., and Eglinton, G. (1986). Molecular geochemical indicators in sediments. *Organic Marine Geochemistry* **305**, 10-31.

Bray, E.E., and Evans, E.D. (1961). Distribution of n-paraffins as a clue to recognition of source beds. *Geochimica et Cosmochimica Acta* **22**, 2-15.

Brennan, P., (1992), Raguba Field; Libya, Sirte Basin, in E.A. Beaumont and N.H. Foster (Ed), Treatise of petroleum geology, Atlas of oil and gas fields, Structural traps, American Association of Petroleum Geologists, 7, 267-289.

Brooks, J., Cornford, C., and Archer, R. (1987). The role of hydrocarbon source rocks in petroleum exploration. *Geological Society, London, Special Publications* **26**, 17-46.

Brooks, J. D., Gould, K., and Smith, J. W. (1969). Isoprenoid hydrocarbons in coal and petroleum. *Nature* **222**, 257-259.

Bu-Argoub, M. F. (1996). Palynological and playnofacies studies of the Upper Cretaceous sequence in well C275-65, Sirt Basin, northeast, Libya. *In* "The geology of the Sirt Basin" (M. T. B. M. J. Salem, A. A. Misallati, and M. A. Sola, ed.), Vol. 1, pp. 419-454. Elsevier, Amsterdam.

Burwood, R. (1997). Petroleum systems of the east Sirte Basin. *American Association of Petroleum Geologists Bulletin* **81**, 1365.

Burwood, R., Redfern, J., and Cope, M. (2003). Geochemical evaluation of East Sirte Basin (Libya) petroleum systems and oil provenance. *Geological Society, London, Special Publications* **207**, 203-240.

Calvert, S., and Pedersen, T. (1992). Organic carbon accumulation and preservation in marine sediments: How important is anoxia? *In* "Organic matter: productivity, accumulation, and preservation in recent and ancient sediments" (J. W. a. J. W. Farrington, ed.), Vol. 533, pp. 231-263. Columbia University Press, New York.

Cassani, F., Gallango, O., Talukdar, S., Vallejos, C., and Ehrmann, U. (1988). Methylphenanthrene maturity index of marine source rock extracts and crude oils from the Maracaibo Basin. *Organic Geochemistry* **13**, 73-80.

Cbpek, P. (1979). Geological Map of Libya, 1: 250,000, Sheet Al Qaryat Ash Sharqiyah, NH 33-6. *In* "Explanatory Booklet". Industrial Research Center, Tripoli.

Ceriani, A., Di Giulio, A., Goldstein, R. and Rossi, C., (2002). Diagenesis associated with cooling during burial: An example from Lower Cretaceous reservoir sandstones (Sirt basin, Libya). *American Association of Petroleum Geologists Bulletin* **86**, 1573-1591.

Chatellier, J. Y., and Slevin, A. (1988). Review of African petroleum and gas deposits. *Journal of African Earth Science* **7**, 561-578.

Clark, J. P., and Philp, R. P. (1989). Geochemical characterization of evaporite and carbonate depositional environments and correlation of associated crude oils in the Black Creek Basin, Alberta. *Bulletin of Canadian Petroleum Geology* **37**, 401-416.

Clementz, D. M. (1979). Effect of Oil and Bitumen Saturation on Source-Rock Pyrolysis: Geologic Notes. *American Association of Petroleum Geologists Bulletin* **63**, 2227-2232.

Clifford, H. J., Grund, R., and Musrati, H. (1980). Geology of a stratigraphic giant: Messla oil field, Libya. *In* "Giant oil and gas fields of the decade 1968-1978" (M. T. Halbouty, ed.), pp. 507-524. American Association of Petroleum Geologists Memoir **30**.

Connan, J. (1984). Biodegradation of crude oils in reservoirs. *In* "Advances in petroleum geochemistry" (J. Brooks and D. H. Welte, eds.), Vol. 1, pp. 299-335. Academic press London.

Connan, J., BourouUec, J., Dessort, D., and Albrecht, P. (1986). The microbial input in carbonate-anhydrite facies of a sabkha paleoenvironment from Guatemala: A molecular approach. *In* "Advances in Organic Geochemistry 1985" (D. Leythaeuser and J. Rullkotter, eds.), pp. 29-50. Pergamon Press, Oxford.

Creaney, S., and Passey, Q. R. (1993). Recurring patterns of total organic carbon and source rock quality within a sequence stratigraphic framework. *American Association of Petroleum Geologists Bulletin* **77**, 386-401.

Cornford, C., Gardner, P., and Burgess, C. (1998). Geochemical truths in large data sets. I: Geochemical screening data. *Organic Geochemistry* **29**, 519-530.

Curiale, J. A., and Odermatt, J. R. (1989). Short-term biomarker variability in the monterey formation, Santa Maria Basin. *Organic Geochemistry* **14**, 1-13.

Czochanska, Z., Gilbert, T., Philp, R., Sheppard, C., Weston, R., Wood, T., and Woolhouse, A. (1988). Geochemical application of sterane and triterpane biomarkers to a description of oils from the Taranaki Basin in New Zealand. *Organic Geochemistry* **12**, 123-135.

Dawson, D., Grice, K., and Alexander, R. (2005). Effect of maturation on the indigenous δD signatures of individual hydrocarbons in sediments and crude oils from the Perth Basin (Western Australia). *Organic Geochemistry* **36**, 95-104.

De Grande, S. M. B., Aquino Neto, F. R., and Mello, M. R. (1993). Extended tricyclic terpanes in sediments and petroleums. *Organic Geochemistry* **20**, 1039-1047.

Demaison, G., and Huizinga, B. J. (1991). Genetic Classification of Petroleum Systems *American Association of Petroleum Geologists Bulletin* **75**, 1626-1643.

Demaison, G. J., and Moore, G. T. (1980). Anoxic environments and oil source bed genesis. *Organic Geochemistry* **2**, 9-31.

Didyk, B., Simoneit, B., Brassell, S. C., and Eglinton, G. (1978). Organic geochemical indicators of palaeoenvironmental conditions of sedimentation. *Nature* **272**, 216-222.

Duan, Y. (2012). Geochemical characteristics of crude oil in fluvial deposits from Maling oilfield of Ordos Basin, China. *Organic Geochemistry*, **52**, 35–43.

Durand, B. (1980). Sedimentary organic matter and kerogen. Definition and quantitative importance of kerogen. *In* "Kerogen, Insoluble Organic Matter from Sedimentary Rocks" (B. Durand, ed.), pp. 13-34. Editions Technip,, Paris.

Eglinton, T., and Douglas, A. (1988). Quantitative study of biomarker hydrocarbons released from kerogens during hydrous pyrolysis. Energy & fuels **2**, 81-88.

Ekweozor, C., and Udo, O. T. (1987). The oleananes: Origin, maturation and limits of occurence in southern Nigeria sedimentary basins. *Organic Geochemistry* **13**, 131-140.

Ekweozor, C. M., and Strausz, O. P. (1983). Tricyclic terpanes in the Athabasca oil sands: their geochemistry. *In* "Advances in Organic Geochemistry 1981" (M. Bjorùy, et al. , ed.), pp. 746-766.

El-Arnauti, A., and Shelmani, M. (1985). Stratigraphic and structural setting. *In* "Palynostratigraphy of North-East Libya" (T. B. and O. B., eds.), Vol. 4, pp. 1-10. British Micropalaeontological Society, London.

El-Alami, M. (1996). Habitat of oil in Abu Attiffel area, Sirt Basin, Libya. *In* "The geology of the Sirt Basin", Vol. 2, pp. 337-347. Elsevier, Amsterdam.

El-Alami, M., Rahouma, S., and Butt, A. A. (1989). Hydrocarbon habitat in the Sirte

basin, northern Libya. *Petroleum Research journal* **1**, 19-30.

El-Gayar, M.S. (2005) Aromatic steroids in Mideastern crude oils: identification and geochemical application. *Petroleum science and technology*, **23**, 971-990.

El-Hawat, A., Missallati, A., Bezan, A., and Taleb, T. (1996). The Nubian sandstone in Sirt Basin and its correlatives. *In* "Geology of the Sirt Basin ", Vol. 2, pp. 3-30. Elsevier, Amsterdam.

Espitalié, J., Laporte, J. L., Madec, M., Marquis, F., Leplat, P., Paulet, J., and Boutefeu, A. (1977). Méthode rapide de caractérisation des roches mètres, de leur potentiel pétrolier et de leur degré d'évolution. *Oil & Gas Science and Technology* **32**, 23-42.

Fang, H., Jianyu, C., Yongchuan, S., and Yaozong, L. (1993). Application of organic facies studies to sedimentary basin analysis: A case study from the Yitong graben, China. *Organic Geochemistry* **20**, 27-42.

Farrimond, P., Bevan, J. C., and Bishop, A. N. (1996). Hopanoid hydrocarbon maturation by an igneous intrusion. *Organic Geochemistry* **25**, 149-164.

Farrimond, P., Bevan, J. C., and Bishop, A. N. (1999). Tricyclic terpane maturity parameters: response to heating by an igneous intrusion. *Organic Geochemistry* **30**, 1011-1019.

Farrimond, P., Taylor, A., and Telns, N. (1998). Biomarker maturity parameters: the role of generation and thermal degradation. *Organic Geochemistry* **29**, 1181-1197.

Futyan, A., and Jawzi, A. H. (1996). The hydrocarbon habitat of the oil and gas fields of north Africa with emphasis on the Sirt Basin. *In* "The geology of the Sirt Basin: Amsterdam, Elsevier" (M. J. Salem, A. S. El-Hawat and A. M. Sbeta, eds.), Vol. 2, pp. 287-307.

Gammudi, M. A., Salem, M. J., Mouzughi, A. J., and Hammuda, O. S. (1996). The ostracod fauna of the Miocene Maradah Formation exposed in the eastern Sirt Basin, Libya. *In* "The geology of the Sirt Basin: Amsterdam, Elsevier" (M. J. Salem, M. T. Busrewil, A. A. Misallati and M. A. Sola, eds.), Vol. 1, pp. 391-418. Elsevier, Amsterdam.

Ghori, K., and Mohammed, R. (1996). The application of petroleum generation modelling to the eastern Sirt Basin, Libya. *In* "Geology of the Sirt Basin: Amsterdam, Elsevier" (M. J. Salem, A. S. El-Hawat and A. M. Sbeta, eds.), Vol. 2, pp. 529-540. Elsevier, Amsterdam.

Goudarzi, G. H. (1980). Structure-Libya. *In* "The geology of Libya", Vol. 3, pp. 879-

892. Academic Press, London.

Grantham, P. (1986). Sterane isomerization and moretane/hopane ratios in crude oils derived from Tertiary source rocks. *Organic Geochemistry* **9**, 293-304.

Grantham, P., and Wakefield, L. (1988). Variations in the sterane carbon number distributions of marine source rock derived crude oils through geological time. *Organic Geochemistry* **12**, 61-73.

Grantham, P. J. (1986). The occurrence of unusual $C_{27}$and C_{29} sterane predominances in two types of Oman crude oil. *Organic Geochemistry* **9**, 1-10.

Guiraud, R., and Bosworth, W. (1997). Senonian basin inversion and rejuvenation of rifting in Africa and Arabia: synthesis and implications to plate-scale tectonics. *Tectonophysics* **282**, 39-82.

Gumati, Y., and Nairn, A. (1991). Tectonic subsidence of the Sirte Basin, Libya. *Journal of Petroleum Geology* **14**, 93-102.

Gumati, Y.D., Kanes, W.H., Schamel, S. (1996). An evaluation of the hydrocarbon potential of the sedimentary basins of Libya. Journal of Petroleum Geology, 19(1), 95-112.

Gumati, Y., and Schamel, S. (1988). Thermal maturation history of the Sirte Basin, Libya. *Journal of Petroleum Geology* **11**, 205-218.

Gumati, Y. D., and Kanes, W. H. (1985). Early Tertiary Subsidence and Sedimentary Facies--Northern Sirte Basin, Libya. *American Association of Petroleum Geologists Bulletin* **69**, 39-52.

Gürgey, K. (1999). Geochemical characteristics and thermal maturity of oils from the Thrace Basin (western Turkey) and western Turkmenistan. *Journal of Petroleum Geology* **22**, 167-189.

Hallett, D. (2002). Petroleum geology of Libya, Elsevier Science.

Hallett, D., and El Ghoul, A. (1996). Oil and gas potential of the deep trough areas in the Sirt Basin, Libya. *In* "The geology of Sirt Basin" (M. J. Salem, A. S. El-Hawat and A. M. Sbeta, eds.), Vol. 2, pp. 455-484. Elsevier, Amsterdam.

Hantschel, T., and Kauerauf, A. I. (2009). "Fundamentals of basin and petroleum systems modeling," Springer Verlag, Berlin Heidelberg.

Harding, T. (1984). Graben hydrocarbon occurrences and structural style. *American Association of Petroleum Geologists Bulletin* **68**, 333-362.

Hase, A., and Hites, R. A. (1976). On the origin of polycyclic aromatic hydrocarbons in recent sediments: biosynthesis by anaerobic bacteria. *Geochimica et Cosmochimica Acta* **40**, 1141-1143.

Head, I. M., Jones, D. M., and Larter, S. R. (2003). Biological activity in the deep subsurface and the origin of heavy oil. *Nature* **426**, 344-352.

Huang, D. F. (1984). Evolution and Hydrocarbon-Forming Mechanism of Terrestrial Organic Matter. *Petroleum Industry Press*.

Huang, D., Zhang, D. and Li, J., (1994). The origin of 4-methyl steranes and pregnanes from Tertiary strata in the Qaidam Basin, China. *Organic Geochemistry*, **22**, 343-348.

Huang, D., Li, J., Zhang, D., Huang, X., and Zhou, Z. (1991). Maturation sequence of Tertiary crude oils in the Qaidam Basin and its significance in petroleum resource assessment. *Journal of Southeast Asian earth sciences* **5**, 359-366.

Huang, W. Y., and Meinschein, W. G. (1979). Sterols as ecological indicators. *Geochimica et Cosmochimica Acta* **43**, 739-745.

Hughes, W. B., Holba, A. G., and Dzou, L. I. P. (1995). The ratios of dibenzothiophene to phenanthrene and pristane to phytane as indicators of depositional environment and lithology of petroleum source rocks. *Geochimica et Cosmochimica Acta* **59**, 3581-3598.

Hunt, J. M. (1996). "Petroleum geochemistry and geology " 2/Ed. W. H. Freeman and Company New York.

Hur, M., Yeo, I., Park, E., Kim, Y.H., Yoo, J., Kim, E., No, M., Koh, J., Kim, S. (2009). Combination of statistical methods and Fourier transform ion cyclotron resonance mass spectrometry for more comprehensive, molecular-level interpretations of petroleum samples. *Analytical chemistry*, **82**, 211-218.

Hussler, G., Chappe, B., Wehrung, P., and Albrecht, P. (1981). C_{27}—C_{29} ring A monoaromatic steroids in Cretaceous black shales. *Nature* **294**, 556 -558.

Ibrahim, M. (1996). Geothermal gradient anomalies of hydrocarbon entrapment; Al Hagfah trough, Sirt Basin, Libya. *In* "The geology of Sirt Basin " (M. J. Salem, A. S. El- Hawat and A. M. Sbeta, eds.), Vol. 2, pp. 419-434. Elsevier, Amsterdam.

Jiamo, F., Guoying, S., Jiayou, X., Eglinton, G., Gowar, A., Rongfen, J., Shanfa, F., and Pingan, P. (1990). Application of biological markers in the assessment of paleoenvironments of Chinese non-marine sediments. *Organic Geochemistry* **16**, 769-779.

Jiang, C., Li, M., Osadetz, K. G., Snowdon, L. R., Obermajer, M., and Fowler, M. G. (2001). Bakken/Madison petroleum systems in the Canadian Williston Basin. Part 2: molecular markers diagnostic of Bakken and Lodgepole source rocks. *Organic Geochemistry* **32**, 1037-1054.

Jones, P., and Philp, R. (1990). Oils and source rocks from Pauls Valley, Anadarko Basin, Oklahoma, USA. *Applied geochemistry* **5**, 429-448.

Jonson, B. A., and Nicoud, D. A. (1996). Integrated exploration for Beda Formation reservoir in the south Zellah Trough (west Sirt Basin, Libya). *In* "The geology of the Sirt Basin" (J. Salem, A. S. El-Hawat and A. M. Sbeta, eds.), Vol. 2, pp. 211-222. Elsevier, Amsterdam.

Killops, S., and Killops, V. (2005). "Introduction to Organic Geochemistry," 2/Ed. Blackwell Publishing, Oxford.

Kolaczkowska, E., Slougui, N. E., Watt, D. S., Maruca, R. E., and Michael Moldowan, J. (1990). Thermodynamic stability of various alkylated, dealkylated and rearranged 17α-and 17β-hopane isomers using molecular mechanics calculations. *Organic Geochemistry* **16**, 1033-1038.

Koscec, B., and Gherryo, Y. S. (1996). Geology and reservoir performance of Messlah oil field, Libya. *In* "the Geology of the Sirt Basin" (J. Salem, A. S. El-Hawat and A. M. Sbeta, eds.), Vol. 3, pp. 365-389. Elsevier, Amsterdam.

Kruge, M. A., Hubert, J. F., Bensley, D. F., Crelling, J. C., Akes, R. J., and Meriney, P. E. (1990a). Organic geochemistry of a Lower Jurassic synrift lacustrine sequence, Hartford Basin, Connecticut, USA. *Organic Geochemistry* **16**, 689-701.

Kruge, M. A., Hubert, J. F., Jay Akes, R., and Meriney, P. E. (1990b). Biological markers in Lower Jurassic synrift lacustrine black shales, Hartford basin, Connecticut, USA. *Organic Geochemistry* **15**, 281-289.

Lafargue, E., Marquis, F., and Pillot, D. (1998). Rock-Eval 6 applications in hydrocarbon exploration, production, and soil contamination studies. *Oil & Gas Science and Technology-Revue de l'Institut Français du Pétrole* **53**, 421-437.

Lambert, M. W. (1993). Internal stratigraphy and organic facies of the Devonian–Mississippian Chatanooga Woodford Shale in Oklahoma and Kansas. *In* "Source rocks in a sequence-stratigraphic framework: American Association of Petroleum Geologists Studies in Geology" (B. J. Katz and L. M. Pratt, eds.), Vol. 37, pp. 163-176.

Lewan, M., Bjorøy, M., and Dolcater, D. (1986). Effects of thermal maturation on

steroid hydrocarbons as determined by hydrous pyrolysis of Phosphoria Retort Shale. *Geochimica et Cosmochimica Acta* **50**, 1977-1987.

Lijmbach, W. (1975). On the Origin of Petroleum. *In* "proceeding 9th world petroleum congress 2", pp. 357-369. Applied Science Publishers, london.

Loutit, T. S., Hardenbol, J., Vail, P. R., and Baum, G. R. (1988). Condensed sections: the key to age determination and correlation of continental margin sequences. *SEPM Special Publications* **42**, 183-213.

Lu, S. T., Ruth, E., and Kaplan, I. R. (1989). Pyrolysis of kerogens in the absence and presence of montmorillonite-I. The generation, degradation and isomerization of steranes and triterpanes at 200 and 300° C. *Organic Geochemistry* **14**, 491-499.

Macgregor, D. S., and Moody, R. T. J. (1998). Mesozoic and Cenozoic petroleum systems of North Africa. *In* "Petroleum Geology of North Africa" (D. S. Macgregor, R. T. J. Moody and D. D. Clark-Lowes, eds.), pp. 201-216. Geological Society, London, Special Publications No.132.

Mackenzie, A., Hoffmann, C., and Maxwell, J. (1981). Molecular parameters of maturation in the Toarcian shales, Paris Basin, France—III. Changes in aromatic steroid hydrocarbons. *Geochimica et Cosmochimica Acta* **45**, 1345-1355.

Mackenzie, A., Patience, R., Maxwell, J., Vandenbroucke, M., and Durand, B. (1980). Molecular parameters of maturation in the Toarcian shales, Paris Basin, France—I. Changes in the configurations of acyclic isoprenoid alkanes, steranes and triterpanes. *Geochimica et Cosmochimica Acta* **44**, 1709-1721.

Mackenzie, A. S. (1984). Application of biological markers in petroleum geochemistry. *In* "Advances in Petroleum Geochemistry" (B. J. and W. D., eds.), Vol. 1, pp. 115-215. Academic Press, London.

Mackenzie, A. S., Lamb, N. A., and Maxwell, J. R. (1982). Steroid hydrocarbons and the thermal history of sediments. *Nature* **295**, 223-226.

Macquaker, J. H. S., Gawthorpe, R. L., Taylor, K. G., and Oates, M. J. (1998). Heterogeneity, stacking patterns and sequence stratigraphic interpretation in distal mudstone successions: examples from the Kimmeridge Clay Formation, UK. In "Shales and Mudstones: Basin Studies, Sedimentology, and Palaeontology " (J. Schieber, W. Zimmerle and P. Sethi, eds.), Vol. 1, pp. 163-186. E. Schweizerbart'sche Verlagsbuchhandlung,, Stuttgart.

Magoon, L., and Dow, W. (1991). The petroleum system-from source to trap. *American Association of Petroleum Geologists memoir **60,*** pp. 655.

Magoon, L. B., and Beaumont, E. A. (1999). Petroleum system *In* "Exploring for oil and gas traps" (E. A. Beaumont and N. H. Foster, eds.), pp. 3.1-3.34. American Association of Petroleum Geologists Treatise of Petroleum Geology.

Mansour, A. T., and Magairhy, I. A. (1996). Petroleum geology and stratigraphy of the southeastern part of the Sirt Basin, Libya. *In* "The geology of Sirt Basin" (M. J. Salem, A. S. El-Hawat and A. M. Sbeta, eds.), Vol. 2, pp. 485-528. Elsevier, Amsterdam.

McCaffrey, M. A., Michael Moldowan, J., Lipton, P. A., Summons, R. E., Peters, K. E., Jeganathan, A., and Watt, D. S. (1994). Paleoenvironmental implications of novel C_{30} steranes in Precambrian to Cenozoic Age petroleum and bitumen. *Geochimica et Cosmochimica Acta* **58**, 529-532.

McKirdy, D., Aldridge, A., and Ypma, P. (1983). A geochemical comparison of some crude oil from pre-Ordovician carbonate rocks. *In* "Advances in organic geochemistry 1981" (M. B. e. al., ed.), pp. 99-107. Wiley, New York.

Meijun, L., Yunlong, J., and Liguo, H. (2003). Geochemical-sequence stratigraphy and its application prospects in lake Basins. *Chinese Journal of Geochemistry* **22**, 164-172.

Mello, M. R., Telnaes, N., Gaglianone, P. C., Chicarelli, M. I., Brassell, S. C., and Maxwell, J. R. (1988). Organic geochemical characterisation of depositional palaeoenvironments of source rocks and oils in Brazilian marginal basins. *Organic Geochemistry* **13**, 31-45.

Moldowan, J. M., Lee, C., Sundararaman, P., Salvatori, T., Alajbeg, A., Gjukic, B., and Demaison, G. J. (1992). Source correlation and maturity assessment of select oils and rocks from the Central Adriatic Basin (Italy and Yugoslavia). *In* "Biological markers in sediments and petroleum" (J. M. Moldowan, P. Albrecht and P. R. P., eds.), pp. 730-401. Prentice Hall, Englewood Cliffs, New Jersey.

Moldowan, J. M., Seifert, W. K., and Gallegos, E. J. (1985). Relationship between petroleum composition and depositional environment of petroleum source rocks. *American Association of Petroleum Geologists Bulletin* **69**, 1255-1268.

Moldowan, J. M., Sundararaman, P., and Schoell, M. (1986). Sensitivity of biomarker properties to depositional environment and/or source input in the Lower Toarcian of SW-Germany. *Organic Geochemistry* **10**, 915-926.

Montgomery, S. (1994). Sirte Basin, North-central Libya–prospects for the future: Petroleum Information Corporation. *Petroleum Frontiers* **11**, 94.

Mueller, E., Philip, R., and Allen, J. (1995). Geochemical characterization and

relationship of oils and solid bitumens from SE Turkey. *Journal of Petroleum Geology* **18**, 289-308.

Murray, A., and Boreham, C. (1992). Organic geochemistry in petroleum exploration. *Australian Geological Survey Organization, Canberra*, 230.

Norgate, C. M., Boreham, C. J., and Wilkins, A. J. (1999). Changes in hydrocarbon maturity indices with coal rank and type, Buller Coalfield, New Zealand. *Organic Geochemistry* **30**, 985-1010.

Othman, R. S., (2003). Petroleum Geology of the Gunnedah-Bowen-Surat Basins, Northern New South Wales, , Ph. D. Dissertation ,University of New South Wales.

Ourisson, G., Albrecht, P., and Rohmer, M. (1979). The hopanoids, paleochemistry and biochemistry of a group of natural products. *Pure and Applied Chemistry* **51**, 709-729.

Ourisson, G., Albrecht, P., and Rohmer, M. (1982). Predictive microbial biochemistry—from molecular fossils to procaryotic membranes. *Trends in Biochemical Sciences* **7**, 236-239.

Ourisson, G., Albrecht, P., and Rohmer, M. (1984). Microbial origin of fossil fuels. *Scientific American* **251**, 44-51.

Parsons, M. G., Zagaar, A. M., and Curry, J. J. (1980). Hydrocarbon occurrences in the Sirte Basin, Libya. (A. D. Miall, ed.), pp. 723-732. Canadian Society of Petroleum Geologists Memoir **6**.

Peakman, T. M., Haven, H. L. T., Rechka, J. R., De Leeuw, J. W., and Maxwell, J. R. (1989). Occurrence of (20R)- and (20S)-Δ8(14) and -Δ14 5α(H)-steranes and the origin of 5α(H),14β(H),17β(H)-steranes in an immature sediment. *Geochimica et Cosmochimica Acta* **53**, 2001-2009.

Pedersen, T., and Calvert, S. (1990). Anoxia vs. Productivity: What Controls the Formation of Organic-Carbon-Rich Sediments and Sedimentary Rocks? *Association of Petroleum Geologists Bulletin* **74**, 454-466.

Peter, K. E., and Moldowan, J. M. (1993). "The biomarker guide: interpreting molecular fossils in petroleum and ancient sediments," Englewood Cliffs, New Jersey.

Peters, K. E. (1986). Guidelines for evaluating petroleum source rock using programmed pyrolysis. *American Association of Petroleum Geologists Bulletin* **70**, 318-329.

Peters, K. E., and Cassa, M. R. (1994). Applied source rock geochemistry. *In* "The Petroleum System—from source to trap" (L. B. Magoon and W. G. Dow, eds.), pp. 93-120. American Association of Petroleum Geologists Memoir **60**.

Peters, K. E., and Moldowan, J. M. (1991). Effects of source, thermal maturity, and biodegradation on the distribution and isomerization of homohopanes in petroleum. *Organic Geochemistry* **17**, 47-61.

Peters, K. E., Moldowan, J. M., Driscole, A. R., and Demaison, G. J. (1989). Origin of Beatrice oil by co-sourcing from Devonian and Middle Jurassic source rocks, inner Moray Firth, United Kingdom. *American Association of Petroleum Geologists Bulletin* **73**, 454-471.

Peters, K. E., Moldowan, J. M., McCaffrey, M. A., and Fago, F. J. (1996). Selective biodegradation of extended hopanes to 25-norhopanes in petroleum reservoirs. Insights from molecular mechanics. *Organic Geochemistry* **24**, 765-783.

Peters, K. E., Moldowan, J. M., and Sundararaman, P. (1990). Effects of hydrous pyrolysis on biomarker thermal maturity parameters: Monterey phosphatic and siliceous members. *Organic Geochemistry* **15**, 249-265.

Peters, K. E., Ramos, L. S., Zumberge, J. E., Valin, Z. C., Scotese, C. R., and Gautier, D. L. (2007). Circum-Arctic petroleum systems identified using decision-tree chemometrics. *American Association of Petroleum Geologists Bulletin* **91**, 877-913.

Peters, K., Snedden, J., Sulaeman, A., Sarg, J. and Enrico, R., (2000). A new geochemical-sequence stratigraphic model for the Mahakam Delta and Makassar Slope, Kalimantan, Indonesia. *American Association of Petroleum Geologists Bulletin* **84**, 12-44.

Peters, K. E., Walters, C. C., and Moldowan, J. M. (2005). The Biomarker Guide, Vol. 1 and 2. pp. 1155. Cambridge University Press, Cambridge.

Philip, B. (1992). Raguba Field; Libya, Sirte Basin. in: Atlas of Oil and Gas Fields; Structural Traps, (Eds.) E.A. Beaumont, N.H. Foster, Vol. 6, American Association of Petroleum Geologists, Treatise of Petroleum Geology, pp. 267-289.

Philp, R. P. (1985). Fossil fuel biomarkers methods in geochemistry and geophysics. *Elsevier, New York* **23**, 292.

Philp, R. P. (2007). Formation and geochemistry of oil and gas. *In* "sediments, Diagenesesis, and sedemntary rocks, Treatise on Geochemistry" (F. T. Mackenzie, ed.), Vol. 7, pp. 223-256.

Philp, R. P., and Gilbert, T. (1986). Biomarker distributions in Australian oils

predominantly derived from terrigenous source material. *Organic Geochemistry* **10**, 73-84.

Pieri, N., Jacquot, F., Mille, G., Planche, J. and Kister, J., (1996). GC-MS identification of biomarkers in road asphalts and in their parent crude oils. Relationships between crude oil maturity and asphalt reactivity towards weathering. *Organic geochemistry*, **25**, 51-68.

Powell, T., and McKirdy, D. (1973). Relationship between ratio of pristane to phytane, crude oil composition and geological environment in Australia. *Nature* **243**, 37-39.

Prince, R. C. (1987). Hopanoids: The world's most abundant biomolecules? *Trends in Biochemical Sciences* **12**, 455-456.

Radke, J., Bechtel, A., Gaupp, R., Püttmann, W., Schwark, L., Sachse, D., and Gleixner, G. (2005). Correlation between hydrogen isotope ratios of lipid biomarkers and sediment maturity. *Geochimica et Cosmochimica Acta* **69**, 5517-5530.

Radke, M. (1987). Organic geochemistry of aromatic hydrocarbons. *In* "Advances in petroleum geochemistry" (J. Brooks and D. Welte, eds.), Vol. 2, pp. 141-207. Academic Press.

Radke, M., Vriend, S., and Schaefer, R. (2001). Geochemical characterization of lower Toarcian source rocks from NW Germany: Interpretation of aromatic and saturated hydrocarbons in relation to depositional environment and maturation effects. *Journal of Petroleum Geology* **24**, 287-307.

Radke, M., and Welte, D. (1983). The methylphenanthrene index (MPI): A maturity parameter based on aromatic hydrocarbons. *In* "Advances in organic geochemistry 1981" (M. Bjorøy, et al. , ed.), pp. 504-512. Wiley Chichester.

Radke, M., Welte, D. H., and Willsch, H. (1982a). Geochemical study on a well in the Western Canada Basin: relation of the aromatic distribution pattern to maturity of organic matter. *Geochimica et Cosmochimica Acta* **46**, 1-10.

Radke, M., Willsch, H., Leythaeuser, D., and Teichmüller, M. (1982b). Aromatic components of coal: relation of distribution pattern to rank. *Geochimica et Cosmochimica Acta* **46**, 1831-1848.

Riediger, C. L. (1997). Geochemistry of potential hydrocarbon source rocks of Triassic age in the Rocky Mountain Foothills of northeastern British Columbia and west-central Alberta. *Bulletin of Canadian Petroleum Geology* **45**, 719-741.

Raymond, A. C., and Murchison, D. G. (1992). Effect of igneous activity on

molecular-maturation indices in different types of organic matter. *Organic Geochemistry* **18**, 725-735.

Risatti, J., Rowland, S., Yon, D., and Maxwell, J. (1984). Stereochemical studies of acyclic isoprenoids—XII. Lipids of methanogenic bacteria and possible contributions to sediments. *Organic Geochemistry* **6**, 93-104.

Roohi, M. (1996a). Geological history and hydrocarbon migration pattern of the central Az Zahrah–Al Hufrah Platform. *In* "The geology of Sirt Basin" (M. J. Salem, A. S. El-Hawat and A. M. Sbeta, eds.), Vol. 2, pp. 435-454. Elsevier, Amsterdam.

Roohi, M. (1996b). A geological view of source-reservoir relationships in the western Sirt Basin. *In* "The geology of Sirt Basin" (M. J. Salem, A. S. El-Hawat and A. M. Sbeta, eds.), Vol. 2, pp. 323-336. Elsevier, Amsterdam.

Rullkötter, J., Mackenzie, A., Welte, D., Leythaeuser, D., and Radke, M. (1984). Quantitative gas chromatography—mass spectrometry analysis of geological samples. Organic Geochemistry **6**, 817-827.

Rullkötter, J., and Marzi, R. (1988). Natural and artificial maturation of biological markers in a Toarcian shale from northern Germany. *Organic Geochemistry* **13**, 639-645.

Rullkötter, J., Meyers, P. A., Schaefer, R. G., and Dunham, K. W. (1986). Oil generation in the Michigan basin: a biological marker and carbon isotope approach. *Organic Geochemistry* **10**, 359-375.

Rusk, D. C. (2001). Libya, Petroleum Potential of the Underexplored Basin Centers--A Twenty-First-Century Challenge. *In* "Petroleum geology of the twenty-first century" (M. J. Downey, J. C. Threet and W. A. Morgan, eds.), pp. 429-452. American Association of Petroleum Geologists Memoir **74**.

Samuel, O.J., Cornford, C., Jones, M., Adekeye, O.A. and Akande, S.O., (2009). Improved understanding of the petroleum systems of the Niger Delta Basin, Nigeria. *Organic Geochemistry*, **40,** 461-483.

Sanford, R. M. (1970). Sarir oil field, Libya--desert surprise. *In* "Geology of giant petroleum fields" (M. T. Halbouty, ed.), pp. 449-476. American Association of Petroleum Geologist Memoir **14**.

Schidlowski, M. (1988). A 3,800-million-year isotopic record of life from carbon in sedimentary rocks. *Nature* **333**, 313-318.

Schimmelmann, A., Lewan, M. D., and Wintsch, R. P. (1999). D/H isotope ratios of kerogen, bitumen, oil, and water in hydrous pyrolysis of source rocks containing kerogen types I, II, IIS, and III. *Geochimica et Cosmochimica Acta*

63, 3751-3766.

Schröter, T. (1996). Tectonic and sedimentary development of the central Zallah trough (West Sirt Basin, Libya). *In* "Geology of the Sirt Basin" (M. J. Salem, A. S. El-Hawat and A. M. Sbeta, eds.), Vol. 3, pp. 123-136. Elsevier, Amsterdam.

Schutter, S. R. (1998). Characteristics of shale deposition in relation to stratigraphic sequence systems tracts. *In* "Shales and Mudstones—Basin Studies, Sedimentology, and Paleontology" (J. Schieber, et al, ed.), pp. 79-107. E. Schweizerhbart'sche, Stuttgart.

Schwark, L., and Empt, P. (2006). Sterane biomarkers as indicators of Palaeozoic algal evolution and extinction events. *Palaeogeography, Palaeoclimatology, Palaeoecology* **240**, 225-236.

Seifert, W., and Moldowan, J. (1986). Use of biological markers in petroleum exploration. *In* "Methods in geochemistry and geophysics" (R. B. Johns), ed.), Vol. 24, pp. 261-290. Amsterdam, Elsevier.

Seifert, W. K., and Michael Moldowan, J. (1978). Applications of steranes, terpanes and monoaromatics to the maturation, migration and source of crude oils. *Geochimica et Cosmochimica Acta* **42**, 77-95.

Seifert, W. K., and Michael Moldowan, J. (1979). The effect of biodegradation on steranes and terpanes in crude oils. *Geochimica et Cosmochimica Acta* **43**, 111-126.

Seifert, W. K., and Moldowan, J. M. (1980). The effect of thermal stress on source-rock quality as measured by hopane stereochemistry. *Physics and Chemistry of the Earth* **12**, 229-237.

Selley, R. C. (1966). Near-shore marine and continental sediments of the Sirte basin, Libya. *Quarterly Journal of the Geological Society* **124**, 419-460.

Selley, R. C. (1971). Structural control of the Miocene sedimentation in the Sirt Basin. *In* "Symposium on the geology of Libya" (C. Gray, ed.), pp. 99-106. University of Libya, Science Faculty, Tripoli, Libya.

Selley, R. C., (1997). The Sirt basin of Libya. *In* "African basins: Sedimentary basins of the World" (R. C. Selley, ed), 3, 27– 37.

Sghair, A. M. A., and El-Alami, M. A. (1996). Depositional environment and diagenetic history of the Maragh Formation, NE Sirt Basin, Libya. *In* "The Geology of the Sirt Basin" (M. J. Salem, A. S. El-Hawat and A. M. Sbeta, eds.), pp. 263-271. Elsevier, Amsterdam.

Shanmugam, G. (1985). Significance of coniferous rain forests and related organic matter in generating commercial quantities of oil, Gippsland Basin, Australia. *American Association of Petroleum Geologists Bulletin* **69**, 1241-1254.

Shi, J., Benshan, W., Lijie, Z., and Zhiqing, H. (1988). Study on diagenesis of organic matter in immature rocks. *Organic Geochemistry* **13**, 869-874.

Simoneit, B. R. T. (1978). The organic chemistry of marine sediments. *Chemical oceanography* **7**, 233-311.

Simoneit, B. R. T., Schoell, M., Dias, R. F., and de Aquino Neto, F. R. (1993). Unusual carbon isotope compositions of biomarker hydrocarbons in a Permian tasmanite. *Geochimica et Cosmochimica Acta* **57**, 4205-4211.

Singh, P. (2008). Lithofacies and sequence stratigraphic framework of the Barnett Shale, northeast Texas. Unpubl, Ph. D. Dissertation, The University of Oklahoma, 181p.

Sinninghe Damsté, J. S., Kenig, F., Koopmans, M. P., Köster, J., Schouten, S., Hayes, J., and de Leeuw, J. W. (1995). Evidence for gammacerane as an indicator of water column stratification. *Geochimica et Cosmochimica Acta* **59**, 1895-1900.

Slatt, R. M. (2006). "Stratigraphic reservoir characterization for petroleum geologists, geophysicists, and engineers," 1/Ed. Elsevier Science Limited, Amsterdam.

Slatt, R. M., and Rodriguez, N. (2011). Comparative sequence stratigraphy and organic geochemistry of North American unconventional gas shales: Commonality or coincidence (abstract). *In* "AAPG Hedberg ", Austin, Texas.

Slatt, R. M., and Rodriguez, N. D. (2012). Comparative sequence stratigraphy and organic geochemistry of gas shales: Commonality or coincidence? *Journal of Natural Gas Science and Engineering* **8**, 68-84

Slatt, R. M., Singh, P., Philp, R. P., Marfurt, K. J., Abousleiman, Y., Brien, N. R. O., and Eslinger, E. (2009). Workflow for stratigraphic characterization of unconventional gas shales. *SPE. Paper Number 119891-MS*

Sofer, Z. (1984). Stable carbon isotope compositions of crude oils: application to source depositional environments and petroleum alteration. *American Association of Petroleum Geologist Bulletin* **68**, 31-49.

Stach, E., Mackowsky, M. T., Teichmüller, M., Taylor, G., Chandra, D., and Teichmüller, R. (1982). "Stach's Textbook of Coal Petrology (2nd edn.) Borntraeger," 3/Ed. Gebruder Borntraeger, Berlin

Stojanović, K., Jovančićević, B., Vitorovi, D., Pevneva, G., S. Golovko, J. A., and

Golovko, A. K. (2007). New maturation parameters based on naphthalene and phenanthrene isomerization and dealkylation processes aimed at improved classification of crude oils (Southeastern Pannonian Basin, Serbia). *Geochemistry International* **45**, 781-797.

Sun, Y., Chen, Z., Xu, S., and Cai, P. (2005). Stable carbon and hydrogen isotopic fractionation of individual n-alkanes accompanying biodegradation: evidence from a group of progressively biodegraded oils. *Organic Geochemistry* **36**, 225-238.

Tawadros, E. (2001). Geology of Egypt and Libya: Balkema, Rotterdam. Elsevier, 468p.

Taylor, G. H.; Teichmueller, M., Davis, A., Diessel, C. F. K., Littke, R., Robert, P., Glick, D. C., Smyth, M., Swaine, D. J., and Vanderbroucke, M. (1998). Organic petrology: A new handbook incorporating some revised parts of Stach's textbook of coal petrology, Gebrüder Borntraeger.

Tegelaar, E., De Leeuw, J., and Sáiz-Jiménez, C. (1989). Possible origin of aliphatic moieties in humic substances. *Science of the total environment* **81**, 1-17.

ten Haven, H., De Leeuw, J., and Schenck, P. (1985). Organic geochemical studies of a Messinian evaporitic basin, northern Apennines (Italy) I: Hydrocarbon biological markers for a hypersaline environment. *Geochimica et Cosmochimica Acta* **49**, 2181-2191.

ten Haven, H. L., Leeuw, J. d., Rullkotter, J., and Damaste, J. S. S. (1987). Restricted utility of the pristane/phytane ratio as a paleoenvironmental indicator. *Nature* **330**, 641-643.

ten Haven, H. L. T., Leeuw, J. W. D., Peakman, T. M., and Maxwell, J. R. (1986). Anomalies in steroid and hopanoid maturity indices. *Geochimica et Cosmochimica Acta* **50**, 853-855.

Thusu, B. (1996). Implication of the discovery of reworked and in-situ Late Palaeozoic and Triassic palynomorphs on the evolution of the Sirt Basin, Libya. *In* "The Geology of Sirt Basin" (M. J. Salem, A. J. Mouzughi and O. S. Hammuda, eds.), Vol. 1, pp. 455-475. Elsevier, Amsterdam.

Tissot, B., Pelet, R., and Ungerer, P. (1987). Thermal history of sedimentary basins, maturation indices, and kinetics of oil and gas generation. *American Association of Petroleum Geologists Bulletin* **71**, 1445-1466.

Tissot, B. P. Welte. D. H. (1984). Petroleum Formation and Occurrence," Springer Verlag, Berlin, New York.

Tourtelot, H. A. (1979). Black shale--its deposition and diagenesis. Clays and Clay Minerals 27, 313-321.

van Aarssen, B. G. K., Bastow, T. P., Alexander, R., and Kagi, R. I. (1999). Distributions of methylated naphthalenes in crude oils: indicators of maturity, biodegradation and mixing. *Organic Geochemistry* **30**, 1213-1227.

van Wagoner, J. C., Mitchum, R. M., Campion, K. M., and Rahmanian, V. D. (1990). Siliciclastic sequence stratigraphy in well logs, cores, and outcrops. *American Association of Petroleum Geologists Methods in Exploration Series 7*, 1-55.

van Wagoner, J. C., Mitchum, R. M., Posamentier, H. W., and Vail, P. R. (1987). Seismic stratigraphy interpretation using sequence stratigraphy, part 2. Key definitions of sequence stratigraphy *In* "Atlas of Seismic stratigraphy" (A. W. Bally, ed.), pp. 11-14. American Association of petroleum Geologists 27.

Volkman, J., Banks, M., Denwer, K., and Aquino Neto, F. (1989). Biomarker composition and depositional setting Tasmanite oil shale from northern Tasmania, Australia (abstract). *In* "14th International Meeting on Organic Geochemistry ", pp. 18-22, Paris.

Volkman, J. K. (1986). A review of sterol markers for marine and terrigenous organic matter. *Organic Geochemistry* **9**, 83-99.

Volkman, J. K. (1988). Biological marker compounds as indicators of the depositional environments of petroleum source rocks. *In* "Lacustrine petroleum source rocks" (A. J. Fleet, K. Kelts and M. R. Talbot, eds.), Vol. 40, pp. 103-122. Geological Society, London, Special Publications.

Wang, H. D. (1993). A geochemical study of potential source rocks and crude oils in the Anadarko Basin, Ph. D. Dissertation, The University of Oklahoma.

Waples, D. W. (1985). "Geochemistry in Petroleum Exploration," International Human Resources Development Corporation, Boston, MA.

Waples, D.W. (1994). Modeling of sedimentary basins and petroleum systems. *In* "The Petroleum System—from source to trap" (L. B. Magoon and W. G. Dow, eds.), pp. 307-322. American Association of Petroleum Geologists Memoir **60**.

Waples, D. W., and Machihara, T. (1990). Application of sterane and tritepane biomarkers in petroleum exploration Bulletin of Canadian Petroleum Geology. *Bulletin of Canadian Petroleum Geology* **3**, 357-380.

Wenger, L., Davis, C., and Isaksen, G. (2001). Multiple controls on petroleum biodegradation and impact on oil quality. *SPE Paper Number 71450-MS*.

Yensepbayev, T., Izart, A., Joltaev, G., Hautevelle, Y., Elie, M. and Suarez-Ruiz, I., (2010). Geochemical characterization of source rocks and oils from the eastern part of the Precaspian and Pre-Uralian Basins (Kazakhstan): Palaeoenvironmental and palaeothermal interpretation. *Organic Geochemistry*, **41,** 242-262.

Younes, M. and Philp, R., (2005). Source rock characterization based on biological marker distributions of crude oils in the southern Gulf of Suez, Egypt. Journal of Petroleum Geology, **28**, 301-317.

Zumberge, J. E. (1984). Source rocks of the La Luna Formation (Upper Cretaceous) in the Middle Magdalena Valley, Colombia. *In* "Petroleum geochemistry and source rock potential of carbonate rocks" (J. G. Palacas, ed.), pp. 127-133. American Association of Petroleum Geologists, Studies in Geology 18.

Appendices

Appendix I. Sedimentary Organic Matter

Definition

Organic matter is produced by plants, microbes and other organisms and accumulates in aqueous environments. The nature of organic matter is different in continental and marine environments. Continental environments are dominated by land plants that accumulate in coastal plain environments and by freshwater algae which accumulate in lakes. Marine environments are dominated by phytoplankton. When organic matter accumulates, it undergoes alteration through many mechanisms. These mechanisms include anaerobic microbial activities that form methane and purely physical or chemical processes like dehydration and oxidation (Tissot and Welte, 1984; Hunt, 1996).

In the sedimentary record, organic matter is the solid material containing organic carbon. Most of the organic matter in sedimentary rocks is animal remains and plants which lived at the time the sediment was deposited. Even though they are derived from organic matter, crude oil and natural gas are not included in this definition (Taylor et al., 1998).

Organic Matter in the Ocean

Phytoplankton are the main source of organic matter in marine environments. The main groups of phytoplankton include diatoms, dinoflagellates, and coccolithophora (Tissot and Welte, 1984). These account for 95% of marine primary production (Killops and Killops, 2005). In the ocean, bacteria are considered an important producer of organic matter in addition to phytoplankton. Bacterial production of

__Note__: Reference list of Appendix I is included in main reference list of dissertation

organic matter is less than that of phytoplankton. Bacteria decompose the dead organic matter and convert it into forms which can be used by aquatic plants and aquatic animals which also use bacteria as food. In the sea water, bacteria can be attached to phytoplankton and other particles suspended in the water. It can be also found on the sea floor, and in the top layer of sediment in shallow to moderate water depths (Tissot and Welte, 1984).

Factors controlling primary productivity:

Since phytoplankton are primary producers, they are the base of the food chain and the foundation of life in the ocean. The factors controlling levels of productivity in surface water are related to the life of phytoplankton. Photosynthesis is an important process in primary production of organic matter. During this process plants, algae and photosynthetic bacteria use light energy to synthesize organic compounds. Photosynthesis starts with the assimilation of CO_2 from the atmosphere by primary photosynthesizers, such as phytoplankton in aquatic environments (Killops and Killops, 2005).

Ocean productivity is primarily controlled by light availability, nutrient concentrations and temperature. Photosynthesis is thought to be the most important form of primary production for at least the past 3.5 billion years (Schidlowski, 1988). Through photosynthesis, CO_2 and water is transformed into high energy carbohydrates:

$CO_2 + H_2O \rightarrow CH_2O$ (organic matter) + O_2

The production of organic matter is not only limited by CO_2 or water in aquatic environments but also by nutrient availability. Phosphorus and nitrogen are the most important nutrients.

Light is a most important factor in primary production. Light affects the rate of photosynthesis and therefore, primary production. In general, photosynthesis and growth of phytoplankton are limited by the depth of the photic zone. The photic zone is the layer that is exposed to suitable sunlight for photosynthesis to occur. However, in the Polar Regions, the depth in the open ocean and turbid coastal water effect the penetration of the light. The depth of the photic zone can be greatly affected by seasonal turbidity. The photic zone in clear oceanic water is generally located at 200 m of the ocean (Killops and Killops, 2005). In some estuaries the light may only penetrate a few centimeters because of the large amount of suspended materials (Killops and Killops, 2005). However, the upper 60 to 80 m of the water column is the main zone of organic matter production (Tissot and Welte, 1984). In tropical oceans, photic zones generally contain very low concentrations of nutrients because nutrients are consumed by the phytoplankton. Phytoplankton production can only occur if nutrients are supplied to the photic zone from the bottom by vertical mixing that can be happened by either turbulence or upwelling. The centers of the mid-latitude oceans have low production rates because the warm surface layers are separated from the deep layers all the time. In these locations, nutrients are only driven by wind (Killops and Killops, 2005). In equatorial regions, the rate of production is moderate throughout the year; the drive mechanism of nutrients is upwelling from shallow depths. In high latitudes, high production occurs on the summer and spring when the

photic zone becomes thick and the surface layers expose to the sun's heat (Pedersen and Calvert, 1990).

The temperature of ocean water is interrelated with illumination and water mixing. The temperature has a great effect on primary productivity. There is certain temperature for various phytoplankton species. For example, dinoflagellates live in warm tropical waters with temperature of 25°C or more while siliceous diatoms prefer the cold water of 5°C to 15°C (Tissot and Welte, 1984).

Settling of Organic Matter

Dead phytoplankton and animals in the ocean supply the organic matter which will sink down into deeper water and the ocean floor. The organic matter undergoes many processes and changes during settling. These processes vary from place to place in the ocean depending on the water depth, level of production, availability of oxidants and sedimentation rate (Bjørlykke, 2010). Part of this organic matter is oxidized during settling and another part is used as food by other organisms such as benthic organisms. Also, some of it undergoes degradation in sediment where the remaining part is buried and some is chemically converted to crude oil (Bjørlykke, 2010).

Breakdown of Organic Matter

Most of the organic matter is oxidized in the water column or on the ocean floor and the nutrients are released into the water and become available for new organic production (Figure 1). The organic matter that is produced in the oceans by phytoplankton is broken down through direct oxidation or by microbiological

processes (Bjørlykke, 2010). In the presence of oxygen, it will break down in a manner as indicated below:

$$CH_2O + O_2 \rightarrow CO_2 + H_2O$$

If oxygen is available, organic matter is rapidly oxidized. As organisms die, organic material suspended in seawater falls through the water column and consumes dissolved oxygen. If water circulation is limited the dissolved oxygen supply will be absent or limited. In this case, sulphate-reducing bacteria, which decompose organic material in an anoxic environment will use the oxygen bound in sulphates or nitrates. The few centimeters directly below the sea floor are usually oxidizing, while depths 5–30 cm below the sea floor may have reducing conditions. Below this redox boundary which is characterized by absence of oxygen, sulphate-reducing bacteria and organic matter react in the following way (Bjørlykke, 2010):

$$NH_3 + H+ + SO_2 \rightarrow NO_3 + H_2S + H_2O$$

$$2CH_2O + 2H+ + SO_4-- \rightarrow H_2S + 2CO_2 + 2H_2O$$

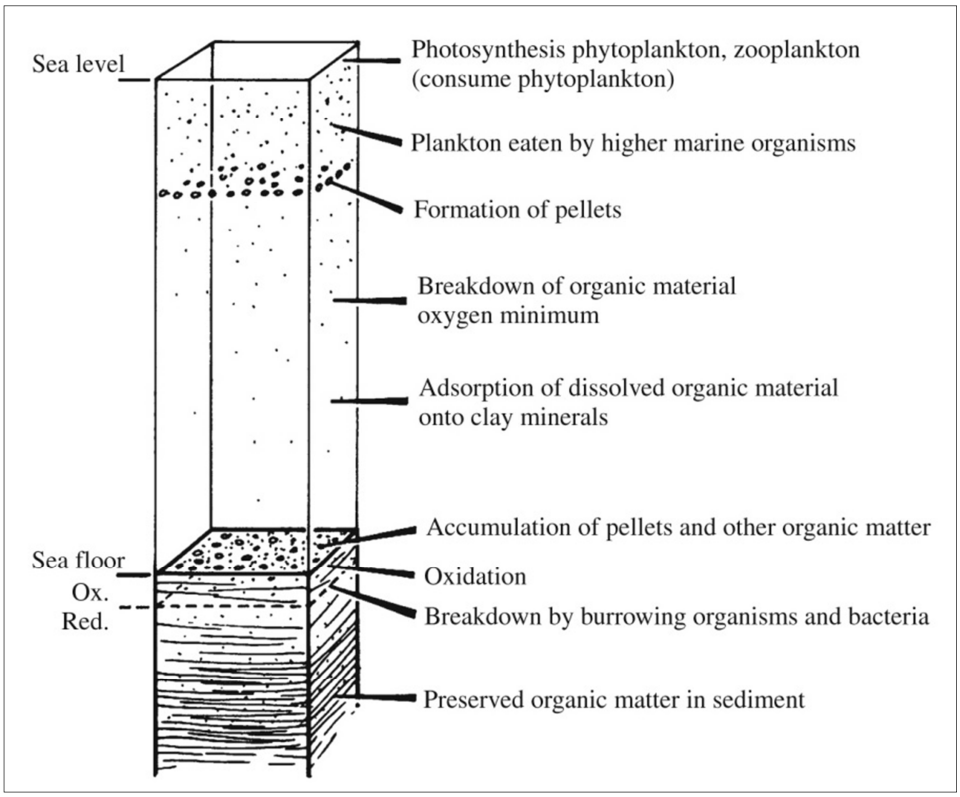


Figure 1. Formation of source rocks. Only a small fraction of the organic matter is preserved. The formation organic-rich source rocks require restricted water circulation and oxygen supply (Bjørlykke, 2010).

Preservation of Organic Matter

Pederson and Calvert, (1990) and Calvert and Pederson (1992) suggested that organic productivity is more important than anoxia and has major control on the high accumulations of organic matter in marine sediments. Therefore, environment with a very high rate of productivity is more likely to produce sediment having rich organic matter than one where the rate of productivity was low or limited.

Figure (2) shows that there is no great difference between two sediments that have similar texture and were deposited under oxic or anoxic conditions in fine grained bottom sediment. However, productivity and preservation are important in the formation of organic-rich rocks (Philp, 2007).

The abundance of organic matter is also controlled by sedimentary environment. The environment of deposition of the organic matter have a big influence on the characteristic of the hydrocarbon generation from organic matter in the sediment, because the environmental processes modify the conditions to be favorable for organisms to grow and partly because the dominant physio-chemical conditions modify the organic material during and directly after deposition (Bissada et al., 1993). According to Bohacs et al. (2005), the accumulation of organic matter in depositional environments is controlled by three main variables: rates of production, destruction, and dilution. The preservation or destruction of organic matter in sedimentary environments is also controlled by three factors: the oxygen supply, microbial activity, and the accumulation rate of the sediment (Demaison and Moore, 1980). Partial preservation requires that the processes of decomposition and oxidation do not eliminate all organic matter before some parts can be preserved in the sediments. In

other words, the rate of organic matter preserved must exceed the rate of destruction (Taylor et al., 1998). The formation of deposits rich in organic matter with high TOC values is controlled by subaquatic depositional environments (Tourtelot, 1979). Therefore, the preservation of organic matter depends both on the organic matter and the depositional environment conditions.

The anoxic aquatic environment is a water body with a very low or absence of oxygen content so all microbial activities are limited or terminated. Anoxic conditions occur where the demand of oxygen in the water column is more than the supply (Figure 3). Demand for oxygen depends on the productivity of the water surface and oxygen supply mainly depends on water circulation, which is controlled by global climatic changes (Demaison and Moore, 1980). Under an oxic water column, aerobic bacteria and other organisms consume organic matter settling from the photic zone while under anoxic, or suboxic water (less than 0.2 ml oxygen/l water), aerobic degradation of organic matter is reduced (Peters et al., 2005).

Sedimentation rate and grain size are of the sediment are also important in the preservation of organic matter. Organic matter is favorably deposited in low permeability fine-grained mud. Fine-grained sediments such as mud exclude rapidly oxygenated water below the sediment water interface, creating anoxic conditions during depositions (Peters et al., 2005). Organic matter that is deposited in a highly reducing environment and rapid sedimentation rate has a greater chance of being preserved than in oxic conditions (Philp, 2007). Preservation of organic matter in anoxic settings is increased compared with oxic settings when they have the same sedimentation rate (Yensepbayev, 2010).

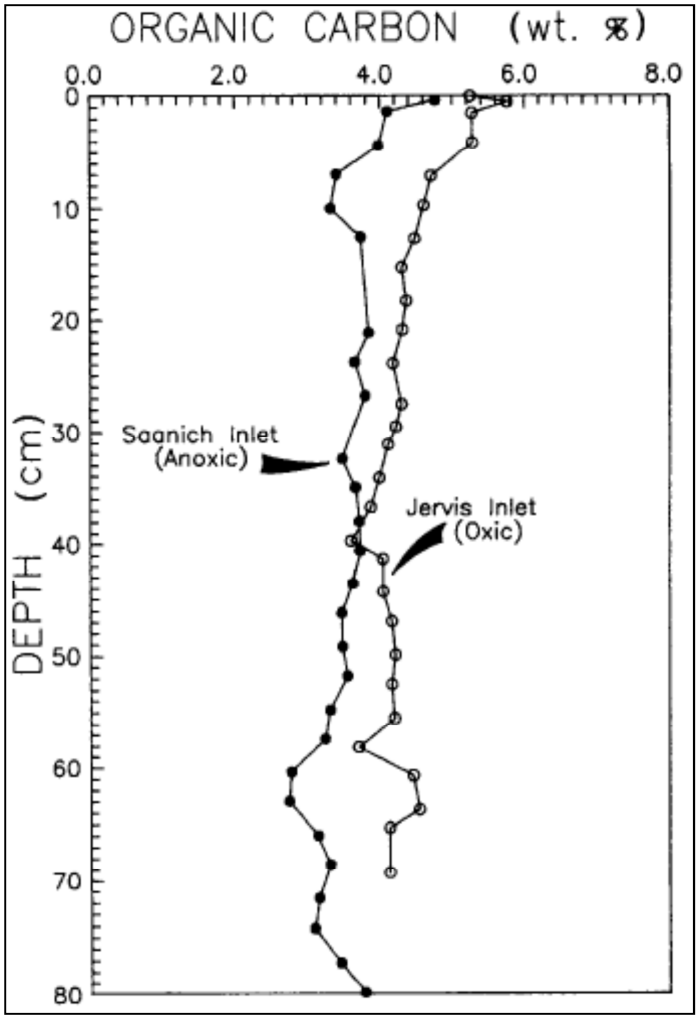


Figure 2. Distribution of two organic carbons with similar texture deposited in different conditions (Pederson and Calvert, 1990).

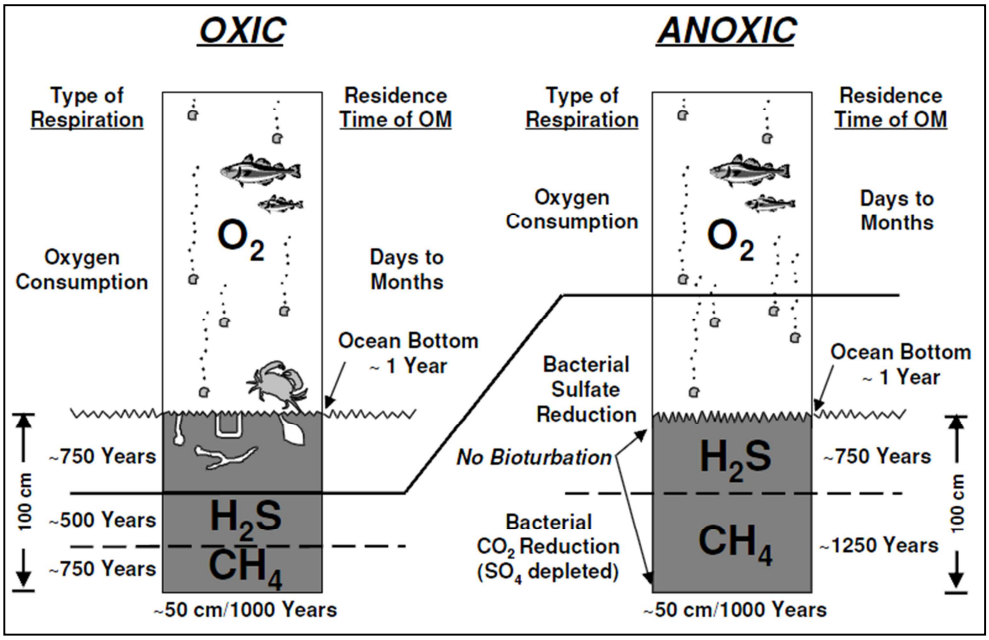


Figure 3. Oxic (left) and anoxic (right) depositional environments generally result in poor and good preservation of deposited organic matter, respectively (modified by Peters et al., 2005 after Demaison and Moore, 1980).

Types of Organic Matter

Most organic matter in sediment may be classified into two major types, sapropelic and humic. The term sapropelic refers to the decomposition and polymerization products of fatty, lipid-rich organic materials such as amorphous organic matter, and planktonic algae deposited in subaquatic muds mainly in marine or lacustrine environments under reducing conditions. The term humic refers to products of peat formation which are mainly land plant material deposited usually in swamps under oxic conditions (Hunt, 1996).

Organic matter can be classified into more detailed groups using microscopic analysis. For example, coal can be divided into three maceral groups (vitrinite, liptinite and inertinite). Each group is divided into subgroups of macerals where each maceral represents a specific source. For example, vitrinite is a maceral commonly associated with a higher land plant input, while alginite and exinite are associated with an algal input (Stach et al., 1982; Tissot and Welte 1984; Taylor et al., 1998).

Kerogen

Kerogen is a very heterogeneous agglomerate of macerals. The complexities of its macerals cause variations in its structures over relatively small distances within a source facies (Philp 2007). The term kerogen refers to organic matter in the sedimentary rocks that is insoluble in the common organic solvents which make it different from the extractable organic matter (Durand 1980; Tissot and Welt, 1984). Kerogen is considered the most abundant organic component on Earth (Brooks et al., 1987). Kerogen is believed to be economically the most important organic matter

because it is a major source for oil and gas. During diagenesis, most organic matter in the sediments is converted by microbiological processes into kerogen. One of the schemes which illustrated the mechanism for kerogen formation is shown in Figure 4. The processes of thermal maturation affect and change the kerogen composition. The subsurface temperature causes chemical reactions that break down small fragments of the kerogen to form oil or gas molecules (Waples, 1985). Oil is mainly generated during catagenesis when kerogen is thermally cracked to hydrocarbons and other compounds such as nitrogen, sulfur and oxygen compounds. Tissot and Welte (1984) summarize the classification of organic matter in sediments (Figure 5).

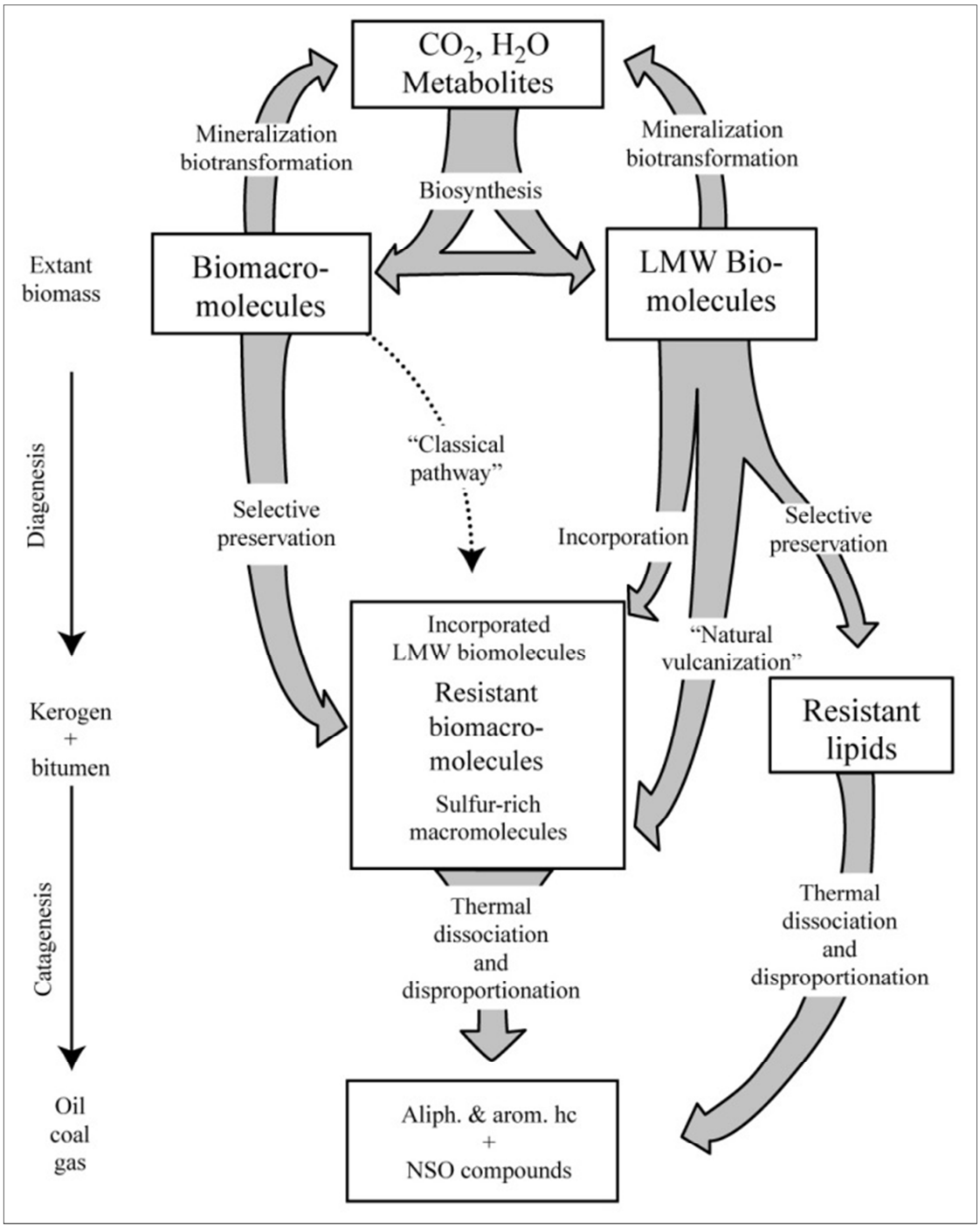


Figure 4. Proposed mechanism for kerogen formation describing the interrelationships between extant biomass, kerogen and fossil fuels. LMW denotes low-molecular-weight (Tegelaar et al., 1989; Philp, 2007).

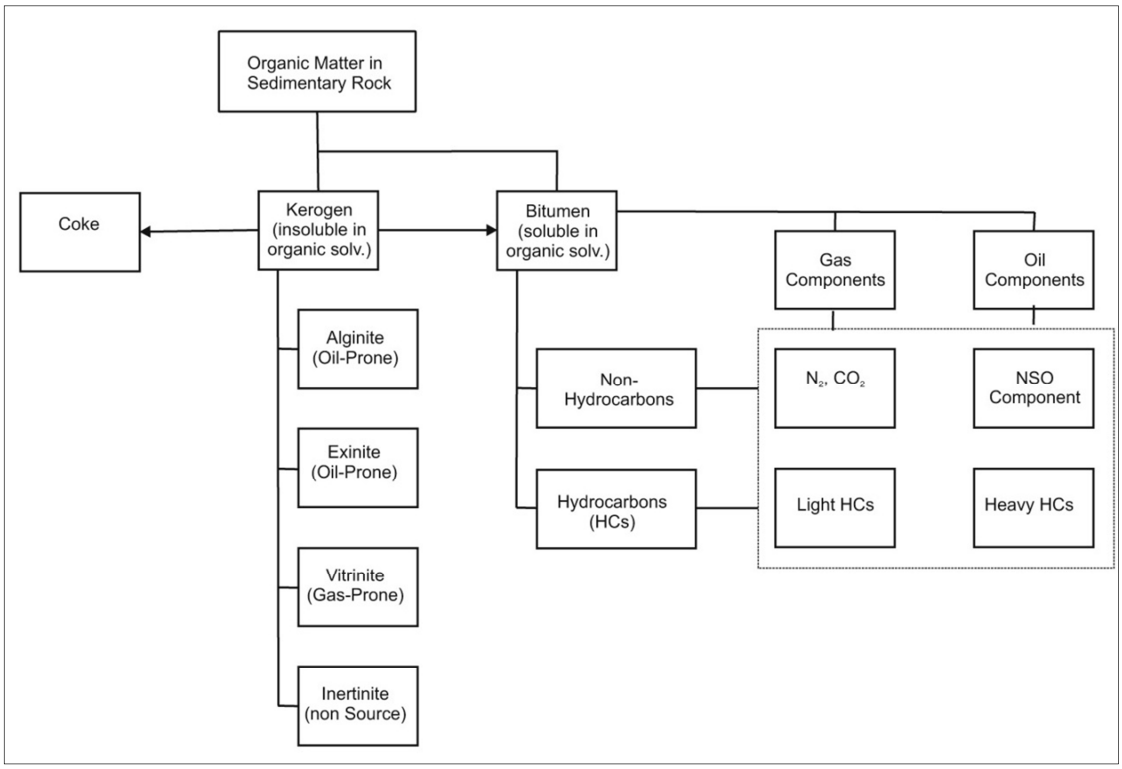


Figure 5. A geochemical fractionation of organic matter (Hantschel and Kauerauf, 2009).

Kerogen Type

Kerogen is subdivided into four main maceral types under the microscope based on optical characterization such as color, fluorescence, and reflectance (Stach et al., 1982; Tissot and Welte, 1984; Hunt 1996; Taylor et al., 1998). The main maceral groups are liptinite, exinite, vitrinite, and inertinite. These classifications of kerogen allow geochemists to identify the depositional environment of organic matter. Occurrence of each kerogen type is dependent on the types of organic matter preserved in a specific sedimentary environment.

Type I: Liptinite fluoresces under UV light and is derived mainly from an algal source, which is rich in lipids formed in lacustrine or lagoonal environments. It is oil-prone and has a high hydrogen index (HI) and a low oxygen index (OI). This type of kerogen is relatively rare compared to the other types.

Type II: Exinite also fluoresces under UV light and is the most abundant among kerogen types. Its source is mainly plant materials (spores, pollen, and cuticle), phytoplankton and bacterial microorganisms in marine sediments. This type is oil and gas-prone and has intermediate HI and OI.

Type III: Vitrinite has a low HI and high OI, therefore, it mainly generates gas. The primary source is higher plant materials. Vitrinite does not fluoresce under UV light. Therefore, it is increasingly reflective at higher levels of maturity. Therefore, vitrinite maceral is widely used as an indicator of source-rock maturity.

Type IV: Inertinite does not fluoresce. It is high in carbon and very low in hydrogen and does not have any effective potential to yield oil or gas. Inertinite is usually considered as dead-carbon (Brooks et al., 1987).

Kerogen can also be divided into the same four types based on chemical analysis. The early method used to characterize kerogen was based on the elemental composition of the kerogen (Tissot and Welte, 1984). This method is a plot of the atomic H/C versus atomic O/C on Van Krevelen diagrams (Figure 6, left). After the development of the Rock-Eval Pyrolysis system, it was found that the HI and OI indices are directly proportional to the H/C and O/C ratios. Therefore, the plot of HI vs. OI replaced the H/C and O/C values on the plot (Hunt, 1996). Now, the diagram is known as modified Van Krevelen diagram (Figure 6, right).

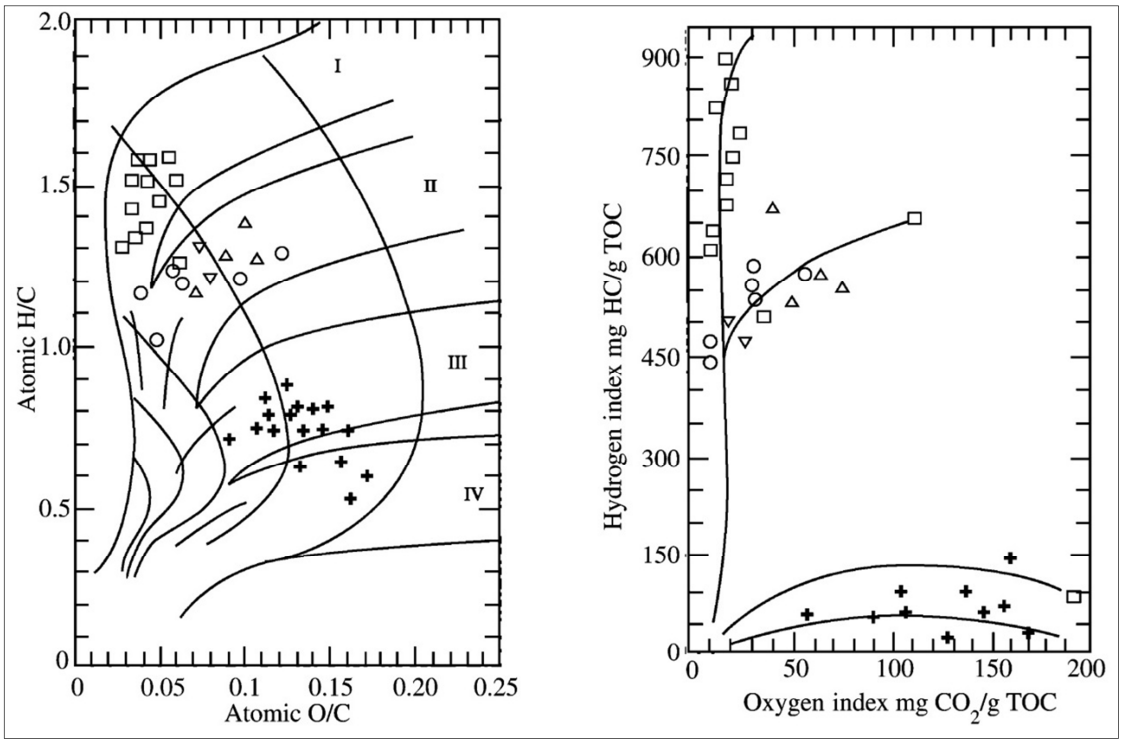


Figure 6. Classification of kerogen to four types based on chemical analysis (Hunt, 1996).

Organic Matter Content within Sequence Stratigraphy

Sequence stratigraphy is a study of genetically related sedimentary facies within a framework of chronostratigraphically significant surfaces within relative sea level changes (van Wagoner et al., 1987 and 1990). Sequence stratigraphy differs from lithostratigraphy in the sense that it takes rock surfaces as laterally continuous and correlative time intervals, rather than lithologic intervals. These intervals are deposited in relative sea-level cycles over geological time. When they are correctly defined, they allow prediction of stratigraphic patterns from terrestrial to deep marine environments, and more importantly, facies, hydrocarbon source, seal rocks, and reservoir (Slatt, 2006). The fundamental unit of sequence stratigraphy is bound by unconformities and their correlative conformities (van Wagoner et al., 1987). These sequences are also subdivided into systems tracts, and then to parasequences which are bound by marine flooding surfaces. Parasequences are stacked regionally and form parasequence sets with distinctive patterns bounded by major marine flooding surfaces. Geochemical data integrated into sequence stratigraphy is referred to as geochemical sequence stratigraphy (Pesters et al., 2000) and deals with both the geochemical characterization and distribution of source rocks relative to sea level changes within a sequence stratigraphy framework.

Lowstand Systems Tracts

Shales occur in systems tracts which can be identified by their predictable characteristics (Schutter, 1998). Lowstand fan shale deposits form during the waning period of proximal fan deposition. It includes allochthonous, waning, turbidite-fine grained sediment and autochthonous hemiplegic sediment (Schutter, 1998). Shale in lowstand fans can be rich or poor in organic matter content depending on the oxygen level. Since these shales of lowstand fans are interbedded with coarse clasts or carbonate, this shale can be good seal rock. However, lowstand wedge shales are relatively high in mud and terrestrial organic matter compared with lowstand fan shales (Schutter, 1998).

Transgressive Systems Tracts

Shales of transgressive systems tracts vary in thickness and continuity depending upon the rate of relative sea level rise. Thin and discontinuous shales are associated with rapid relative sea level rise while thick shales are deposited under slow relative sea level (Schutter, 1998). On a larger scale, transgressive tracts represent upward fining successions leading to condensed section (Macquaker et al., 1998).

Highstand Systems Tracts

Highstand systems tracts represent coarsening upward successions. Shales in these systems tracts will be non-calcareous shales which are associated with high amount of a siliciclastic component; carbonates are associated with calcareous shales (Schutter, 1998). The organic matter in highstand shales will be low and diluted with siliciclastic input.

Condensed Section

Condensed sections are associated with maximum flooding surfaces and are deposited during rising sea level and cover a large area of the basin. Condensed sections accumulate during the late transgressive systems tracts (TST), and therefore, they act as a boundary between TST and HST (Schutter, 1998). Condensed sections are widespread and are low-energy deposits resulting from relatively constant, low sedimentation rates. Condensed sections commonly concentrate and preserve organic matter (Creaney and Passey, 1993). The sediments are fine grained and lack coarse terrigenous particles. They usually contain skeletal remains of pelagic organisms which may be used to estimate the age of the sediments (Loutit et al., 1988).

Geochemical Sequence Stratigraphy Parameters

Integrated with sequence stratigraphy, organic geochemistry can be used to study the source rock potential within a sequence stratigraphic framework and predict the hydrocarbon characters of reservoirs. Therefore, it can be directly applied in petroleum geochemistry studies. There are many parameters that can be used as proxies to investigate the characterics of organic matter within a sedimentary sequence.

Organic Matter Content and Type

Organic matter is usually characterized by the total organic carbon content (TOC) and reflects changes of sea level within a sequence stratigraphic framework. The maximum total organic carbon in a vertical marine sequence likely correlates with the maximum flooding surface (Bohacs and Isaksen, 1991; Creaney and Passey, 1993). Low oxygen conditions at the sediment/water interface, rate of degradation of organic

matter, and sedimentation rate are the principal controls on organic matter accumulation (Creaney and Passey, 1993). TOC decreases above the maximum flooding surface due to increasing sediment dilution during high-stand progradation. In addition to this, TOC also decreases below maximum flooding surface with the higher sedimentation rate of the older transgressive systems tracts (Meijun, et al., 2003). However, potential source rocks can be found in all three systems tracts, but the richest source rock are generally found in the condensed section within transgressive systems tracts (Philp, 2007).

Creaney and Passey (1993) explain recurrent patterns in the vertical distribution of TOC in marine source rocks using sequence stratigraphic concepts. The highest TOC content in a shale sequence will be at the maximum flooding surfaces (condensed section) and the organic material will be increasingly oil prone. The LST sediments have lower TOC contents than TST/CS. The organic matter is relatively enriched in terrestrial (Type III) or type IV constituents (Lambert et al., 1993). Therefore, organic matter of LST will be gas prone.

Relative Hydrocarbon Potential

The relative hydrocarbon potential parameter (RHP) was proposed by Fang et al., (1993). RHP is calculated as (S1 + S2)/TOC, where S1, S2 and TOC can be obtained from Rock-Eval. TOC = measure of the rock's richness; S1= measure of the amount of free hydrocarbons present in the rocks. S1 is measured during the first stage of pyrolysis at the fixed temperature of 300º C; and S2 = measure of the hydrocarbons formed by cracking the kerogen at higher temperature.

RHP reflects oxygenation conditions in the depositional environment (Fang et al., 1993; Slatt and Rodriguez, 2011). It can be related to relative sea level fluctuations within a sequence stratigraphic framework (Slatt and Rodriguez, 2011). Therefore, sequence stratigraphy of shales provide a powerful tool not only for regional-to-local stratigraphic correlations but also for high-grading stratigraphic intervals most favorable for preservation of organic matter (ductile), gas storage, and hydraulic fracturing (organic-poor, relatively brittle; Slatt and Rodriguez, 2011). RHP represents the variation in organic facies within the sedimentary sequence. High RHP indicates anoxic conditions with high hydrogen content and usually associated with TST. However, low RHP refers to oxic conditions with low hydrogen content is usually associated with LST. It was reported that the variations in the degree of oxic to anoxic conditions as recorded by the RHP data trend are related to relative sea level changes and sequence stratigraphic interpretation. The high RHP intervals are associated with maximum flooding surfaces where the intervals with the highest oxygenation correlate with the interpreted position of the sequence boundary (Singh, 2008). Increasing RHP indicates that more organic matter is preserved is under anoxic conditions in the stratigraphic sequence (Slatt et al., 2009).

Appendix II. Total Organic Carbon and Rock Eval Pyrolysis Results for Source Rock Samples.

Well Name	Depth (ft)	Carbonate (wt%)	TOC (wt% HC)	S1 (mg HC/g)	S2 (mg HC/g)	S3 (mg CO2/g)	Tmax (°C)	HI (S2x100/TOC)	OI (S3x100/TOC)	S2/S3 (mg HC/mg CO2)	S1/TOC	PI (S1/(S1+S2)
BBB1-6	10465	56.79	0.83	0.32	2.02	0.28	440	244	34	7	39	0.14
BBB1-6	10525	60.63	0.69	0.22	1.42	0.21	439	206	31	7	32	0.13
BBB1-6	10645	59.71	0.84	0.35	2.15	0.24	440	255	28	9	42	0.14
BBB1-6	10705	62.41	1.29	0.40	3.61	0.33	440	280	26	11	31	0.10
BBB1-6	10765	50.20	1.74	0.37	4.93	0.40	439	283	23	12	21	0.07
BBB1-6	10825	58.37	2.31	0.79	9.42	0.44	439	408	19	21	34	0.08
BBB1-6	10885	50.62	2.12	0.60	8.47	0.43	440	400	20	20	28	0.07
BBB1-6	10945	56.55	3.16	1.63	16.36	0.39	439	518	12	42	52	0.09
BBB1-6	11005	35.23	3.85	2.00	18.31	0.37	438	476	10	49	52	0.10
BBB1-6	11065	46.58	4.77	2.90	24.21	0.41	443	508	9	59	61	0.11
BBB1-6	11095	53.47	5.35	5.48	28.17	0.47	439	527	9	60	102	0.16
BBB1-6	11185	49.21	3.48	2.04	16.35	0.37	441	470	11	44	59	0.11
BBB1-6	11335	58.17	4.76	2.84	20.47	0.42	440	430	9	49	60	0.12
BBB1-6	11425	51.72	5.24	4.30	23.13	0.39	441	441	7	59	82	0.16
H1-6	9990	20.21	0.53	0.24	0.36	0.12	426	68	23	3.00	45.45	0.40
H1-6	10025	27.15	0.39	0.11	0.27	0.13	439	69	33	2.08	28.06	0.29
H1-6	10065	20.94	0.50	0.17	0.32	0.12	445	64	24	2.67	33.93	0.35
H1-6	10095	23.85	0.48	0.12	0.31	0.12	428	65	25	2.58	25.05	0.28

TOC: Total Organic Carbon, wt%; S1: Volatile hydrocarbon (HC) content, mg HC/g rock; S2: Remaining HC generative potential, mg HC/g rock; S3: Carbon dioxide content, mg CO2/g rock; HI: Hydrogen Index = S2 x 100 / TOC, mg HC/ g TOC; OI: Oxygen Index = S3 x 100 / TOC, mg CO2/ g TOC: Production index = S1/ (S1+S2).

Appendix II. (continued)

Well Name	Depth (ft)	Carbonate (wt%)	TOC (wt% HC)	S1 (mg HC/g)	S2 (mg HC/g)	S3 (mg CO2/g)	Tmax (°C)	HI (S2x100/TOC)	OI (S3x100/TOC)	S2/S3 (mg HC/mg CO2)	S1/TOC	PI (S1/(S1+S2)
HHH1-6	10355	21.37	0.94	0.51	0.82	0.28	442	87	30	2.93	54.14	0.38
HHH1-6	10415	14.23	1.04	0.56	1.14	0.23	446	110	22	4.96	53.85	0.33
HHH1-6	10475	26.34	0.40	0.13	0.25	0.08	441	63	20	3.13	32.50	0.34
EEEE1-6	13275	15.47	2.9	28.39	7.18	0.59	421	248	20	12	979	0.80
EEEE1-6	13315	15.24	2.78	29.8	7.3	0.69	422	263	25	11	1072	0.80
EEEE1-6	13415	33.14	2.3	33.31	6.54	0.7	428	284	30	9	1448	0.84
EEEE1-6	13745	33.52	2.73	35.7	7.33	0.59	427	268	22	12	1308	0.83
EEEE1-6	13835	35.91	2.4	28.43	7.39	0.69	424	308	29	11	1185	0.79
EEEE1-6	14045	46.39	1.8	20.86	5.36	0.54	430	298	30	10	1159	0.80
FFFF1-6	9955	67.14	0.34	0.3	0.26	0.34	414	76	100	0.76	88	0.54
FFFF1-6	10015	61.55	0.25	0.19	0.15	0.26	422	60	104	0.58	76	0.56
FFFF1-6	10075	55.07	0.25	0.26	0.16	0.21	391	65	85	0.76	105	0.62
FFFF1-6	10135	54.56	0.25	0.24	0.12	0.3	370	49	121	0.40	97	0.67
FFFF1-6	10195	44.13	0.36	0.28	0.2	0.22	368	56	61	0.91	78	0.58
FFFF1-6	10375	19.09	0.52	0.31	0.27	0.24	363	52	46	1.13	60	0.53
FFFF1-6	10495	27.47	0.47	0.29	0.3	0.3	363	64	64	1.00	62	0.49
FFFF1-6	10555	42.67	0.89	0.35	0.56	0.64	396	63	72	0.88	39	0.38

TOC: Total Organic Carbon, wt%; S1: Volatile hydrocarbon (HC) content, mg HC/g rock; S2: Remaining HC generative potential, mg HC/g rock; S3: Carbon dioxide content, mg CO2/g rock; HI: Hydrogen Index = S2 x 100 / TOC, mg HC/ g TOC; OI: Oxygen Index = S3 x 100 / TOC, mg CO2/ g TOC: Production index = S1/ (S1+S2).

Appendix II. (continued)

Well Name	Depth (ft)	Carbonate (wt%)	TOC (wt% HC)	S1 (mg HC/g)	S2 (mg HC/g)	S3 (mg CO2/g)	Tmax (°C)	HI (S2x100/TOC)	OI (S3x100/TOC)	S2/S3 (mg HC/mg CO2)	S1/TOC	PI (S1/(S1+S2)
FF13-6	10825	43.08	0.28	0.08	0.09	0.16	432	33	58	0.56	29	0.47
FF13-6	11095	21.46	0.79	0.18	0.36	0.27	417	46	34	1.33	23	0.33
FF13-6	11215	59.64	0.38	0.14	0.16	0.18	402	42	47	0.89	37	0.47
FF13-6	11345	40.33	0.38	0.1	0.11	0.14	340	29	37	0.79	27	0.48
FF13-6	11405	31.76	0.41	0.12	0.16	0.13	389	39	31	1.23	29	0.43
FF13-6	11505	40.62	0.32	0.1	0.1	0.13	376	31	41	0.77	31	0.50
FF13-6	11595	56.37	0.24	0.08	0.09	0.11	366	38	46	0.82	33	0.47
NN1-6	12885	52.64	0.753	1.46	1.04	0.61	434	138	81	1.70	193.89	0.58
NN1-6	12945	56.39	0.768	1.24	0.92	0.68	436	120	89	1.35	161.46	0.57
NN1-6	13005	62.07	0.873	1.87	0.92	0.92	435	105	105	1.00	214.20	0.67
NN1-6	13065	47.55	1.27	2.43	1.72	0.98	436	135	77	1.76	191.34	0.59
NN1-6	13125	53.39	1.21	2.14	1.25	0.9	437	103	74	1.39	176.86	0.63
NN1-6	13185	54.03	1.03	2.31	1.15	0.81	435	112	79	1.42	224.27	0.67
NN1-6	13245	62.56	0.854	1.14	0.96	0.7	436	112	82	1.37	133.49	0.54

TOC: Total Organic Carbon, wt%; S1: Volatile hydrocarbon (HC) content, mg HC/g rock; S2: Remaining HC generative potential, mg HC/g rock; S3: Carbon dioxide content, mg CO2/g rock; HI: Hydrogen Index = S2 x 100 / TOC, mg HC/ g TOC; OI: Oxygen Index = S3 x 100 / TOC, mg CO2/ g TOC: Production index = S1/ (S1+S2).

Appendix II. (continued)

Well Name	Depth (ft)	Carbonate (wt%)	TOC (wt% HC)	S1 (mg HC/g)	S2 (mg HC/g)	S3 (mg CO2/g)	Tmax (°C)	HI (S2x100/TOC)	OI (S3x100/TOC)	S2/S3 (mg HC/mg CO2)	S1/TOC	PI (S1/(S1+S2)
Z1-6	13225	68.77	0.637	0.48	0.34	0.72	413	53	113	0.47	75.35	0.59
Z1-6	13315	72.88	0.67	0.24	0.09	2.33	403	13	348	0.04	35.82	0.73
Z1-6	13685	72.43	1.65	1.08	0.38	0.35	463	23	21	1.09	65.45	0.74
Z1-6	13775	77.04	2.05	1.43	0.55	0.39	510	27	19	1.41	69.76	0.72
Z1-6	13955	56.13	1.55	0.99	0.57	0.43	421	37	28	1.33	63.87	0.63
Z1-6	14055	38.9	1.47	0.93	0.5	0.44	413	34	30	1.14	63.27	0.65
Z1-6	14235	36.23	1.5	0.82	0.47	0.4	358	31	27	1.18	54.67	0.64
Z1-6	14325	38.53	1.74	0.96	0.47	0.27	415	27	16	1.74	55.17	0.67
Z1-6	14415	37.6	1.4	0.76	0.39	0.32	362	28	23	1.22	54.29	0.66
Z1-6	14515	26.1	1.32	0.8	0.57	0.39	381	43	30	1.46	60.61	0.58
C65-47	6415	58.27	0.53	0.09	1.11	0.35	434	208	66	3.17	16.85	0.08
C65-47	6605	47.29	0.52	0.09	0.72	0.4	433	137	76	1.80	17.18	0.11
C65-47	6725	38.48	0.49	0.13	0.47	0.45	430	96	92	1.04	26.64	0.22
C65-47	6915	16.56	0.86	0.07	1.33	0.33	455	156	39	4.03	8.19	0.05
C65-47	7205	37.62	0.44	0.14	0.43	0.28	433	97	63	1.54	31.53	0.25
C65-47	7375	16.98	0.42	0.05	0.16	0.17	436	38	40	0.94	11.79	0.24
C65-47	7505	29.34	0.43	0.06	0.25	0.21	432	58	49	1.19	13.99	0.19

TOC: Total Organic Carbon, wt%; S1: Volatile hydrocarbon (HC) content, mg HC/g rock; S2: Remaining HC generative potential, mg HC/g rock; S3: Carbon dioxide content, mg CO2/g rock; HI: Hydrogen Index = S2 x 100 / TOC, mg HC/ g TOC; OI: Oxygen Index = S3 x 100 / TOC, mg CO2/ g TOC: Production index = S1/ (S1+S2).

Appendix II. (continued)

Well Name	Depth (ft)	Carbonate (wt%)	TOC (wt% HC)	S1 (mg HC/g)	S2 (mg HC/g)	S3 (mg CO2/g)	Tmax (°C)	HI (S2x100/TOC)	OI (S3x100/TOC)	S2/S3 (mg HC/mg CO2)	S1/TOC	PI (S1/(S1+S2)
ZZZ1-6	12135	18.04	0.479	0.12	0.33	0.43	421	69	90	0.77	25.05	0.27
ZZZ1-6	12255	27.41	0.438	0.2	0.32	0.36	387	73	82	0.89	45.66	0.38
ZZZ1-6	12345	42.04	0.417	0.18	0.36	0.41	430	86	98	0.88	43.17	0.33
ZZZ1-6	12465	29.71	0.422	0.12	0.31	0.42	427	73	100	0.74	28.44	0.28
ZZZ1-6	12505	20.9	0.41	0.11	0.18	0.34	379	44	83	0.53	26.83	0.38
ZZZ1-6	12595	19.2	0.623	0.21	0.69	0.4	436	111	64	1.73	33.71	0.23
ZZZ1-6	12675	19.86	0.413	0.13	0.28	0.3	420	68	73	0.93	31.48	0.32
ZZZ1-6	12715	17.88	0.47	0.09	0.3	0.37	421	64	79	0.81	19.15	0.23
ZZZ1-6	12755	23.05	0.375	0.06	0.19	0.41	410	51	109	0.46	16.00	0.24
ZZZ1-6	12875	21.56	0.448	0.11	0.39	0.5	432	87	112	0.78	24.55	0.22
ZZZ1-6	12915	21.77	0.432	0.15	0.34	0.57	422	79	132	0.60	34.72	0.31
ZZZ1-6	13035	15.46	0.487	0.11	0.2	0.31	380	41	64	0.65	22.59	0.35
ZZZ1-6	13115	28.39	0.431	0.09	0.19	0.74	401	44	172	0.26	20.88	0.32
ZZZ1-6	13195	14.63	0.466	0.06	0.09	0.26	367	19	56	0.35	12.88	0.40
ZZZ1-6	13315	16	0.384	0.06	0.1	0.27	348	26	70	0.37	15.63	0.38
ZZZ1-6	13395	23.64	0.368	0.07	0.11	0.4	393	30	109	0.28	19.02	0.39
ZZZ1-6	13475	11.55	0.459	0.08	0.16	0.28	384	35	61	0.57	17.43	0.33
ZZZ1-6	13555	18.14	0.438	0.04	0.11	0.51	396	25	116	0.22	9.13	0.27
ZZZ1-6	13635	10.21	0.446	0.08	0.16	0.25	388	36	56	0.64	17.94	0.33
ZZZ1-6	13715	11.63	0.439	0.07	0.11	0.29	372	25	66	0.38	15.95	0.39

TOC: Total Organic Carbon, wt%; S1: Volatile hydrocarbon (HC) content, mg HC/g rock; S2: Remaining HC generative potential, mg HC/g rock; S3: Carbon dioxide content, mg CO2/g rock; HI: Hydrogen Index = S2 x 100 / TOC, mg HC/ g TOC; OI: Oxygen Index = S3 x 100 / TOC, mg CO2/ g TOC: Production index = S1/ (S1+S2).

Appendix III Source Rock Geochemical Data

Depth (ft)	Pr/Ph	Pr/C_{17}	Ph/C_{18}	C_{27}/C_{17}	CPI
10465	0.89	0.54	0.56	0.08	1.17
10705	1.40	0.52	0.55	0.08	1.04
10765	1.62	0.49	0.50	0.05	1.14
10825	1.45	0.47	0.49	0.09	1.26
10885	1.37	0.47	0.49	0.08	1.21
10945	1.42	0.53	0.51	0.08	1.19
11005	1.44	0.52	0.54	0.12	1.19
11065	1.23	0.49	0.52	0.10	1.17
11095	1.42	0.55	0.56	0.17	1.19
11185	1.34	0.47	0.48	0.14	1.23
11335	1.27	0.47	0.47	0.18	1.20
11425	1.26	0.54	0.51	0.78	1.02

Pr/Ph = pristane/phytane; Pr/C_{17} = pristane/n-heptadecane; Ph/C_{18} = phytane/n-octadecane; CPI = Carbon Preference Index ; C_{17}/C_{27} = n-heptadecane/C_{27} normal alkane.

Appendix III (continued)

Depth (ft)	Ts/ (Ts+Tm)	22S/ (22S+22R)	$C_{23}Tr/C_{30}\alpha\beta$	$C_{30}\beta\alpha/C_{30}\alpha\beta$	C_{29}/C_{30}	$C_{24}Tri/C_{23}Tri$	24Tet/ 24Te+26Tri	C35/ (C_{31}-C_{35})	G/C_{31}R
10465	0.66	0.59	0.14	0.11	0.48	0.04	0.02	0.29	0.26
10765	0.70	0.57	0.12	0.09	0.44	0.04	0.02	0.37	0.33
10825	0.70	0.58	0.15	0.09	0.42	0.03	0.02	0.28	0.24
10885	0.69	0.57	0.16	0.10	0.42	0.04	0.02	0.28	0.32
10945	0.71	0.57	0.17	0.08	0.40	0.04	0.02	0.26	0.26
11005	0.72	0.57	0.18	0.08	0.39	0.04	0.03	0.25	0.26
11065	0.74	0.56	0.20	0.08	0.39	0.04	0.03	0.23	0.23
11095	0.74	0.58	0.22	0.08	0.39	0.04	0.03	0.27	0.24
11185	0.72	0.56	0.17	0.10	0.40	0.03	0.03	0.23	0.26
11335	0.70	0.55	0.29	0.10	0.33	0.06	0.06	0.23	0.30
11425	0.72	0.54	0.28	0.09	0.39	0.05	0.03	0.21	0.32

Ts/(Ts+Tm) = ratio of C_{27} 18α(H)-22,29,30-trisnorneohopane/ C_{27} 18α(H)-22,29,30trisnorneohopane + C_{27} 17α(H)-22,29,30-trisnorhopane; 22S/(22S+22R) = ratio of C_{32} αβ homohopane 22S/ C_{32} αβ- homohopane 22S + 22R; $C_{23}Tr/C_{30}\alpha\beta$ = C_{23} tricyclic terpane /C_{30} αβ-hopane; $C_{30}\beta\alpha/C_{30}\alpha\beta$ = C_{30} βα-hopane /C_{30} αβ-hopane; C_{29} αβ/$C_{30}\alpha\beta$ = ratio of C_{29} αβ-hopane / C_{30} αβ-hopane; $C_{24}Tr/C23Tr$ = C_{24} tricyclic terpane /C_{23} tricyclic terpane; $C_{24}Te/24Tet$ +26Tet = C_{24} tetracyclic terpane/ 24 tetracyclic terpane +26 tetracyclic terpane; C_{35}/ sum of C_{31}–C_{35} homohopanes; G/C_{31}R= gammacerane/ C_{31} αβ homohopane 22R.

Depth (ft)	20S/ (20S+20R)	ββ/ (ββ+αα)	Dia/27R	Pre/27R	27R/29R	28R/29R	%27R	%28R	%29R
10465	0.44	0.51	0.82	1.41	1.46	1.07	41	30	28
10765	0.46	0.56	0.82	0.96	1.64	1.19	43	31	26
10825	0.48	0.59	1.16	1.26	1.56	1.35	40	35	26
10885	0.46	0.58	0.91	1.00	1.82	1.18	45	29	25
10945	0.47	0.60	1.19	1.44	1.62	1.11	43	30	27
11005	0.47	0.63	1.06	1.37	1.84	1.14	46	29	25
11065	0.47	0.61	0.98	1.30	1.89	1.12	47	28	25
11095	0.45	0.62	1.11	2.04	1.55	1.03	43	29	28
11185	0.45	0.60	0.95	1.25	1.47	1.09	41	31	28
11335	0.48	0.59	1.10	1.54	1.45	1.08	41	31	28
11425	0.48	0.62	1.31	1.64	1.48	1.09	41	31	28

20S/(20S+20R) = C_{29} ααα-sterane 20S/C_{29} ααα-sterane 20S + 20R; ββ/(ββ+αα) = C_{29} αββ-sterane 20S+20R/C_{29} ααα + αββ-sterane 20S + 20R; 27Dia/27R = C_{27} βα-diasterane 20S/C_{27} αα-sterane 20R; 27R/29R = C_{27} αα-sterane 20R /C_{29} αα-sterane 20R.28R/$_{29}$R = C_{28} αα-sterane 20R /C_{29} αα-sterane 20R; Preg/27R = C_{21} pregnane/C_{27} αα-sterane 20R; %27R = percentage of C27 αα 20R to sum C_{27}, C28, C_{29} αα 20R steranes; %28R = percentage of C_{28} αα 20R to sum C_{27}, C28, C_{29} αα 20R steranes; %29R = percentage of C_{29} αα20Rto sum C27,

Appendix IV Crude Oil Geochemical Data

Sample	Form.	Pr/Ph	Pr/C_{17}	Ph/C_{18}	C_{17}/C_{27}	CPI
C65	Gialo	1.66	2.33	1.67	4.76	---
4B2-6		1.61	98.34	39.5		---
C98-6		1.53	0.54	0.4	5.34	1.15
4I2-6		1.48	0.59	0.46	4.90	1.09
C229-6	Zaltan	1.35	0.59	0.48	3.85	1.08
J3-6		1.53	0.74	0.56	3.51	1.1
4G1-6		1.47	0.59	0.46	4.04	1.09
4J2-6		1.76	0.49	0.35	4.04	1.1
B5-47	Bayda	1.45	0.7	0.55	3.74	1.13
4B1-6	Waha	1.44	0.55	0.44	3.80	1.12
2D12-6		1.45	0.54	0.42	6.51	1.15
C35-47	Kalash	1.24	0.76	0.72	4.07	1.13
B3-93		1.49	0.76	0.61	4.29	1.13
S9-47	Tagrifet	1.3	0.57	0.51	4.91	1.13
4R1-6	Gargaf	2.12	0.4	0.24		1.15
3M2A-6		1.76	0.42	0.28	4.07	1.08
2F16-6		1.68	0.11	0.07	4.54	1.13
2U9A-6		1.71	0.38	0.26	5.79	1.12

Pr/Ph = pristane/phytane; Pr/C_{17} = pristane/n-heptadecane; Ph/C_{18} = phytane/n-octadecane; CPI = Carbon Preference Index ; C_{17}/C_{27} = n-heptadecane/C_{27} normal alkane.

Appendix IV (continued)

Sample	Form.	Ts/ (Ts+Tm)	22S/ (22S+22R)	$C_{23}Tr/C_{30}\alpha\beta$	$C_{30}\beta\alpha/C_{30}\alpha\beta$	C_{29}/C_{30}	$C_{24}Tri/C_{23}Tri$	24Tet/ 24Te+26Tri	C35/ (C_{31}-C_{35})	$G/C_{31}R$
C65	Gialo	0.62	0.53	0.33	0.12	0.53	0.66	0.24	0.07	0.34
4B2-6		0.62	0.54	0.28	0.12	0.49	0.68	0.24	0.09	0.36
C98-6	Zaltan	0.67	0.52	0.3	0.09	0.46	0.65	0.23	0.08	0.32
4I2-6		0.76	0.59	0.31	0.12	0.37	0.71	0.22	0.08	0.39
C229-6		0.61	0.53	0.24	0.12	0.50	0.69	0.24	0.08	0.36
J3-6		0.54	0.56	0.22	0.09	0.53	0.66	0.25	0.08	0.37
4G1-6		0.62	0.52	0.27	0.13	0.49	0.67	0.24	0.08	0.34
4J2-6		0.68	0.53	0.42	0.1	0.56	0.63	0.28	0.08	0.29
B5-47	Bayda	0.61	0.52	0.28	0.11	0.50	0.68	0.21	0.07	0.34
4B1-6	Waha	0.72	0.52	0.23	0.11	0.42	0.69	0.14	0.07	0.30
2D12-6		0.49	0.56	0.22	0.13	0.59	0.63	0.32	0.11	0.57
C35-47	Kalash	0.49	0.53	0.25	0.1	0.57	0.66	0.20	0.09	0.46
B3-93		0.54	0.52	0.32	0.11	0.55	0.61	0.17	0.08	0.47
S9-47	Tagrifet	0.6	0.52	0.27	0.11	0.49	0.62	0.26	0.03	0.27
4R1-6	Gargaf	0.71	0.53	5.78		0.61	0.7	0.21	0.08	
3M2A-6		0.57	0.68	8.75		0.91	0.68			
2F16-6		0.48	0.62	0.23		0.58	1.38			
2U9A-6		0.67	0.59	3.65		0.62	0.66	0.08	0.00	

Ts/(Ts+Tm) = ratio of C_{27} 18α(H)-22,29,30-trisnorneohopane/ C_{27} 18α(H)-22,29,30trisnorneohopane + C_{27} 17α(H)-22,29,30-trisnorhopane; 22S/(22S+22R) = ratio of C_{32} αβ homohopane 22S/ C_{32} αβ- homohopane 22S + 22R; C23Tr/C30αβ = C_{23} tricyclic terpane /C_{30} αβ-hopane; $C_{30}\beta\alpha/C30\alpha\beta$ = C_{30} βα-hopane /C_{30} αβ-hopane; C_{29} αβ/C30αβ = ratio of C_{29} αβ-hopane / C_{30} αβ-hopane; $C_{24}Tr/C_{23}Tr$ = C_{24} tricyclic terpane /C_{23} tricyclic terpane; $C_{24}Te/24Tet$ + 26Tet = C_{24} tetracyclic terpane/ 24 tetracyclic terpane +26 tetracyclic terpane; C_{35}/ sum of C_{31}–C_{35} homohopanes; G/C_{31}R= gammacerane/ C_{31} αβ homohopane 22R.

Sample	Form.	20S/ (20S+20R)	ββ/ (ββ+αα)	Dia/27R	Pre/27R	27R/29R	28R/29R	%27R	%28R	%29R
C65	Gialo	0.44	0.6	0.88	0.55	1.67	1.07	45	29	27
4B2-6		0.5	0.59	1.05	0.64	1.31	1.11	38	33	29
C98-6	Zaltan	0.46	0.63	1.29	0.75	1.35	1.12	39	32	29
4I2-6		0.45	0.65	1.82	1	1.13	1.13	35	35	31
C229-6		0.44	0.59	1.02	0.54	1.31	1.12	38	33	29
J3-6		0.42	0.58	0.81	0.45	1.18	1.05	36	33	31
4G1-6		0.44	0.6	0.98	0.56	1.41	1.09	40	31	29
4J2-6		0.42	0.6	1.13	1	1.36	1.05	40	31	29
B5-47	Bayda	0.43	0.59	0.62	0.38	1.46	1.23	40	33	27
4B1-6	Waha	0.45	0.64	0.9	0.57	1.5	1.1	42	30	28
2D12-6		0.47	0.57	0.83	0.43	1.25	1.08	38	32	30
C35-47	Kalash	0.49	0.5	0.33	0.19	1.39	1.19	39	33	28
B3-93		0.49	0.52	0.45	0.27	1.46	1.27	39	34	27
S9-47	Tagrifet	0.45	0.59	0.97	0.65	1.35	1.06	40	31	29
4R1-6	Gargaf	0.52	0.67	1.79	7.93	3.62	1.91	55	29	15
3M2A-6		0.55	0.71	4.94	7.76	2.78	1.91	49	34	18
2F16-6		0.41	0.59	0.53	0.51	1.51	1.36	39	35	26
2U9A-6		0.43	0.67	2.96	3.72	2.15	1.04	50	27	23

20S/(20S+20R) = C_{29} ααα-sterane 20S/C_{29} ααα-sterane 20S + 20R; ββ/(ββ+αα) = C_{29} αββ-sterane 20S+20R/C29 ααα + αββ-sterane 20S + 20R; 27Dia/27R = C_{27} βα-diasterane 20S/C_{27} αα-sterane 20R; 27R/29R = C_{27} αα-sterane 20R /C_{29} αα-sterane 20R.28R/29R = C_{28} αα-sterane 20R /C_{29} αα-sterane 20R; Preg/27R = C_{21} pregnane/C_{27} αα-sterane 20R; %27R = percentage of C_{27} αα 20R to sum C_{27}, C_{28}, C_{29} αα 20R steranes; %28R = percentage of C_{28} αα 20R to sum C_{27}, C_{28}, C_{29} αα 20R steranes; %29R = percentage of C_{29} αα20Rto sum C_{27}, C_{28}, C_{29} αα 20R steranes.

Appendix IV (continued)

Sample	Form.	I/(I+II) Mono	I/(I+II) Tri	MPI1	MPI2	MPI3	MPR	DBT/P	MDBT/ MP	Rc(rw)1.35	Rc(b)1.7
C65	Gialo	0.17	0.17	0.68	0.71	0.65	0.79	0.24	0.23	0.81	0.70
4B2-6		0.14	0.18	0.62	0.71	0.61	0.84	0.29	0.35	0.77	0.66
C98-6		0.19	0.21	0.65	0.68	0.63	0.75	0.14	0.12	0.79	0.67
4I2-6		0.17	0.21	0.58	0.65	0.56	0.8	0.18	0.12	0.75	0.63
C229-6		0.15	0.17	0.57	0.69	0.58	0.93	0.28	0.24	0.74	0.62
J3-6	Zaltan	0.11	0.11	0.65	0.65	0.65	0.7	0.34	0.28	0.79	0.68
4G1-6		0.16	0.15	0.68	0.61	0.66	0.56	0.23	0.7	0.81	0.69
4J2-6		0.19	0.3	0.69	0.68	0.7	0.76	0.6	0.22	0.81	0.70
B5-47	Bayda	0.12	0.11	0.61	0.63	0.59	0.66	0.32	0.2	0.77	0.65
4B1-6	Waha	0.18	0.19	0.6	0.61	0.58	0.6	0.11	0.2	0.76	0.64
2D12-6		0.12	0.14	0.63	0.7	0.64	0.86	0.23	0.12	0.78	0.66
C35-47	Kalash	0.07	0.06	0.6	0.6	0.55	0.59	0.47	0.19	0.76	0.64
B3-93		0.1	0.08	0.63	0.6	0.6	0.58	0.25	0.19	0.82	0.71
S9-47	Tagrifet	0.16	0.2	0.69	0.65	0.68	0.64	0.23	0.15	0.78	0.66
4R1-6	Gargaf	0.72	0.79	1.41	1.54	2.16	2.1	0.06	0.03	1.46	2.23
3M2A-6		0.53	0.78	0.8	0.87	0.8	1.05	0.21	0.07	1.82	2.56
2F16-6		0.51	0.27	2.03	2.01	2.15	2.13	0.02	0.02	1.08	1.88
2U9A-6		0.57	0.82	1.1	1.29	0.94	1.4	0.18	0.03	1.64	2.39

I/(I+II) Mono= C_{21}+C_{22}/(C_{21}+C_{22}+C_{27} to C_{29}) 20S and 20R Monoaromatic steroid; I/(I+II) Tri= C_{20}+C21/(C_{20}+C_{21}+C_{26} to C_{28} 20S and 20 R Triaromatic steroid; MPI 1 = 1.5 (2-MP + 3-MP)/(P + 1-MP + 9-MP); MPI 2 = 3 (2-MP)/(P + 1-MP + 9-MP); MPI3= (2- +3-MP)/1- + 9- MP) MPI 3 = (%3-MP + %2-MP)/(%9-MP + %1-MP); MDBT/MP = (4-MDBT+ 3+2-MDBT+1-MDBT)/(3-MP+2-MP+9-MP+1-MP) ; RC(rw) = 0.6 MPI 1 + 0.4 (for Rm<1.35%); RC(rw) = - 0.6 MPI 1 + 2.3 (for Rm>1.35%); Rc(b) = 0.7 MPI 1 + 0.22 (for Rm < 1.7%); Rc(b)= - 0.55 MPI 1 + 3.0 (for Rm > 1.7%)

Appendix IV (continued)

Table shows Stable carbon and hydrogen isotope values of oil samples.

Sample	**Form.**	**$\delta^{13}C$**	**δD**	**$\delta^{13}C_{Sat}$**	**$\delta^{13}C_{Arom.}$**
C65	Gialo	-27.34	-124.8		
4B2-6		-27.16	-126.6		
C98-6		-27.72	-117.6		
4I2-6		-27.81	-131.9		
C229-6	Zaltan	-27.83	-131.6	-28.33	-26.9
J3-6		-27.81	-127.9		
4G1-6		-27.68	-132.7		
4J2-6		-27.37	-123.2		
B5-47	Bayda	-28.54	-133.6		
4B1-6	Waha	-27.88	-135.8	-28.1	-26.75
2D12-6		*-28.05*	*-98.4*		
C35-47	Kalash	-28.93	-126.8		
B3-93		-28.87	-134.7		
S9-47	Tagrifet	-28.6	-120.6	-28.73	-26.96
4R1-6	Gargaf	-27.5	-99.5	-27.63	-26.02
3M2A-6		-28.06	-110.2	-27.9	-26.43
2F16-6		-29.37	-86.1	-29.35	-27.9
2U9A-6		-27.45	-92.8	-27.46	-25.91

Appendix V. Absolute Concentration Of Source Rock Samples Normalized to Saturate Fraction (µg/g)

Depth (ft)	C_{19}/3	C_{23}Tri	C_{26}Tri R	C_{26}Tri S	C_{24}Tet	Ts	Tm	C_{29} αβ	C_{30} αβ	C_{31} S
10465	28	52	7	7	17	79	48	185	383	123
10765	11	38	10	10	11	69	31	145	327	121
10825	8	47	14	13	11	71	31	130	313	109
10885	7	53	17	15	13	80	48	145	342	112
10945	16	130	39	41	28	193	108	309	776	234
11005	12	102	32	30	21	139	55	214	555	171
11065	18	124	42	39	25	158	96	242	624	183
11095	27	108	29	29	21	124	43	191	489	134
11185	12	91	29	30	18	122	44	208	519	155
11425	19	228	83	85	44	287	163	314	807	207

Depth (ft)	C_{31} R	C_{30} G	C_{32} S	C_{32} R	C_{33} S	C_{33} R	C_{34} R	C_{34} R	C_{35} S	C_{35} R
10465	76	20	66	47	37	23	14	8	4	3
10765	75	25	76	57	52	33	21	12	6	3
10825	71	17	72	53	50	32	21	11	6	3
10885	74	24	71	54	48	31	21	12	6	4
10945	155	40	147	110	93	57	40	21	11	10
11005	115	30	112	85	72	47	33	18	10	7
11065	152	35	119	92	77	51	36	19	11	8
11095	110	26	82	60	46	30	22	11	7	7
11185	129	33	101	79	66	44	32	19	11	11
11425	188	61	128	106	77	51	39	22	15	15

Appendix V. (continued)

Depth (ft)	Preg	27Dia	27ααS	27ααR	28ααS	28ααR	29ααs	29ααR	30ααS	30ααR
10465	28	35	34	43	29	31	23	29	7	5
10765	17	31	24	38	27	27	19	23	7	7
10825	17	35	26	31	26	26	18	20	7	7
10885	19	40	25	44	26	29	21	24	7	8
10945	50	107	61	90	59	62	49	56	16	11
11005	37	72	44	68	39	42	33	37	12	8
11065	41	85	50	86	50	51	40	46	13	9
11095	39	61	39	54	36	36	29	35	11	7
11185	28	59	43	63	39	46	35	43	14	9
11425	63	154	92	118	80	87	75	80	24	16

Appendix VI. Absolute Concentration of Crude Oil Samples Normalized to Saturate Fraction (µg/g)

Sample	Form.	C_{19}Tri	C_{23}Tri	C_{26}Tri R	C_{26}Tri S	C_{24}Tet	Ts	Tm	C_{29} αβ	C_{30} αβ	C_{31} S
C65	Gialo	17	181	53	51	33	137	84	291	551	175
4B2-6		6	78	23	23	15	64	40	136	280	92
C98-6		12	155	51	55	18	173	67	287	678	221
4I2-6		20	162	47	47	44	129	136	423	720	214
C229-6		12	112	30	30	18	98	48	170	373	123
J3-6	Zaltan	21	162	50	48	28	153	49	195	524	183
4G1-6		14	160	52	49	32	147	95	336	666	218
4J2-6		5	70	20	19	13	56	47	170	318	104
B5-47	Bayda	9	94	29	28	18	76	47	172	348	114
4B1-6	Waha	17	122	33	33	25	112	53	166	294	104
2D12-6		8	130	43	41	23	96	61	232	461	129
C35-47	Kalash	4	115	39	36	19	63	67	261	459	144
B3-93		4	83	28	26	11	45	38	144	263	71
S9-47	Tagrifet	11	119	39	37	26	113	76	220	448	135
4R1-6	Gargaf	26	38	0	0	0	7	3	4	7	1
3M2A-6		23	77	25	23	13	25	19	8	9	4
2F16-6		0	2				1	2	5	9	3
2U9A-6		24	82	28	29	5	63	31	14	22	8

Appendix VI. (continued)

Sample	Form.	C_{31} R	C_{30} G	C_{32} S	C_{32} R	C_{33} S	C_{33} R	C_{34} R	C_{34} R	C_{35} S	C_{35} R
C65	Gialo	154	52	122	94	86	55	61	30	27	31
4B2-6		80	28	64	51	48	31	36	19	20	20
C98-6	Zaltan	204	62	165	133	126	85	79	46	33	44
4I2-6		169	96	150	115	102	67	79	50	49	53
C229-6		114	36	90	72	66	44	44	26	20	30
J3-6		125	48	134	104	95	64	70	36	28	39
4G1-6		192	69	157	122	117	78	82	46	40	50
4J2-6		81	30	71	53	50	33	36	19	16	21
B5-47	Bayda	104	35	84	67	63	42	48	26	21	26
4B1-6	Waha	92	26	74	60	47	32	38	21	19	19
2D12-6		119	40	86	68	59	41	40	23	18	23
C35-47	Kalash	124	57	93	69	72	48	50	30	28	37
B3-93		66	31	46	36	36	24	25	14	12	18
S9-47	Tagrifet	124	33	87	69	53	35	47	21	10	8
4R1-6	Gargaf	1	0	0	0	0	0	0	0	0	0
3M2A-6		2	0	0	0		0	0	0		0
2F16-6		2	1	2	1	1	1	1	1	1	0
2U9A-6		5	4	5	0		0	0	0		0

Appendix VI. (continued)

Sample	Form.	Preg	27Dia	27*aaS*	27*aaR*	28*aaS*	28*aaR*	29*aas*	29*aaR*	30*aaS*	30*aaR*
C65	Gialo	66	159	75	120	76	77	55	72	21	17
4B2-6		29	65	39	45	35	38	34	34	10	9
C98-6	Zaltan	44	109	48	59	50	49	37	44	12	9
4I2-6		66	176	67	66	76	67	49	59	17	11
C229-6		58	155	84	109	85	93	66	83	30	29
J3-6		20	51	39	45	35	41	28	39	11	12
4G1-6		36	89	46	64	46	49	36	45	13	10
4J2-6		60	105	50	60	45	46	32	44	11	9
B5-47	Bayda	33	75	59	88	54	74	46	60	20	14
4B1-6	Waha	63	140	73	111	72	81	60	74	23	15
2D12-6		45	123	76	104	82	89	73	83	19	14
C35-47	Kalash	22	49	68	111	58	95	79	80	22	18
B3-93		17	37	40	62	37	54	41	43	12	10
S9-47	Tagrifet	43	98	44	67	48	52	40	49	16	10
4R1-6	Gargaf	70	31	6	9	6	5	3	2	1	0
3M2A-6		45	51	6	6	8	4	3	2	0	
2F16-6		1	2	1	1	1	1	1	1	0	0
2U9A-6		69	120	17	19	21	9	7	9	2	

Appendix VII Principal Component Analysis (PCA)

Factor loadings:

	F1	F2	F3	F4	F5
Ts/ (Ts+Tm)	0.102	-0.508	-0.667	0.235	-0.372
22S/ (22S+22R)	0.631	0.136	0.443	0.591	0.066
C_{23}Tri/$C_{30}\alpha\beta$	0.890	-0.377	0.243	0.014	-0.020
C_{29}/C_{30}	0.711	-0.144	0.566	-0.042	0.336
C_{24}Tri/ C_{23}Tri	0.300	0.881	-0.015	0.195	-0.111
20S/ (20S+20R)	0.446	-0.432	0.497	-0.314	-0.331
ββ/ (βββ+αα)	0.696	-0.373	-0.290	0.468	-0.192
Dia/27R	0.723	-0.479	0.224	0.430	0.039
Pre/27R	0.914	-0.350	0.077	-0.078	-0.096
27R/29R	0.902	-0.244	-0.059	-0.323	-0.097
28R/29R	0.812	-0.072	0.332	-0.247	-0.358
%27R	0.845	-0.312	-0.219	-0.296	0.119
%28R	-0.242	0.379	0.682	0.263	-0.440
%29R	-0.926	0.166	-0.043	0.299	0.076
I/(I+II) Mono	0.972	0.103	-0.187	0.013	0.012
I/(I+II) Tri	0.931	-0.262	-0.128	0.099	0.131
MPI1	0.675	0.696	-0.185	-0.043	0.029
MPI2	0.740	0.624	-0.218	-0.012	0.044
MPI3	0.719	0.563	-0.231	-0.229	-0.121
MPR	0.800	0.496	-0.235	-0.061	-0.033
DBT/P	-0.497	-0.311	0.286	-0.124	0.474
MDBT/MP	-0.555	-0.242	-0.066	-0.110	-0.012
Rc(rw)1.35	0.943	-0.167	0.112	0.104	0.169
Rc(b)1.7	0.972	0.048	0.051	0.086	0.133
$\delta^{13}C$	0.061	-0.657	-0.519	0.179	0.095
δD	0.727	0.435	-0.084	0.072	0.348

Appendix VII. (continued)

Contribution of the variables (%):

	F1	F2	F3	F4	F5
Ts/ (Ts+Tm)	0.075	5.678	16.755	3.640	11.425
22S/ (22S+22R)	2.874	0.409	7.377	23.044	0.363
C_{23}Tri/$C_{30}\alpha\beta$	5.728	3.118	2.228	0.014	0.034
C_{29}/C_{30}	3.655	0.454	12.058	0.119	9.297
C_{24}Tri/ C_{23}Tri	0.651	17.082	0.008	2.518	1.022
20S/ (20S+20R)	1.439	4.103	9.301	6.524	9.040
ββ/ (βββ+αα)	3.499	3.056	3.175	14.429	3.025
Dia/27R	3.777	5.038	1.894	12.195	0.123
Pre/27R	6.040	2.698	0.222	0.398	0.763
27R/29R	5.886	1.312	0.131	6.888	0.769
28R/29R	4.767	0.114	4.154	4.034	10.567
%27R	5.161	2.141	1.810	5.797	1.170
%28R	0.423	3.152	17.492	4.550	15.935
%29R	6.192	0.602	0.069	5.883	0.471
I/(I+II) Mono	6.836	0.235	1.313	0.010	0.011
I/(I+II) Tri	6.263	1.504	0.614	0.641	1.424
MPI1	3.290	10.639	1.294	0.123	0.069
MPI2	3.955	8.554	1.792	0.009	0.160
MPI3	3.742	6.978	2.016	3.469	1.203
MPR	4.625	5.408	2.076	0.245	0.088
DBT/P	1.789	2.130	3.083	1.022	18.496
MDBT/MP	2.227	1.286	0.166	0.803	0.011
Rc(rw)1.35	6.430	0.613	0.473	0.714	2.360
Rc(b)1.7	6.829	0.051	0.099	0.484	1.457
$\delta^{13}C$	0.027	9.489	10.135	2.105	0.742
δD	3.823	4.156	0.264	0.342	9.973

Appendix VII. (continued)

Squared cosines of the variables:

	F1	F2	F3	F4	F5
Ts/ (Ts+Tm)	0.010	0.258	**0.445**	0.055	0.139
22S/ (22S+22R)	**0.398**	0.019	0.196	0.349	0.004
C_{23}Tri/$C_{30}\alpha\beta$	**0.793**	0.142	0.059	0.000	0.000
C_{29}/C_{30}	**0.506**	0.021	0.320	0.002	0.113
C_{24}Tri/ C_{23}Tri	0.090	**0.777**	0.000	0.038	0.012
20S/ (20S+20R)	0.199	0.187	**0.247**	0.099	0.110
ββ/ (βββ+αα)	**0.484**	0.139	0.084	0.219	0.037
Dia/27R	**0.523**	0.229	0.050	0.185	0.001
Pre/27R	**0.836**	0.123	0.006	0.006	0.009
27R/29R	**0.814**	0.060	0.003	0.104	0.009
28R/29R	**0.660**	0.005	0.110	0.061	0.128
%27R	**0.714**	0.097	0.048	0.088	0.014
%28R	0.059	0.143	**0.465**	0.069	0.193
%29R	**0.857**	0.027	0.002	0.089	0.006
I/(I+II) Mono	**0.946**	0.011	0.035	0.000	0.000
I/(I+II) Tri	**0.866**	0.068	0.016	0.010	0.017
MPI1	0.455	**0.484**	0.034	0.002	0.001
MPI2	**0.547**	0.389	0.048	0.000	0.002
MPI3	**0.518**	0.317	0.054	0.053	0.015
MPR	**0.640**	0.246	0.055	0.004	0.001
DBT/P	**0.247**	0.097	0.082	0.015	0.224
MDBT/MP	**0.308**	0.058	0.004	0.012	0.000
Rc(rw)1.35	**0.890**	0.028	0.013	0.011	0.029
Rc(b)1.7	**0.945**	0.002	0.003	0.007	0.018
$\delta^{13}C$	0.004	**0.432**	0.269	0.032	0.009
δD	**0.529**	0.189	0.007	0.005	0.121

Values in bold correspond for each variable to the factor for which the squared cosine is the largest

Factor scores:

Observation	F1	F2	F3	F4	F5
C65	-1.091	-0.879	-1.426	-0.540	0.766
4B2-6	-1.870	-0.805	0.043	0.067	-0.545
C98-6	-1.258	-0.434	-0.977	0.599	-0.800
4I2-6	-1.737	-0.381	-0.470	2.679	-2.153
C229-6	-2.103	-0.074	-0.058	0.225	-0.267
J3-6	-2.610	0.331	0.565	0.613	0.741
4G1-6	-2.434	-0.922	-0.881	-0.316	-0.088
4J2-6	-1.714	-1.136	-0.804	0.238	1.635
B5-47	-2.152	0.095	0.362	-0.488	-0.362
4B1-6	-1.595	-1.015	-1.842	0.232	-1.204
2D12-6	-1.418	0.793	1.092	-0.051	1.170
C35-47	-2.691	0.562	2.512	-1.906	0.791
B3-93	-2.248	0.359	2.018	-1.639	-0.668
S9-47	-1.748	0.122	-0.155	-0.375	0.182
4R1-6	8.996	-0.619	-2.135	-2.810	-1.360
3M2A-6	8.336	-3.103	4.259	1.416	-0.247
2F16-6	3.930	8.051	0.143	0.809	-0.121
2U9A-6	5.408	-0.946	-2.245	1.245	2.532